32024

National Library of Canada / Bibliothèque nationale du Canada

CANADIAN THESES ON MICROFICHE / *THÈSES CANADIENNES SUR MICROFICHE*

NAME OF AUTHOR/*NOM DE L'AUTEUR* NAGI AZZOUZ MANSOUR

TITLE OF THESIS/*TITRE DE LA THÈSE* NONLINEAR ANALYSIS OF TWO TERMINAL MICROWAVE ACTIVE CIRCUITS

UNIVERSITY/*UNIVERSITÉ* U OF ALBERTA

DEGREE FOR WHICH THESIS WAS PRESENTED/ *GRADE POUR LEQUEL CETTE THÈSE FUT PRÉSENTÉE* Ph.D.

YEAR THIS DEGREE CONFERRED/*ANNÉE D'OBTENTION DE CE GRADE* 1977

NAME OF SUPERVISOR/*NOM DU DIRECTEUR DE THÈSE* Dr W.A.G. VOSS

Permission is hereby granted to the NATIONAL LIBRARY OF CANADA to microfilm this thesis and to lend or sell copies of the film.

The author reserves other publication rights, and neither the thesis nor extensive extracts from it may be printed or otherwise reproduced without the author's written permission.

L'autorisation est, par la présente, accordée à la BIBLIOTHÈQUE NATIONALE DU CANADA de microfilmer cette thèse et de prêter ou de vendre des exemplaires du film.

L'auteur se réserve les autres droits de publication; ni la thèse ni de longs extraits de celle-ci ne doivent être imprimés ou autrement reproduits sans l'autorisation écrite de l'auteur.

DATED/*DATÉ* Jan 3, 1977 SIGNED/*SIGNÉ* N. A. Mansour

PERMANENT ADDRESS/*RÉSIDENCE FIXÉ* #301 – 8510 – 111 St.
EDMONTON
ALBERTA CANADA

NL-91 (3-74)

National Library of Canada

Cataloguing Branch
Canadian Theses Division

Ottawa, Canada
K1A 0N4

Bibliothèque nationale du Canada

Direction du catalogage
Division des thèses canadiennes

NOTICE

The quality of this microfiche is heavily dependent upon the quality of the original thesis submitted for microfilming. Every effort has been made to ensure the highest quality of reproduction possible.

If pages are missing, contact the university which granted the degree.

Some pages may have indistinct print especially if the original pages were typed with a poor typewriter ribbon or if the university sent us a poor photocopy.

Previously copyrighted materials (journal articles, published tests, etc.) are not filmed.

Reproduction in full or in part of this film is governed by the Canadian Copyright Act, R.S.C. 1970, c. C-30. Please read the authorization forms which accompany this thesis.

THIS DISSERTATION
HAS BEEN MICROFILMED
EXACTLY AS RECEIVED

AVIS

La qualité de cette microfiche dépend grandement de la qualité de la thèse soumise au microfilmage. Nous avons tout fait pour assurer une qualité supérieure de reproduction.

S'il manque des pages, veuillez communiquer avec l'université qui a conféré le grade.

La qualité d'impression de certaines pages peut laisser à désirer, surtout si les pages originales ont été dactylographiées à l'aide d'un ruban usé ou si l'université nous a fait parvenir une photocopie de mauvaise qualité.

Les documents qui font déjà l'objet d'un droit d'auteur (articles de revue, examens publiés, etc.) ne sont pas microfilmés.

La reproduction, même partielle, de ce microfilm est soumise à la Loi canadienne sur le droit d'auteur, SRC 1970, c. C-30. Veuillez prendre connaissance des formules d'autorisation qui accompagnent cette thèse.

LA THÈSE A ÉTÉ
MICROFILMÉE TELLE QUE
NOUS L'AVONS REÇUE

NL-339 (3/77)

THE UNIVERSITY OF ALBERTA

NONLINEAR ANALYSIS OF TWO TERMINAL MICROWAVE ACTIVE CIRCUITS

by

(C)

NAGI A. MANSOUR

A THESIS

SUBMITTED TO THE FACULTY OF GRADUATE STUDIES AND RESEARCH

IN PARTIAL FULFILLMENT OF THE REQUIREMENTS FOR THE DEGREE

OF DOCTOR OF PHILOSOPHY

DEPARTMENT OF ELECTRICAL ENGINEERING

EDMONTON, ALBERTA

SPRING, 1977

THE UNIVERSITY OF ALBERTA

FACULTY OF GRADUATE STUDIES AND RESEARCH

The undersigned certify that they have read, and recommend to the Faculty of Graduate Studies and Research, for acceptance, a thesis entitled NONLINEAR ANALYSIS OF TWO TERMINAL MICROWAVE ACTIVE CIRCUITS submitted by NAGI AZZOUZ MANSOUR in partial fulfilment of the requirements for the degree of Doctor of Philosophy in Electrical Engineering.

.....
Supervisor

.....

.....

.....

.....

.....
External Examiner

Date: December 24, 1976

ABSTRACT

A nonlinear model characterizing two terminal microwave active circuits under dynamic and steady state conditions is developed and represented by two nonlinear differential equations. The model is applicable to oscillators and amplifiers, and considers the admittance dependence on both RF voltage and frequency up to the sixth order. The model response to harmonically time dependent signals with slowly varying amplitude and frequency is discussed. Either discrete or analytically characterized data can be employed in the model.

The model is applied to Impatt diode oscillators and the computed transient and steady state solutions are compared with experimental data. A technique for measuring large signal admittance parameters is developed and is used to obtain the model parameters of an Impatt diode and its embedding circuitry.

In order to measure transient behaviour of Impatt diode oscillators, a new oscillator designed for pulsed operation and a new frequency discriminator was developed. Some of the results measured on a circuit compared favourably with those obtained from the model using the measured parameters.

The transient response is also evaluated for two hypothetical oscillators in which a semiconductor wafer, as characterized in the literature, is embedded. The results indicate the sensitivity of the transients to the embedding circuitry.

As a practical application of the bias modulated oscillator, a digital modulation scheme which operates at rates up to 40 Mb/s has been suggested.

ACKNOWLEDGMENT

The author wishes to express his appreciation for the assistance of many people during the course of this work:

To Dr. W.A.G. Voss, for his valuable advice, encouragement and guidance during the supervision of this work, to Dr. J. Nigrin for the period of his co-supervision, and for the many helpful discussions, to Dr. W.R. Tinga for his generosity and valuable comments, to Dr. C.G. Englefield for his helpful assistance, and to Dr. D.J. Marsden, who served on the doctoral committee.

Thanks are also extended to Dr. H.K. Chaurasia and Mr. C.M.B. Walker for their help and patience in editing the manuscript, to Mrs. M. Yiu for her excellent typing of this thesis,to Mrs. M.K. Mounteer for her assistance in many ways, to Mr. J. Fearn and Mr. A. Huizinga for their excellent technical assistance, to Mr. K. Doerbecker and Mr. G. Fij of the machine shop for their help in fabricating the various components used in the experimental work.

The author also thanks his wife, Greta and his son, Tamer for their patience and encouragement.

The following organizations are acknowledged for their support: The Atomic Energy Establishment of Egypt, The Department of Electrical Engineering, The University of Alberta and The National Research Council of Canada.

TABLE OF CONTENTS

		Page
CHAPTER I	INTRODUCTION	1
CHAPTER II	METHODS FOR DYNAMIC STUDIES ON MICROWAVE CIRCUITS EMPLOYING ONE-PORT ACTIVE DEVICES	5
2.1	Introduction	5
2.2	General circuit approach	9
2.3	Passive circuit characterization	11
2.4	Active circuit model	17
2.5	Model characterization	29
2.6	Theoretical description of a free-running negative conductance oscillator	35
CHAPTER III	BASIC THEORIES OF NEGATIVE CONDUCTANCE SOLID STATE OSCILLATORS	42
3.1	Introduction	42
3.2	Equivalent circuit of a negative conductance microwave oscillator	45
3.3	Oscillators: under steady-state and transient state conditions	47
3.3.1	Analysis of a highly simplified model of a two terminal oscillator circuit	47
3.3.2	Build up and limitation of amplitude of oscillation	51
3.4	Kurokawa's simple theory of oscillators: free-running oscillators	55
3.4.1	Equivalent circuit	56
3.4.2	Impedance locus, device line, and operating point	58

		Page
CHAPTER III - Cont'd		
3.4.3	Effects of distant reflection	58
3.4.4	Onset of oscillation: transient and steady state conditions	63
3.4.5	Stability of free-running oscillators	66
CHAPTER IV	IMPATT DIODES	68
4.1	Introduction	68
4.2	Device structure and dc characteristics	69
4.3	Basic principles of Impatt operation	76
4.4	Small- and large-signal operation	79
CHAPTER V	MEASUREMENT OF LARGE-SIGNAL ADMITTANCE OF IMPATT DIODES AND ASSOCIATED PASSIVE CIRCUITS FOR OSCILLATORS	88
5.1	Introduction	88
5.2	Experimental arrangement for admittance measurements	91
5.3	Error network; system error characterization	96
5.4	Insertion network characterization	103
5.5	Determination of the diode admittance and RF voltage	108
5.6	Evaluation of the passive circuit admittance	109
5.7	Experimental procedure	110
5.8	Discussion of results; examination of sources of error	114

		Page
CHAPTER VI	INSTANTANEOUS POWER AND FREQUENCY MEASUREMENTS	127
6.1	Basic principles of instantaneous power and frequency systems	127
6.2	Single hybrid tee discriminator: principle of operation	130
6.3	Instantaneous power and frequency measuring system	136
CHAPTER VII	THEORETICAL STUDY ON TRANSIENT AND STEADY STATES IN OSCILLATORS	146
7.1	Introduction	146
7.2	Derivation of equations and parameters describing steady and transient states in oscillators	148
7.2.1	Evaluation of the active device d-coefficients	151
7.2.2	Passive circuit d-coefficients evaluation	153
7.2.3	The computation of the quasistationary angular frequency $\bar{\omega}$	153
7.3	Steady state solutions	155
7.4	Transients in Impatt diode oscillators	157
CHAPTER VIII	EXPERIMENTAL STUDIES ON IMPATT DIODE OSCILLATORS	175
8.1	Design of Impatt diode oscillator and the measurement system	175
8.1.1	The resonator circuit	176
8.1.2	The bias circuit	181

		Page
CHAPTER VIII - Cont'd		
8.2	Transient and CW measurements on the oscillators	185
8.3	Bias modulated Impatt diode oscillators	199
CHAPTER IX	SUMMARY AND CONCLUSIONS	210
REFERENCES		216
APPENDIX I		222
APPENDIX II		230
APPENDIX III		240

LIST OF TABLES

Table		Page
5.1	Effect of errors on the measured diode conductance and susceptance due to a change in the return gain and phase.	119
5.2	Measured microwave impedance, Z_m , and the same calculated at plane AA'.	120
7.1	The two sets of resonator parameters used to evaluate the passive circuit admittance for circuits A and B of Fig. 7.4.	167
7.2	Hypothetical and developed oscillator parameters of Eq. (7.22).	174
8.1	Specifications of HP 5082-0437 and HP 5082-0431 Impatt diodes.	186
8.2	Theoretical and experimental steady state solutions (frequency and power) of the two Impatt diodes used.	188
8.3	Operating conditions under changing duty cycle from 50% to 10%.	204
8.4	Operating conditions under fixed (50%) duty cycle and changing pulse period from 60 ns to 300 ns.	204

LIST OF FIGURES

Figure		Page
2.1	Representation of microwave circuit by two separate passive and active sections.	10
3.1	Schematic diagram of a microwave oscillator.	43
3.2	Equivalent circuit representation of a microwave oscillator with separate resonant circuits representing each mode.	43
3.3	Equivalent circuit of a microwave oscillator designed to operate in a single frequency mode.	48
3.4a	Equivalent circuit of a solid state microwave oscillator tuned to one mode of oscillation.	48
3.4b	Highly simplified equivalent circuit of a microwave oscillator.	48
3.5	Electronic conductance vs. RF signal amplitude.	54
3.6	Equivalent circuit of a free-running microwave oscillator.	57
3.7	Impedance locus and device line.	57
3.8	Formation of a loop in the impedance locus.	60
3.9a	Variation of the operating point with change in the position of impedance locus.	62
3.9b	Explanation of the jump of operating point.	62
3.10	Typical frequency and power tuning hysteresis of a multiple-tuned oscillator.	65
3.11	The onset of oscillation in a single tuned oscillator.	65

Figure		Page
4.1	Imput diode equivalent circuit at $V < V_b$.	70
4.2	Read diode.	70
4.3	One-sided abrupt p-n junction diode.	73
4.4	p-i-n diode.	74
4.5	Read diode structure, field distribution, and voltage and current waveforms.	78
4.6	Read diode: Idealized negative resistance vs. transit angle.	82
4.7	Effect of doping profile on conductance for 1) Read, 2) abrupt, 3) Missawa (uniform avalanche) profiles.	82
4.8	Small-signal admittance plane plot for Ge n^+-p-p^+ diode.	84
4.9	Diode admittance (susceptance vs. conductance) as a function of frequency and RF voltage amplitude.	86
5.1	Arrangement for the measurement of Impatt diode large-signal admittance.	92
5.2	Cross-sectional view of Impatt diode amplifier: consisting of an Impatt diode, a single slug transformer and a waveguide circulator.	94
5.3	Measurement system representation for evaluating the Impatt diode admittance.	98
5.4	Measurement system representation for evaluating error network parameters.	98
5.5	Circuit of the reflection type amplifier.	98
5.6	The measured reflection coefficient, Γ_m, and the corresponding measured and the corrected value Γ_{AA}, at 5.7 GHz.	101

Figure			Page
5.7		The measured reflection coefficient, Γ_m, and the corresponding measured and corrected value $\Gamma_{AA'}$, at 6.5 GHz.	102
5.8		Real and imaginary parts of Impatt diode impedance ($Z_D=R_D + jX_D$) as a function of bias voltage ($V < V_b$) at 5.7 GHz for diode #1.	107
5.9		C-V characteristics of Impatt diodes #1 and #2.	111
5.10	(a)	Large-signal admittance, Y_D, of Impatt diode #1 as a function of RF voltage and frequency at constant dc current of 25 mA.	115
	(b)	Circuit admittance, Y_c, as a function of frequency, as seen by the diode embedded in a 7 mm coaxial resonator.	
5.11	(a)	Large-signal admittance, Y_D, of Impatt diode #2 as a function of RF voltage and frequency at constant dc current of 25 mA.	116
	(b)	Circuit admittance, Y_c, as a function of frequency, as seen by the diode embedded in a 7 mm coaxial resonator.	
5.12		Diode negative conductance as a function of RF voltage amplitude for various fixed frequencies for diode #2 (I_{dc} = 25 mA).	118
5.13		The effect of errors in the C-V measurements on the measured diode conductance vs. RF voltage curves at 5.9 GHz (diode #1).	123
5.14		The effect of errors in the C-V measurements on the diode susceptance vs. RF voltage curves at 5.9 GHz (diode #1).	124
5.15		The effect of errors in the C-V measurements on the measured diode admittance vs. RF voltage curves at 5.9 GHz (diode #1).	125

Figure		Page
6.1	Illustrating the basic principle of the operation of the microwave instantaneous frequency measuring system.	128
6.2	Single hybrid tee frequency discriminator.	131
6.3	Polar display of the discriminator response (P = 10 mW, ℓ = 1.78 cm).	135
6.4	Input VSWR of the single hybrid tee discriminator.	135
6.5	Experimental arrangement for the calibration of instantaneous power and frequency measuring system.	137
6.6	Detectors dc voltage sensitivities.	139
6.7	Constant power and frequency response of the instantaneous measuring system.	140
6.8	Practical RF modulating system to check the accuracy of the instantaneous power and frequency measuring system.	142
6.9	The two RF envelopes recorded by the X- and Y-detectors.	143
6.10	Enlarged section of the constant power and frequency curves of Fig. 6.7 showing the results extracted from the traces in Fig. 6.9.	144
7.1	Overall iterative scheme for the calculations of steady state voltage amplitude, A, and frequency $\bar{w} + x$.	156
7.2	Overall iterative scheme for the calculation of the dynamic solution by using forward iterative scheme.	158
7.3	Overall iterative scheme for the calculation of the dynamic solution using backward iterative method.	159

Figure		Page
7.4	(a) Impatt diode admittance as a function of RF voltage amplitude and frequency at a current density of 200 A/cm.	162
	(b) Passive circuit admittance, Y_c, as a function of frequency for circuit A (Table 7.1).	
	(c) Passive circuit admittance as a function of frequency for circuit B (Table 7.1).	
7.5a	Cross-sectional view of a 7 mm coaxial-type resonator embedding the Impatt diode. R_1, R_2, R_3, XL_2 and XL_3 are the resonator parameters (Table 7.1).	163
7.5b	Equivalent circuit of an Impatt diode oscillator.	164
7.6	Buildup of power in a realistic oscillator for two sets of the 7 mm coaxial resonator parameters.	165
7.7	Buildup of frequency in a realistic oscillator for two sets of the 7 mm coaxial resonator parameters.	166
7.8	Buildup of power (a) and frequency (b) in the Impatt diode oscillator using diode #2 (Ch. VIII).	169
7.9	Device line and impedance locus superimposed on a part of Impatt diode admittance characteristics.	171
7.10	Device line and impedance locus superimposed on the measured Impatt diode admittance characteristics, diode #2 ($\bar{\omega}$ = 5.886 GHz).	173
8.1	Arrangement for the measurement of transients in Impatt diode oscillators.	177
8.2	Cross-sectional view of the Impatt diode oscillator used in the measurement of the transients.	178
8.3	Cross-sectional view of the 7 mm coaxial cavity with end mounted Impatt diode.	180

Figure		Page
8.4	Bias circuit as seen from pulse generator terminals.	183
8.5	Modulating pulse (500 mV/cm), diode current (100 mV/cm) and two RF envelopes recorded by the X- and Y-detectors (20 mV/cm) for diode #2.	190
8.6	A reproduced copy of Fig. 8.5 with the time scale adjusted for a 10 ns delay caused by the measurement system.	192
8.7	System calibration for instantaneous frequency and at different instance of time on the RF envelopes of Fig. 8.5.	194
8.8	Measured and calculated power waveforms of the Impatt diode oscillator.	195
8.9	Measured and calculated time dependence of the frequency of the Impatt diode oscillator.	197
8.10	Diode current (100 mV/cm) and two RF envelopes (20 mV/cm) recorded by the X- and Y-detectors for a modulating pulse with duty cycle of 0.5.	202
8.11	Diode current (100 mV/cm) and two RF envelopes (20 mV/cm) recorded by the X- and Y-detectors for a modulating pulse with duty cycle of 0.2.	203
8.12	Frequency variation, for pulses of 30 ns ON time, as a function of the duty cycle between two instances for which the power changes between its maximum value and 87% of this value.	206
8.13	Decay time of the RF envelopes as a function of the duty cycle due to a 30 ns ON pulse.	206
8.14	Instantaneous frequency at maximum power level vs. pulse periods (50% ON time pulses).	207

Figure		Page
8.15	Modulation scheme for utilizing bias modulated Impatt diode oscillator for the transmission of data at nearly 40 Mbits/s.	208

LIST OF SYMBOLS

A = Ch. III: RF current amplitude flowing through the active device.

Ch. IV: diode area.

Otherwise = A(t): time dependent applied RF voltage amplitude.

A,B,C and D = the fundamental parameters of the insertion network.

a,b,c and 1 = normalized parameters of the insertion network.

AN,BN,CN and 1 = elements of the error network matrix.

A_o = peak amplitude of the driving RF voltage for CW excitation.

A_{mh}, B_{ph} = constants depending upon the embedding circuitry and active device.

a_{mh}, b_{ph} = coefficients dependent on the active device, embedding circuitry and the bias voltage V_o.

$a_{m,h,g}$, $b_{m,h,g}$ = the m-th coefficient of the g-harmonic component with an amplitude A^h.

a_m = simplified notation for $a_{m,o,o}$

A^o = dA/dt.

$a_n,\ldots,a_o$ = characteristic parameters of the passive circuit.

a_i = normalized incident wave at the i-th port (i = 1,2,3,4).

$b_n, \ldots, b_o$ = characteristic parameters of the passive circuit.

b_i = normalized emerging wave from the i-th port ($i = 1,2,3,4$).

b_{ij} = emerging wave from the i-th port to the j-th port.

${}_{KL}b^{d}_{p,2h,g}$ = the p-th coefficient for the g-th harmonic component with an amplitude A^{2h} of the active device in the KL subrectangle $[A_k, A_{k+1}] \times [\omega_L \times \omega_{L+1}]$.

${}_{L}b^{c}_{p,o,o}$ = the p-th coefficient of the passive circuit in the L-interval.

${}_{KL}b_{p,2h,g} = {}_{KL}b^{d}_{p,2h,g}$; except for Eqs.(2.63) to (2.68) = the total oscillator b-coefficients.

$B(A_k^2, \omega_L^2)$ = active device susceptance determined at the points A_k^2 and ω_L^2.

$B(A_M^2, \omega_N^2)$ = active device susceptance determined at the points A_M^2 and ω_N^2.

$B_{MN}(A^2, \omega^2)$ = bicubic spline interpolate for the active device susceptance determined at the points A^2 and ω^2 in the MN subrectangle $[A_M, A_{M+1}] \times [\omega_N, \omega_{N+1}]$.

$B(A^2, \omega^2)$ = active device susceptance at the points A^2 and ω^2.

$B_D(A^2, \omega^2) = B(A^2, \omega^2)$.

$\bar{B}_{MN}(A^2, \omega^2)$ = susceptance of the complementary device admittance at the points A^2 and ω^2 in the MN subrectangle.

B_D = diode susceptance.

$B_c(\omega)$ = circuit susceptance.

$_N B_c(\omega^2)$ = spline interpolate for B_c in the N-th interval.

B = total circuit susceptance of the oscillator.

$\bar{B}$ = total circuit complementary susceptance of the oscillator.

B_{en} = device electronic susceptance at the n-th harmonic.

B_e = device electronic susceptance.

B_ℓ = load susceptance.

B_n, C_n = Ch. VII: nonlinear coefficients of the equations representing the steady state of the oscillator.

C = Ch. II: passive circuit capacitance

Ch.III: equivalent capacitance of the highly simplified oscillator circuit.

Ch.VIII: bypass capacitors.

C_n = circuit capacitance at the n-th harmonic.

C_ℓ = equivalent load capacitance.

C_r = equivalent capacitance of the cavity.

C_e = equivalent capacitance of the device.

C_c = equivalent passive circuit capacitance.

$C(V)$ = bias voltage dependent capacitance of the Impatt diode wafer $(V < V_b)$.

$C(V_j) = C_j$ = diode wafer capacitance at bias voltage V_j.

$C(V_{j+1}) = C_{j+1}$ = diode wafer capacitance at bias voltage V_{j+1}.

C_{av} = the average of the capacitances C_j and C_{j+1} at bias voltages V_j and V_{j+1}, respectively.

C_p = package capacitance.

C_H = heat sink capacitance to ground.

$KL^{c\mathcal{E}}_{2m}$, $KL^{c\mathcal{E}}_{2m+1,2}$, $KL^{c\mathcal{E}}_{2m,2}$ and $KL^{c\mathcal{E}}_{2m+1}$ = active device coefficients in the KL subrectangle $[A_k, A_{k+1}] \times [\omega_L, \omega_{L+1}]$, which are functions of A and the device d-coefficients.

$MN^{c\mathcal{E}}_{2m}$, $MN^{c\mathcal{E}}_{2m+1,2}$, $MN^{c\mathcal{E}}_{2m,2}$ and $MN^{c\mathcal{E}}_{2m+1}$ = active device coefficients in the MN subrectangle.

CW = constant frequency wave.

$d'_{p,h}$ = (p,h)-th coefficient of the general model of the active device derived from the $b_{p,h,g}$ coefficients.

$d_{p,h}$ = (p,h)-th coefficient of the simplified model of the active device derived from the $b_{p,h,g}$ coefficients.

$d_{p,o}$ = p-th coefficient of the circuit derived from the $b^c_{p,o,o}$ coefficient.

dBm = dB with reference to mW.

D = Ch. II: $= \frac{\partial}{\partial \omega}$

Ch. V : diode junction diameter (cm).

E = electric field (V/cm).

$E_{in}(t)$ = voltage amplitude of the measured signal.

E_{out} = measured output voltage.

E_{d_1}, E_{d_2} = dc output voltages of diodes #1 and #2.

f = frequency in GHz.

f(t) = driving force.

$F_1, \ldots, F_N$ = functional values of either circuit conductance or $B_c(\omega)/\omega$.

$F_N(\omega^2)$ = spline interpolate for G_c or $B_c(\omega)/\omega$ in the N-th interval.

g_{ij} = the ij-th coefficient of the bicubic spline fitting for the active device conductance.

g = hole and electron generation recombination rates.

G = Ch. II: passive circuit conductance pp. 6-7.

: total circuit conductance of the oscillator p. 39.

Ch.III: equivalent circuit conductance of the highly simplified oscillator circuit.

$G[\omega^2(t)]$ = conductance operator for non-CW operation.

${}_LG(\omega^2)$ = the spline interpolate in the L-th interval for the passive circuit conductance.

$G_m(\omega_L^2)$ = the m-th coefficient of the spline in the L-th interval for the passive circuit conductance (m = 1,2,3,4).

${}_{KL}G(A^2, \omega^2)$ = the spline interpolate in the KL subrectangle $[A_k, A_{k+1}] \times [\omega_L, \omega_{L+1}]$ for the active device conductance.

$G(A_k^2, \omega_L^2)$ = the active device conductance determined at the points A_k^2 and ω_L^2.

$GM_{ij}(A_k^2, \omega_L^2)$ = the ij-th coefficient of the expansion of the device conductance as a function of A^{2i} and ω^{2j} for the KL subrectangle.

$G(A_M^2, \omega_N^2)$ = the active device conductance determined at the points A_M^2 and ω_N^2.

$GM_{ij}(A_M^2, \omega_N^2)$ = the ij-th coefficient of the expansion of the device conductance as a function of A^{2i} and ω^{2j} for the MN subrectangle.

$G_{MN}(A^2, \omega^2)$ = the spline interpolate in the MN subrectangle $[A_M, A_{M+1}] \times [\omega_N, \omega_{N+1}]$ for the active device conductance.

$\bar{G}$ = total circuit complementary conductance of the oscillator.

G_{en} = device electronic conductance at the n-th harmonic.

G_n = circuit conductance at the n-th harmonic.

G_ℓ = load conductance.

G_e = device electronic conductance.

G_r = shunt conductance of the cavity.

G_c = equivalent passive circuit conductance.

$|G_e|_o$ = absolute value of G_e at zero RF voltage amplitude.

$\bar{G}_{MN}(A^2, \omega^2)$ = the spline interpolate in the MN subrectangle for the active device complementary conductance.

$G_c(\omega)$ = circuit conductance.

${}_N G_c(\omega^2)$ = spline interpolate for G_c in the N-interval.

G_D = diode conductance.

i = $i(t)$: current response of the active device.

i_i = $i_i(t)$: externally injected current.

$i_c(t)$ = passive circuit current.

$i_D(t)$ = active device current.

I_o = peak amplitude of RF current for the constant CW case.

$I(t)$ = complex time varying current amplitude for the modulated CW case.

$\tilde{i}(t)$ = microwave frequency component of the current $i(t)$.

$I_o(t)$ = bias component of the current $i(t)$.

$I_f(t)$ = amplitude of the f-th component of the RF current.

$I^*_{-f}(t)$ = complex conjugate of $I_f(t)$.

I_{2f+1} = odd harmonic component of $I_f(t)$.

I_{2f} = even harmonic component of $I_f(t)$.

I_1 = complex current amplitude at the fundamental frequency.

$i_{KL}(t)$ = fundamental frequency component of the current response of the active device in the KL rectangle $[A_k, A_{k+1}] \times [\omega_L, \omega_{L+1}]$.

$_L i_c(t)$ = passive circuit current in the L-interval.

I = fundamental frequency component of the device current.

I_{dc} = dc bias current.

J_o = dc current density.

J_{inj} = avalanche current density.

J_{ind} = external current density.

J_p, J_n = electron and hole current densities (A/cm^2).

k = Ch.IV: Boltzman constant (1.38×10^{-23} Joule/°K)

Ch. V: constant = 9.91×10^{30} for Si.

L = Ch. II: passive circuit inductance.

Ch.III: equivalent inductance of the highly simplified oscillator circuit.

$L(\frac{d}{dt})$ = linear differential commutative operator.

$L(j\omega_o)$ = function operator in $j\omega_o$ for the CW case.

$L(j\omega + \frac{d}{dt})$ = differential function operator to operate on $i(t)$ for the modulated CW case.

L_r = equivalent inductance of the cavity.

L_1 = equivalent inductance of the coupling iris.

L_e = equivalent inductance of the device.

L_c = equivalent passive circuit inductance.

ℓ = plunger position with respect to the reference plane AA'.

ℓ_1, ℓ_2 = physical length of channels No. 1 and No. 2, respectively.

L_p = Ch. VII: package inductance

Ch.VIII: DC supply input inductance.

LF = low frequency.

M_n = mutual inductance for the n-th harmonic.

$N(\frac{d}{dt})$ = linear differential commutative operator.

$N(j\omega_o)$ = function operator in $j\omega_o$ for the CW case.

$N(j\omega + \frac{d}{dt})$ = differential function operator to operate on $v(t)$ for the modulated CW case.

N_D, N_A = donor and acceptor densities (cm^{-3}).

$N_x(j)$ = impurity concentration in (j+1,j) interval.

p,n = hole and electron densities (cm^{-3}).

P_{in} = incident power.

P_{out} = output power.

P = CW oscillator power.

q = electronic charge (C).

Q = quality factor.

$r(t)$ = response of the microwave passive circuit.

RF = microwave frequency.

$R_e(A)$ = equivalent device resistance.

R_a = equivalent resistance representing loss in the cavity.

R_L = load resistance.

$R_D(V)$ = resistance of unswept region of the Impatt diode at bias voltage $V < V_b$.

R = real part of the diode terminal impedance.

RG = return gain.

R_1, R_2 and R_3 = resonator parameters - Ch. VII.

R_b = bias current measuring resistor.

R_s = pulse generator source resistance.

R_T = load termination.

$S[\omega^2(t)]$ = susceptance operator for the modulated CW case.

$S(A_k^2, \omega_L^2) = B(A_k^2, \omega_L^2)/\omega_L$.

S_{ij} = hybrid tee scattering parameters.

s_{ij} = the ij-th coefficient of the bicubic spline fitting for the active device susceptance.

$S_{KL}(A^2, \omega^2)$ = spline interpolate in the KL subrectangle for the active device B/ω.

$SM_{ij}(A_k^2, \omega_L^2)$ = the ij-th coefficient of the expansion of the device B/ω as a function of A^{2i} and ω^{2j} for the KL subrectangle.

$S_{MN}(A^2, \omega^2)$ = the spline interpolate in the MN subrectangle for the actice device B/ω.

$S(A_M^2, \omega_N^2)$ = the active B/ω determined at the points A_M^2 and ω_N^2.

$SM_{ij}(A_M^2, \omega_N^2) = SM_{ij}(A_k^2, \omega_L^2)$; at M = k and N = L.

t = time.

T = absolute temperature.

$v_{s\ell}$ = scattering limited velocity of the charge carriers.

v = v(t) = applied terminal voltage.

V(t) = complex time varying voltage amplitude.

$\tilde{v}(t)$ = microwave frequency component of the voltage v(t).

$V_o(t)$ = bias component of the voltage v(t).

$V^*(t)$ = complex conjugate of V(t).

V = bias voltage.

V_{RF_n} = RF voltage amplitude of the n-th harmonic.

V_o = Ch. III: RF signal amplitude at t = 0.

V_{bias} = V.

V_b = dc breakdown voltage.

V_a = the voltage drop across the avalanche region.

V_{dc} = dc voltage output from the network analyzer proportional to the phase angle of the reflection coefficient.

V_+ = voltage amplitude of the incident wave at plane AA'.

V_{RF} = RF voltage across the diode.

W = width of the depletion region.

$x^{\cdot} = \frac{d\phi}{dt}$.

$x^{o} = \frac{dx}{dt}$.

$X_e(A)$ = equivalent device electronic reactance.

x_A = width of the avalanche region.

X-det = response of the detector in H-arm of the hybrid tee.

XL_2, XL_3 = resonator parameters.

$X_D(V)$ = reactance of the diode at bias voltage V.

$Y_c(j\omega_o)$ = passive circuit CW admittance.

$Y_c[j\omega(t)]$ = admittance operator for the modulated CW case.

Y_D' = admittance characterizing the general model of the actice device.

Y_D = admittance of the simplified model of the active device.

Y_e = passive circuit admittance.

$\bar{Y}$ = total circuit complementary admittance of the oscillator.

Y = total circuit admittance of the oscillator.

Y_D = diode admittance.

Y(short) = admittance of the short circuit.

Y-det = response of the detector in the E-arm of the hybrid tee.

Y_{MN} = the active device admittance determined at the points A_M^2 and ω_N^2.

$Y(A^2,\omega^2)$ = the active device admittance as a function of A^2 and ω^2.

Y_e = device electronic admittance.

Y_E = transformed circuit admittance as seen by the packaged diode.

$Z_e(A)$ = device electronic impedance.

$Z_c(\omega)$ = circuit impedance.

$Z_e(0)$ = device impedance at zero RF voltage amplitude.

Z_o = characteristic impedance of the transmission line.

Z_a = normalized impedance at plane AA' looking towards the diode.

$Z(V)$ = impedance of the active layer of the Impatt diode at bias voltage V.

Z_m = measured normalized microwave impedance at plane AA' looking towards the diode at $V < V_b$.

α = Ch. II: positive constant characterizing the device.

Ch.III: oscillation growth factor.

Ch. V : attenuation coefficient of the transmission line.

α_n = ionization rate of the electrons.

α_p = ionization rate of the holes.

$\langle\alpha\rangle$ = average ionization rate of charge carriers.

α' = derivative of the ionization rate with respect to the electric field.

β = phase coefficient of the transmission line.

γ = positive constant characterizing the device.

γ_d = diode voltage sensitivity.

Γ = reflection coefficient.

Γ_m = measured reflection coefficient.

$\Gamma_{AA'}$ = reflection coefficient at plane AA'.

$\Delta R_D(j)$ = incremental change of the diode resistance for a voltage change $\Delta V = V_{j+1} - V_j$.

ΔC = change in the diode capacitance between voltages V_j and V_{j+1}.

ΔV = change in the bias voltage $(V_{j+1} - V_j)$.

δ = error parameter controlling the iteration procedure for the evaluation of the steady state solution.

ε = dielectric constant (F/cm).

θ = transit angle.

$\rho(j)$ = diode wafer resistivity in the interval j, j+1 (Ω.cm).

ϕ = Ch.III: constant phase angle of v at t = 0.

Ch. V : phase constant of the reflection coefficient in degrees.

Otherwise = $\phi(t)$: time dependent phase of the applied RF voltage v(t).

ϕ_o = constant phase of the CW driving force.

$\bar{\omega}$ = quasistationary frequency.

ω = Kurokawa: time and phase dependent angular frequency operator.

Ch. III: angular frequency of oscillations.

Otherwise: angular frequency.

ω_o = CW angular frequency.

$\omega(t)$ = instantaneous angular frequency.

$[\omega(t)]$ = angular frequency operator.

ω_L = angular frequency at the start of the L-interval.

ω_a = resonant angular frequency of an LC circuit.

ω' = real part of the complex angular frequency ω.

ω_r = avalanche resonant angular frequency.

μ_p, μ_n = hole and electron mobilities ($cm^2/V.s$).

λ_g = guided wavelength.

CHAPTER I

INTRODUCTION

Microwave one port active semiconductor devices are finding wide applicability in the output stages of many communications systems requiring RF power levels of the order of 5 to 10 watts. High reliability, long-life and extreme compactness are inherent characteristics of semiconductor devices and therefore fully solid state microwave systems are a considerable improvement over existing tube or hybrid types[1,2]. In the communications context, the two most important solid state devices are the Impatt and the Gunn diodes. In particular, the Impatt diode, capable of delivering up to 12 watts at 6 GHz [3], is the most powerful solid state CW microwave source presently available [4].

A significant area of growth in the communications industry is in computer based high speed data transmission, where digital microwave systems play the major role [5,6]. Design trends for these systems indicate the strong possibility of the Impatt diode being used even more extensively in the near future. The modulation schemes most likely to be adopted for digital communications are phase and frequency shift keying in which the problem of amplitude nonlinearity inherent in solid state devices is not significant [7-9].

It is unlikely that the Impatt diode, or any other solid state device will immediately replace tube devices in the near future. Rather, solid state technology will be applied selectively to perform specific system functions while freely capitalizing on the advantages of an all solid state approach. For this reason, and to ensure successful implementation in new system concepts, a precise knowledge of the characteristics and limitations of these solid state devices is essential.

The electrical characteristics and properties of microwave circuits are governed by the active device. In system applications, either in oscillator or amplifier circuitry, the interaction between the active device and the circuit is very important for design considerations. Under transient conditions, the dynamic characteristics of the circuit account for this interaction and yield the transient response of the circuit.

To optimize efficiency and economy, which are key figures of merit in power applications, the active devices are strongly driven into the nonlinear region. Consequently any detailed description of the dynamic behaviour of active circuits, which is of primary importance to the designers, is very complex, and requires extensive numerical calculations. The numerical methods are usually very different, depending upon the type of active device. To simplify the calculations,

either the active device is very accurately described while only simple external circuitry is assumed, or in the opposite approach, external circuitry is accurately described and combined with an idealized negative conductance device possessing Van der Pol's cubic nonlinearity [10]. The latter approach can only be applied to the simplest of these devices, such as the tunnel diode. On the other hand, high power devices have nonlinear dependence of both conductance and susceptance on RF voltage and frequency. Consequently they are poorly approximated by a cubic nonlinearity. Hence in dynamic studies on these circuits a more accurate method based on detailed characteristics of the given active device must be employed.

The presentation of this thesis starts with the development of a general model characterizing the dynamic and steady states of nonlinear microwave active circuits. The application to free-running oscillators is then described. Chapter III develops the basic theories of negative conductance solid state oscillators in the form of a simplified model. The basic principles of Impatt diodes, their structure, DC characteristics and operation under small and large signal conditions are discussed in Chapter IV. Chapter V describes the measurement technique and method used to evaluate the large signal admittance of Impatt diodes together with their embedding

circuitry. A new frequency discriminator to measure the instantaneous power and frequency is discussed in Chapter VI. The model developed in Chapter II has been used for a theoretical study of the transient and steady state behaviour of the oscillator in Chapter VII. The results are applied to the Impatt diode oscillator in particular, using the large signal parameters determined in Chapter V. The following chapter deals with experimental studies on Impatt diode oscillators, and the results are compared with the theoretical predictions from the previous chapter. This chapter also discusses the operation of a bias modulated oscillator and develops a digital modulation scheme for transmitting data at rates up to 40 Mb/s. The concluding Chapter IX summarizes the findings of this study, and presents suggestions for further work.

CHAPTER II

METHODS FOR DYNAMIC STUDIES ON MICROWAVE CIRCUITS EMPLOYING ONE-PORT ACTIVE DEVICES

2.1 Introduction

Microwave active solid state devices are usually very small compared to the guided wavelength so that the electric and magnetic fields do not vary significantly along their dimensions. Therefore, conventional circuit theory can be used in the analysis of these devices even up to the millimeter wavelength range. The device response to a single frequency excitation, which may be either RF voltage or current depending on the embedding circuitry, contains an appreciable number of harmonics the amplitudes of which depend upon the signal strength. The higher harmonics, however, are greatly attenuated by tuning the high Q embedding circuitry to the fundamental frequency. This enables the active device to be uniquely characterized at the signal frequency by a nonlinear immittance dependent upon the signal amplitude and frequency. Consequently, equivalent circuit representation can be employed when investigating the active circuit response to unmodulated CW signals. The steady state amplitude and phase of the device response at

the signal frequency can be obtained by solving nonlinear algebraic circuit equations. However, in many applications, some additional information is vital, e.g. stability and noise properties of the steady state solution, response of the active circuit to modulated signals (in particular nonlinear and phase distortion, AM to PM conversion) and intermodulation characteristics of the device. The desired method must be suitable for dynamic studies on active one-port circuits exposed to both CW and modulated signals in order to give some insight into these problems and therefore facilitate better circuit designs.

The oldest method for dynamic studies on one-port devices is that developed by Van der Pol [10] for negative conductance oscillations. He approximated the current response of the device, i, by

$$i = -\alpha v + \gamma v^3 \qquad (2.1)$$

where v is the applied voltage and α, γ are positive constants characterizing the given device. Representing the embedding circuitry by a single tuned parallel resonant circuit, whereby all package parasitic and device susceptances are included in the embedding circuitry, Van der Pol arrived at the following second order nonlinear differential equation:

$$\frac{d^2v}{dt^2} + \frac{1}{C}\,(G - \alpha + \gamma v^2)\,\frac{dv}{dt} + \frac{1}{LC}\,v = \frac{1}{C}\,\frac{di_i}{dt} \qquad (2.2)$$

where L, C and G are positive circuit parameters and i_i is the externally injected current. To solve the above equation, Van der Pol proposed a method of slowly varying parameters which was later refined by Bogoliubov [11]. According to this method, the solution is sought in the form

$$v(t) = A(t)\sin[\bar{\omega}\, t + \phi(t)] \ . \qquad (2.3)$$

Thus, the rapid time variation of v(t) is assumed to be harmonic, being characterized by a carrier or quasi-stationary angular frequency $\bar{\omega}$, and the slow variations of v(t) are described by the unknown functions A(t) and $\phi(t)$ which satisfy the relationships

$$\frac{dA}{dt} << \bar{\omega}\, A \ ; \qquad \frac{d\phi}{dt} << \bar{\omega} \ . \qquad (2.4)$$

In other words, A(t) and $\phi(t)$ are functions which are slowly varying in time intervals comparable to $2\pi/\bar{\omega}$. Substituting Eq. (2.3) into Eq. (2.2), two first order differential equations are obtained from which A(t) and $\phi(t)$ can be conveniently evaluated using numerical methods.

There are a few serious short comings when applying Van der Pol's approach to active solid state devices. First, solid state devices are characterized by nonlinear conductance as well as susceptance; Kuno [12] has recently extended the method by including nonlinear

inductance . Secondly, because of the single tuned circuit representation of the embedding circuitry, the active solid state microwave circuit, which usually operates in a wide frequency band, cannot be well described. Finally, the active device is described by means of various constants, e.g. γ, which are rather general and cannot be accurately determined for a given device.

Many present dynamic studies are based on a method developed by Kurokawa [13] in 1969 for noise and stability investigations on CW oscillators. Kurokawa expresses the diode voltage and current in the form

$$v(t) = A(t)\ \mathrm{Re}\{\exp\ j[\bar{\omega}t + \phi(t)]\}\ .$$

He does not restrict the passive circuitry to a single tuned model. Instead, he uses a generalized immittance expression in which the ω-factor is replaced by the operator

$$\omega \longrightarrow [\bar{\omega} + \frac{d\phi}{dt} - j\ \frac{d}{dt}]$$

and the active device is represented by its large signal immittance. Expanding the immittance expression around $\bar{\omega}$, Kurokawa derives two first order differential equations for $\phi(t)$ and $A(t)$. Since the coefficients in these equations are related to the device immittance, this method can describe a particular device accurately. The great potential of this method lies in the studies on steady state CW operation and small noise disturbances.

Since the device nonlinearities are not fully taken into account, this method is hardly suitable for the study of active devices exposed to strongly modulated or transient signals.

In 1972, another method was proposed by Gustafsson, Hansson and Lundström [14]. Representing the active circuit by a feedback model containing a nonlinear element, they were able to apply a describing function technique. Since this technique has been intensively used in the study of nonlinear control systems, considerable experience is made available for the study of nonlinear problems at microwave frequencies. When dealing with strongly modulated signals, this technique is only slightly better than Kurokawa's approach.

Sections 2.2 to 2.5 of this chapter deal with the development of a theoretical technique for the characterization of nonlinear microwave active circuits. This technique is applied to free-running oscillators in section 2.6.

2.2 General circuit approach

When studying the dynamic behaviour of a microwave circuit in which is embedded an active one-port device, it is very useful to divide the circuit into a passive one-port circuit and an active one-port device, as shown in Fig. 2.1. In this manner it is possible to

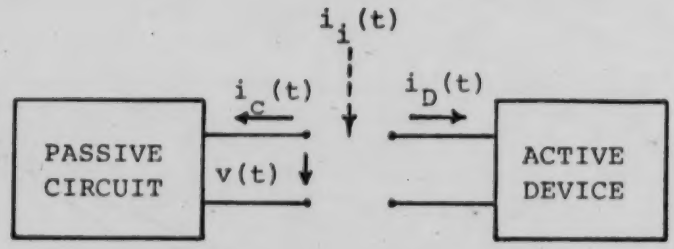

Fig. 2.1 Representation of microwave circuit by two separate passive and active sections.

separate the characteristics of the nonlinear active element that vary relatively slowly with frequency from those of the passive circuit which vary rapidly with frequency.

Assuming the terminal voltage, v(t), to be the driving force, the operation of the complete active circuit is described by

$$i_c[v(t)] + i_D[v(t)] = 0 \ . \qquad (2.5)$$

If the active circuit is disturbed by an externally injected signal, i_i, the above relation, which is essentially Kirchhoff's current law, will change to

$$i_c[v(t)] + i_D[v(t)] = i_i(t) \ . \qquad (2.6)$$

If the current response of the network to the applied terminal voltage can be determined, the voltage at the terminals of the active device, excited by any externally injected signal, can be evaluated using Eq. (2.6). Knowing the terminal voltage (at the terminals of the passive circuit), the current flowing into the passive circuit, $i_c(t)$, can be evaluated. Using linear circuit techniques, the current and voltage anywhere in the passive circuit can thus be determined.

2.3 Passive circuit characterization

In analogy with low frequency networks, the driving force, f(t), and the corresponding response

of a passive microwave circuit, r(t), are related by [15]

$$\left(a_n \frac{d^n}{dt^n} + \ldots + a_1 \frac{d}{dt} + a_o\right) r(t) = \left(b_p \frac{d^p}{dt^p} + \ldots + b_1 \frac{d}{dt} + b_o\right) f(t) \tag{2.7}$$

where $a_o, \ldots, a_n$, $b_o, \ldots, b_n$ are characteristic parameters of the given circuit. Depending on the circuit excitation, the terminal voltage can be either the driving force itself, as is assumed in this study, or the circuit response. Eq. (2.7) can be written in operator notation as

$$L\left(\frac{d}{dt}\right)\{r(t)\} = N\left(\frac{d}{dt}\right)\{f(t)\} \tag{2.8}$$

where the linear differential commutative operators, L and N, operate on the functions enclosed in the { } brackets.

The circuit response to an unmodulated CW driving force can be evaluated from Eq. (2.8) by Fourier transforming it into an algebraic equation. The steady state amplitudes of the driving force and the circuit response are then related through a frequency dependent circuit immittance.

A single frequency CW voltage excitation

$$f(t) = v(t) = A_o e^{j\omega_o t} \tag{2.9}$$

produces a current response r(t), which will have the general form:

$$r(t) = i(t) = I_o \exp(j\omega_o t) = \exp(j\omega_o t) Y_c(j\omega_o) A_o \ . \qquad (2.10)$$

The actual physical signals are given by Re{v(t)} and Re{i(t)}. The term $Y_c(j\omega_o)$, called the passive circuit CW admittance, will be given by

$$Y_c(j\omega_o) = \frac{I_o}{A_o} = \frac{N(j\omega_o)}{L(j\omega_o)} \qquad (2.11)$$

where $N(j\omega_o)$ and $L(j\omega_o)$ follow directly from the Fourier transform of Eq. (2.7)†.

For a modulated CW driving force, the evaluation of the circuit response is relatively complicated. Then the dirving force is usually given by

$$f(t) = v(t) = A(t) \exp j(\bar{\omega}t + \phi(t)) = V(t) \exp j\bar{\omega}t \qquad (2.12)$$

where $\bar{\omega}$ is the quasistationary angular frequency. The signal V(t) is the complex time-varying voltage amplitude which has a magnitude A(t) and a phase angle $\phi(t)$, where both A and ϕ are real quantities.

The general circuit response can be expressed in a form similar to Eq. (2.12), i.e.

---

† The operator argument of N and L changes depending on whether one is treating modulated or CW signals, or on whether one is operating in the time or frequency domain.

$$r(t) = i(t) = I(t)\exp j\bar{\omega}t \tag{2.13}$$

where $I(t)$ is the complex, time-varying current amplitude. Differentiating Eqs. (2.12) and (2.13), we obtain

$$\frac{d^n v(t)}{dt^n} = \exp j\bar{\omega}t\left[j\bar{\omega} + \frac{d}{dt}\right]^n \{V(t)\} \tag{2.14}$$

and

$$\frac{d^n i(t)}{dt^n} = \exp j\bar{\omega}t\left[j\bar{\omega} + \frac{d}{dt}\right]^n \{I(t)\} \quad . \tag{2.15}$$

Thus the derivatives of v and i for the modulated frequency case and for the constant CW case can be symbolically expressed in the same way if one replaces the algebraic factor $(j\bar{\omega})$ of the latter by the differential factor $(j\bar{\omega} + \frac{d}{dt})$, which then operates on the slowly varying complex amplitudes of the non-constant CW quantities. Substituting Eqs. (2.14) and (2.15) into Eq. (2.7), and utilizing the operator notation of Eq. (2.8), we obtain

$$L\left[j\bar{\omega} + \frac{d}{dt}\right]\{i(t)\} = N\left[j\bar{\omega} + \frac{d}{dt}\right]\{v(t)\} \quad . \tag{2.16}$$

Analogous to the CW case, we can define a linear admittance operator, $Y_c[j\omega(t)]$, for the non-CW case by

$$Y_c[j\omega(t)] = Y_c\left[j\bar{\omega} + \frac{d}{dt}\right] = \frac{N\left[j\bar{\omega} + \frac{d}{dt}\right]}{L\left[j\bar{\omega} + \frac{d}{dt}\right]} \quad . \tag{2.17}$$

The complex amplitude of the current response is then given by

$$I(t) = Y_c[j\omega(t)]\{A(t)\ \exp j\phi(t)\} \quad . \tag{2.18}$$

The admittance operator $Y_c[j\omega(t)]$ operates on the term in the { } brackets in this notation. We can also define the frequency operator

$$[\omega(t)] = [\bar{\omega} - j\frac{d}{dt}] \tag{2.19}$$

where $\omega(t)$ is the instantaneous frequency, and $\bar{\omega}$ is the quasistationary frequency. The instantaneous frequency of $v(t)$ is

$$\omega(t) = \frac{d}{dt}(\bar{\omega}t + \phi(t)) = \bar{\omega} + \frac{d\phi}{dt} \quad . \tag{2.20}$$

In many microwave applications, the amplitude $A(t)$ and phase angle $\phi(t)$ usually change insignificantly within one RF period, i.e.

$$\frac{dA}{dt} << \bar{\omega}A \quad ; \quad \frac{d\phi}{dt} << \bar{\omega} \quad . \tag{2.21}$$

Accordingly, the admittance operator can be expanded into a Taylor series about $\bar{\omega}$:

$$Y_c[j\omega(t)] = Y_c[j\bar{\omega} + \frac{d}{dt}] = \sum_{n=0}^{\infty} \frac{d^n Y(j\bar{\omega})}{d\bar{\omega}^n} \frac{1}{n!} (\frac{d^n}{dt^n}) \quad . \tag{2.22}$$

Substituting for $(\frac{d}{dt})$ from Eq. (2.19) into Eq. (2.22) and using the result for Y_c in Eq. (2.18), we have

$$I(t) = \left(\sum_{n=0}^{\infty} \frac{d^n Y(j\bar{\omega})}{d\bar{\omega}^n} \frac{1}{n!} (j\omega(t) - j\bar{\omega})^n \right) \{A(t) \exp j\phi(t)\} \quad . \tag{2.23}$$

Equation (2.23) is known as the Carson-Fry series [15].

The convergence of this series was discussed by Stumpers [15] for FM modulated signals. Stumpers pointed out that any terminated series approximating Eq. (2.23) must be discussed together with the remainder since the complete series may not be convergent for frequencies far removed from $\bar{\omega}$.

Inspection of Eq. (2.23) reveals that the operator $Y_c[j\omega(t)]$ will be composed of terms $j\omega$, $(j\omega)^2$, $(j\omega)^3$, etc.. Separating the real and imaginary parts of $Y_c[j\omega(t)]$ results in

$$Y_c[j\omega(t)] = G[\omega^2(t)] \pm j\omega(t)S[\omega^2(t)] \qquad (2.24)$$

where $G[\omega^2(t)]$ and $S[\omega^2(t)]$ are conductance and capacitive (plus sign) or inductive (negative sign) susceptance operators, respectively. In Eq. (2.24), the $[\omega^2(t)]$ is an operator which, by using Eq. (2.19), is given by

$$[\omega^2(t)] = [(\bar{\omega} - j\frac{d}{dt})^2] = [\bar{\omega}^2 - 2j\bar{\omega}\frac{d}{dt} - \frac{d^2}{dt^2}]. \qquad (2.25)$$

Expanding $G[\omega^2(t)]$ and $S[\omega^2(t)]$ by a Taylor series about $\bar{\omega}^2$, we obtain using Eq. (2.25),

$$G[\omega^2(t)] = \sum_{n=0}^{\infty} \frac{d^n G(\bar{\omega}^2)}{d(\bar{\omega}^2)^n} \frac{1}{n!} (\omega^2(t) - \bar{\omega}^2)^n \qquad (2.26)$$

and

$$S[\omega^2(t)] = \sum_{n=0}^{\infty} \frac{d^n S(\bar{\omega}^2)}{d(\bar{\omega}^2)^n} \frac{1}{n!} (\omega^2(t) - \bar{\omega}^2)^n \; . \qquad (2.27)$$

Substitution of these results into (2.24) yields the desired passive circuit non-CW admittance operator:

$$Y_c[j\omega(t)] = \sum_{n=0}^{\infty} \left\{ \frac{d^n G(\bar{\omega}^{-2})}{d(\bar{\omega}^{-2})^n} \pm j\omega(t) \frac{d^n S(\bar{\omega}^{-2})}{d(\bar{\omega}^{-2})^n} \right\} \frac{(\omega^2(t) - \bar{\omega}^{-2})^n}{n!} . \tag{2.28}$$

Then the current amplitude is given by substituting Eq. (2.28) into Eq. (2.18)

$$I(t) = \sum_{n=0}^{\infty} \left\{ \frac{d^n G(\bar{\omega}^{-2})}{d(\bar{\omega}^{-2})^n} \pm j\omega(t) \frac{d^n S(\bar{\omega}^{-2})}{d(\bar{\omega}^{-2})^n} \right\} \frac{(\omega^2(t) - \bar{\omega}^{-2})^n}{n!} \times \{A(t) \exp j\phi(t)\} . \tag{2.29}$$

The convergence restriction applying to Eq. (2.23) also holds for Eq. (2.29). Since the frequency deviation (usually a few percent) at microwave frequencies is usually within the series convergence interval, a finite number of terms will approximate the current amplitude with the desired accuracy for practical purposes.

2.4 Active circuit model

The relation between the terminal voltage and the current response of a nonlinear active circuit can be obtained from Eq. (2.7) by allowing the coefficients $a_o,\ldots,a_n$ and $b_o,\ldots,b_p$ to depend on the driving force. Expressing this dependence as a power series, Eq. (2.7) becomes

$$\sum_{m=0}^{M}\left[\sum_{h=0}^{H}\left(A_{mh}v^{h}(t)\right)\frac{d^{m}i(t)}{dt^{m}}\right]=\sum_{p=0}^{P}\left[\sum_{h=0}^{H}\left(B_{ph}v^{h}(t)\right)\frac{d^{p}v(t)}{dt^{p}}\right] \tag{2.30}$$

where A_{mh} and B_{ph} are constants depending both on the nature of the embedding circuitry and the active device. For $H = 0$, the above equation simplifies to the relation describing passive circuits (Eq. (2.7)) and for $M = 0$, $P = 0$ and $A_{mh} = 0$ for $h > 0$, the above relation is reduced to a generalized Van der Pol's equation for active devices. For nonzero M, P and H the current response of the active circuit is generally a nonlinear function of the driving force, as well as its derivatives, and its integrals.

Unlike the case for the passive circuits, the bias components here cannot be disregarded, and the terminal voltage and current will have the form

$$v(t) = V_o(t) + \tilde{v}(t) \tag{2.31}$$

and

$$i(t) = I_o(t) + \tilde{i}(t) \tag{2.32}$$

where $V_o(t)$ and $I_o(t)$ are the slowly varying bias components and $\tilde{v}(t)$ and $\tilde{i}(t)$ are the microwave frequency (RF) components. The time dependence is assumed implied in the following derivations (e.g., $I_o(t) = I_o, \ldots,$ etc.) for the purpose of simplicity of the expressions. Substituting Eq. (2.31) and Eq. (2.32) into Eq. (2.30) yields

$$\sum_{m=0}^{M}\sum_{h=0}^{H} A_{mh}(V_o+\tilde{v})^h \frac{d^m(I_o+\tilde{i})}{dt^m} = \sum_{p=0}^{P}\sum_{h=0}^{H} B_{ph}(V_o+\tilde{v})^h \frac{d^p(V_o+\tilde{v})}{dt^p} \tag{2.33}$$

By expanding the above summation in $(V_o+\tilde{v})^h$, collecting like terms in $\tilde{v}^h$ and then separating the bias and LF, and the RF components, Eq. (2.33) yields

$$\sum_{m=0}^{M}\left(a_{mo}\frac{d^m I_o}{dt^m}\right) + \left[\sum_{m=0}^{M}\left(\sum_{h=1}^{H} a_{mh}\tilde{v}^h \frac{d^m\tilde{i}}{dt^m}\right)\right]_{LF}$$

$$= \sum_{p=0}^{P}\left(b_{po}\frac{d^p V_o}{dt^p}\right) + \left[\sum_{p=0}^{P}\left(\sum_{h=1}^{H} b_{ph}\tilde{v}^h \frac{d^p\tilde{v}}{dt^p}\right)\right]_{LF} \tag{2.34}$$

and

$$\left[\sum_{m=0}^{M}\left(\sum_{h=0}^{H} a_{mh}\tilde{v}^h \frac{d^m\tilde{i}}{dt^m}\right)\right]_{RF} = \sum_{h=1}^{H}\left[\sum_{p=0}^{P}\left(b_{ph}\frac{d^p V_o}{dt^p}\right) - \sum_{m=0}^{M}\left(a_{mh}\frac{d^m I_o}{dt^m}\right)\right]\tilde{v}^h$$

$$+ \left[\sum_{p=0}^{P}\left(\sum_{h=0}^{H} b_{ph}\tilde{v}^h \frac{d^p\tilde{v}}{dt^p}\right)\right]_{RF} \tag{2.35}$$

where

$$a_{mo} = A_{mo} + A_{m1}V_o + A_{m2}V_o^2 + \ldots,$$
$$a_{m1} = A_{m1} + 2A_{m2}V_o + 3A_{m3}V_o^2 + \ldots,$$
$$\vdots$$
$$\text{etc.}$$

and

$$b_{po} = B_{po} + B_{p1}V_o + B_{p2}V_o^2 + \ldots,$$
$$b_{p1} = B_{p1} + 2B_{p2}V_o + 3B_{p3}V_o^2 + \ldots,$$
$$\vdots$$
$$\text{etc..}$$

In Eqs. (2.34) and (2.35), the coefficients a_{mh} and b_{ph} depend not only on the active device and embedding circuitry but also on the bias voltage V_o.

In case of low efficiency two terminal devices, e.g. Impatt-, Transferred electron- or Barrit diodes, the rectification components, expressed by the $[\ ]_{LF}$ terms in Eq. (2.34) are insignificant compared to the bias terms. Then only the bias terms, as expressed by

$$\sum_{m=0}^{M} \left(a_{mo} \frac{d^m I_o}{dt^m}\right) = \sum_{p=0}^{P} \left(b_{po} \frac{d^p V_o}{dt^p}\right) \qquad (2.36)$$

describe sufficiently well the dynamics of the bias conditions. Only for very large signals, can the rectification and time-dependent thermal conditions affect the bias components of active solid state devices. Because of large time constants in the bias circuit and large thermal time constants of the mounted active device, the changes of the bias conditions in microwave amplifiers and oscillators are very slow as compared to the signal modulation. In oscillators specifically designed for bias modulation, the almost step-like changes of the bias voltage are usually so short that most of the oscillation transients take place under nearly constant bias conditions. Moreover, since the signal modulation has hardly any effect on the bias conditions, the dynamics of RF signals in active circuits are usually well described by

$$\left(\sum_{m=0}^{M} \left(\sum_{h=0}^{H} a_{mh} \tilde{v}^h \frac{d^m \tilde{i}}{dt^m}\right)\right)_{RF} = \left(\sum_{p=0}^{P} \left(\sum_{h=0}^{H} b_{ph} \tilde{v}^h \frac{d^p \tilde{v}}{dt^p}\right)\right)_{RF} \qquad (2.37)$$

where the coefficients a_{mh} and b_{ph} are time independent.

The coefficients in the above differential equation depend on the terminal voltage (driving force). In many applications (negative conductance amplifiers and oscillators), single carrier frequency operation (as to the power and energy flow) is the desired operational mode. Hence, a single carrier voltage, either externally excited or self-generated, is the desired voltage waveform at the device terminals. In practice, however, the terminal voltage is composed of a number of harmonic frequency components. Their amplitudes depend upon the amplitude of the corresponding components of the nonlinear device current response and the impedance of the embedding circuitry at that particular harmonic frequency. Because of the very nature of microwave circuits, the impedance of the embedding microwave circuitry does not decrease monotonically to zero with increasing frequency. However, except, for example, in oscillators with tuned harmonics, this impedance is usually insignificant at harmonic frequencies. Very often the device capacitance acts as a low-pass filter, drastically reducing the higher harmonic voltage components at the device terminals. Then the single carrier driving force

$$\tilde{v}(t) = \frac{A(t)}{2}\left(e^{j[\bar{\omega}t+\phi(t)]} + e^{-j[\bar{\omega}t+\phi(t)]}\right) \qquad (2.38a)$$

very well approximates the operating conditions of many

active devices. The quantities A(t) and $\phi(t)$ are slowly varying functions of time, obeying the restrictions given by Eq. (2.21). No other restriction is imposed on these functions. Thus, a large variety of signals are described by Eq. (2.38a), e.g. frequency and/or amplitude modulated signals; single or multiple frequency modulation; transient signals and two or more signals with closely spaced carrier frequencies. In some cases it may not be possible to separate the slowly varying part of the signal into its amplitude and phase components. Then the driving force has to be expressed by

$$\tilde{v}(t) = \frac{V(t)\ e^{j\bar{\omega}t} + V^*(t)\ e^{-j\bar{\omega}t}}{2}$$

$$= \mathrm{Re}[V(t)]\ \cos\bar{\omega}t + \mathrm{Im}[V(t)]\ \sin\bar{\omega}t \qquad (2.38b)$$

where V(t) is the complex time-varying voltage amplitude and the following derivation should be carried out for the above driving force.

In theoretical studies of active microwave circuits, single frequency excitation, while considerably simplifying the mathematical treatment, is usually assumed. Only one exponential term (the one used in the passive circuits) is considered in almost all studies. In noise and stability investigations, this does not introduce any significant error. However to properly describe the nonlinear operation of the active device with strongly

modulated signals, both the exponential terms (which express the real driving function) have to be considered. No harmonic restrictions are imposed on the circuit response, which is expressed in the form

$$\tilde{i}(t) = \sum_{\substack{f\neq 0 \\ -F}}^{F} I_f(t) e^{jf\bar{\omega}t} \quad . \tag{2.39}$$

Here, $\sum_{f\neq 0}$ denotes the summation of all terms with the exception of the bias term, i.e. $f\neq 0$, and the complex amplitudes which satisfy

$$I_f(t) = I^*_{-f}(t) \tag{2.40}$$

carry information on both the amplitude and the phase of a particular current component.

The summation in $\tilde{v}^h$ from Eq. (2.37) is expanded using Eq. (2.38a) and if like terms are collected, the summation in $\tilde{v}^h$ can be written as:

$$\sum_{h=0}^{H} [a_{mh}\tilde{v}^h(t)] = \sum_{g=-\frac{H}{2}}^{H/2} \sum_{h=|g|}^{H/2} (a_{m,2h,2g} A^{2h}(t) e^{j2g[\bar{\omega}t+\phi(t)]})$$

$$+ \sum_{g=-\frac{H-1}{2}}^{\frac{H-1}{2}} \sum_{h=|g|}^{\frac{H-1}{2}} (a_{m,2h+1,2g+1} A^{2h+1}(t) e^{j(2g+1)[\bar{\omega}t+\phi(t)]}) \tag{2.41}$$

Similarly, differentiating Eq. (2.39) m times and Eq. (2.38a) p times yields

$$\frac{d^m \tilde{i}(t)}{dt^m} = \sum_{\substack{f\neq 0 \\ -F}}^{F} e^{jf\bar{\omega}t}\left(jf\bar{\omega} + \frac{d}{dt}\right)^m \{I_f(t)\} \qquad (2.42)$$

and

$$\frac{d^p \tilde{v}(t)}{dt^p} = e^{j\bar{\omega}t}\left(j\bar{\omega} + \frac{d}{dt}\right)^p \left\{\frac{A(t)}{2}\, e^{j\phi(t)}\right\} + e^{-j\bar{\omega}t}\left(-j\bar{\omega} + \frac{d}{dt}\right)^p \left\{\frac{A(t)}{2} e^{-j\phi(t)}\right\} \qquad (2.43a)$$

$$= \sum_{s=-1,1} e^{js\bar{\omega}t}\left(js\bar{\omega} + \frac{d}{dt}\right)^p \left\{\frac{A(t)}{2}\, e^{js\phi(t)}\right\} . \qquad (2.43b)$$

In Eq. (2.41), the summations are carried out to the highest integral number $H/2$ or $\frac{H-1}{2}$ and the coefficients $a_{m,h,g}$ with different g's are related through simple algebraic relations to the coefficients a_{mh} of Eq. (2.37).

Substituting Eqs. (2.41)-(2.43) into Eq. (2.37) yields

$$\left(\sum_{f\neq 0} \sum_{m=0}^{M} \left[\sum_{g=-H/2}^{H/2} \sum_{h=|g|}^{H/2} \left(a_{m,2h,2g} A^{2h}(t) e^{j[(2g+f)\bar{\omega}t + 2g\phi(t)]}\right) \right.\right.$$
$$\left. + \sum_{g=-\frac{H-1}{2}}^{\frac{H-1}{2}} \sum_{h=|g|}^{\frac{H-1}{2}} \left(a_{m,2h+1,2g+1} A^{2h+1}(t) e^{j[(2g+1+f)\bar{\omega}t + (2g+1)\phi(t)]}\right) \right]$$
$$\left. \times \left(jf\bar{\omega} + \frac{d}{dt}\right)^m \{I_f(t)\} \right)_{RF}$$
$$= \left(\sum_{s=-1,1} \sum_{p=0}^{P} \left[\sum_{g=-H/2}^{H/2} \sum_{h=|g|}^{H/2} b_{p,2h,2g} A^{2h}(t) e^{j[(2g+s)\bar{\omega}t + 2g\phi(t)]} \right.\right.$$
$$\left. + \sum_{g=-\frac{H-1}{2}}^{\frac{H-1}{2}} \sum_{h=|g|}^{\frac{H-1}{2}} b_{p,2h+1,2g+1} A^{2h+1}(t) e^{j[(2g+1+s)\bar{\omega}t + (2g+1)\phi(t)]} \right]$$
$$\left. \times \left(js\bar{\omega} + \frac{d}{dt}\right)^p \left\{\frac{A(t)}{2}\, e^{js\phi(t)}\right\} \right)_{RF} . \qquad (2.44)$$

The above set of nonlinear differential equations for complex current amplitudes describes the active device response to a single-carrier driving force with non-constant amplitude. Even if all the parameters a and b were known, the complexity of the above description would make it unsuitable for any numerical studies. The description of the active device response becomes simpler if all passive circuit elements between the device terminals and the active device itself, namely all device package parasitics, very often involving energy storage elements, are included into the external passive circuitry. The transformation of the nonlinear device quantities into the terminal quantities is then eliminated. Furthermore, since the external circuitry is assumed to present an infinite admittance at the device terminals at all frequencies other than the fundamental frequency, the current of this simplified active circuit does not contribute to higher harmonic generation. Thus

$$a_{m,h,g} = 0 \qquad \text{for } |g| > 0 \,, \quad |h| > 0 \qquad (2.45)$$

and the equation set (2.44) reduces to a set of uncoupled differential equations with constant coefficients. Thus Eq. (2.44) reduces to

$$\left[\sum_{f\neq 0}\sum_{m=0}^{M} a_{m,o,o}\, e^{jf\bar{\omega}t}\left(jf\bar{\omega}+\frac{d}{dt}\right)^{m} f(t)\right]_{RF}$$

$$= \left[\sum_{s=-1,1}\left(\sum_{p=0}^{P}\left(\sum_{g=-H/2}^{H/2}\sum_{h=|g|}^{H/2} b_{p,2h,2g} A^{2h}(t) e^{j[(2g+s)\bar{\omega}t+2g\phi(t)]}\right.\right.\right.$$

$$+ \sum_{g=-\frac{H-1}{2}}^{\frac{H-1}{2}}\sum_{h=|g|}^{\frac{H-1}{2}} b_{p,2h+1,2g+1} A^{2h}(t) e^{j[(2g+1+s)\bar{\omega}t+(2g+1)\phi(t)]}\Big)$$

$$\left.\left.\left. \times\left(js\bar{\omega}+\frac{d}{dt}\right)^{p}\right)\left\{\frac{A(t)}{2}\, e^{js\phi(t)}\right\}\right]_{RF} \qquad (2.46)$$

If in the above equation, one considers the current amplitudes of odd and even harmonics separately, then for the odd order one gets:

$$I_{2f+1} = \left(\sum_{m=0}^{M} a_m\left(j(2f+1)\bar{\omega}+\frac{d}{dt}\right)^{m}\right)^{-1}\left(\sum_{p=0}^{P}\left(\sum_{h=f}^{H/2} b_{p,2h,2f} A^{2h}(t) e^{j2f\phi(t)}\right.\right.$$

$$\left.\left.\times\left(j\bar{\omega}+\frac{d}{dt}\right)^{p}\left\{\frac{A(t)}{2}\, e^{j\phi(t)}\right\} + b_{p,2h+2,2f+2} A^{2h+2}(t) e^{j(2f+2)\phi(t)}\right.\right.$$

$$\left.\left.\times\left(-j\bar{\omega}+\frac{d}{dt}\right)^{p}\left\{\frac{A(t)}{2}\, e^{-j\phi(t)}\right\}\right) \qquad (2.47a)$$

and the corresponding expression for the even order is of the form:

$$I_{2f} = \left(\sum_{m=0}^{M} a_m (j2f\bar{\omega} + \frac{d}{dt})^m \right)^{-1} \left\{ \sum_{p=0}^{P} \left(\sum_{h=f}^{\frac{H-1}{2}} b_{p,2h-1,2f-1} \right. \right.$$

$$\times A^{2h-1}(t) e^{j(2f-1)\phi(t)}$$

$$\times (j\bar{\omega} + \frac{d}{dt})^p \{ \frac{A(t)}{2} e^{j\phi(t)} \} + b_{p,2h+1,2g+1} A^{2h+1}(t) e^{j(2g+1)\phi(t)} \Big)$$

$$\left. \times (-j\bar{\omega} + \frac{d}{dt})^p \{ \frac{A(t)}{2} e^{-j\phi(t)} \} \right\} \quad (2.47b)$$

where $a_{m,o,o} = a_m$, $b_{p,h,g} = 0$ for $h > H$ and $f \geq 0$ in Eq. (2.47a) and $f > 0$ in Eq. (2.47b).

Equations (2.47) can be regarded as generalized admittance relations describing the current response of an active device to a single carrier driving force with nonconstant amplitude. The amplitudes of the current response are nonlinear functions of the applied voltage amplitude, its derivatives and its integrals. Knowing both sets of the coefficients, i.e. a and b, the current response of the active device could be evaluated for any amplitude and frequency of the driving force. Disregarding the fact that it may be very difficult to find the appropriate sets of coefficients, the above description of the active device response is still extremely complex. It would lead to integro-differential equations, and is hardly useful for numerical studies. The active device description can be

significantly simplified by the following choice of the a coefficients

$$a_o = 1 \; ; \quad a_m = 0 \quad \text{for} \quad m > 0 \; . \tag{2.48}$$

Then the square-bracketed [ ] differential operator in Eqs.(2.47) reduces to unity and the components of the current response are given by

$$I_{2f+1} = \sum_{p=0}^{P} \sum_{h=f}^{H/2} [b_{p,2h,2f} A^{2h}(t) e^{j2f\phi(t)} (j\bar{\omega}+\frac{d}{dt})^p \{\frac{A(t)}{2} e^{j\phi(t)}\}$$

$$+ b_{p,2h+2,2f+2} A^{2h+2}(t) e^{j(2f+2)\phi(t)} (-j\bar{\omega}+\frac{d}{dt})^p \{\frac{A(t)}{2} e^{-j\phi(t)}\}] \tag{2.49a}$$

$$I_{2f} = \sum_{p=0}^{P} \sum_{h=f}^{\frac{H-1}{2}} [b_{p,2h-1,2f-1} A^{2h-1}(t) e^{j(2f-1)\phi(t)} (j\bar{\omega}+\frac{d}{dt})^p \{\frac{A(t)}{2} e^{j\phi(t)}\}$$

$$+ b_{p,2h+1,2f+1} A^{2h+1}(t) e^{j(2f+1)\phi(t)} (-j\bar{\omega}+\frac{d}{dt})^p \{\frac{A(t)}{2} e^{-j\phi(t)}\}] \tag{2.49b}$$

In this simpler description, the current response of an active device is a nonlinear function of the voltage amplitude and its derivatives. Thus, a given set of b parameters will accurately describe the device response in a more or less limited frequency range at large amplitudes of the applied voltage. Using numerical methods based on bicubic spline approximation, both the

b parameter evaluation and the current response description for any amplitude and frequency of the driving force can be accomplished in a piece-wise manner.

2.5 Model characterization

The previously described techniques are designed for studies on active microwave circuits with non-constant CW signals. For a constant CW driving force characterized by

$$A(t) = A_o \; ; \qquad \phi(t) = \phi_o = 0 \tag{2.50}$$

the techniques simplify to a conventional steady state approach involving large signal immittance relations at the basic frequency component. Thus by substituting the values of $A(t)$ and $\phi(t)$ given by Eq. (2.50) into Eq. (2.47a) and rearranging terms in powers of $\bar{\omega}^{-2}$ and A_o^2, the admittance of the general model characterizing an active device is given by

$$Y'_D = \frac{I_1}{A_o} = \frac{\sum_{p=0}^{\frac{P-1}{2}} \sum_{h=0}^{H/2} (-1)^p (d'_{2p,2h} + j\bar{\omega} d'_{2p+1,2h}) A_o^{2h} \bar{\omega}^{-2p}}{\sum_{m=0}^{M} a_m (j\bar{\omega})^m} \tag{2.51}$$

where I_1 is the complex current amplitude at the

fundamental frequency and, according to Eq. (2.49a), the admittance of the simpler active circuit model is given by

$$Y_D = \frac{I_1}{A_o} = \sum_{p=0}^{\frac{P-1}{2}} \sum_{h=0}^{H/2} (-1)^p (d_{2p,2h} + j\bar{\omega} d_{2p+1,2h}) A_o^{2h} \bar{\omega}^{2p} \qquad (2.52)$$

where the summation is carried out to the highest integral number $\frac{P-1}{2}$ and H/2. The factor 1/2 in Eqs. (2.51) and (2.52) is absorbed in the $b_{p,h,g}$ coefficients. In this case, the admittance of the passive circuit is given by

$$Y_c = \sum_{p=0}^{\frac{P-1}{2}} (-1)^p (d_{2p,o} + j\bar{\omega} d_{2p+1,o}) \bar{\omega}^{2p} \quad . \qquad (2.53)$$

In Eqs. (2.51)-(2.53) the d coefficients are related to the b coefficients by

$$d_{2p,2h} = b_{2p,2h,o} + b_{2p,2h,2}$$

and (2.54)

$$d_{2p+1,2h} = b_{2p+1,2h,o} - b_{2p+1,2h,2}$$

where $b_{p,h,g} = 0$ if $h = 0$ and $g > 0$.

Since they are described by linear differential operators, passive circuits are uniquely characterized by a single set of coefficients which can be valuated from circuit admittance measurements. Active circuits are described

by nonlinear differential operators, which are not commutative, and thus two sets of coefficients uniquely describe active circuits. In analogy with passive circuits, the large signal admittance of active circuits provides one set of matching conditions while the other set of conditions should be provided by some other nonlinear characteristics of the circuit. Even if two proper sets of conditions are known, the evaluation of coefficients may be extremely difficult. Based on theoretical studies, one can sometimes guess one set of coefficients, e.g. in the case of Impatt diodes $a_o = 1$, $0 < a_1 < 1$ and $a_2 = a_3 = \ldots = 0$. A single set of unknown coefficients then remains. In amplifier and oscillator applications, the large signal considerations are of primary importance while the nonlinearities associated with higher powers of derivatives of the terminal voltage are of minor importance. In these applications, the simpler model of the active device, for which the single set of coefficients can be determined using the device large signal immittance, is more than adequate for dynamic studies.

If the passive or actice circuit admittances are analytically specified, the differentiation of the admittance expression can yield the model coefficients. Most often, however, the admittances are specified by a series of measured or calculated data points at different signal frequencies and amplitudes. Even though numerical differentiation can be used, the natural cubic and bicubic

spline curve fitting (into the characteristics of a given passive and active circuit) is most efficient.

The natural cubic spline, the first two derivatives of which are continuous, was shown to best approximate the curve joining data points with minimum curvature. Given a set of M data points, e.g., $\omega_1^2,\ldots,\omega_M^2$, a computer routine returns the spline coefficients in each of the (M-1) intervals. The spline interpolate in the L-th interval, $(\bar{\omega}_L^{-2} - \bar{\omega}_{L+1}^{-2})$, can then be constructed by

$$G_L(\omega^2) = \sum_{m=1}^{4} G_m(\omega_L^2)\,(\omega^2 - \omega_L^2)^{m-1} \quad . \qquad (2.55)$$

More than three data points are needed for the evaluation of the spline coefficients. The approximation accuracy increases with the number of given data points. The coefficients in a given interval, which are related to the first three derivatives of the approximation function at the interval boundaries, depend on all data points. Thus the effect of nonsystematic errors of individual data points on the numerical derivatives is inherently reduced resulting in "smooth derivatives" [16] (this property is partially attributable to the best approximation characteristic, and partially to the minimum curvature property of the cubic spline). Unlike a Taylor series approximation, the question of convergence is irrelevant here. Since all spline coefficients are equally important, none of them can be neglected without

seriously reducing the approximation accuracy.

The natural bicubic spline is fitted through M × N functional values, e.g. $G_{1,1},\ldots,G_{M,N}$, corresponding to two sets of grid points, e.g. $A_1,\ldots,A_m$, $\omega_1,\ldots,\omega_N$. The computer routine returns the coefficients of the bicubic spline interpolate on the KL subrectangle $[A_K,A_{K+1}] \times [\omega_L, \omega_{L+1}]$ in a 4 by 4 matrix. The spline interpolate is then given by

$$G_{KL}(A^2,\omega^2) = \sum_{i=1}^{4}\sum_{j=1}^{4} g_{ij}(A^2 - A_K^2)^{i-1}(\omega^2-\omega_L^2)^{j-1} \quad . \quad (2.56)$$

To evaluate the d coefficients, the device admittance data Y_{KL} should be first expressed as

$$Y_{KL} = G(A_K^2,\omega_L^2) + j\omega_L \frac{B(A_K^2,\omega_L^2)}{\omega_L^2}$$

$$= G(A_K^2,\omega_L^2) + j\omega_L S(A_K^2,\omega_L^2) \quad . \quad (2.57)$$

Finding the spline interpolates for the G and S functions

$$G_{KL}(A^2,\omega^2) = \sum_{i=0}^{3}\sum_{j=0}^{3} GM_{ij}(A_K^2,\omega_L^2)\, A^{2i}\, \omega^{2j}$$

$$S_{KL}(A^2,\omega^2) = \sum_{i=0}^{3}\sum_{j=0}^{3} SM_{ij}(A_K^2,\omega_L^2)\, A^{2i}\, \omega^{2j} \quad (2.58)$$

and equating the coefficients from Eq. (2.58) and Eq. (2.52) at various powers of A and ω, the d coefficients can be numerically evaluated. Since the $b_{p,h,o}$ and

$b_{p,h,2}$ coefficients are linked through simple algebraic relations, they can be evaluated from the known d coefficients using the formulas

$$d_{2p,o} = b_{2p,o,o} \quad ; \quad b_{2p,o,2} = 0$$

$$d_{2p,2h} = \frac{2h+1}{h} b_{p,2h,2} = \frac{2h+1}{h+1} b_{p,2h,o} \tag{2.59}$$

and

$$d_{2p+1,2h} = \frac{1}{h} b_{2p+1,2h,2} = \frac{1}{h+1} b_{2p+1,2h,o} \cdot$$

The fundamental frequency component of the current response of the given device to the nonconstant CW driving force which is given by Eq. (2.49a) can then be analytically evaluated from

$$i_{KL}(t) = \mathrm{Re}\left\{ e^{j\omega t} \left(\sum_{p=0}^{7} \left(\sum_{h=0}^{3} {}_{KL}b_{p,2h,o} A^{2h}(t) \left(j\omega_L + \frac{d}{dt}\right)^p \left\{ \frac{A(t)}{2} e^{j\phi(t)} \right\} \right.\right.\right.$$

$$\left.\left.\left. + {}_{KL}b_{p,2h+2,2} A^{2h+2}(t) e^{j2\phi(t)} \left(-j\omega_L + \frac{d}{dt}\right)^p \left\{ \frac{A(t)}{2} e^{-j\phi(t)} \right\} \right) \right) \right\} \tag{2.60}$$

where the b coefficients are related through the numerical spline coefficients to all admittance data points of the given active device. In analogy with $i_{KL}(t)$,

under nonconstant CW driving force, by using Eqs. (2.13), (2.17) and (2.18), the passive circuit current may be analytically evaluated from

$$
\begin{aligned}
{}_{L}i_{c}(t) &= \mathrm{Re}\left[e^{j\omega t}\,{}_{L}Y_{c}\left[j\omega_{L} + \frac{d}{dt}\right]\{A(t)e^{j\phi(t)}\}\right] \\
&= \mathrm{Re}\left[e^{j\omega t}\sum_{p=0}^{7} {}_{L}b^{c}_{p,o,o}\left(j\omega_{L} + \frac{d}{dt}\right)^{p}\{A(t)e^{j\phi(t)}\}\right]
\end{aligned}
\tag{2.61}
$$

where the b^{c} coefficients are related through the numerical spline coefficients of the circuit for the interval L.

The above technique will be applied for the analysis of free-running oscillators as these have wide applications in communication systems. The resulting method can be extended to analyze injection locked oscillators and amplifiers.

2.6 Theoretical description of a free-running negative conductance oscillator

Operation of a free-running oscillator is described by Eq. (2.5). This nonlinear differential equation together with proper initial conditions uniquely describes the time dependent terminal voltage of an active device.

If the transients in the bias circuit can be disregarded and the embedding circuitry is designed to ensure single frequency oscillation, then Eq. (2.5) will describe the transients of the RF oscillations. In this case, only the fundamental frequency components of both the active device and the passive circuitry may be considered. Substituting for the device current as given by Eq. (2.60), and for the proper circuit current (Eq. (2.61)) into Eq. (2.5), the following differential equation for the unknown, slowly varying amplitude A(t) and phase $\phi(t)$ of the RF oscillations can be obtained

$$\sum_{p=0}^{7}\Bigg(\sum_{h=0}^{3} {}_{KL}b^{d}_{p,2h,o}A^{2h}(t)\left(j\omega_L + \frac{d}{dt}\right)^{p}\{A(t)e^{j\phi(t)}\}$$

$$+ {}_{KL}b^{d}_{p,2h,2}A^{2h}(t)e^{j2\phi(t)}\left(-j\omega_L + \frac{d}{dt}\right)^{p}\{A(t)e^{-j\phi(t)}\}$$

$$+ {}_{L}b^{c}_{p,o,o}\left(j\omega_L + \frac{d}{dt}\right)^{p}\{A(t)e^{j\phi(t)}\}\Bigg) = 0 \ . \qquad (2.62)$$

In Eq. (2.62) the b coefficients are related to a few discrete admittance values of both the embedding circuit and the active device. Combining the terms on the left hand side of Eq. (2.62), the differential

equation characterizing the slowly varying components of the terminal voltage can be obtained

$$\sum_{p=0}^{7}\Big(\sum_{h=0}^{3} KL^{b}_{p,2h,o}A^{2h}(t)\left(j\omega_L+\frac{d}{dt}\right)^{p}\{A(t)e^{j\phi(t)}\} + KL^{b}_{p,2h,2}A^{2h}(t)e^{j2\phi(t)}\left(-j\omega_L+\frac{d}{dt}\right)^{p}\{A(t)e^{-j\phi(t)}\}\Big) = 0 \tag{2.63}$$

where

$$KL^{b}_{p,o,o} = L^{b^c}_{p,o,o} + KL^{b^d}_{p,o,o}\ ;\ KL^{b}_{p,o,2} = 0 \tag{2.64a}$$

and

$$KL^{b}_{p,2h,o} = KL^{b^d}_{p,2h,o}\quad ;\quad KL^{b}_{p,2h,2} = KL^{b^d}_{p,2h,2} \tag{2.64b}$$

If a proper KL-subrectangle is used, i.e. the instantaneous voltage amplitude and $d\phi/dt$ are within the limits $A_k \le A(t) \le A_{k+1}$ and $0 \le d\phi/dt \le \omega_{L+1} - \omega_L$, then the differential equation (2.63) describes accurately the dynamic conditions of a given active microwave circuit. Performing the differentiation, separating the real and imaginary parts and neglecting the higher order derivatives of the products of the amplitude and phase, the following set of differential equations can be derived in the slowly varying quantities A(t) and $\phi(t)$:

$$A^{o}\sum_{n=0}^{6}\frac{x^{n}}{n!}D^{n+1}\bar{B}+A\sum_{n=0}^{6}\frac{x^{n}}{n!}D^{n}G+\frac{x^{o}A}{2}\sum_{n=1}^{6}\frac{x^{n-1}}{(n-1)!}D^{n+1}\bar{B}=0 \tag{2.65a}$$

and

$$A^{o}\sum_{n=1}^{6}\frac{x^{n+1}}{n!}D^{n}\bar{G}+A\sum_{n=1}^{6}\frac{x^{n}}{n!}D^{n}B+\frac{x^{o}A}{2}\sum_{n=1}^{6}\frac{x^{n-1}}{(n-1)!}D^{n+1}\bar{G}=0 \tag{2.65b}$$

where in Eq. (2.65) D is an operator representing partial differentiation with respect to ω, $x = d\phi/dt$, $A^{o} = dA/dt$, G and B are the total circuit conductance and susceptance of the oscillator, $\bar{G}$ and $\bar{B}$ are the total circuit complementary conductance and susceptance of the oscillator. The two nonlinear equations of (2.65) may be written in a form suitable for steady and transient (numerical) solutions in oscillators as

$$A^{o} = (R_3R_5 - R_6R_2)/(R_6R_1 - R_3R_4) \tag{2.66a}$$

and

$$x^{o} = (R_2R_4 - R_1R_5)/(R_6R_1 - R_3R_4) \tag{2.66b}$$

where

$$R_1 = \sum_{n=0}^{6}\frac{x^{n}}{n!}D^{n+1}\bar{B}$$

$$R_2 = \sum_{n=0}^{6}\frac{x^{n}}{n!}D^{n}G$$

$$R_3 = \sum_{n=1}^{6}\frac{x^{n-1}}{(n-1)!}D^{n+1}\bar{B}$$

$$R_4 = \sum_{n=1}^{6}\frac{x^{n+1}}{n!}D^{n}\bar{G}$$

$$R_5 = \sum_{n=1}^{6} \frac{x^n}{n!} D^n B$$

$$R_6 = \sum_{n=1}^{6} \frac{x^{n-1}}{(n-1)!} D^{n+1} \bar{G} \quad .$$

In Eqs. (2.65) and (2.66), the Y and $\bar{Y}$ are related to the passive and active circuit parameters through the following equations:

$$Y = G + jB$$

$$= \sum_{m=0}^{3} \{[{}_L d_{2m,o} + (-1)^m {}_{KL}c\mathcal{D}_{2m}]\omega^{2m}$$

$$+ j[{}_L d_{2m+1,o} + (-1)^m {}_{KL}c\mathcal{D}_{2m+1,2}]\omega^{2m+1}\} \qquad (2.67)$$

and

$$\bar{Y} = \bar{G} + j\bar{B}$$

$$= \sum_{m=0}^{3} \{[(-1)^{m+1} {}_{KL}c\mathcal{D}_{2m,2} - {}_L d_{2m,o}]\omega^{2m}$$

$$+ j[{}_L d_{2m+1,o} + (-1)^m {}_{KL}c\mathcal{D}_{2m+1}]\omega^{2m+1}\} \quad . \qquad (2.68)$$

In these equations, the ${}_L d$ parameters characterizing the passive circuit in the L-interval are related to the b^c coefficients of Eq. (2.64a) through the equations given by Eq. (2.54) for h = 0. They are directly computed from coefficients evaluated by fitting the discrete admittance values of the passive circuit to the one-

dimensional cubic spline. The $c\mathcal{D}$'s are nonlinear functions of the voltage amplitude A up to the sixth order and can be written as

$$ {}_{KL}c\mathcal{D}_{2m} = \sum_{n=0}^{3} (-1)^m {}_{KL}d_{2m,2n} A^{2n} \quad , \; m = 0,1,2,3 $$

$$ {}_{KL}c\mathcal{D}_{2m+1,2} = \sum_{n=0}^{3} (-1)^m {}_{KL}d_{2m+1,2n} A^{2n} \quad , \; m = 0,1,2,3 $$

$$ {}_{KL}c\mathcal{D}_{2m,2} = \sum_{n=0}^{3} \frac{(-1)^m}{(2n+1)} {}_{KL}d_{2m,2n} A^{2n} \quad , \; m = 1,2,3 $$

$$ {}_{KL}c\mathcal{D}_{2m+1} = \sum_{n=0}^{3} (-1)^m (2n+1) {}_{KL}d_{2m+1,2n} A^{2n}, \; m = 0,1,2,3 $$

The active device parameters ($c\mathcal{D}$'s) can be determined for any subrectangle KL depending on the value of the amplitude A and that of the instantaneous frequency $\bar{\omega}+ x$. The d's, here, are the active device parameters and are given in terms of the b coefficients through Eq. (2.54). They are calculated from the coefficients resulting from the bicubic spline which fits the device large signal admittance data.

The transients of a given oscillator, with known d coefficients (passive and active circuit parameters), can be studied by solving the nonlinear equations (2.66), simultaneously in A and x. This may only be achieved for a given set of initial conditions (for A and x). The physically acceptable initial conditions, in free-

running oscillators, are those which correspond (i) to the start of oscillations or (ii) those corresponding to the almost steady state. The solutions give the amount of time taken by the oscillations to build up to the steady state amplitude and frequency, which is an important factor in the design of bias modulated solid state oscillators. Because of the complexity of calculations, Eqs. (2.66) can only be solved numerically on a digital computer.

CHAPTER III

BASIC THEORIES OF NEGATIVE CONDUCTANCE SOLID STATE OSCILLATORS

3.1 Introduction

In practice, negative conductance solid state oscillators comprise an active device such as Impatt, Transferred electron or Tunnel diodes, with a suitable passive circuit. In the schematic diagram, Fig. 3.1, the oscillator is represented by a waveguide cavity containing a negative conductance device. An adjustable short circuit plunger and a slide-screw tuner or other suitable device optimizes the output power. In practice, the cavity may take various forms, cylindrical or coaxial, for example. In the case where the output port is of the coaxial form, the slide screw tuner is most likely replaced by slug tuners. Coupling to the load may be accomplished through either a window or a probe.

Because the dimensions of the semiconductor chip are generally very small compared to the free space wave length, at the fundamental frequency of oscillation, the conventional voltage and current values can be determined at the terminals of the active device. Therefore, even though equivalent circuit components for various devices may have differing voltage and frequency

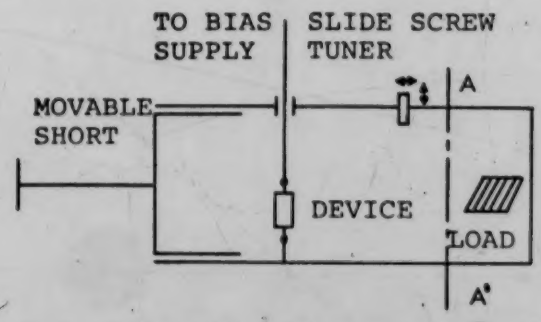

Fig. 3.1 Schematic diagram of a microwave oscillator.

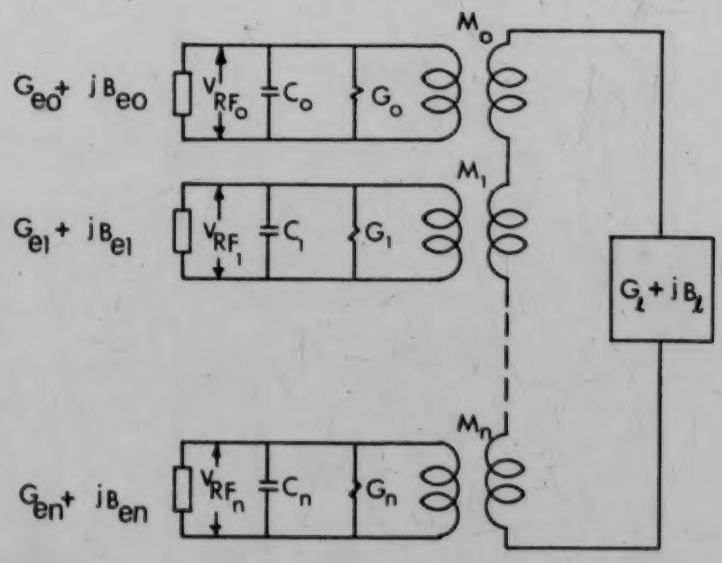

Fig. 3.2 Equivalent circuit representation of a microwave oscillator with separate resonant circuits representing each mode.

dependence, the general theory for negative conductance oscillators will be the same for any active device.

If the harmonic content in the waveguide at the output port is small, at each harmonic frequency the device sees an impedance un-affected by the load condition. Under these circumstances, the active device admittance at the fundamental frequency exhibits a certain nonlinear behaviour necessary for it to achieve a stable operating condition.

In general, the current and voltage wave forms generated by an active device are nonsinusoidal. Depending on the embedding circuitry, it can be assumed that either the voltage or the current contains the basic frequency component only (voltage or current excitation of the active element) while the device response, i.e. current or voltage, contains a number of harmonics. By Fourier analysis of the oscillator wave forms or by measuring the large signal admittance, it is possible to obtain the large signal admittance of the active devices as defined by:

$$I = Y_e A = (-G_e + jB_e) A \qquad (3.1)$$

where A and I are the fundamental frequency components of the device voltage and current; Y_e is the device's electronic admittance. The electronic parameters of the device, i.e., G_e and B_e, are nonlinear functions of the

oscillation frequency, ω_o, and the voltage amplitude, A, and also depend on the device bias and thermal conditions. On the other hand, the passive circuit admittance is a nonlinear function of frequency only.

Circuit models must take into account the inherent nonlinearity of the active device. To aid the understanding of the operation of microwave oscillators, a very simple oscillator model is first introduced and the behaviour of these oscillators under transient and steady state conditions is examined. Later in this chapter Kurokawa's geometric model of [17] microwave oscillators based on device line and impedance locus will be briefly presented to discuss the behaviour of negative conductance solid state oscillators.

3.2 Equivalent circuit of a negative conductance microwave oscillator

Unlike their counterparts at lower frequencies, microwave resonant cavity parameters are defined based upon the choice of relevant field quantities. The stored magnetic and electric energies in the electromagnetic field inside the cavity determine the equivalent inductance and capacitance, whereas ohmic losses in the resonator walls and dielectric losses determine the equivalent conductance. A cavity can resonate at an infinite number of frequencies.

A microwave cavity without excessive losses which is coupled by some arbitrary transducer to a waveguide is accurately represented by the equivalent circuit shown in Fig. 3.2. The parallel resonance circuits, of resonant frequencies ω_o, $\omega_{o1},\ldots,\omega_{on}$, represent the resonant modes of the microwave cavity. The load admittance $(G_\ell + jB_\ell)$ is coupled to each of the resonator modes by the mutual inductance M_n of a coupling element having a self inductance L_1. An active element within the cavity can excite these modes and is characterized by admittances $(G_{eo} + jB_{eo}),\ldots,(G_{en} + jB_{en})$. The electronic admittances $(G_{em} + jB_{em})$ are defined as the ratio of RF current to RF voltage at the appropriate terminal pair; that is,

$$Y_{em} = G_{em} + jB_{em} = \frac{(i_{RF})_m}{(v_{RF})_m} \qquad (3.2)$$

where $m = 0,1,2,\ldots,n$.

Resonators for oscillators are normally designed to possess fairly well-separated modes, permitting oscillation only in the vicinity of the desired frequency. According to the Foster Reactance [18,19] Theorem the behaviour of a resonator within a narrow range near the selected frequency may be represented by retaining the parts of the circuit representing the corresponding mode, Fig. 3.3. In this diagram:

G_r = shunt conductance of the cavity

L_r, C_r = equivalent inductance and capacitance

L_1 = equivalent inductance of the coupling iris (window)

M = mutual inductance between L_1 and L_r.

The diode package and bias circuit losses and reactances are lumped with those of the cavity since the diode is mounted inside the cavity.

3.3 Oscillators: under steady state and transient state conditions

3.3.1 Analysis of a highly simplified model of a two terminal oscillator circuit

In this section a simplified analysis for microwave oscillators is introduced. Although such a simplified model cannot represent the complete behaviour of microwave oscillators, the analysis helps to explain some of their features.

The equivalent circuit of a two terminal microwave oscillator developed in the last section (Fig. 3.3) can be transformed into the simplified form shown in Fig.3.4a. The electronic susceptance, B_e, may be considered to result from an equivalent inductance L_e or capacitance C_e. Therefore, Fig. 3.4a may be reduced to the simplified form in Fig. 3.4b, in which

$$G = G_e + G_r + G_\ell \quad , \tag{3.3a}$$

$$C = C_e + C_r + C_\ell \tag{3.3b}$$

and

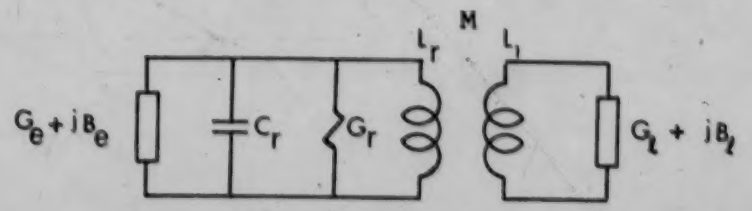

Fig. 3.3 Equivalent circuit of a microwave oscillator designed to operate in a single frequency mode.

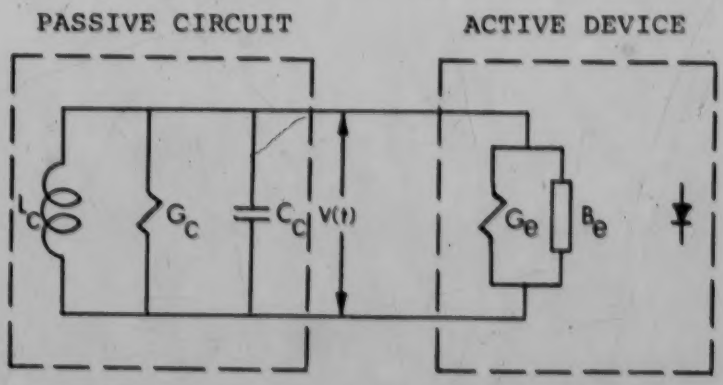

Fig. 3.4a Equivalent circuit of a solid state microwave oscillator tuned to one mode of oscillation.

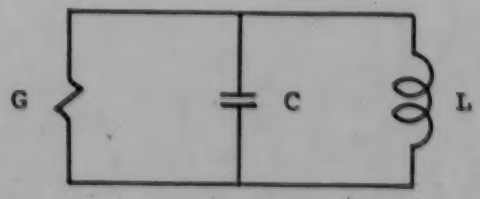

Fig. 3.4b Highly simplified equivalent circuit of a microwave oscillator.

$$L = 1/(1/L_e + 1/L_r + 1/L_\ell) \quad . \qquad (3.3c)$$

Since B_e can be either inductive or capacitive, L_e and C_e are not present simultaneously in the equivalent circuit.

The electronic admittance, Y_e, is not constant with amplitude and frequency; hence the relation between the voltage across the active device and the current through it is not linear. Since one consequence of non-linearity of circuit elements is the generation of harmonics in current and voltage, it follows that variations of Y_e with amplitude and frequency are always associated with the presence of harmonics. A strictly rigorous analysis would have to take harmonics into account or else show that the presence of harmonics has negligible effect upon the steady state frequency and amplitude. Because the following treatment is intended to be of value principally in explaining qualitatively some of the observed characteristics of oscillator behaviour, harmonics of the driving force (voltage or current) will be neglected. It may also be noted that the dependence of B_e upon the amplitude causes some change in the frequency as the amplitude of oscillation builds up.

Under the rather severe assumption that all parameters in the circuit of Fig. 3.4b are constant and linear, summation of the currents at one of the nodal

points yields the following differential equation for the voltage v across the elements:

$$\frac{d^2v}{dt^2} + \frac{G}{C}\frac{dv}{dt} + \frac{v}{CL} = 0 \ . \qquad (3.4)$$

The solution of Eq. (3.4) is

$$v = V_o e^{\alpha t} \sin(\omega t + \phi) \qquad (3.5)$$

in which

$$\alpha = -\frac{G}{2C} = -(G_\ell + G_r + G_e)/2C$$

$$= -(G_e + G_c)/2C \qquad (3.6)$$

$$\omega = \sqrt{1/LC - G^2/4C^2} = \sqrt{1/LC - \alpha^2} \qquad (3.7)$$

and the constants V_o and ϕ are the amplitude and phase angle of the voltage at t = 0, respectively.

Eq. (3.7) shows that the circuit can be oscillatory only if $|G| < 2\sqrt{\frac{C}{L}}$. Examination of Eqs. (3.5) and (3.6) discloses that since the resonator and load conductances G_r and G_ℓ are positive, sustained sinusoidal oscillation is possible only if the electronic conductance G_e is negative and equal to or greater in magnitude than G_c. If G_e is negative and equal in magnitude to G_c, α is zero and the oscillation is of constant amplitude. Theoretically, if G_e is negative and greater in magnitude than G_c, the amplitude of oscillation will increase continuously. However, the magnitude of G_e is dependent on

the amplitude of oscillation. G_e may remain constant or increase in magnitude for some amplitude range, but there is always an amplitude above which it decreases. Eventually, an equilibrium amplitude is reached at which the dynamic value of G_e is equal in magnitude to G_c. What the value of the equilibrium amplitude may be depends upon the manner in which G_e varies with amplitude, the resonator losses, and the load. The time which oscillations require to reach the steady state amplitude depends upon the behaviour of G_c with frequency as well as the effect of voltage amplitude and frequency on G_e.

Eq. (3.5) indicates that, since v is zero when V_o is zero, oscillation cannot take place unless initiated in some manner. In an actual case, the thermal motion of electrons sets up random pulses which will initiate oscillation if the static value of G_e at zero amplitude is negative and $|G_e| > G_c$.

3.3.2 Buildup and limitation of amplitude of oscillation

Eqs. (3.4)-(3.7) indicate whether or not sustained oscillation is possible; whether the amplitude at any instant is constant, increasing or decreasing; and the frequency at which oscillation takes place. They give no indication of the equilibrium amplitude of oscillation, the manner in which the amplitude builds up, or how the equilibrium amplitude varies with circuit parameters.

The equilibrium amplitude of oscillation can be determined only if the manner in which the electronic conductance G_e varies with amplitude of oscillation is known. However, if a curve of G_e versus amplitude can be constructed, a simple graphical method may be used. The trend of such curves is shown in Fig. 3.5 along with a curve of G_c versus amplitude. Useful qualitative information concerning the behaviour of oscillators may be derived from the analysis of the curves in the figure even though it does not necessarily represent any particular oscillator. If $G_e < 0$ and $|G_e|_o \geq G_c$, the exponent α in Eq. (3.6) is zero or positive. Any small initial voltage V_o resulting from random noise or other circuit disturbance initiates oscillation. When $|G_e|_o$ exceeds G_c the exponent α is initially positive and the amplitude of oscillation increases. As the amplitude increases, $|G_e|$ decreases, until the amplitude reaches the value corresponding to the intersection of the $|G_e|$ and G_c curves. Further increase of amplitude would cause $|G_e|$ to become smaller than G_c. Consequently, α would become negative. The amplitude would therefore decrease to the value corresponding to the intersection. This analysis indicates that the intersection of the curves corresponds to a condition of stable equilibrium in the circuit and that sustained oscillation takes place at the amplitude corresponding to this point.

The curves in Fig. 3.5 show that the amplitude of oscillation can be increased by two methods. The value of G_c may be reduced by changing the load or the resonator loss or the $|G_e|$ curve may be raised, which is ordinarily accomplished by changing one or more of the operating parameters of the electronic device which affect the negative electronic conductance. In some oscillators, however, the magnitude of the electronic conductance increases at low amplitudes, as indicated, for example, by the curves of Fig. 3.5. Again, oscillation cannot start unless $|G_e|_o$ is equal to or greater than G_c. For curve (a) of Fig. 3.5, $|G_e|_o$ just exceeds G_c and α is very small, but positive. As the amplitude increases, $|G_e|$ also increases, α grows, and the amplitude increases more rapidly. The action is cumulative and the amplitude increases rapidly until it reaches a value corresponding to the intersection of the curves at point P. If the curve of the electronic conductance is then raised by changing some parameter of the source of electronic conductance, the amplitude increases continuously with change in the parameter. When the parameter is changed in the opposite direction, so as to lower the curve of electronic conductance, the amplitude decreases continuously with change of parameter until the curve becomes tangent to the G_c line, as shown by curve (b) of Fig. 3.5. Any further lowering of the electronic conductance

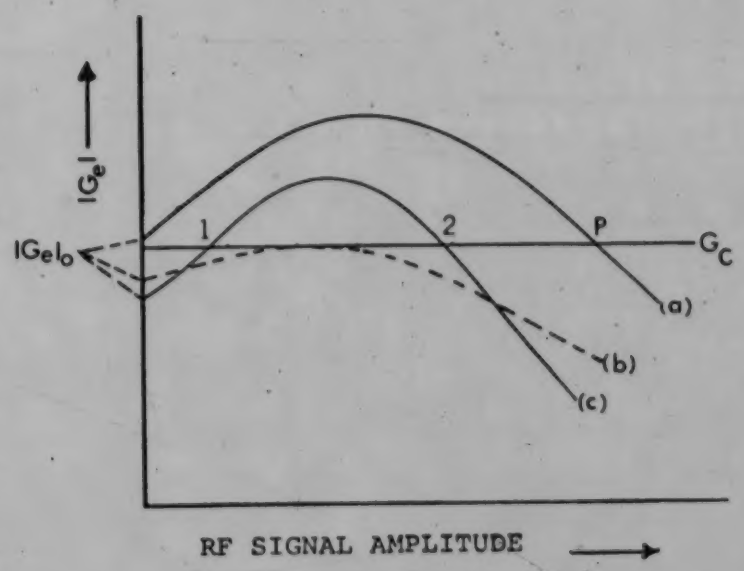

Fig. 3.5 Electronic conductance, vs. RF signal amplitude.

curves causes $|G_e|$ to be smaller than G_c and α to be negative, whereupon oscillation ceases. It can then be started again only by raising the curve to a point at which $|G_e|_o$ exceeds G_c and the amplitude again jumps to that corresponding to point P.

If the electronic conductance curve has a maximum, as shown in all G_e-curves of Fig. 3.5, and $|G_e|_o$ is adjusted to a value that is somewhat smaller than G_c, as in (c) of Fig. 3.5, the oscillation is not self-starting. However, if the circuit is driven by external means to an amplitude equal to or greater than that corresponding to intersection 1 of the conductance curves, the amplitude will increase abruptly to the value corresponding to intersection 2 and oscillation will continue when the driving force is removed.

3.4 Kurokawa's simple theory of oscillators: free-running oscillators

In practical oscillators, the device impedance is a function of both amplitude and frequency of the RF current through the device. A graphical approach may clarify the behaviour of oscillators even when a simplified version of the device impedance has been used.

The characteristics of negative conductance oscillators will be presented along the lines proposed by Kurokawa's simple theory of oscillators [13,17,20].

Since the model proposed considers the equivalent circuit of the oscillator in series representation, the impedance concepts will be the most convenient to use.

3.4.1 Equivalent circuit

In this theory, the active device is treated as a general impedance, $-Z_e(A)$, with real and imaginary parts, $R_e(A)$ and $X_e(A)$, which are arbitrary functions of the amplitude of the RF current, A, through the device, driving a general passive impedance $Z_c(\omega)$. The dependence of the device impedance on the frequency is neglected. This is justifiable since the device impedance is usually a slowly varying function of ω as compared to the circuit impedance. For the purposes of qualitative analysis this dependence of $-Z_e(A)$ on ω will not affect the results of the discussion, but simplify the analysis considerably. The equivalent circuit for the proposed model is shown in Fig. 3.6. The equation for free-running oscillation is given by

$$[Z_c(\omega) - Z_e(A)]\, I = 0 \ . \qquad (3.8)$$

This indicates that the total impedance times the current is equal to zero; namely, there is no applied voltage. Because of its simplicity, the oscillator model represented by Eq.(3.8) reveals a number of important aspects of microwave solid state oscillators. Some of those

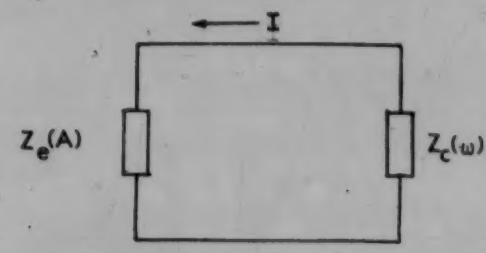

Fig. 3.6 Equivalent circuit of a free-running microwave oscillator.

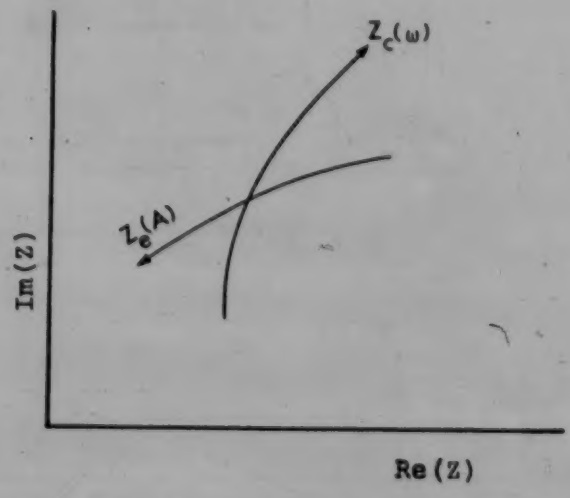

Fig. 3.7 Impedance locus and device line.

related to free running-oscillators will be considered.

3.4.2 Impedance locus, device line, and operating point

To demonstrate the real meaning of Eq. (3.8), the locus of the circuit impedance and that of the negative of the device impedance are drawn on the complex plane by varying ω and A, as shown in Fig. 3.7. The locus of $Z_c(\omega)$ is called the impedance locus and that of $Z_e(A)$ is called the device line. The arrows indicate the directions of increasing ω and A. The intersection of these two loci correspond to

$$Z_c(\omega) = Z_e(A) \quad . \tag{3.9}$$

When the RF current amplitude flowing through the device is A, the point corresponding to $Z_e(A)$ is called the operating point. If I is finite and Eq. (3.8) is satisfied, $Z_c(\omega)$ must be equal to $Z_e(A)$. Consequently, in steady state, the operating point is located at the intersection between the impedance locus and the device line. The steady state oscillation frequency and amplitude can be determined at the intersection point of the two loci.

3.4.3 Effects of distant reflection

With this much understanding of the device line and impedance locus, typical behaviour of microwave oscillators like the one illustrated in Fig. 3.1 can be

discussed. First, the probable shape of the impedance locus must be deduced. This can be done conveniently on the Smith chart. The vector drawn from the center to a given impedance point on the Smith chart indicates the corresponding reflection at the reference plane where the impedance is measured.

Reflections in an oscillator circuit, exhibit a phase rotation with a change in frequency at a rate determined by the electrical distance of the reflector from the active device. The longer the distance the quicker the rotation. Physical structures near the device, such as the short circuit plunger or the waveguide post used to bias the device, create large reflections which rotate slowly. On the other hand, the slide screw tuner which is located at a distance from the device gives a reflection which rotates quickly. Because of this quick rotation, the tip of the resultant vector most probably draws a loop or loops on the Smith chart as illustrated in Fig. 3.8. Consequently, it is most likely that the impedance locus has loops. It may be worth mentioning that the distant reflection has less tendency to form loops when the main reflection vector rotates quickly. One way to avoid loops in the impedance locus is to make the Q of the close-in circuit as high as other conditions permit and the distant reflection as small as possible.

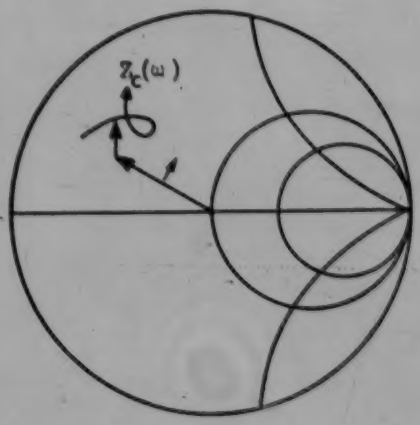

Fig. 3.8 Formation of a loop in the impedance locus.

If adjustments are made in some suitable circuit component such as the short circuit plunger, the position of the impedance locus changes with a loop downwards as shown in Fig. 3.9a. The operating point P_1 first moves to the right as indicated by P_2 but as soon as the upper edge of the loop separates from the device line, the operating point jumps to the left. Fig. 3.9b will help understand the detailed behaviour near the upper edge of the loop. As the operating point P_a, approaches the upper edge of the loop, the intersecting angle becomes small. This indicates that the oscillation becomes noisy. If the locus is moved to the position indicated by the dotted line, the intersection disappears. No steady state oscillation is possible near the upper edge of the loop. Consequently, the operating point jumps to the other intersection P_b. If the maximum power point is located at the position indicated by X, the power initially increases as the locus moves downward, since the operating point approaches the maximum power point. But when the operating point jumps to P_b, the power suddenly decreases and the frequency increases as illustrated in Fig. 3.10. If the adjustment is reversed, the locus moves upward, the operating point moves to the right, and the frequency as well as the power follow a different path; and when the lower edge of the loop separates from the device line, the frequency and power

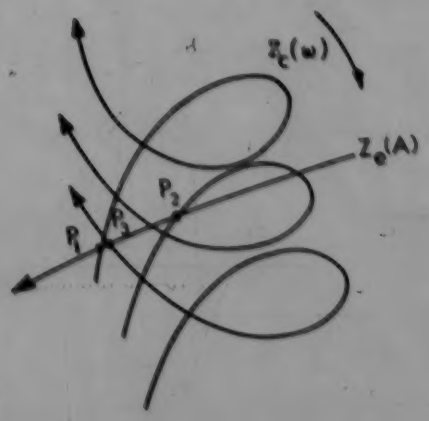

Fig. 3.9a Variation of the operating point with change in the position of impedance locus.

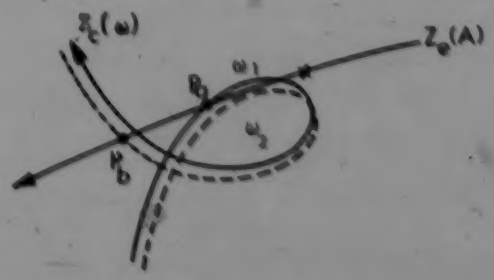

Fig. 3.9b Explanation of the jump of operating point.

suddenly jump again. In this particular case, both frequency and power decrease. This behaviour is typical of microwave solid state oscillators having distant reflections and in accord with experience. In practice, however, the impedance locus may contain many loops and the loops move in various directions while changing their sizes. The result is a more complicated and frustrating oscillator behaviour.

Similar complications will arise when the bias supply is adjusted while keeping the rest of the circuit unchanged. In this case, the device line moves with respect to a stationary impedance locus resulting in an almost identical effect.

3.4.4 Onset of oscillation: transient and steady state conditions

In this section, the steady and transient state conditions of a microwave oscillator will be discussed along the lines proposed by Kurokawa [17].

Because of the white-band noise in the lossy components, there will be present in the embedding circuitry small RF currents of proper frequency after the bias supply is turned on. Under these conditions, the equation of the free-running oscillation is approximated by

$$[Z_c(\omega) - Z_e(0)]\, I = 0 \qquad (3.10)$$

where $-Z_e(0)$ is the small-signal device impedance. Since I is small but nonzero because of the switch-on disturbances or noise, and since $Z_c(\omega)$ is not equal to $Z_e(0)$ for any real ω, ω must be complex. The real part will be expressed by ω' and the imaginary part by $-\alpha$. Since the time factor corresponding to $\omega' - j\alpha$ is $e^{j\omega' t}\, e^{\alpha t}$, positive α indicates the amplitude is increasing with time and negative α indicates a decreasing amplitude. A concrete example in which $Z_c(\omega)$ represents a series resonant circuit will help make the point clear. $Z_c(\omega)$ is given by

$$Z_c(\omega) = j(\omega L - \frac{1}{\omega C}) + R_a + R_L \qquad (3.11)$$

where R_a represents the loss in the cavity and R_L the load. In the vicinity of resonance, $Z_c(\omega)$ is approximated by

$$Z_c(\omega) \approx 2j(\omega - \omega_a)L + R_a + R_L \qquad (3.12)$$

$$= 2j(\omega' - \omega_a)L + 2\alpha L + R_a + R_L \qquad (3.13)$$

where

$$\omega_a = \frac{1}{\sqrt{LC}} \quad . \qquad (3.14)$$

The impedance locus, the locus of $Z_c(\omega)$ with real ω, is a straight line parallel to the imaginary axis. The α-constant locí are all parallel to the impedance locus and the ω'-constant loci are perpendicular to it. The right-hand side of the impedance locus corresponds to

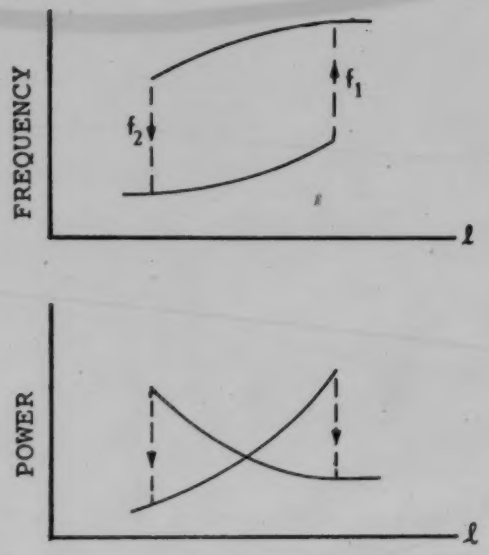

Fig. 3.10 Typical frequency and power tuning hysteresis of a multiple-tuned oscillator.

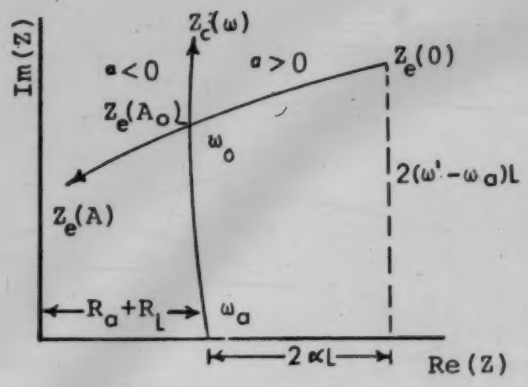

Fig. 3.11 The on-set of oscillation in a single tuned oscillator.

positive α's and the left-hand side to negative α's as indicated in Fig. 3.11. In this diagram $Z_e(0)$ corresponds to a positive α. Consequently, if Eq. (3.10) holds, α must be positive whenever $I \neq 0$. In other words, the circuit device interaction forces the current amplitude to increase. As the current amplitude increases, the operating point moves left along the device line toward the intersection with the impedance locus. The figure indicates that the frequency as well as the amplitude, in general, changes as the operating point moves since the value of ω' changes along the device line. Since α is positive and the amplitude increases as long as the operating point is located on the right-hand side of the impedance locus, amplitude growth continues until the operating point reaches the intersection satisfying $Z_c(\omega_o) - Z_e(A_o) = 0$, or equivalently

$$2L(\omega_o - \omega_a) + X_e(A_o) = 0 , \qquad R_a + R_L - R_e(A_o) = 0 \qquad (3.15)$$

where ω_o and A_o are the frequency and amplitude corresponding to the intersection and $X_e(A)$ is the imaginary part of $-Z_e(A)$.

3.4.5 Stability of free-running oscillators

If the amplitude increases beyond the intersection, the circuit-device interaction forces the current to

decrease since the left-hand side of the impedance locus corresponds to negative α's. Consequently, the operating point returns to the intersection. In other words, the intersection in Fig. 3.11 results in a stable steady state operating point.

In case if the impedance locus has a loop, there could be more than one intersection between the impedance locus and the device line. The same arguments developed above can be used to differentiate between stable and unstable operating points. If two stable operating points happen to occur, the starting history of oscillation will determine which operating point is functional.

CHAPTER IV

IMPATT DIODES

4.1 Introduction

Impatt (IMPact ionization Avalanche Transit Time) diodes are two-terminal devices utilizing the combined effects of avalanche breakdown and transit time to transform part of the dc energy into RF energy in a certain frequency range (from the circuit point of view, the real part of the diode impedance is negative in this frequency range). A p-n junction can be operated in its Impatt mode when it is biased into reverse avalanche breakdown and mounted in a proper microwave cavity. At the present time, the Impatt diode is one of the most powerful solid state sources of microwave power. A CW efficiency of as high as 35.6% (with 2.9 W output power) at 10.4 GHz has been reported [21]. A hi-lo Schottky-barrier GaAs Impatt diode has given a CW power of 12 W at 6 GHz [3].

The possibility of producing high frequency oscillations from a reverse-biased p-n junction device operating under avalanche breakdown conditions was first discussed in 1958 by Read [22], who first proposed the Read structure (in p-n-i-n configuration) which has a peculiar doping profile. Later, Missawa showed that a

negative conductance of Impatt nature can be presented by any p-n junction diode with almost any doping profile [23].

In this chapter, the device structure and its dc characteristics are considered first. Section 4.3 describes the basic principles of operation of the Read diode. Small- and large-signal analyses are discussed in section 4.4.

4.2 Device structure and dc characteristics

A p-n junction is the simplest Impatt structure. When reverse biased, mobile charges from the regions close to the metallurgical junction are swept away by the field, leaving a positively charged (n-region) and a negatively charged (p-region) depletion region. At the same time, a small reverse saturation current flows. As the bias voltage increases, the depletion layer becomes thicker and the unswept portion decreases. These unswept portions of the "p" and "n" sides introduce a resistance which degrades diode efficiency [24]. When $V_{bias} < V_b$ (V_b is the breakdown voltage), the introduced depletion zone acts as a nonlinear capacitor. Fig. 4.1 shows the equivalent circuit for a p-n junction diode at a given bias voltage V ($V < V_b$). In this figure $R_D(V)$ and $C(V)$ depend on the semiconductor characteristics.

If the reverse bias voltage is increased to the value of V_b, the junction breaks down so that a small

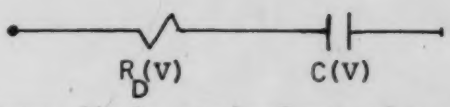

Fig. 4.1 Imput diode equivalent circuit at $V < V_b$, where V = bias voltage and V_b = breakdown voltage.

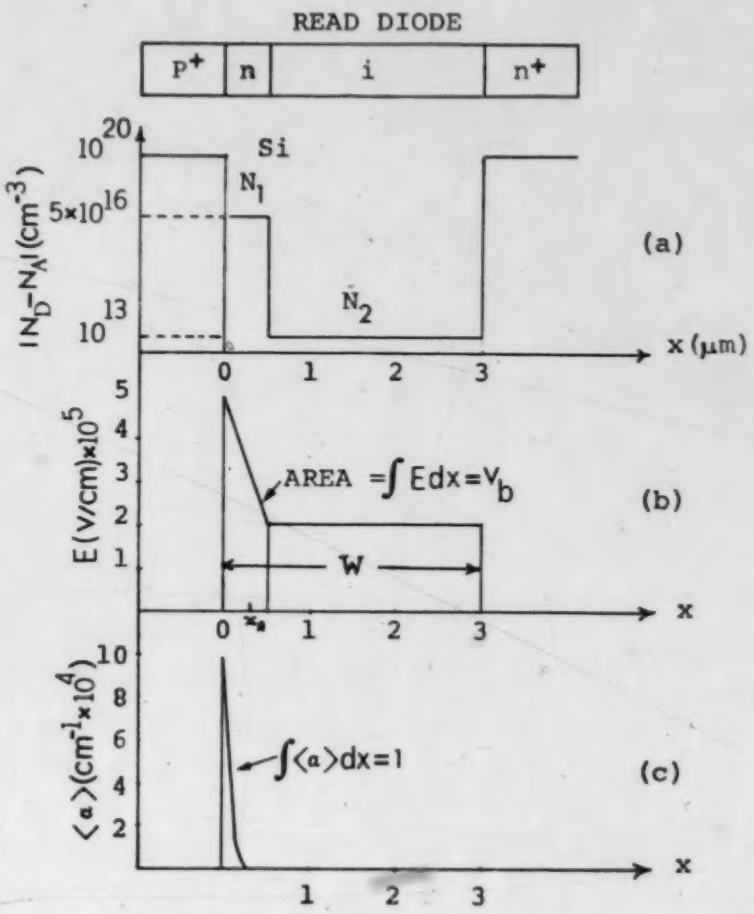

Fig. 4.2 Read diode
(a) doping profile (p^+nin^+),
(b) electric field distribution, and
(c) ionization integrand at breakdown.

increase of the bias voltage beyond this critical value results in a large current flow. This large current is the result of an impact ionization producing multiplication of electrons and holes in the depletion region of the junction. This phenomenon is known as avalanche breakdown.

Impatt diodes are designed in various structures. The Read diode, the one-sided abrupt p-n junction, the two-sided abrupt p-n junction, the p-i-n diode and the lo-hi-lo structure are the most commonly used structures [25]. The Read diode is a convenient structure for analytical purposes and for obtaining an understanding of the physics of the Impatt diode operation, but it is difficult to manufacture. One and two sided abrupt p-n junctions are easier to fabricate but very difficult to analyze. Impatt mode oscillations are obtained from these more practical diode structures in much the same manner as from the Read diode. The most widely used Impatt diode structure has been the one-sided abrupt p^+-n-n^+ junction (p^+-n-n^+ is used instead of p-n in order to reduce the diode parasitic resistance) which will be used in the experimental part of this study.

Fig. 4.2 shows the doping profile, the electric field distribution, and the ionization integrand at breakdown condition for an idealized Read diode (p^+-n-i-n^+) or its dual (n^+-p-i-p^+). The ionization integrand is

$$\langle\alpha\rangle \equiv \alpha_n \exp[-\int_x^W (\alpha_n - \alpha_p)\, dx'] \qquad (4.1)$$

where α_n and α_p are the ionization rates of electrons and holes, respectively, and W is the depletion region width.

The avalanche breakdown condition is given by

$$\int_0^W \langle\alpha\rangle dx = 1 \ . \qquad (4.2)$$

The avalanche region is highly localized. Therefore, because of the strong dependence of α's on the electric field, most of the multiplication process occurs in a narrow region near the highest field, between $0 \leq x \leq x_A$ where x_A is defined as the width of the avalanche region.

The voltage drop across the avalanche region is called V_a. Both x_A and V_a have profound effects on the optimum current density and the maximum efficiency of an Impatt diode [25].

The corresponding results (the doping profile, the electric field distribution and the ionization integrand) for a typical one-sided abrupt p-n junction are shown in Fig. 4.3. Again, there is a noticeable, highly localized avalanche region. Fig. 4.4 shows the results for a p-i-n diode which has a uniform field across the intrinsic layer. The avalanche region in this case corresponds to the full intrinsic layer width. The

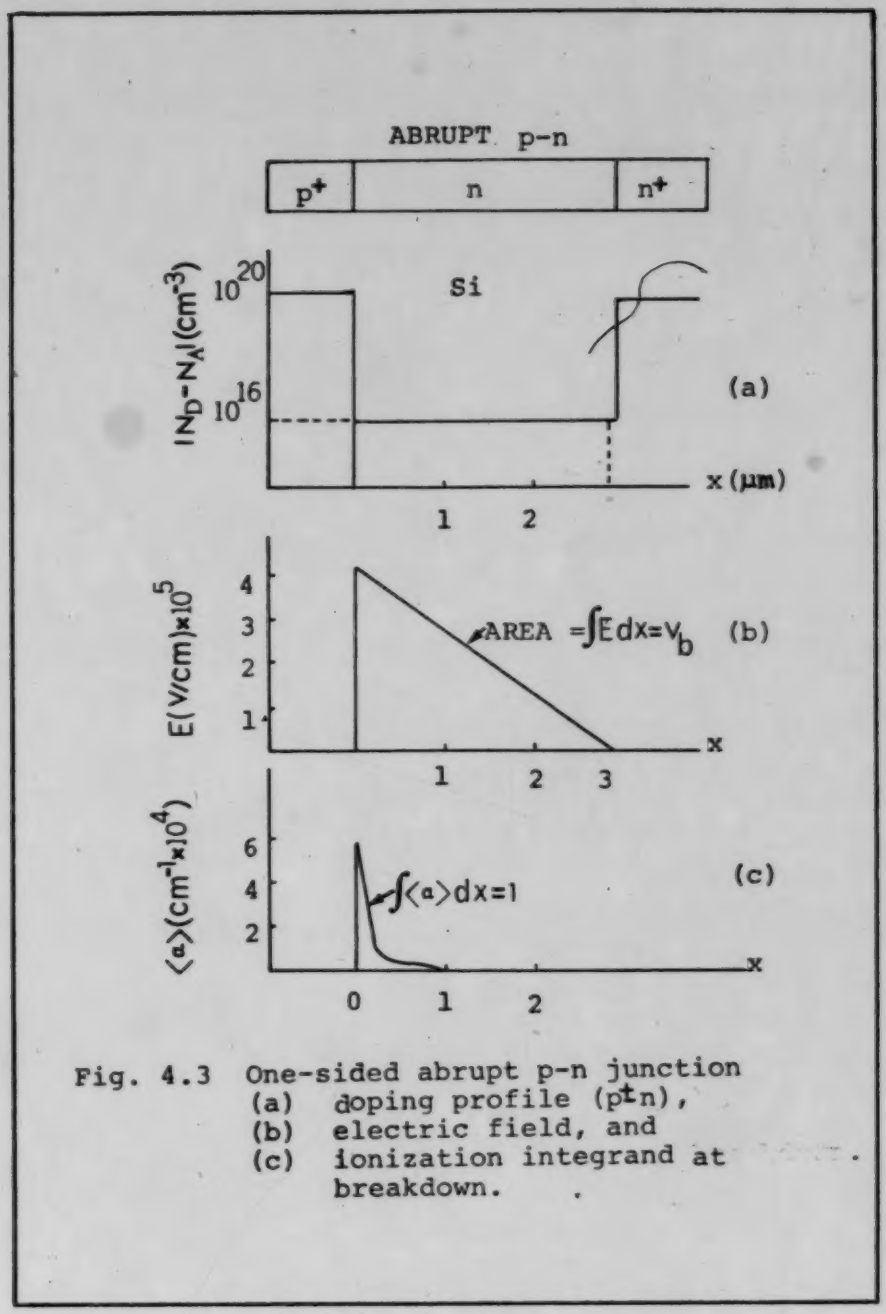

Fig. 4.3 One-sided abrupt p-n junction
(a) doping profile (p^+n),
(b) electric field, and
(c) ionization integrand at breakdown.

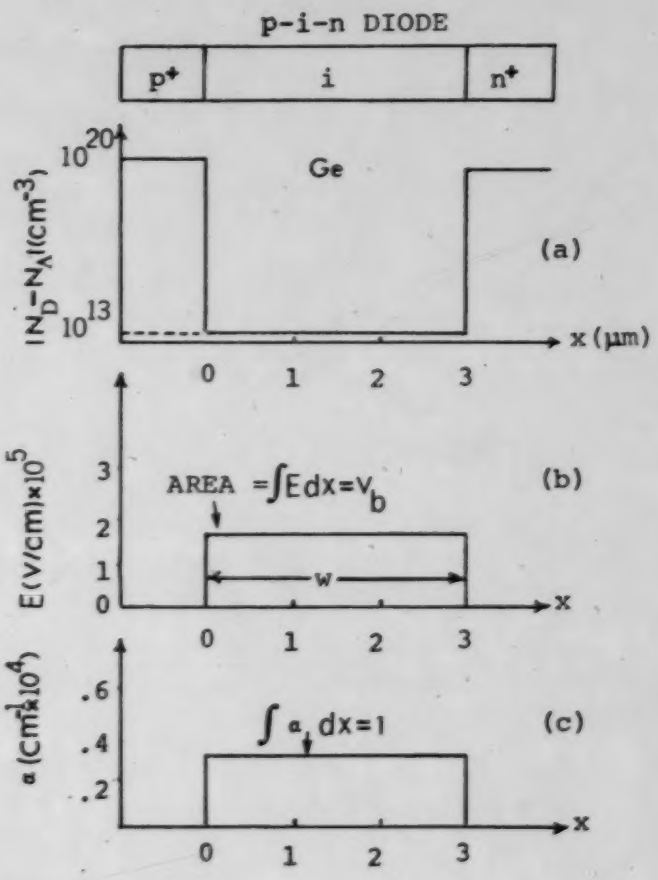

Fig. 4.4 p-i-n diode
(a) doping profile (p-i-n),
(b) electric field, and
(c) ionization integrand at breakdown.

breakdown voltage, the maximum electric field and the depletion layer width can be calculated from the breakdown condition and the field dependence of the ionization rates. Schroeder and Haddad [26] carried out some computations on several diode structures. According to their calculations an n^+-p structure has a higher breakdown voltage with respect to the p^+-n case of the same doping concentrations. The breakdown voltage for the asymmetrical two-sided Si and GaAs diodes is higher than that of the one-sided diodes of the same doping level. In general terms, the breakdown voltage depends mainly on the doping profile, the semiconductor material and the width of the avalanche and depletion regions.

For a simple structure as n^+-p or p^+-n, the doping profile can be accurately deduced from the measured voltage dependence of the junction capacitance. For more complex structures, there is no simple procedure for evaluating the doping profile. Therefore, only in the case where the internal structure of the diode, its junction geometry, and its doping profile are known, can the Impatt terminal characteristics be evaluated. Unfortunately, manufacturers do not supply any information concerning the detailed structure of the diode.

4.3 Basic principles of Impatt operation

A good understanding of the ac characteristics of Impatt diodes can best be obtained by considering the operation of a Read diode [22,27,28]. The structure, field distribution, and current waveforms for a reverse-biased Read diode are shown in Fig. 4.5. The Read diode consists of two regions: a narrow avalanche region (p-region) in which carrier multiplication by impact ionization occurs, and a drift region (intrinsic region) in which the carriers drift at saturated or field-independent velocities. No impact ionization occurs in the drift region.

The negative conductance or resistance of a Read diode is attributed to a phase shift between the current through the diode and the voltage across it. This phase shift consists of two components. There is a phase delay in the external circuit current caused by the avalanche multiplication process and a delay caused by the finite transit time of the charge carriers drifting through the drift region.

The phase delay caused by the avalanche process results from the fact that the rate of generation of electron-hole pairs in the avalanche region is proportional both to the electric field and to the density of electrons and holes already present in the region. If a small RF voltage of sufficiently high frequency is

assumed to be applied along with a dc voltage near breakdown across the diode, the rate of generation of electron-hole pairs will exceed the rate at which the pairs leave the avalanche region. Thus, the carrier density in the avalanche region will grow exponentially with time as long as the RF and dc voltages add to give a total field above breakdown. When the RF voltage changes sign and subtracts from the dc voltage, causing the field to fall below breakdown, the avalanche multiplication process drops almost to zero, causing the current to decrease. Thus the avalanche current will have its maximum when the RF field goes through zero. Thus, as shown in Fig. 4.5, the avalanche process contributes a 90° inductive phase lag to the current generated in the avalanche region. This current is then injected into the drift region of the diode. The current induced in the external circuit by this charge, drifting through the drift region at a saturated drift velocity, is shown at the bottom of Fig. 4.5. It is obvious that the fundamental component of the external current is more than 90° out of phase with the RF voltage, causing the resistance or the conductance of the diode to be negative.

Thus a net transfer of energy into the ac field from the dc field has occurred, and the ac voltage can grow. In an appropriate circuit, self-sustained oscillation can be obtained.

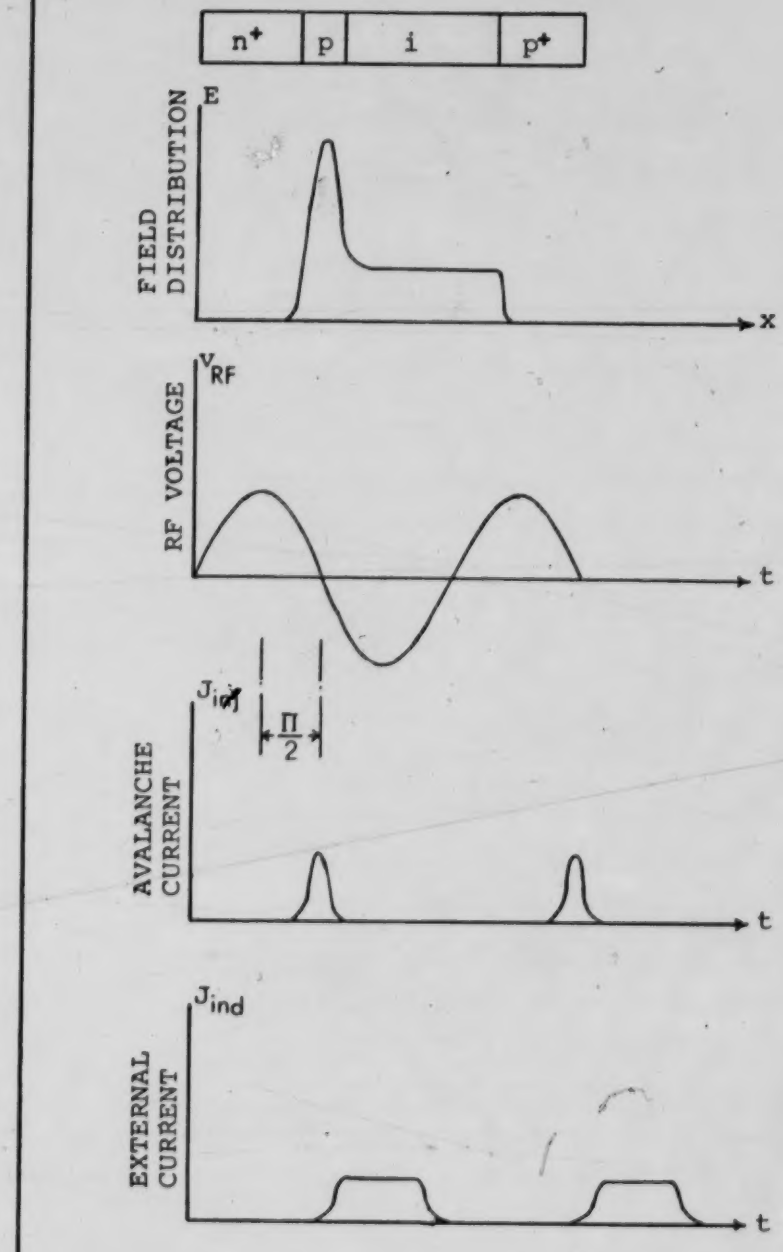

Fig. 4.5 Read diode structure, field distribution, and voltage and current waveforms.

4.4 Small- and large-signal operation

The equations which govern the operation of an Impatt diode are Poisson's equation and the continuity equations for holes and electrons. In one dimension, these equations are

$$\frac{\partial E}{\partial x} = \frac{q}{\epsilon} (N_D - N_A + p - n) \tag{4.3}$$

$$\frac{\partial p}{\partial t} = g - \frac{1}{q} \frac{\partial J_p}{\partial x}$$

and

$$\frac{\partial n}{\partial t} = g + \frac{1}{q} \frac{\partial J_n}{\partial x} \tag{4.4}$$

where

$$J_p = q p \mu_p E - k T \mu_p \frac{\partial p}{\partial x}$$

$$J_n = q n \mu_n E + k T \mu_n \frac{\partial n}{\partial x}$$

where

E	electric field (V/cm)
q	electronic charge (C)
ϵ	dielectric constant (F/cm)
N_D, N_A	donor and acceptor densities (cm^{-3})
p, n	hole and electron densities (cm^{-3})
J_p, J_n	hole and electron current densities (A/cm^2)
g	hole and electron generation recombination rates
μ_p, μ_n	hole and electron mobilities ($cm^2/V.s$)

k Boltzmann constant (1.38×10^{-23} Joule/°K)

T absolute temperature (°K)

Usually, several simplifying assumptions are made in order to obtain a closed form solution for the diode small-signal admittances. In many small-signal studies, ionization coefficients of electrons and holes are assumed to be equal, and recombination effects together with the diffusion current are neglected. Even with these assumptions, closed form solutions are obtainable only for simple structures such as the Read and the p-i-n structures. For more complicated structures, solutions are usually obtained by the use of the digital computers.

Small-signal analysis of a Read diode gives the following expression for the real part of the diode terminal impedance [29]

$$R \simeq \frac{W}{A\varepsilon\omega} \frac{1}{1 - \frac{\omega^2}{\omega_r^2}} \left(\frac{1 - \cos\theta}{\theta}\right) \qquad (4.6)$$

where W is the depletion region width, A the diode area, θ the transit angle given by $\omega W/v_{s\ell}$ ($v_{s\ell}$ is the scattering limited velocity of charge carriers) and ω_r the avalanche resonant frequency given by

$$\omega_r \equiv \sqrt{\frac{2\alpha' v_{s\ell} J_o}{\varepsilon}}$$

in which the quantity α' is the derivative of the ioniza-

tion rate with respect to the electric field and J_o is the dc current density. From Eq. (4.6), the diode negative resistance can only be negative if $\omega > \omega_r$.

The variation of the negative resistance with the transit angle is plotted in Fig. 4.6. The peak value occurs near $\theta = \pi$. For transit angles larger than π and approaching $3\pi/2$, the negative resistance of the device decreases rapidly.

The negative conductance at a fixed operation frequency as a function of the biasing dc current density is shown in Fig. 4.7(a) for the Read diode (p^+-n-i-n^+), the abrupt p^+-n junction, and the p-i-n diode. This figure shows that the negative conductance for a Read diode rises to a maximum value at a relatively low current density, then decreases, and eventually disappears at current density at which the avalanche resonant frequency (which is proportional to $\sqrt{J_o}$, Ref. [30]) equals the operating frequency. The other structures show very similar characteristics. However, the conductance at low current density is smaller and the peak negative conductance occurs at larger current for the abrupt junction. Even larger current density is needed for the Misawa (p-i-n) diode.

At a fixed current density, the negative conductance versus operating frequency for the above structures is shown [30] in Fig. 4.7(b). The Read diode has a relatively

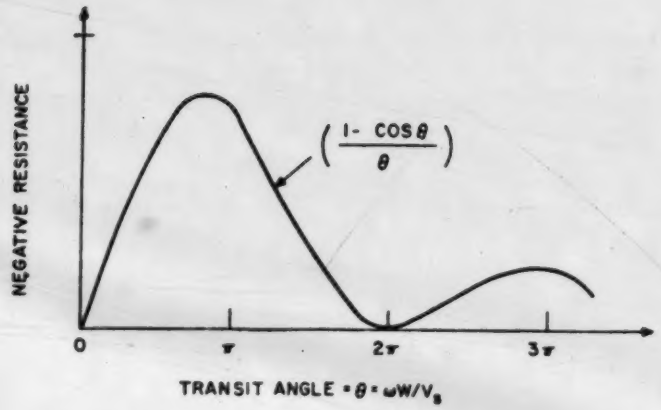

Fig. 4.6 Read diode: Idealized negative resistance vs. transit angle.

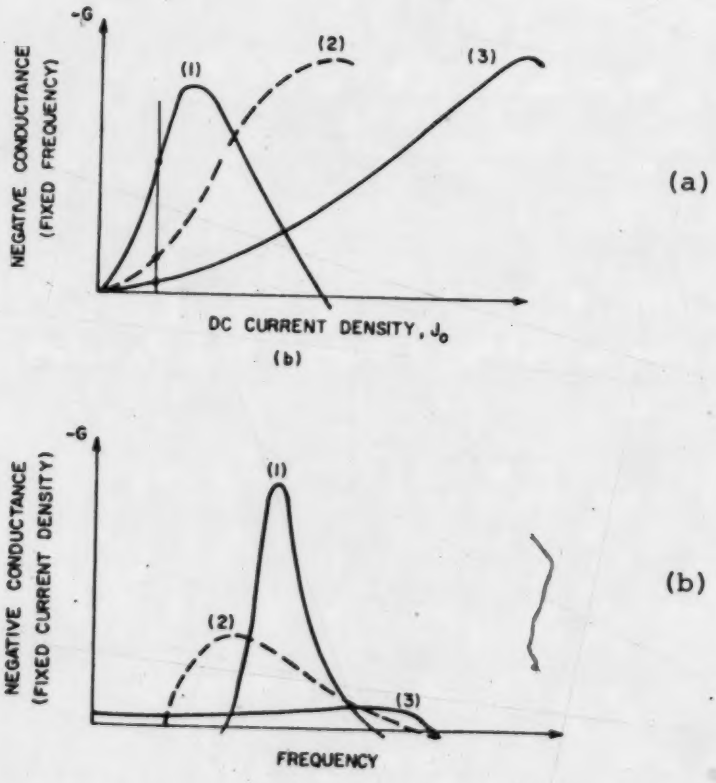

Fig. 4.7 Effect of doping profile on conductance for 1) Read, 2) abrupt, 3) Missawa (uniform avalanche) profiles. (Reproduced from Ref. [30]).

(a) Negative conductance vs. dc current at one frequency.

(b) Negative conductance vs. frequency at constant dc current density.

narrow peak around the transit time frequency. A wider frequency range is obtainable from the abrupt p-n junction with some reduction of peak conductance value due to nonoptimum phase relation. The reason that the negative conductance disappears at low frequencies (small θ) is that space charge in the drift space can exhibit a large positive resistance at low frequencies [31]. The Misawa diode, however, exhibits a small negative conductance, nearly constant at frequencies from zero to $\theta = 2\pi$.

The foregoing discussion has considered the small-signal conductance of several diode structures to be a function of the dc bias current and frequency. However, the dependence of the diode susceptance on the bias current and operation frequency is also important. The sensitivity of the small-signal diode admittance to the bias current and frequency, as given by C.A. Bracket [32] (for n^+-p-p^+ structure), is shown in Fig. 4.8. In Fig. 4.8, the admittance characteristic is seen to be very similar to that of the Read diode [22]. Generally over an appreciable frequency range, the diode susceptance decreases and the diode conductance increases with the increase in the dc bias voltage.

At large current densities the simplifying assumptions used in the small signal theories are not justified. Small-signal results are useful only at the initial

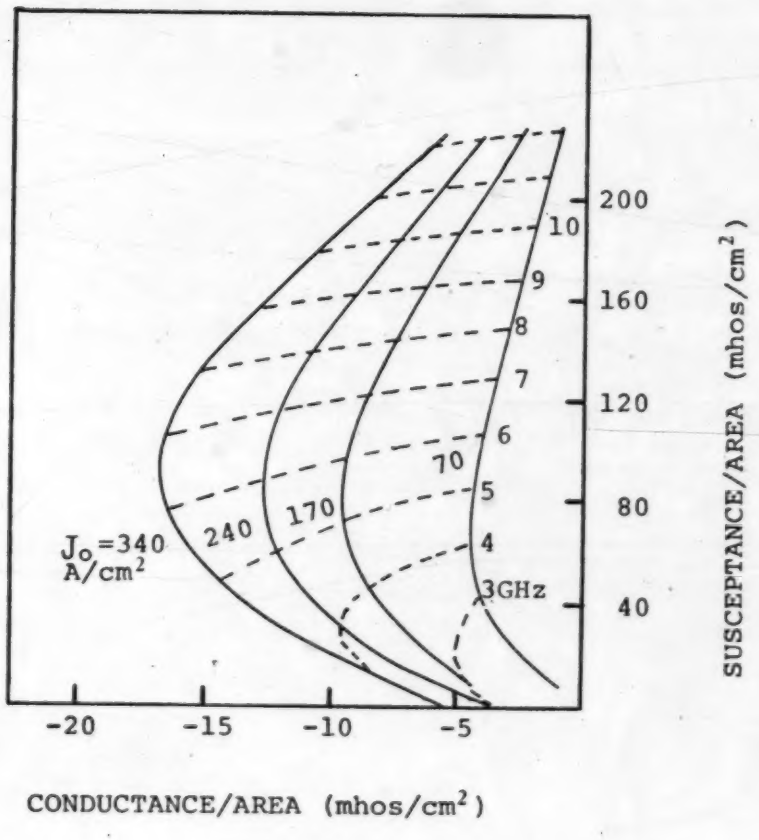

Fig. 4.8 Small signal admittance plane plot for Ge $n^{+}p$-p^{+} diode from Gummel-Scharfetter program. (Reproduced from Ref. [32]).

stages of oscillator design in order to indicate the oscillation frequency and the maximum negative conductance obtained under certain bias conditions. Under normal operating conditions, e.g. in an oscillator circuit, the RF voltage is comparable to the bias voltage and the diode RF characteristics become amplitude dependent.

Under large-signal conditions the ionization rates for holes and electrons depend strongly on the electric field. This causes the multiplication current to respond nonlinearly to the large voltage amplitude across the avalanche zone [33]. In this case, the conduction current will have a high harmonic content.

Several large-signal analyses have been undertaken which provide insight into the nonlinear properties of the Impatt diode [22,28,34, 8] . The most accurate and complete of these, a numerical solution, was given in 1969 by Scharfetter and Gummel [28]. Basically, the program they used performs a simultaneous time-dependent solution of Poisson's equation, the current equations, and the continuity equations for a one dimensional structure. Included in the program are accurate expressions for electron and hole mobilities, ionization rates, and thermal generation and recombination. Although these studies probably give a most accurate and detailed theoretical description of the large-signal operating conditions,

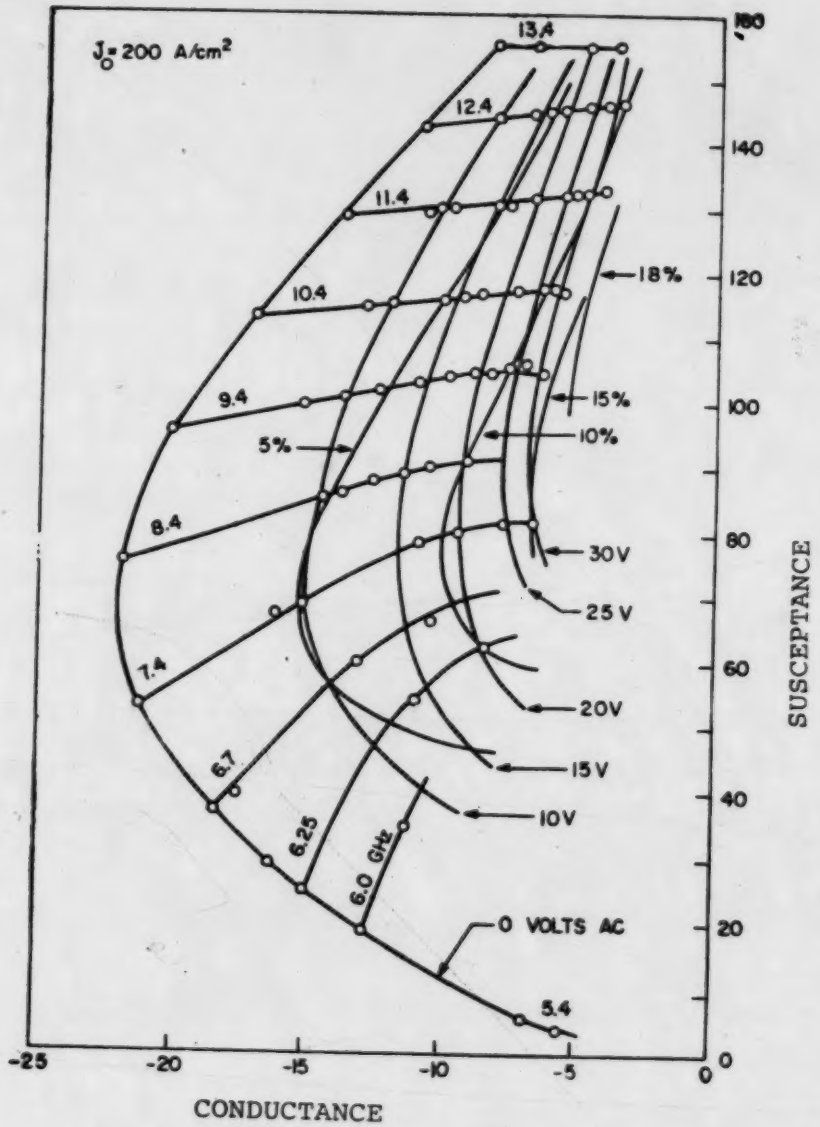

Fig. 4.9 Diode admittance (susceptance vs. conductance) as a function of frequency and RF voltage amplitude, with the resultant efficiency indicated. Current density 200 A/cm^2. (After Gummel and Scharfetter [28]).

the large computational time necessary generally precludes detailed studies of the operating characteristics under a wide range of parameter variations.

Fig. 4.9 is a compact presentation of the important results of their calculations [28] for a Read structure. In most cases, the diode susceptance increases with increasing RF voltage amplitude, whereas the diode negative conductance decreases. The results show diode efficiencies as high as 18%, although neither oscillator power nor efficiency is saturated at that point. It is difficult, with that program, to determine the maximum efficiency or power output because these quantities depend on the proper termination of the harmonics of the fundamental frequency; these constraints are not known a priori.

Since 1969, most of the effort in Impatt large signal studies have been directed toward reducing the computational time required for obtaining a solution [8,34], without causing a significant reduction in accuracy.

CHAPTER V

MEASUREMENT OF LARGE SIGNAL ADMITTANCE OF IMPATT DIODES AND ASSOCIATED PASSIVE CIRCUITS FOR OSCILLATORS

5.1 Introduction

The theoretical models of the active and passive circuits developed earlier can be implemented in practical applications, such as oscillators, only if the active device, e.g., Impatt diode, is accurately characterized. Accordingly a technique for the measurement of large signal admittance and the associated passive circuitry is described. This technique, together with the theoretical models, will provide an accurate method for dynamic studies on Impatt diode active circuits.

Several authors [9,28,35-38] have published methods and/or results of microwave impedance measurements on packaged diodes. However, in order to accurately evaluate the active wafer parameters, it is necessary to measure precisely the parasitics and impedance transformation properties of the diode package, the leads, and the measuring circuit. So far, this has been achieved by the use of two techniques. In one technique these elements are represented by a 2-port network connecting the measuring system to the diode wafer, then the parameters of the 2-port network can be determined by standard measurements [39,40]. This technique, however, requires

replacing the diode wafer by three known impedances for calibration purposes. This necessitates the use of identical dummy packages for the three reference impedances. To accurately substitute for the diode under consideration, the diode packages must be fabricated in the same manufacturing batch, which is commercially unpracticable. Furthermore, replacing the diode by these packages for calibration, one may change the actual RF conditions as seen by the diode, since the reference plane may shift slightly. Accordingly, it is difficult to attain a reasonable measurement accuracy. The second technique used relies on the capacitance vs voltage (C-V) characteristic below breakdown of the Impatt diode, which can be measured accurately at 1 MHz. Gewartowski et al [36] and Itto et al [37] used this technique to obtain the parameters of the 2-port network connecting the measuring system to the diode wafer. However, the parameters characterizing their 2-port network are not uniquely determined.

Even though a considerable amount of work has been carried out in improving the microwave measurement techniques for Impatt diodes, the measurement accuracy is still very limited [41]. The magnitude of the packaged diode's negative resistance is of the order of 10 ohms or less, for practical diodes. Under conditions of low dc currents, high RF voltages, or maximum power outputs,

this magnitude can be as low as 3 ohms. Van Iperen and Tjassens [41] claim that it is questionable whether the standard VSWR (slotted line technique) or reflection coefficient measurement techniques are sensitive enough to produce highly accurate results at these low impedances. They advocate the use of a microwave impedance bridge method that requires a very stable frequency source and critically machined components. However, their method is very time consuming, especially when the measurements are made at several frequencies.

Under large-signal conditions, the accuracy of the measurements is further restricted because the Impatt diode is a nonlinear device and will produce harmonics of the fundamental frequency during the measurements. However, if the diode is terminated in a 50 Ω line, the impedance at various harmonics is also 50 Ω and the harmonic content is well defined. The disadvantage of this arrangement is that a large amount of input RF power is needed to drive the diode into large-signal conditions. Diodes in matched resonator mounts of reflection type amplifiers can be carefully designed to reduce the contribution of the second harmonic, while reasonable power levels can be used in the measurements.

The technique developed here for the measurement of large-signal admittance of Impatt diodes can be summarized as follows. The measurement system, the diode

parasitics and diode package up to a defined imaginary plane intersecting the active wafer are characterized by two 2-port networks. By knowing the parameters of these networks, the admittance of the active wafer can be directly determined at various frequencies and for different RF power levels. The error parameters associated with the first network are evaluated by measuring the response of the measuring system to different known impedances corresponding to various positions of a precision movable short. Replacing the movable short with the Impatt diode mounted in an amplifier assembly, the parameters of the second network can be evaluated by measuring the impedance of the Impatt diode at various dc voltages below breakdown. In the present system, the signal frequency as well as the RF power level can be easily adjusted without physically disturbing the diode. The measurement system has a 50 dB dynamic range and is easy to use for measurements at different frequencies. The active diode and passive circuit admittances are measured using the HP 8410A network analyzer.

5.2 Experimental arrangement for admittance measurements

Fig. 5.1 is a block diagram which illustrates the set up for the admittance measurements on Impatt diodes under both small- and large-signal conditions. One of the two isolators is used to isolate the TWT amplifier from

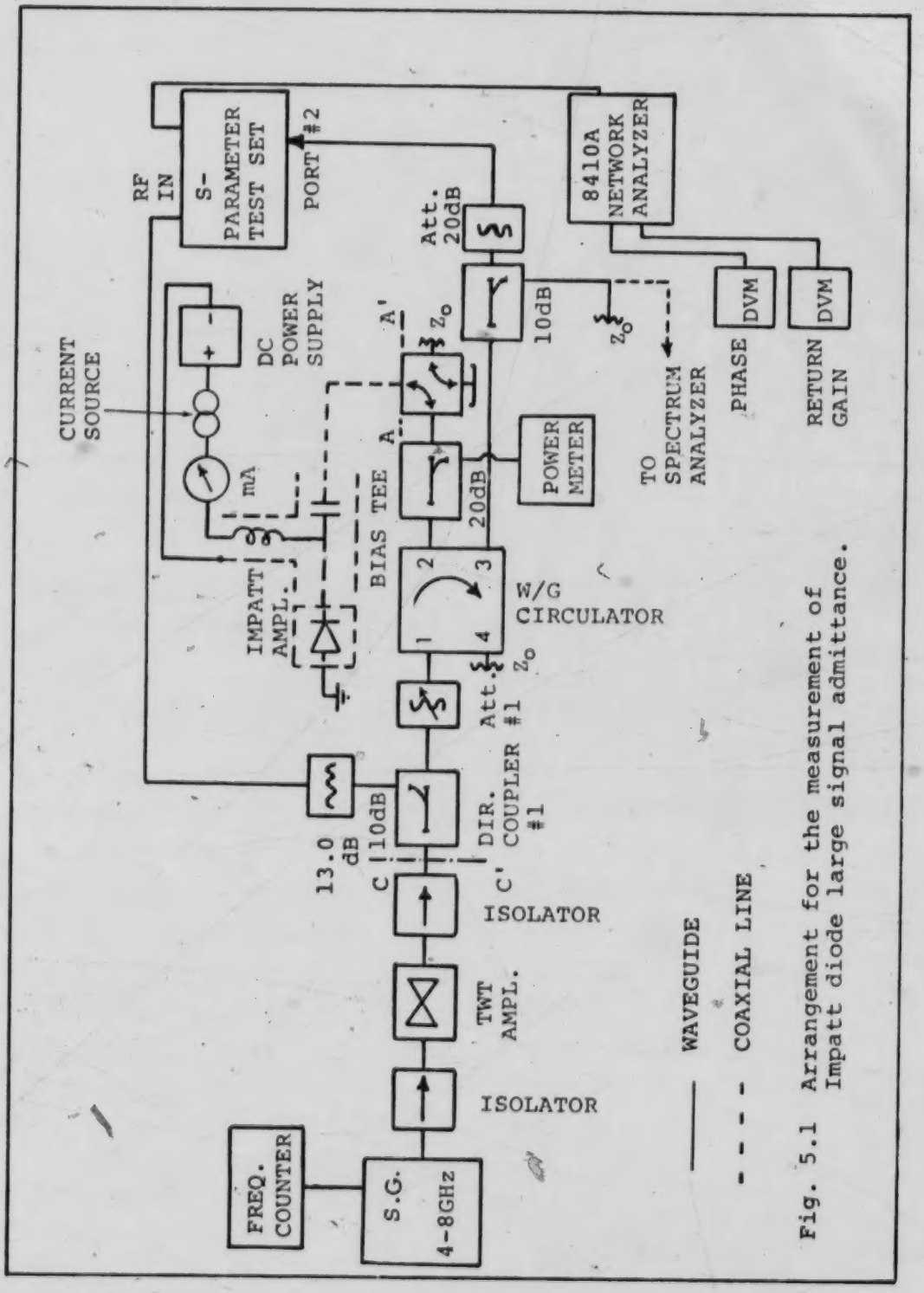

Fig. 5.1 Arrangement for the measurement of Impatt diode large signal admittance.

the klystron source and the other is used to isolate the TWT amplifier from the rest of the system. The TWT amplifier has a maximum gain of 30 dB.

The diode functions as the active element of a reflection type amplifier. The schematic diagram of this amplifier is shown in Fig.5.2. It consists of a waveguide circulator, an impedance transformer with a movable slug for tuning purposes and an Impatt diode. A coaxial transformer matches the 50 Ω characteristic impedance of the transmission line to that of the diode chip. This transformer has a movable slug which allows measurements to be carried out in a frequency range from 5.7 to 6.6 GHz without disturbing the measuring system. The waveguide circulator is used to separate the waves incident on and reflected from the diode.

The principle of operation of the measuring system is simple and can be summarized as follows. The output power of the TWT amplifier is split into two signals by means of the directional coupler #1. The signal in the secondary arm is attenuated by the 13 dB attenuator to the reference power level of the network analyzer. In the main arm of directional coupler #1, the second signal is attenuated, by attenuator #1, directed through the circulator and finally directed into the diode. At a specific power level and frequency, a reading is taken first switching the RF energy into the diode, and then

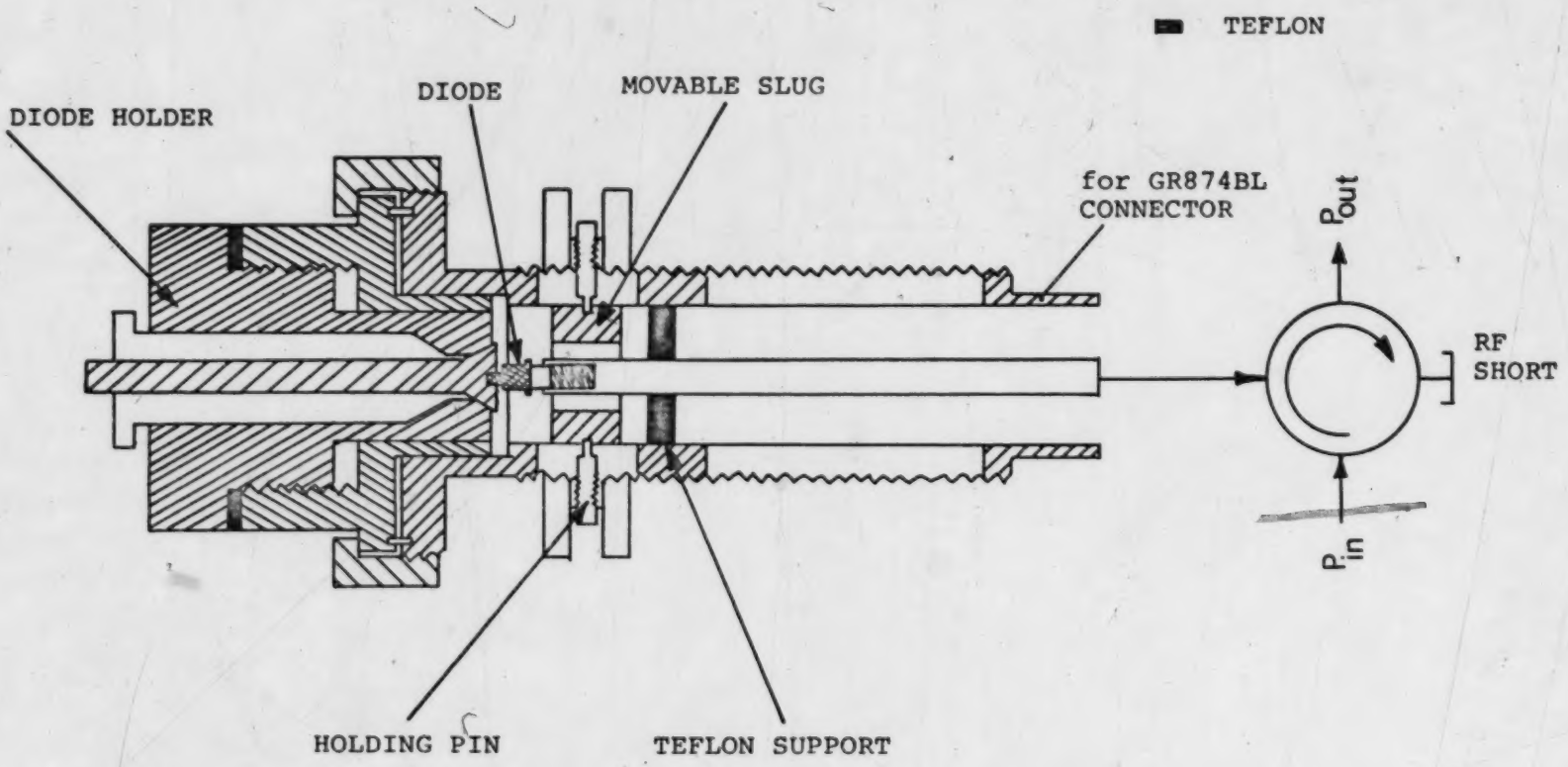

Fig. 5.2 Cross-sectional view of Impatt diode amplifier: consisting of an Impatt diode, a single slug transformer and a waveguide circulator.

switching it into an RF short which serves as an accurate reference impedance. This procedure is repeated at each frequency and power level. Therefore, the data is referenced to the accurately known reflection coefficient of the RF short to minimize the effects of the slow drift of the network analyzer. The reflected signal from the diode is compared with the reference signal within the network analyzer.

The characteristics of the microwave circuitry are governed by the circulator, its bandwidth and isolation being the most important parameters. As the diode is mounted on a precision 50 ohm connector, it has excellent matching characteristics (VSWR < 1.05) to frequencies beyond 18 GHz. However, the four-port circulator has a narrow bandwidth (as $\mathcal{J}$-band components are used) and outside this frequency range it presents a highly reactive impedance. Thus, any second harmonic components generated by the Impatt diode would be largely reflected from the circulator and confined within the diode mount. In this situation, the RF voltage incident upon the Impatt diode will have some second harmonic content present. Another important aspect of the characteristics of the four-port circulator is the isolation between ports 1 and 3 (see Fig. 5.1). This isolation describes the degree of attenuation experienced by the incident RF in reaching the path of the reflected signal. The isolation of the four-port

circulator used here was greater than 30 dB between ports 1 and 3.

Measured data consist essentially of two sets of dc voltages. One is proportional to the return gain, RG, and the other to the phase angle of the reflection coefficient, ϕ, such that ϕ(degrees) = V_{dc}(mV)/10. The return gain is defined as negative return loss in decibels and is converted to the reflection coefficient (Γ) by

$$\Gamma = 10^{RG/20} \, e^{j\phi 2\pi/360} \quad . \qquad (5.1)$$

5.3 Error network; system error characterization [42,43]

All measurement systems introduce systematic errors into the measured results. In precision measurements, these errors must be greatly reduced by either designing a system very close to the ideal one or else by using a system which can be calibrated in situ by substituting reference standards for the device under test. At microwave frequencies, the former approach has usually proven to be impractical. This is because high frequency signals must be measured using such devices as directional couplers, circulators, switches, and other components which cannot be designed with ideal properties. The end result is a large measurement error. Furthermore, in using network analyzers for impedance measurements, the

slow drift in the low frequency circuitry creates a serious problem, especially when making point-by-point measurements of small impedance changes.

Fortunately, at microwave frequencies, one can use impedance standards such as movable shorts. In this case, the response of the system to different positions of a movable short may be used to evaluate a set of error parameters characterizing the error network shown in Fig. 5.3. These error parameters are utilized to correct the measured results.

The error network representing the measurement system between planes CC' and AA' can be characterized by replacing the Impatt amplifier and its bias components at plane AA' (see Fig. 5.1) by a precision movable short as mentioned earlier. The error network of the measurement system has to be measured at each frequency and power level by recording the return gain and phase for different short positions. The reflection coefficient $\Gamma_{AA'}$ due to the RF short (Fig. 5.4) is transformed into an input reflection coefficient Γ_m through the error network. For a known error network, the functional dependence between Γ_m and $\Gamma_{AA'}$ has the form of a bilinear transformation [43]

$$\Gamma_m = \frac{AN\,\Gamma_{AA'} + BN}{CN\,\Gamma_{AA'} + 1} \tag{5.2}$$

where $\Gamma_{AA'}$ is the reflection coefficient at plane AA' due

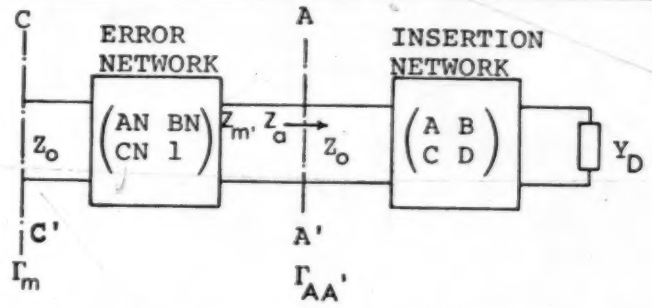

Fig. 5.3 Measurement system representation for evaluating the Impatt diode admittance.

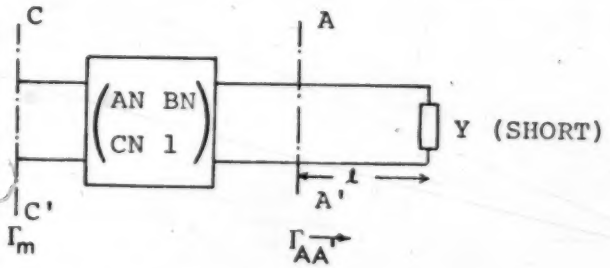

Fig. 5.4 Measurement system representation for evaluating error network parameters.

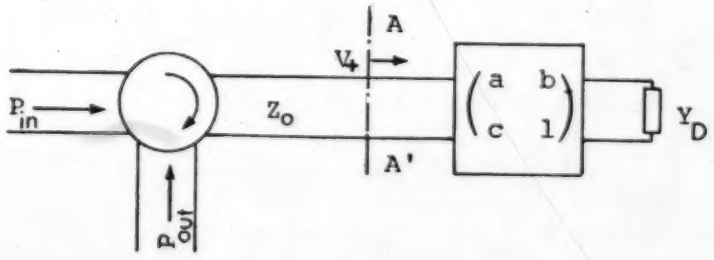

Fig. 5.5 Circuit of the reflection type amplifier.

to the sliding short circuit at a distance ℓ. It is given by

$$\Gamma_{AA'} = -e^{-2\ell(\alpha + j\beta)} \qquad (5.3)$$

where ℓ is the plunger position with respect to the reference plane AA',

α is the attenuation coefficient of the transmission line,

and β is the phase coefficient of the transmission line. However, available precision shorts behave almost ideally and therefore Eq. (5.3) may be simplified to

$$\Gamma_{AA'} = -e^{-j4\pi\ell/\lambda_g} \qquad (\alpha = 0) \qquad (5.4)$$

where λ_g is the guided wavelength.

There will be m equations of the type (5.2) corresponding to m positions of the short. Since each of the quantities AN, BN and CN are complex numbers, there are six unknowns to be determined. This could be accomplished by solving six independent equations derived from three separate measurements. Therefore, if a large number of measurements are taken to determine AN, BN and CN, systematic errors could be minimized by utilizing numerical optimization techniques. This can be achieved by considering three measurements and thus obtaining three equations from Eq.(5.2) and then using a numerical routine for arriving at the values of AN, BN and CN.

These values are then taken to initialize the optimization routine. It has been found that the optimized values of AN, BN and CN do not depend upon the choice of the initializing values.

The measurement system has been calibrated using the above procedure at various positions of the movable short for the frequencies 5.7, 5.9, 6.2 and 6.5 GHz. Figs. 5.6 and 5.7 show the measured reflection coefficient, Γ_m , and the corresponding adjusted and corrected values, $\Gamma_{AA'}$, for frequencies 5.7 and 6.5 GHz, respectively. It can be noted from the figures that the measured reflection coefficient values lie on the unity circle after correction. It may also be noted that the calibration procedure is frequency dependent as indicated by the value of the phase difference between the corrected and uncorrected results at the two extreme frequencies used, this phase difference being greater at the lowest frequency.

In order to evaluate the active Impatt diode admittance, the impedance determined at AA' is transformed to an imaginary plane at the semiconductor chip. This is done by the use of the a, b and c parameters which will be defined in the following section.

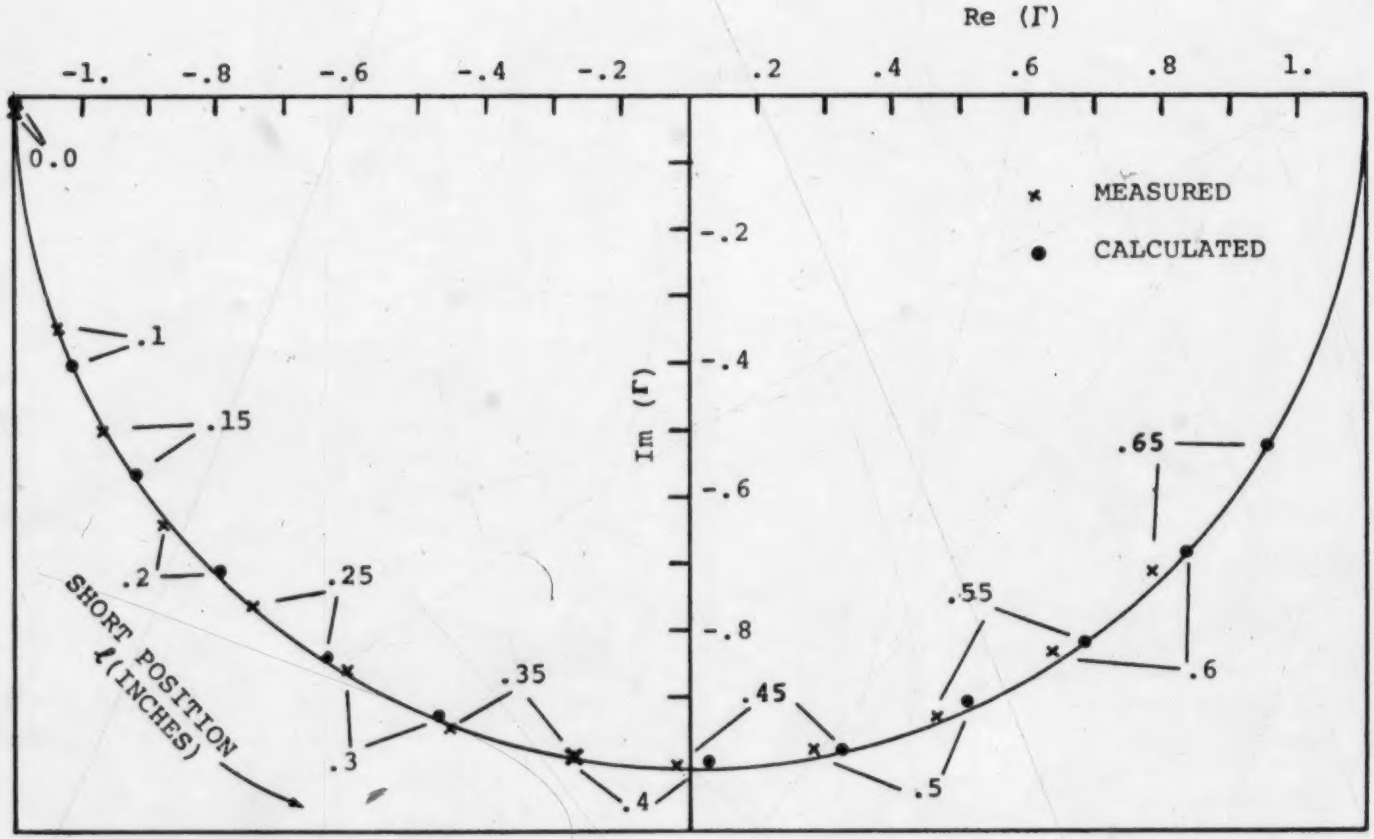

Fig. 5.6 The measured reflection coefficient, Γ_m, and the corresponding measured and corrected value $\Gamma_{AA'}$, using the AN, BN and CN parameters for various short positions at 5.7GHz (Diode #1).

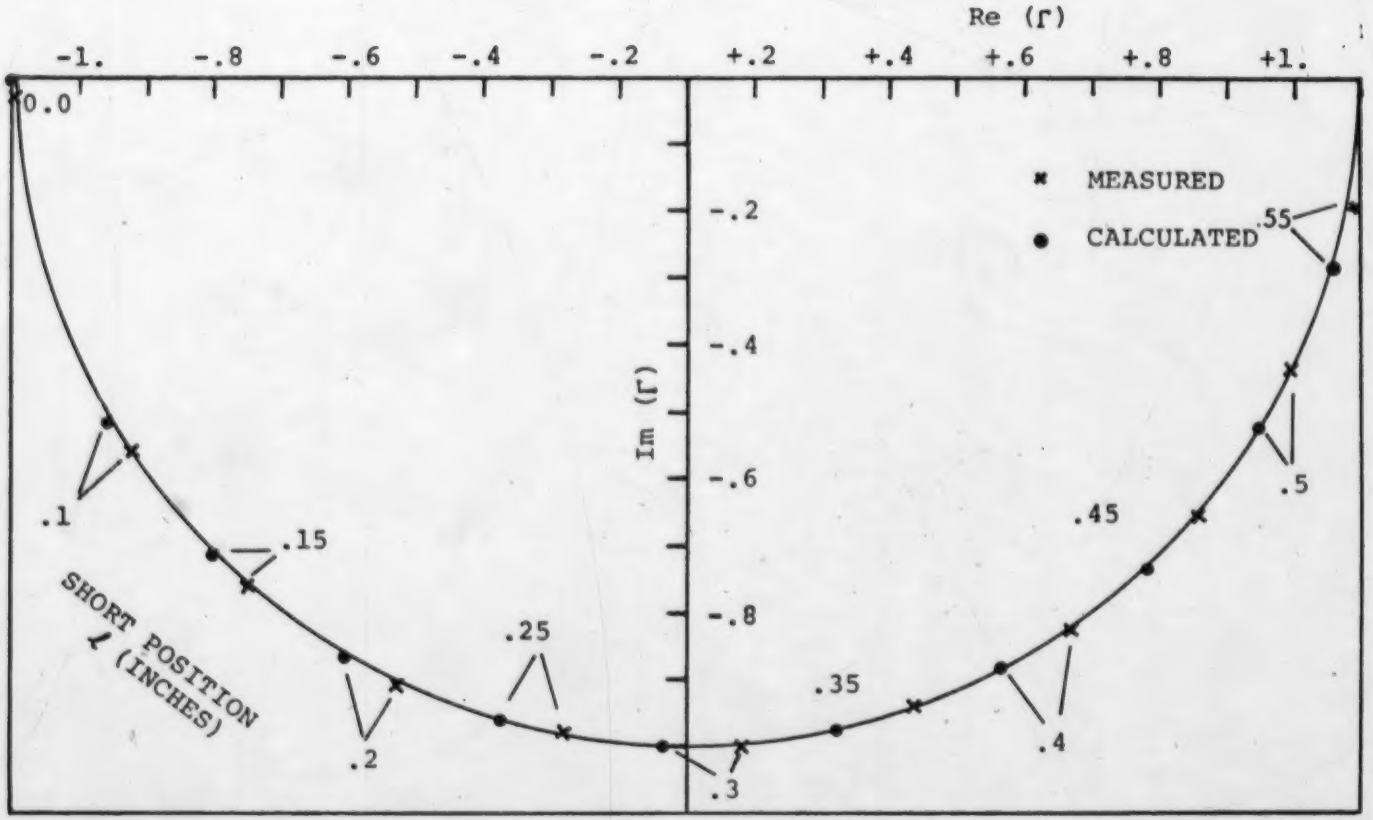

Fig. 5.7 The measured reflection coefficient, Γ_m, and the corresponding measured and corrected value $\Gamma_{AA'}$, using the AN, BN and CN parameters for various short positions at 6.5GHz (Diode #1).

5.4 Insertion network characterization

The insertion network may be fully characterized by three complex parameters a, b and c. Three terminations can be used to fully determine these parameters; also systematic errors in the measured results can be minimized by using a large number of terminations. However, replacing the diode by the other three terminations, viz., an open, a short or a known load, may change the diode RF conditions. In the case of the Impatt diode, impedance below breakdown voltage can be substituted for the above terminations as it has a known impedance for a given bias voltage.

When the bias voltage of the diode is smaller than V_b , the impedance Z_D of the active layer of an Impatt diode is given by

$$Z_D(V) = R_D(V) - j/\omega C(V)$$

$$= R_D(V) + jX_D(V) \qquad (5.5)$$

where $R_D(V)$ and $C(V)$ are the resistance of the unswept region and the bias voltage dependent capacitance, respectively. Both $R_D(V)$ and $C(V)$ decrease with the increase of the reverse bias voltage.

Generally, any two-port insertion network is characterized by the fundamental parameters A, B, C and D (Fig. 5.3) [44]. The transmission line characteristic

impedance is denoted as Z_o. The necessary circuit parameters are determined by measuring the normalized impedance Z_m, looking from the AA' plane towards the diode. Z_m is given by

$$Z_m = \frac{AZ_D + B}{Z_o(CZ_D + D)} \quad . \tag{5.6}$$

Four such equations are required to evaluate the A, B, C and D parameters. Since only reciprocal elements form the insertion network, Eq. (5.6) can be simplified to [37]

$$Z_m = \frac{aZ_D + b}{cZ_D + 1} \quad . \tag{5.7}$$

where

$$\begin{aligned} a &= A/(Z_o D) \\ b &= B/(Z_o D) \\ c &= C/D \\ 1 &= AD - CB = Z_o D^2 (a - bc) \quad . \end{aligned} \tag{5.8}$$

a, b and c can be determined by evaluating Z_D for three bias voltages (from the C-V characteristics below breakdown) and microwave impedance measurement of Z_m at the same three dc bias points. This procedure can be summarized as follows:

1. At various bias voltages below breakdown the capacitance of the diode wafer may be measured accurately with a Boonton 71 A, 1 MHz, capacitance bridge. The C-V

characteristics are thus determined for a range of bias voltages (V) between zero and just below breakdown. Fortunately, for Impatt diodes based on a one-sided abrupt p-n junction it is possible to evaluate the incremental change in the diode resistance [36] $\Delta R_D(j)$ (over a certain bias range below breakdown voltage) as a function of bias voltage with the help of the C-V characteristics. The incremental change (ΔR_D) of the diode resistance which corresponds to the change of voltage ΔV (in the interval designated j, $\Delta V = V_{j+1} - V_j$) has been expressed by [36]

$$\Delta R_D(j) = \varepsilon \rho(j) \left(\frac{1}{C(V_j)} - \frac{1}{C(V_{j+1})} \right) \qquad (5.9)$$

where

$\rho(j)$ is the diode wafer resistivity in the interval j,j+1,

ε is the dielectric constant (ε = 1.036 pF/cm for Si [36]),

$C(V_j)$ and $C(V_{j+1})$ are the diode wafer capacitances at bias voltage of V_j and V_{j+1}, respectively.

The resistivity $\rho(j)$ for n-type Si (in units Ω.cm) is approximated using the expression [45]

$$\ln \rho(j) = 28.3637 - 0.7861 \ln N_x(j) \qquad (5.10)$$

where

$$N_x(j) = \frac{k (C_{av})^3 \Delta V}{D^4 \Delta C} \ (cm^{-3}) \qquad (5.11)$$

and

$$C_{av} = \frac{1}{2}(C_j + C_{j+1}) \qquad \text{(pF)}$$

$$\Delta C = C_j - C_{j+1} \qquad \text{(pF)}$$

$$\Delta V = V_{j+1} - V_j \qquad \text{(volts)}$$

D = junction diameter (cm)

k = a constant = 9.91×10^{30} for Si

$N_x(j)$ = impurity concentration in (j+1,j) interval.

The approximations are valid for $5 \times 10^{16} > N_x > 5 \times 10^{17}$. This range is appropriate for diodes intended for normal Impatt mode operation at frequencies in the 3 to 8 GHz range. At each bias interval j, there will be a specific $N_x(j)$ and $\rho(j)$, for which $\Delta R_D(j)$ is determined. For the p^+-n-n^+ abrupt junction Impatt, the diode resistance R_D can be assumed approximately zero ohms at a bias sufficiently close to break down. Taking this resistance as a reference and extrapolating in terms of ΔR_D, it is possible to arrive at the value R_D corresponding to any bias voltage. Therefore, the diode impedance Z_D ($Z_D = R_D + jX_D$) can be evaluated at different bias voltages. Fig. 5.8 shows X_D and R_D as functions of the bias voltage for one of the diodes used in the measurements.

2. Reflection measurements are then made at the same bias voltages at the desired microwave frequency. From

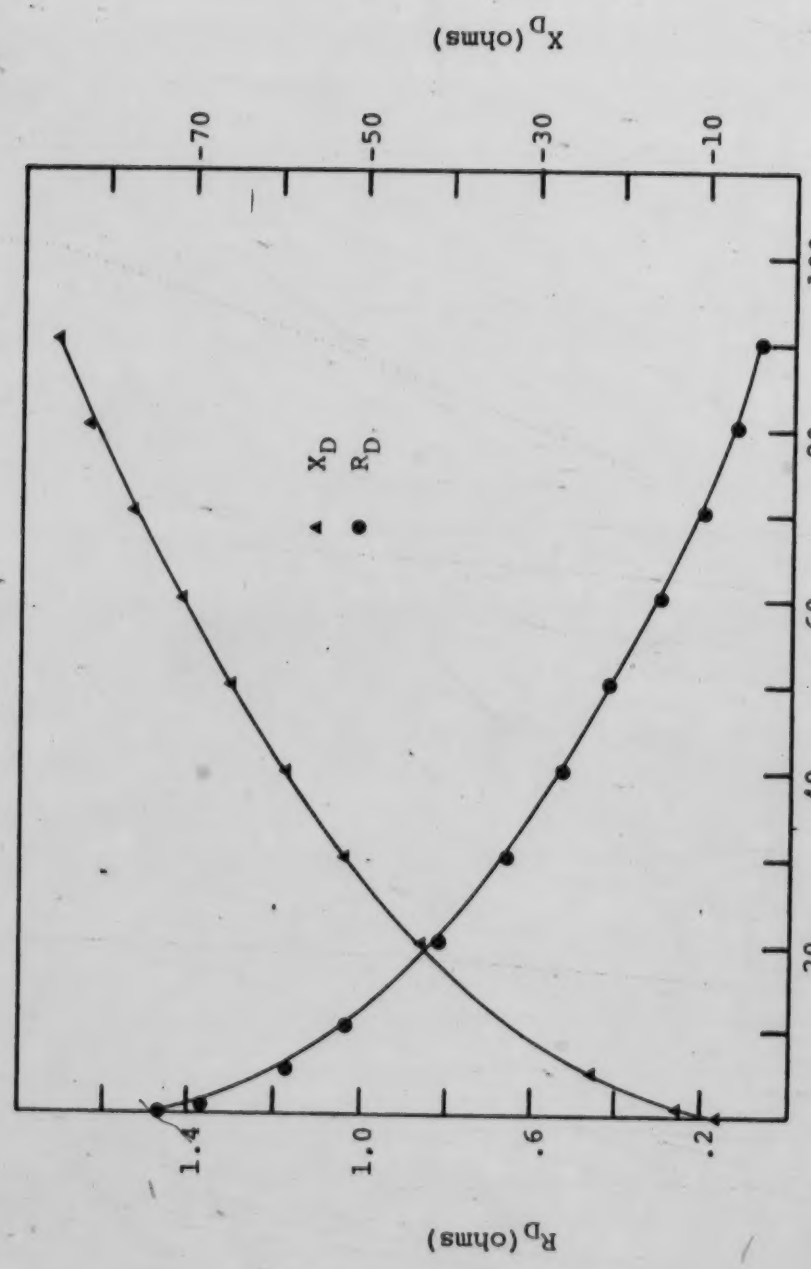

Fig. 5.8 Real and imaginary parts of Impatt diode impedance ($Z_D=R_D + jX_D$) as a function of bias voltage ($V<V_b$) at 5.7GHz for diode #1.

these measurements, Z_m as a function of the dc bias may be determined.

Once the a, b and c parameters (of the insertion network) are known, the Impatt electronic admittance and the RF voltage across the diode can be obtained as outlined in the following section.

5.5 Determination of the diode admittance and RF voltage [37]

When the bias voltage becomes larger than V_b, the diode is characterized by an admittance Y_D with a negative real part, and the circuit of Fig. 5.5 can be operated as a reflection type amplifier. The normalized impedance Z_a of the diode (normalized to the characteristic impedance Z_o of the transmission line) can be measured as a function of input RF signal levels. The electronic admittance Y_D is then given by

$$Y_D = (cZ_a - a)/(b - Z_a) = -G_D + jB_D \quad . \qquad (5.12)$$

The RF voltage v_{RF} applied across Y_D, the diode admittance, can be calculated as follows. Using the boundary condition at AA' plane, Fig. 5.5, and the definition of the A, B, C and D parameters, the following equations are derived [37]

$$V_+ = \frac{1}{2}(DZ_o + B)\left(\frac{A + Z_oC}{DZ_o + B} + Y_D\right) v_{RF} = \frac{1}{2} DZ_o(b+1)\left(\frac{a+c}{b+1} + Y_D\right) v_{RF}$$

$$P_{in} = \frac{1}{2}|V_+|^2/Z_o = \frac{1}{8} Z_o|D|^2|(b+1)Y_D+a+c|^2|v_{RF}|^2 \qquad (5.13)$$

where V_+ is the voltage amplitude of the incident wave at the AA' plane. Substituting Eq. (5.8) into Eq. (5.13), v_{RF} is obtained

$$v_{RF} = (8|a-bc|P_{in})^{\frac{1}{2}}|a+c+(b+1)Y_D| \quad . \qquad (5.14)$$

Using Eq. (5.12) and Eq. (5.14), Y_D as well as v_{RF} are calculated.

5.6 Evaluation of the passive circuit admittance

To perform dynamic studies on Impatt diode oscillators, both the active device admittance and the passive circuit admittance seen by the diode are to be evaluated. In this section, the measurement of the admittance of the embedding circuitry, to be treated in Chapter VII, will be discussed. The methods developed to obtain the parameters of the matrices characterizing the two networks are repeated here. But in evaluating the latter network, the oscillator under consideration is to be placed at plane AA' (Fig. 5.1). Once these parameters are derived, then, by transformation of the 50 ohm characteristic impedance of the line, Z_o, to the plane AA', the passive circuit admittance can be determined at the frequencies of interest. Thus the circuit admittance is given by

$$Y_c = \frac{cZ_o + a}{Z_o + b} \quad . \qquad (5.15)$$

5.7 Experimental procedure

These measurements involve the determination of large-signal Impatt diode admittances together with the admittance parameters of its associated passive circuitry in a practical oscillator (to be treated in Chapter VIII). The active measurements are performed over a range of power levels between -20 dBm and 23 dBm and at a number of frequencies lying between 5.7 GHz to 6.5 GHz. A diode RF voltage range of 0.5 to 25 volts corresponds to the power levels mentioned above. The two diodes, Hp 5082-0437 and Hp 5082-0431, used in the measurements have a junction area of 10^{-4} cm^2 as obtained with microscopic measurements of the diameters of several damaged diodes taken from the same manufactured batch.

The capacitance measurements at 1 MHz (C-V characteristics) are made using a Boonton meter, a diode mount with an APC-7 precision connector, a digital meter and a high resolution dc-power supply. The measured capacitance is that of the wafer plus the diode package. The package capacitance is accounted for by initially adjusting the Boonton meter to zero with an empty package placed in a specially designed diode mount. Measurements are typically made at thirteen voltages in the range from zero to 100 V (100 V is slightly less than V_b). Fig. 5.9 shows the behaviour of the junction capacitance with bias voltage for the two diodes. The junction

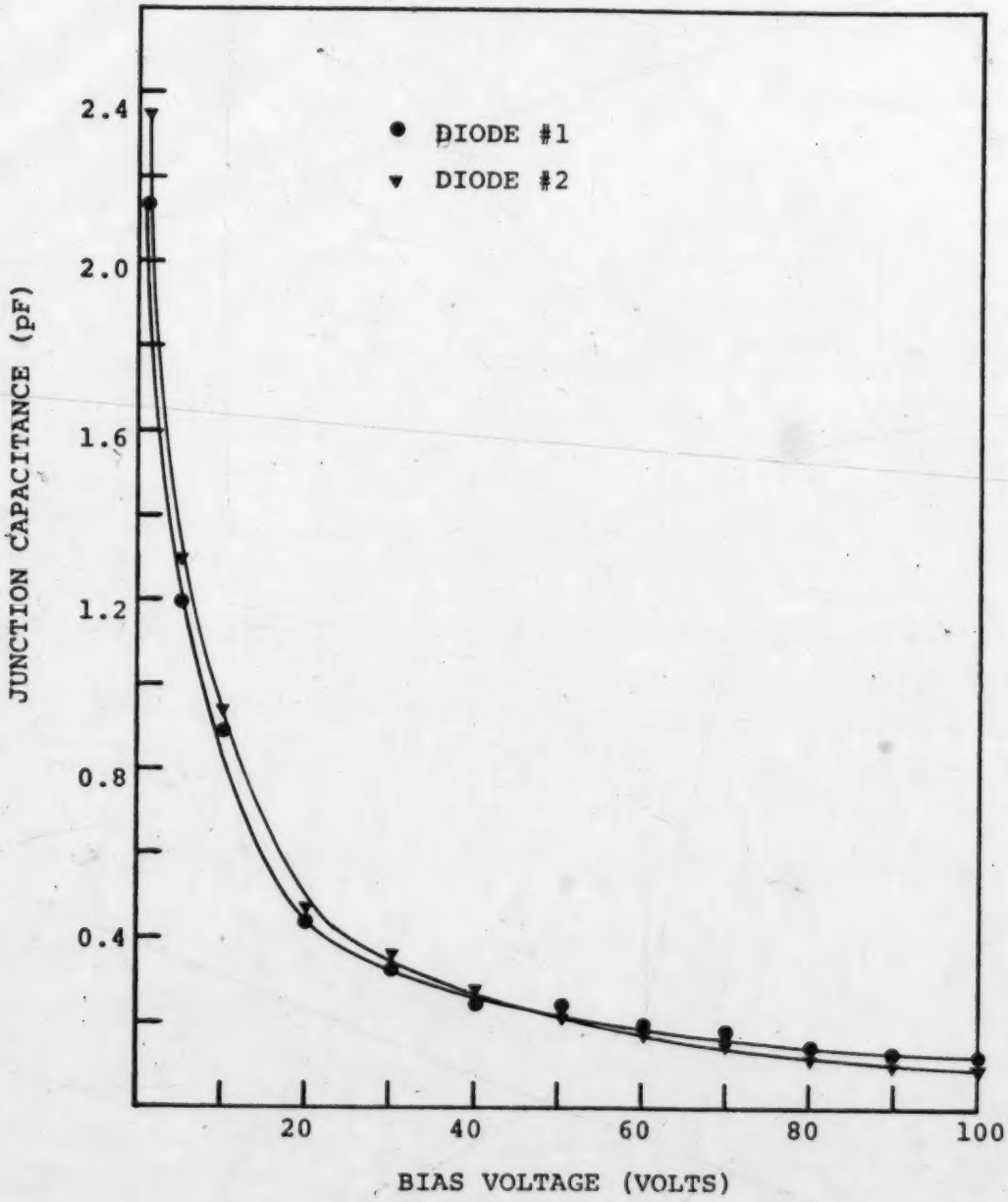

Fig. 5.9 C-V characteristics of Impatt diodes #1 & #2.

capacitances at 100 volts are .31 pF for diode #1 and .289 pF for diode #2.

Reflection measurements with the network analyzer are carried out at a specific frequency and at several power levels between -20 dBm and 23 dBm, as follows.

1. Characterization of the error network, at the desired frequency is done at 0 dBm only, because it is experimentally found to be independent of the power level used. With the precision movable short placed at a plane AA' (Fig. 5.1), reflection coefficients are recorded for thirteen positions of the short. This data is used to determine the AN, BN and CN parameters of the network.

2. For microwave measurements below and above breakdown, the Impatt amplifier is tuned to the proper frequency. This is done by replacing the movable short at plane AA' with the Impatt amplifier. The klystron and the TWT amplifier are replaced by a sweep oscillator (4-8 GHz) for swept frequency measurements. The diode parasitics are tuned to the desired frequency by changing the position of the slug until a gain of about 10 dB is observed on the phase gain display of the network analyzer. Then the measurement system is returned to its original arrangement with the klystron source and TWT amplifier replacing the sweep oscillator. The system is then left to stabilize (for at least one hour) at

the desired power level and frequency.

3. Reflection measurements are made with the values of voltages ($V < V_b$) being the same as those utilized in the determination of the diode C-V characteristics. The data obtained are combined with the diode impedances as calculated from the C-V measurements in order to determine the a, b and c parameters of the insertion network. It should be mentioned that for each measurement, the return gain and phase are recorded, once for the RF signal directed into the diode and then again for the signal reflected back from the RF short (by using the RF switch). This procedure enables the correction of each measurement to the reference RF short. In this case, the drift in the measurement due to the low frequency circuitry within the network analyzer is minimized.

4. The diode bias voltage is then increased to a value above the breakdown for which a suitable dc current is established. The RF power into the diode is varied between 23 dBm and -20 dBm (which is within the capability of the Hp diodes used), and the return gain and phase are recorded.

5. Steps 1 to 4 are repeated at the frequencies of interest.

6. The results are then processed by a computer program (see Appendix 1) in order to evaluate the active admittance of the Impatt diode (Eq. (5.12)) and the

corresponding RF voltage amplitude across this diode (Eq. (5.14)).

However, in order to evaluate the passive circuit admittance seen by the diode embedded in a practical oscillator, the experimental procedure (developed above to evaluate the parameters of the two networks) is repeated. But, in evaluating the insertion network parameters, the Impatt amplifier is to be replaced by the oscillator under consideration and the microwave measurements taken below breakdown voltages are to be performed at a power level of -20 dBm. This power level is adequate, since passive measurements are independent of the power level used.

5.8 Discussion of results; examination of sources of error

The junction conductances and susceptances for the two diodes as a function of the RF voltage amplitude and frequency are shown in Figs. 5.10(a) and 5.11(a). This representation is useful in the characterization of Impatt diode oscillator and amplifier circuits. These curves have shapes similar to those predicted by both the theoretical studies [28,38] as well as the experimental results published for Si diodes [36,46]. These also resemble the curves obtained by Bracket [32] for the small-signal admittance of Germanium diodes

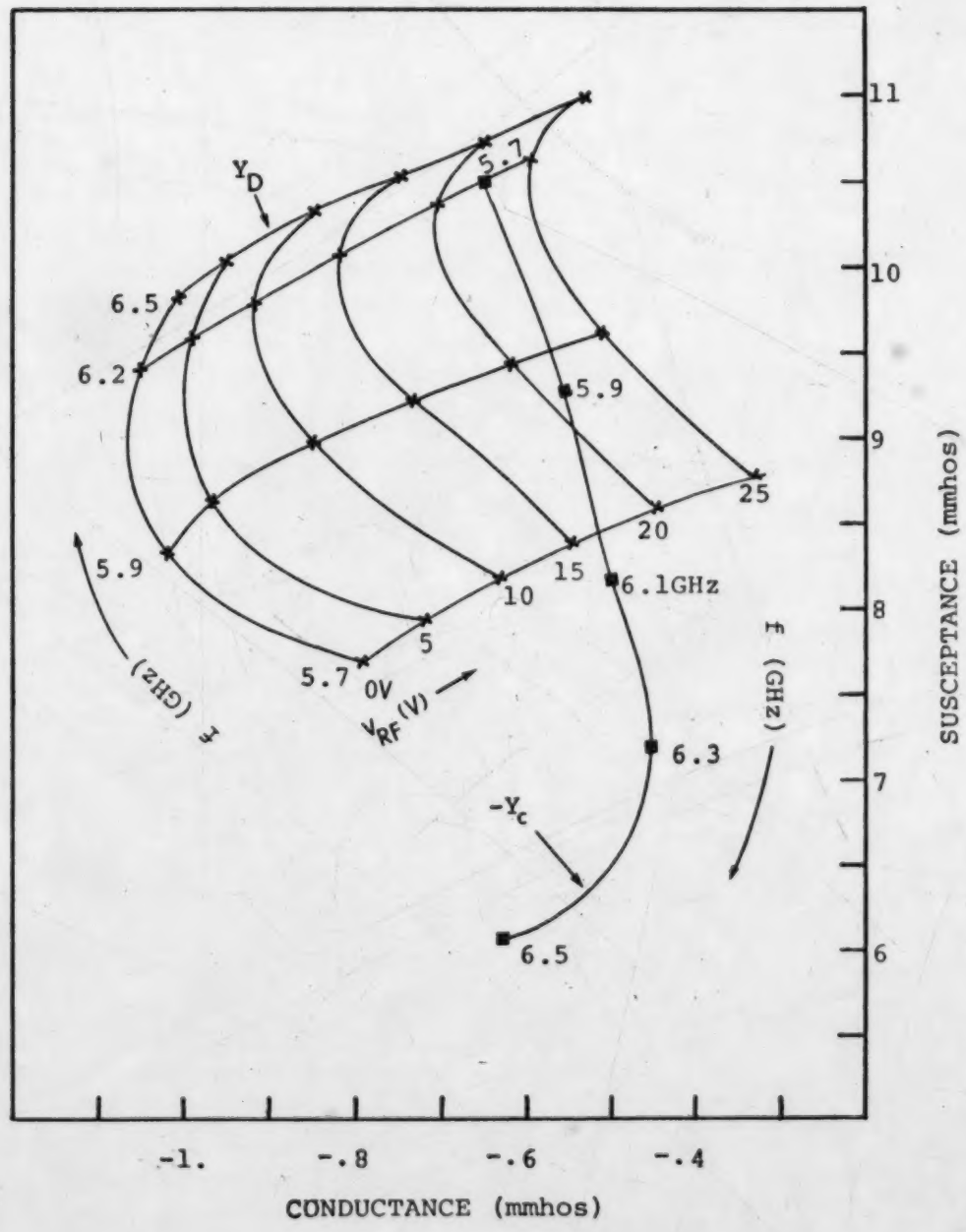

Fig. 5.10 (a) Large signal admittance, Y_D, of Impatt diode #1 as a function of RF voltage and frequency at constant dc current of 25mA.
(b) Circuit admittance, Y_c, as a function of frequency, as seen by the diode embedded in a 7 mm coaxial resonator.

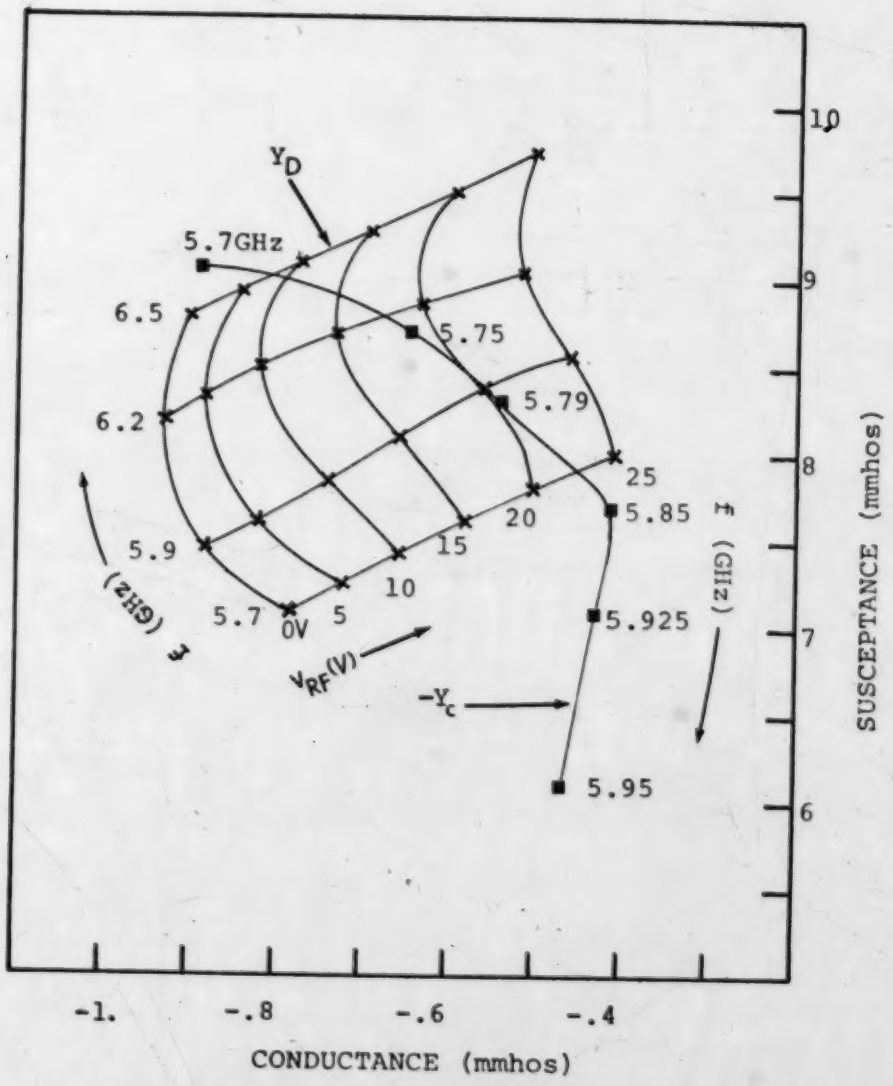

Fig. 5.11 (a) Large signal admittance, Y_D , of Impatt diode #2 as a function of RF voltage and frequency at constant dc current of 25mA.
(b) Circuit admittance, Y_c , as a function of frequency, as seen by the diode embedded in a 7 mm coaxial resonator.

(see Fig. 4.8). In Figs. 5.10(a) and 5.11(a), the wafer susceptance is seen to increase with increasing RF voltage , whereas the negative conductance of the diode decreases. The latter effect can be observed on the characteristics showing the dependence of the diode conductance on the RF voltage (Fig. 5.12 for diode #2). This criterion results in an observed decrease in the efficiency of RF power generation. In oscillator design, there is a trade off between the RF voltage level obtainable and the diode efficiency. It can also be noted that the decrease in negative conductance with the increase in RF voltage constitutes the basis of stability in oscillators (refer to Chapter III). Figs.5.10(b) and 5.11(b) show the circuit admittance seen by the diode vs frequency when the diode #1 and #2 respectively are embedded in the oscillator to be developed in Chapter VIII.

It was mentioned in Section 5.3 that measurement errors arise in the course of microwave experiments. The errors associated with the measurement technique can be divided into two categories:

1. The measured data
2. The network solution.

In the first category, the main errors are due to the inaccuracy in the measurement of the diode C-V characteristics. It has been estimated that the reflection

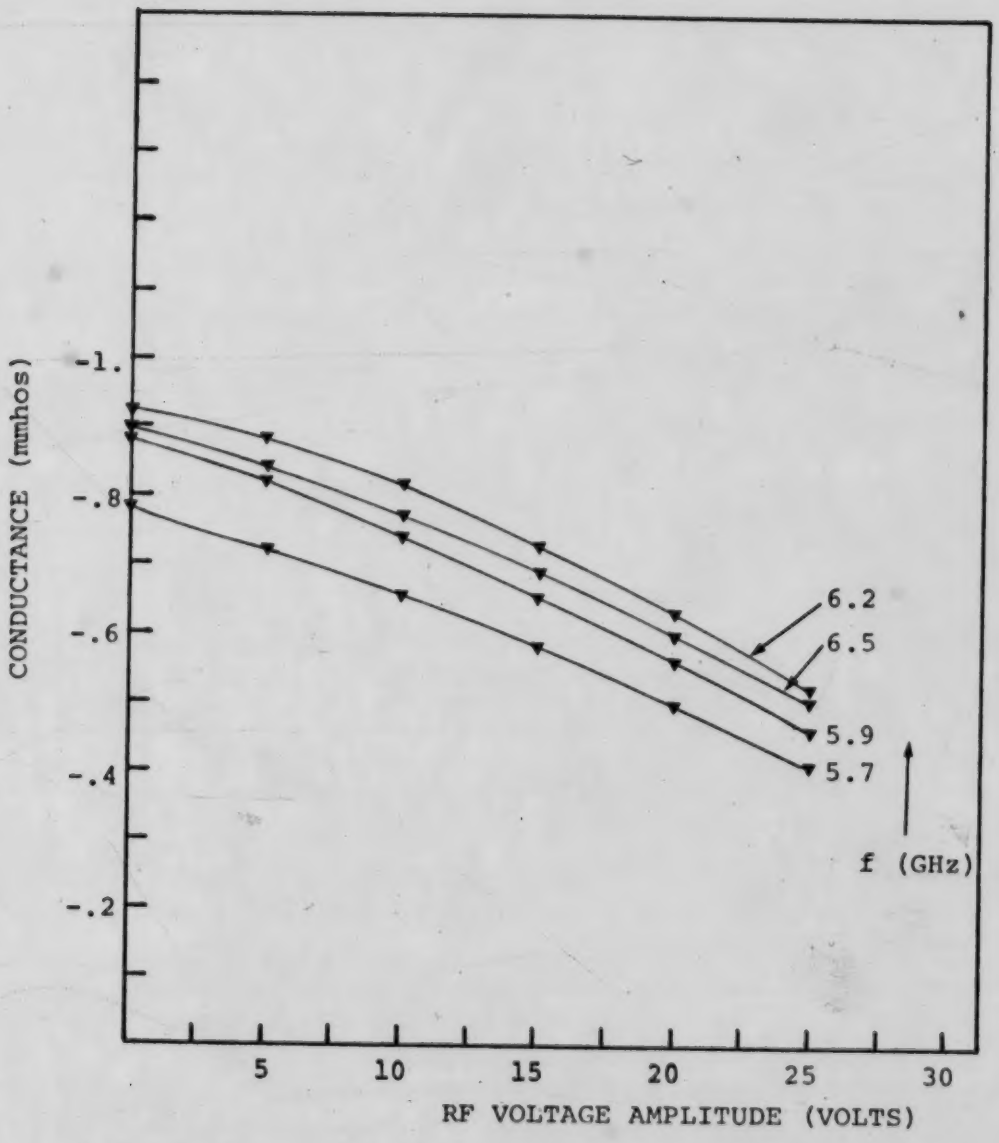

Fig. 5.12 Diode negative conductance as a function of RF voltage amplitude for various fixed frequencies for diode #2 (I_{dc} = 25mA).

Table 5.1. Effect of errors on the measured conductance and susceptance due to a change of 0.04 dB in return gain, RG, and 0.25° in phase for diode #1 at 5.9 GHz

RF voltage (V)	Measured values		A change in RG = 0.04 dB				A change in phase = 0.25°			
	Cond.	Susc.	Cond.	% Errors	Susc.	% Errors	Cond.	% Errors	Susc.	% Errors
1.916	-1.01209	8.50129	-1.01232	0.0	8.50072	0.0	-1.01156	0.0	8.50166	0.0
9.356	-.86333	8.89087	-.86476	0.17	8.8890	0.0	-.86159	0.2	8.88949	0.1
15.6	-.70985	9.24005	-.71295	0.4	9.23767	0.0	-.70762	0.3	9.23709	0.03
26.36	-.47990	9.63517	-.48554	1.2	9.63325	0.0	-.47812	0.4	9.62982	0.06

Table 5.2. Measured microwave impedance, Z_m, and the same calculated using the evaluated a, b and c parameters at plane AA' of Fig. 5.3 (for diode #1 at 5.9 GHz).

Bias voltage ($V < V_b$)	Normalized measured Z_m at AA'		Calculated Z_m using a, b and c parameters at plane AA'			
	$Re(Z_m)$	$Im(Z_m)$	$Re(Z_m)$	% Error	$Im(Z_m)$	% Error
0	0.07821	1.06611	0.07862	0.5	1.06568	0.04
20	0.07826	0.96609	0.07863	0.5	0.96532	0.08
60	0.08048	0.80312	0.0812	0.9	0.80420	0.13
100	0.08891	0.59944	0.08923	0.4	0.60008	0.1

measurement data are accurate to within 0.04 dB in return gain values and 0.25° in phase values. For typical diodes biased at I_{dc} = 25 mA (Table 5.1), errors of this magnitude result in conductance and susceptance errors of about 2%. For each measurement of the return gain and phase, the error due to the instrument drift has been minimized by first making a measurement and then calibrating by switching over to an RF reference short circuit. Evaluation of the network parameters (AN,... and a,...) based on either the calculated reflection coefficients ($\Gamma_{AA'}$) for the evaluation of the error network, or impedances, (insertion network) results in an error in the value of these parameters by not more than 3% (Table 5.2). Table 5.2 shows Z_m, the measured normalized impedance along with the corresponding values calculated by using the a, b and c parameters in Eq. (5.7). Thirteen microwave measurements together with the corresponding evaluated Impatt impedances below breakdown are used to obtain the optimized a, b and c parameters of the insertion network. When twelve or even eleven, rather than thirteen microwave measurements were used to evaluate these parameters and then in turn used to calculate the microwave impedances at the drop out points, no effect could be detected in the measured conductances and susceptances up to the seventh decimal place.

The effect of the error due to inaccurately measuring the diode C-V characteristics is demonstrated by considering diode #1 as an example. The diode admittance at 5.9 GHz is then evaluated, first by using the measured C-V characteristics, then for 95% of the ordinate values, and finally by considering 90% of the ordinate values. Figs. 5.13, 5.14 and 5.15 show the effect of the error in the C-V characteristic on the measured diode conductance, susceptance and admittance, respectively. It can be noted from these figures that, generally, the values of susceptance and conductance decrease on reducing the capacitance values in the diode C-V characteristics. A computed error in the susceptance values of about 5% in the 95% case and 10% for the 90% case is obtained from the graphs of Fig. 5.14. The uniformity in the amount of error obtained for the span of the RF voltages considered is due to the small change in diode susceptances in this range ($\sim$1.2 times).

At this point it must be emphasized that the above example is for demonstration purposes only. In practice, a typical expected error in the C-V characteristics obtained through experimental measurements is not greater than 0.05 pF. Such an error arises due to the use of an empty package to compensate for the value of C_p. This error does not result in a corresponding error of more than 2% in the measured diode conductance and

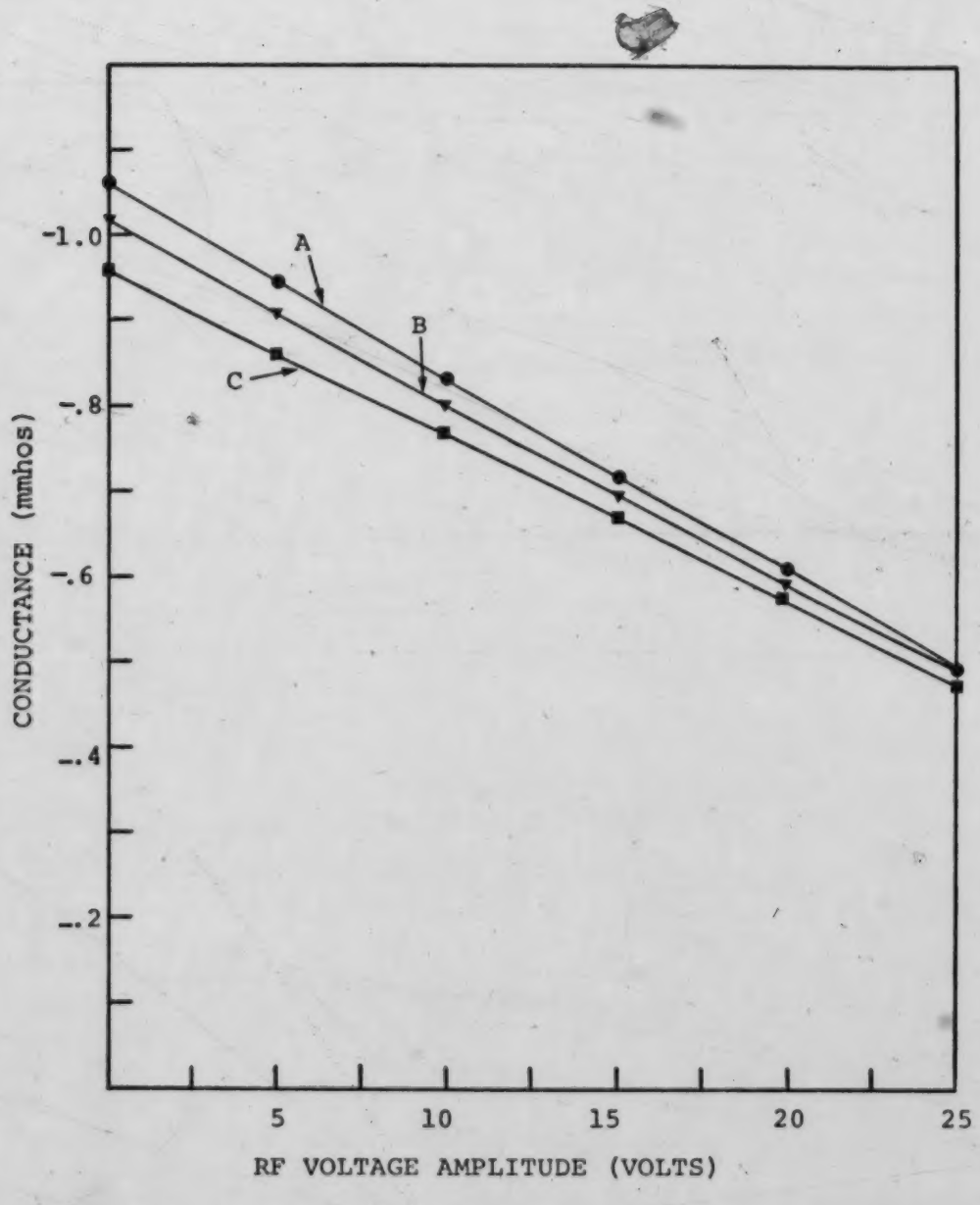

Fig. 5.13 The effect of errors in the C-V measurements on the measured diode conductance vs. RF voltage curves at 5.9GHz (diode #1). Deduced conductance based on:
(A) measured diode capacitances,
(B) on 95% of the measured diode capacitances,
(C) on 90% of the measured diode capacitances.

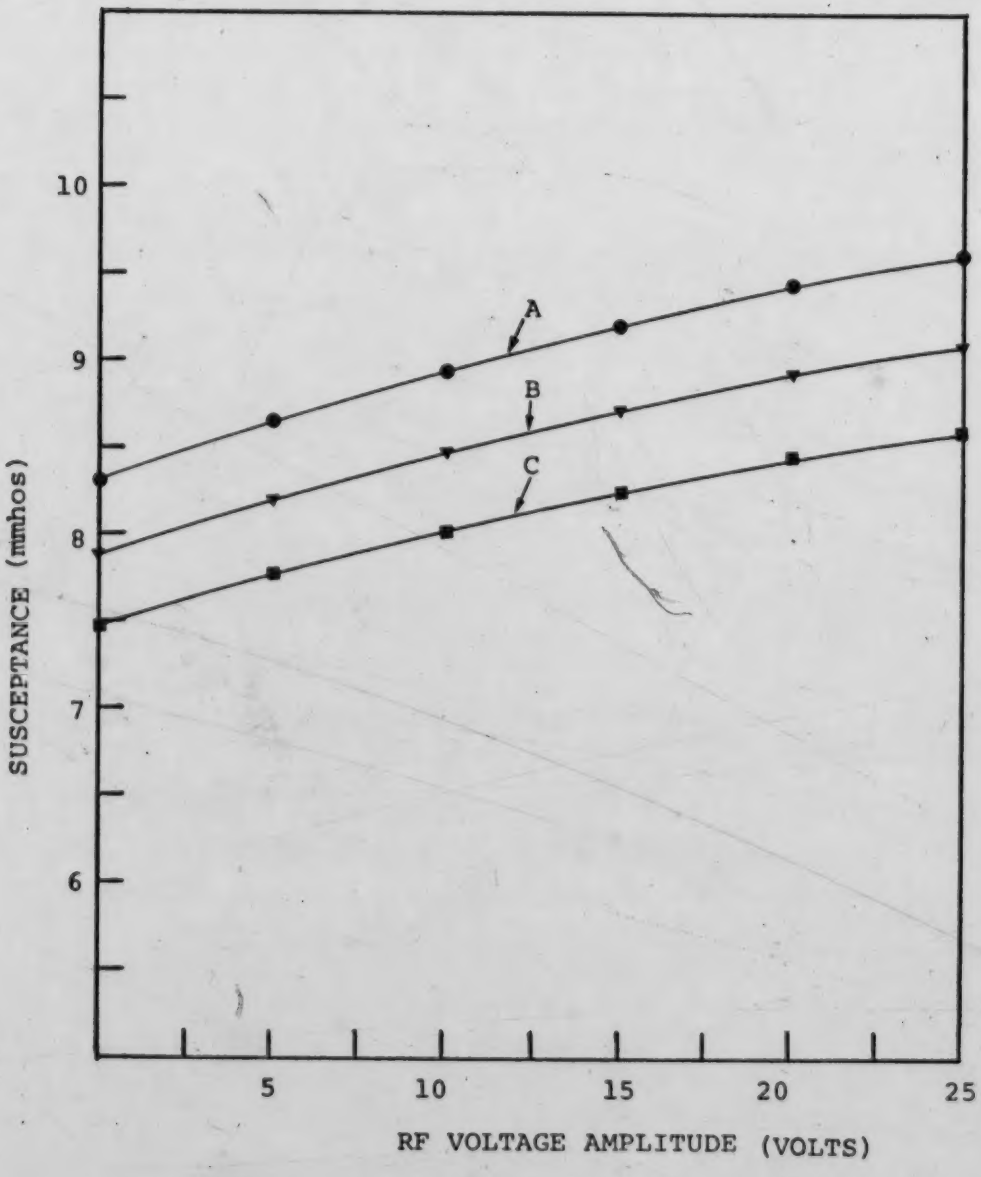

Fig. 5.14 The effect of errors in the C-V measurements on the diode susceptance vs. RF voltage curves at 5.9GHz (diode #1). Deduced susceptance based on:
(A) measured diode capacitances,
(B) on 95% of the measured diode capacitances,
(C) on 90% of the measured diode capacitances.

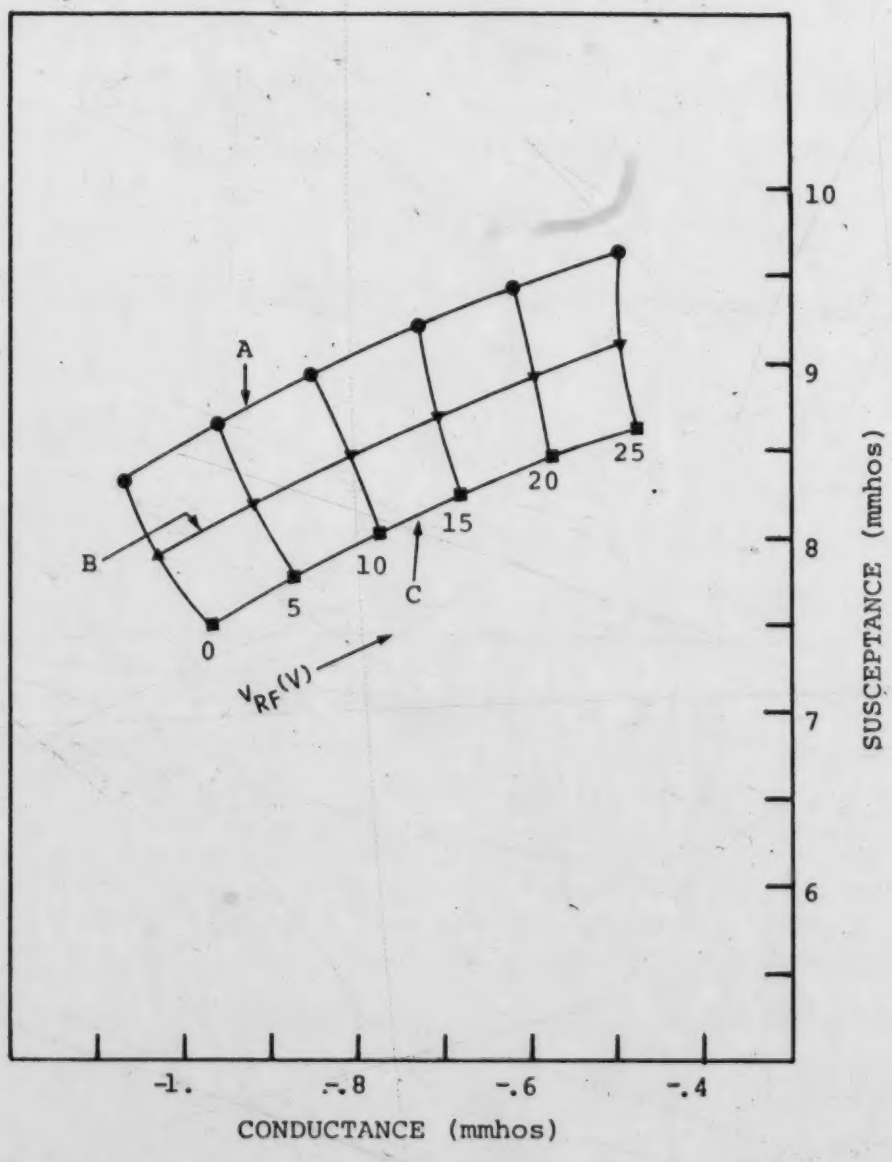

Fig. 5.15 The effect of errors in the C-V measurements on the measured diode admittance vs. RF voltage curves at 5.9GHz (diode #1). Deduced admittance based on:
(A) measured diode capacitances,
(B) 95% of the measured diode capacitances,
(C) 90% of the measured diode capacitances.

susceptance.

Since the errors in the method of measurement are independent of each other, the cumulative error is likely to be of the order of 12%.

CHAPTER VI

INSTANTANEOUS POWER AND FREQUENCY MEASUREMENTS

6.1 Basic principles of instantaneous power and frequency systems

In order to compare the theoretically computed oscillator transients with those experimentally predicted, an instantaneous frequency and amplitude measuring system is required. Since measurements are carried out in the microwave frequency range, the system required must be capable of measuring signals with nanosecond changes of power and frequency.

The present instantaneous frequency measuring systems [47] are more or less complex versions of phase discriminators [48-51]. In all microwave phase discriminators [48], Fig. 6.1, the measured signal is divided by a power splitter (either a 3-dB hybrid or hybrid tee) into two channels commonly consisting of two transmission lines of different electrical length βL_1 and βL_2 (β represents the frequency-dependent phase constant of the lines). The signals from the outputs of the two channels are then combined in a power combiner (usually similar to a power splitter). Because of the signal interference, the envelope of the output signal is proportional to the amplitude and frequency of the measured signal. Square-law detection, unity

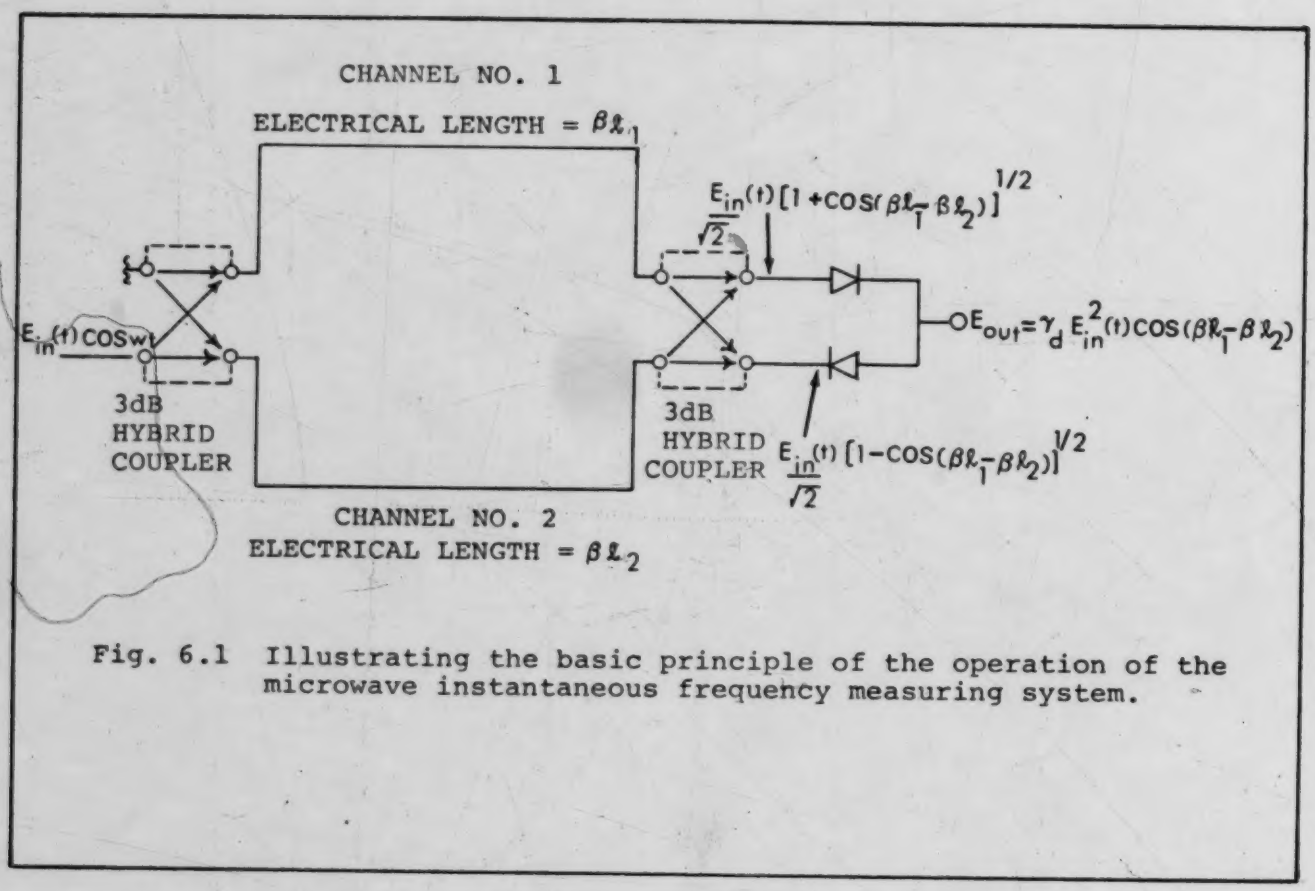
CHANNEL NO. 1
ELECTRICAL LENGTH = βℓ1
E_in(t) [1 + cos(βℓ1 − βℓ2)]^1/2 / √2
E_in(t) cos ωt
3dB HYBRID COUPLER
3dB HYBRID COUPLER
E_in(t) [1 − cos(βℓ1 − βℓ2)]^1/2 / √2
E_out = γ_d E_in^2(t) cos(βℓ1 − βℓ2)
CHANNEL NO. 2
ELECTRICAL LENGTH = βℓ2

Fig. 6.1 Illustrating the basic principle of the operation of the microwave instantaneous frequency measuring system.

VSWR (assumed for calculation convenience) results in a net output voltage [48]

$$E_{out} = E_{d_1} \pm E_{d_2} = \gamma_d E_{in}^2(t) \cos \beta (\ell_1 - \ell_2) \quad (6.1)$$

where $E_{in}(t)$ is the voltage amplitude of the measured signal and γ_d is the diode voltage sensitivity (matched diodes are assumed).

However, these systems have several disadvantages which can be summarized as follows:

(1) The need for cutting and mounting two rigid transmission lines with different accurately defined lengths.

(2) A new piece of transmission line is required for any slight adjustments, or a change in the center frequency.

(3) When using two magic tees as power combiners or splitters a complicated geometry has to be used. This results in higher VSWR values which degrade the performance of the system.

Instantaneous frequency measuring systems are usually complex and expensive. In commercial instantaneous frequency measuring systems, where cost and circuit complexity are not the limiting factors, the above mentioned problems are less important. If one does not need the sophisticated features of the expensive instantaneous frequency measuring systems, the novel

frequency discriminator, which has been developed during this study, gives all needed information with minimum requirements on microwave components. Principles of operation of the new discriminator together with its characteristics and calibration procedures are described in this chapter.

6.2 Single hybrid tee discriminator: principle of operation

The single hybrid tee discriminator [52] is schematically shown in Fig. 6.2. It consists of an ordinary hybrid tee, a transmission line terminated by a movable short circuit, and two crystal detectors which match and terminate the E- and H-arms of the tee. The principle of operation is also simple. The measured signal, represented by an incident normalized wave a_1, enters the hybrid tee via the 1 arm and is split, almost equally, into the H, E, and 2 arms giving rise to emerging waves b_{13}, b_{14}, b_{12} and b_{11}. The wave b_{12} enters the auxiliary transmission line and travels a distance ℓ before being reflected by the line short circuit. The incident wave returning to the hybrid tee via the 2 arm, is given by

$$a_2 = -b_{12} \exp(-2j\beta\ell) \qquad (6.2)$$

where b_{12} is the total wave emerging from the 2 arm and β is the frequency-dependent phase of the transmission

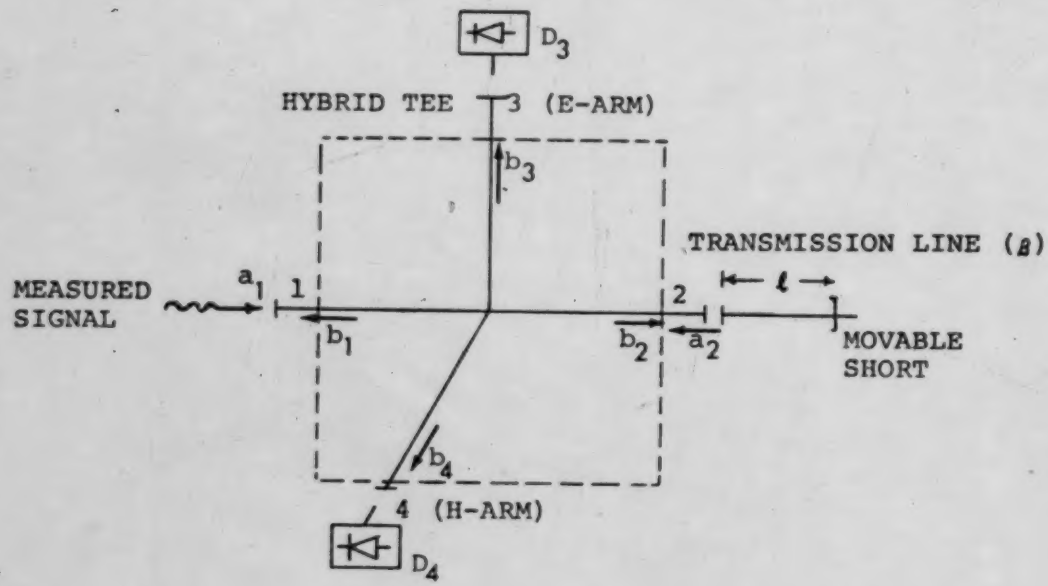

Fig. 6.2 Single hybrid tee frequency discriminator.

line. The a_2 wave undergoes similar splitting as the wave a_1 giving rise to emerging waves b_{23}, b_{24}, b_{21} and b_{22}. Since the phase difference of the waves b_{13} and b_{23} depends on the factor $(2\beta\ell)$, the waves in the E- and H-arms interfere. The envelope of the signals emerging from the E- and H-arms thus depends on the amplitude and frequency of the measured signal.

A scattering matrix representation is used for quantitative description of the discriminator properties. Because of the isotropy and symmetry conditions, the scattering parameters of the hybrid tee satisfy [53]

$$S_{ij} = S_{ji} \quad (i,j = 1,2,3,4);\ S_{14} = S_{24};\ S_{13} = -S_{23}. \tag{6.3}$$

Assuming an incident normalized wave a_1, match terminated E- and H-arms and match termination of the 2 arm for the wave a_2, waves emerging from the 1, 3 and 4 arms are

$$b_1 = a_1[S_{11} - DS_{12}^2 \exp(-j2\beta\ell)] \tag{6.4}$$

$$b_3 = a_1 S_{13}[1 + DS_{12} \exp(-j2\beta\ell)] \tag{6.5}$$

$$b_4 = a_1 S_{14}[1 - DS_{12} \exp(-j2\beta\ell)] \tag{6.6}$$

where $D = [1 + S_{22}\exp(-j2\beta\ell)]^{-1} \simeq |D|\exp j\phi \simeq 1$. Assuming square-law detection, the discriminator net output voltage is

$$E_{out} = E_{d_3} - E_{d_4}$$

$$= E_{in}^2(t) < (\gamma_{d_3}|S_{13}|^2 + \gamma_{d_4}|S_{14}|^2)|D||S_{12}| 2\cos(2\beta\ell - \phi_{12} - \phi)$$

$$+ (\gamma_{d_3}|S_{13}|^2 - \gamma_{d_4}|S_{14}|^2)(1+|D|^2|S_{13}|^2) > \qquad (6.7)$$

where γ_{d_3} and γ_{d_4} are voltage sensitivities of the diodes D_3 and D_4 and ϕ_{12} is the phase angle of the S_{12} vector. The input VSWR of the discriminator, which can be evaluated from Eq. (6.4), varies in the limits

$$\frac{1 - |S_{11}| + |D||S_{12}|^2}{1 + |S_{11}| - |D||S_{12}|^2} < \text{VSWR} < \frac{1 + |S_{11}| + |D||S_{12}|^2}{1 - |S_{11}| - |D||S_{12}|^2} \qquad (6.8)$$

depending on the signal frequency and the length of the transmission line.

The discriminator output voltage depends on the S_{12} parameter according to Eq. (6.7). Since the amplitude of the S_{12} parameter for a lossless waveguide E-H tee is related to the reflection coefficients of the 1, 3, and 4 arms by [54]

$$|S_{12}|^2 = \frac{|S_{33}|^2 + |S_{44}|^2}{2} - |S_{11}|^2 , \qquad (6.9)$$

only nonmatched hybrids, usually characterized by $|S_{33}| > 0.2$ and $|S_{44}| > 0.2$, will provide a useful sensitivity. Scattering parameters of a typical hybrid tee depend very little on frequency in a sub-gigahertz

bandwidth (e.g., in the range of 5.7-6.5 GHz, the parameters of a C622A Microlab hybrid tee are as follows: $|S_{11}| \approx |S_{22}| = 0.08\text{-}0.1$; $|S_{13}| = 0.65\text{-}0.60$; $|S_{14}| = 0.60\text{-}0.54$; and $|S_{12}| = 0.46\text{-}0.52$) and the shape of the discriminator response is determined by the cosine term. Thus the response curve of the single tee discriminator is very similar to that of an ordinary phase discriminator.

The results of experimental investigations on a single hybrid tee discriminator are graphically shown in Figs. 6.3 and 6.4. To eliminate the effects of signal dependent sensitivities of detector diodes on the measured response curve, power meters were employed for the measurement of the output signals of the E- and H-arms. The polar display of the E- and H-arm output powers is shown in Fig. 6.3 for various frequencies. The x-y coordinates represent output power normalized to the input power. Triangles and dots indicate experimental and theoretical data, respectively. As can be seen, the agreement with respect to absolute values is very good while the phases do not agree as well. This is because of relatively poor accuracy in the measurement of the phase angles of the tee-scattering parameters. In the polar display of the discriminator outputs, the distance and phase angle of a displayed point uniquely determine the instantaneous power and frequency of the measured signal. The input VSWR of the single tee discriminator

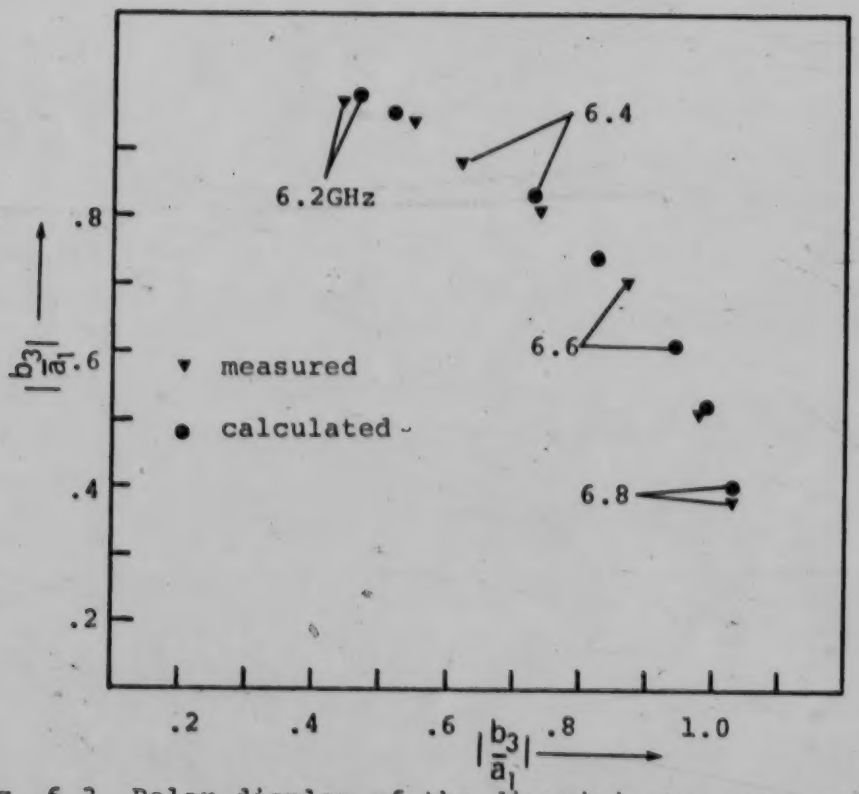

Fig. 6.3 Polar display of the discriminator response (P = 10mW, L = 1.78cm).

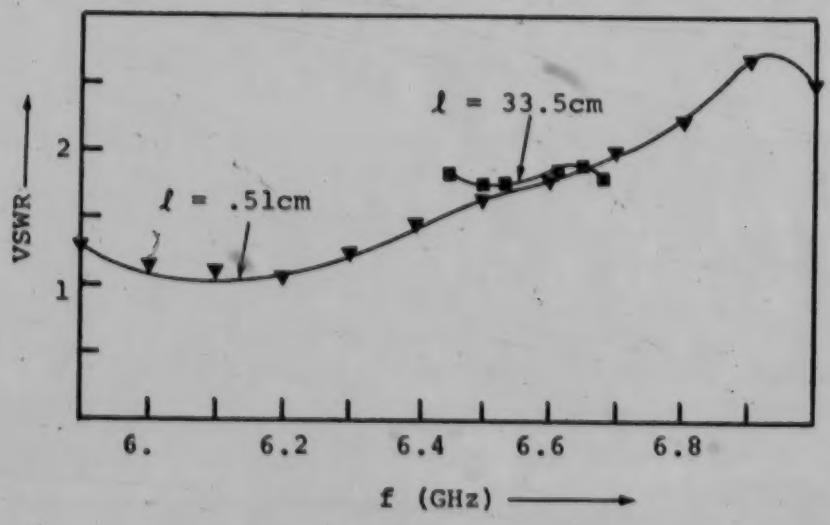

Fig. 6.4 Input VSWR of the single hybrid tee discriminator.

is within the limits 1.35 < VSWR < 2.08 in the frequency range of 5.9-6.8 GHz. A 6 dB attenuator in the discriminator input line will reduce the input VSWR to 1.08 < VSWR < 1.20. The discriminator input VSWR is shown in Fig. 6.4 for two different lengths of transmission line. The input VSWR lies within the predicted range.

6.3 Instantaneous power and frequency measuring system

The instantaneous power and frequency measuring system is essentially the single hybrid tee frequency discriminator combined with a directional coupler, to sample the input power together with an isolator to isolate the discriminator from the rest of the system. Prior to instantaneous power and frequency measurements, the measuring system should be calibrated using the procedure discussed below. Fig. 6.5 shows a block diagram of the system used for calibration purposes. Added to the single hybrid tee discriminator are a J-band (4-8 GHz) signal generator, a frequency counter, two isolators, an attenuator (0-20 dB), a TWT amplifier and a power meter. The first isolator is used to isolate the signal generator from the rest of the system and in this case the generator sees a constant load within the frequency range of interest. On the other hand the second isolator is used to isolate the TWT from the measuring system since reflected

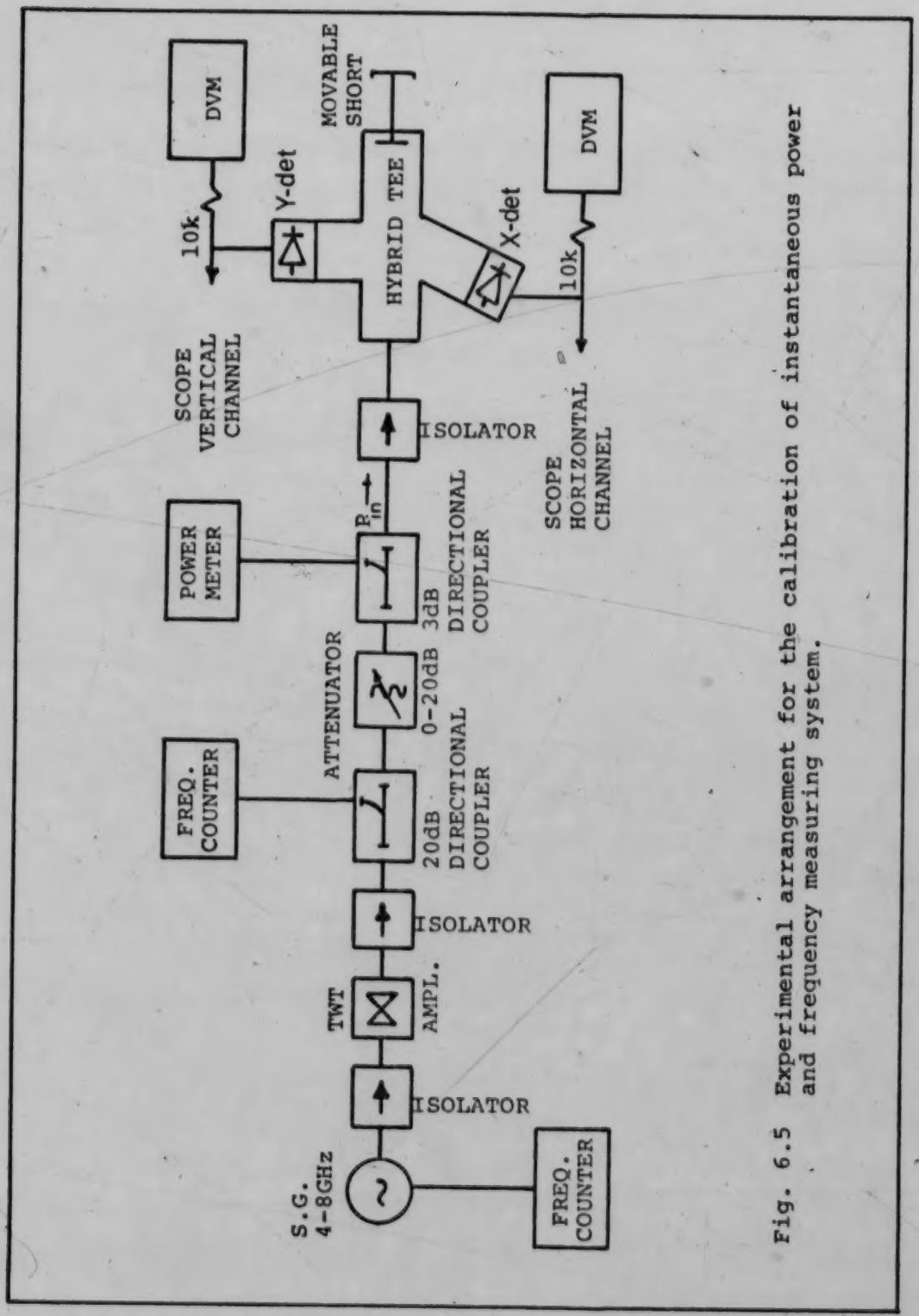

Fig. 6.5 Experimental arrangement for the calibration of instantaneous power and frequency measuring system.

signals could cause frequency and power instabilities at the output of the TWT amplifier. The same system will be used, in the next chapter, to measure Impatt oscillator transients merely by replacing the signal generator and the TWT by the oscillator to be characterized. The crystal detectors used to record the dc voltage from the tee E- and H-arms are HP 423A which will be called D_3 and D_4, respectively. A detected power of as low as 130 μW for D_3 and 70 μW for D_4 corresponds to dc voltages of 0.4 mV and 0.1 mV, respectively. Fig. 6.6 shows the detectors response to input signal levels at the frequencies of 5.8, 6.0 and 6.2 GHz in the frequency range of interest. It can be observed from these plots that the voltage sensitivities of the two crystal detectors are different.

For a given frequency, and with an unattenuated CW signal, the input power is adjusted to the maximum power required. Then, at the various power levels (5-90 mW), the D_3 and D_4 responses are recorded sequentially. These steps are repeated for the frequencies 5.7, 5.8, 5.9, 6, 6.1 and 6.2 GHz. The constant power and constant frequency curves displayed in Fig. 6.7 will be of help for instantaneous power and frequency measurements. It can be seen that the curves are not exactly circular due to the different sensitivities of the crystal detectors. They are similar in

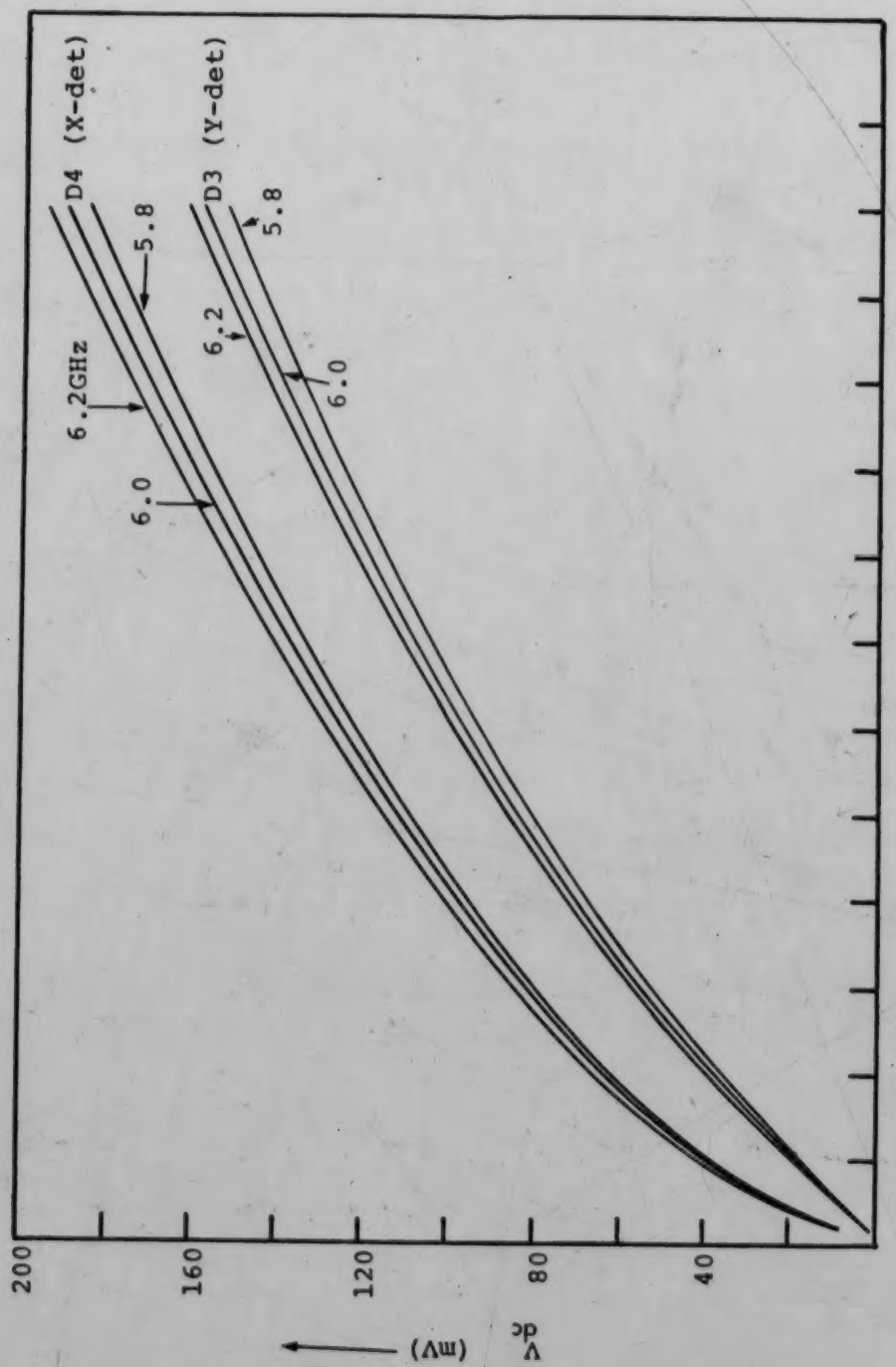

Fig. 6.6 Detectors dc voltage sensitivities.

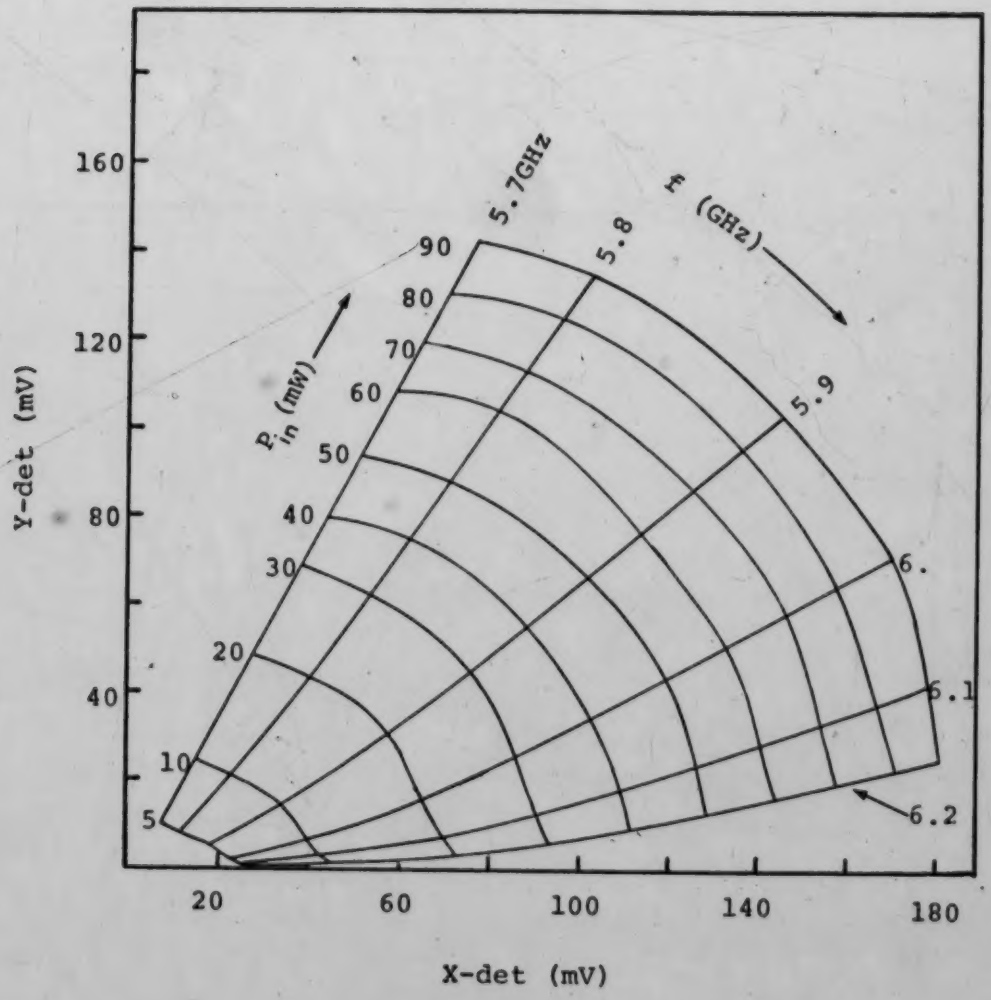

Fig. 6.7 Constant power and frequency response of the instantaneous measuring system.

shape to the curve derived theoretically using the scattering matrix concepts and the curve measured with the help of two power meters (Fig. 6.3).

The calibration curves of Fig. 6.7 show the power and frequency characteristics of the measuring system under CW signal operation. In order to use these curves for instantaneous (power and frequency) measurements of oscillator transients, the capability of the system to instantaneously measure the power and frequency of pulsed modulated signals has to be demonstrated. For this purpose, a similar calibration system was set up for pulsed measurements (Fig. 6.8). The differences were minor consisting essentially of the addition of a pulsed modulation stage in the RF path. This helped further to confirm the accuracy of the system in practical operation. In Fig. 6.8, the isolator following the signal generator is essential in presenting constant load conditions to the generator that maintains a constant input RF signal (6 GHz), especially during the ON conditions of the PIN line. Under pulsed operations, the power meter is used to measure the average input power. Knowing the duty cycle of the modulated signal, the peak power could be easily evaluated from these measurements.

The RF signal was modulated with pulses of amplitude = 3 volts, duration = 1 μsec. and repetition rate of 500 kHz. A PIN diode was the modulating element

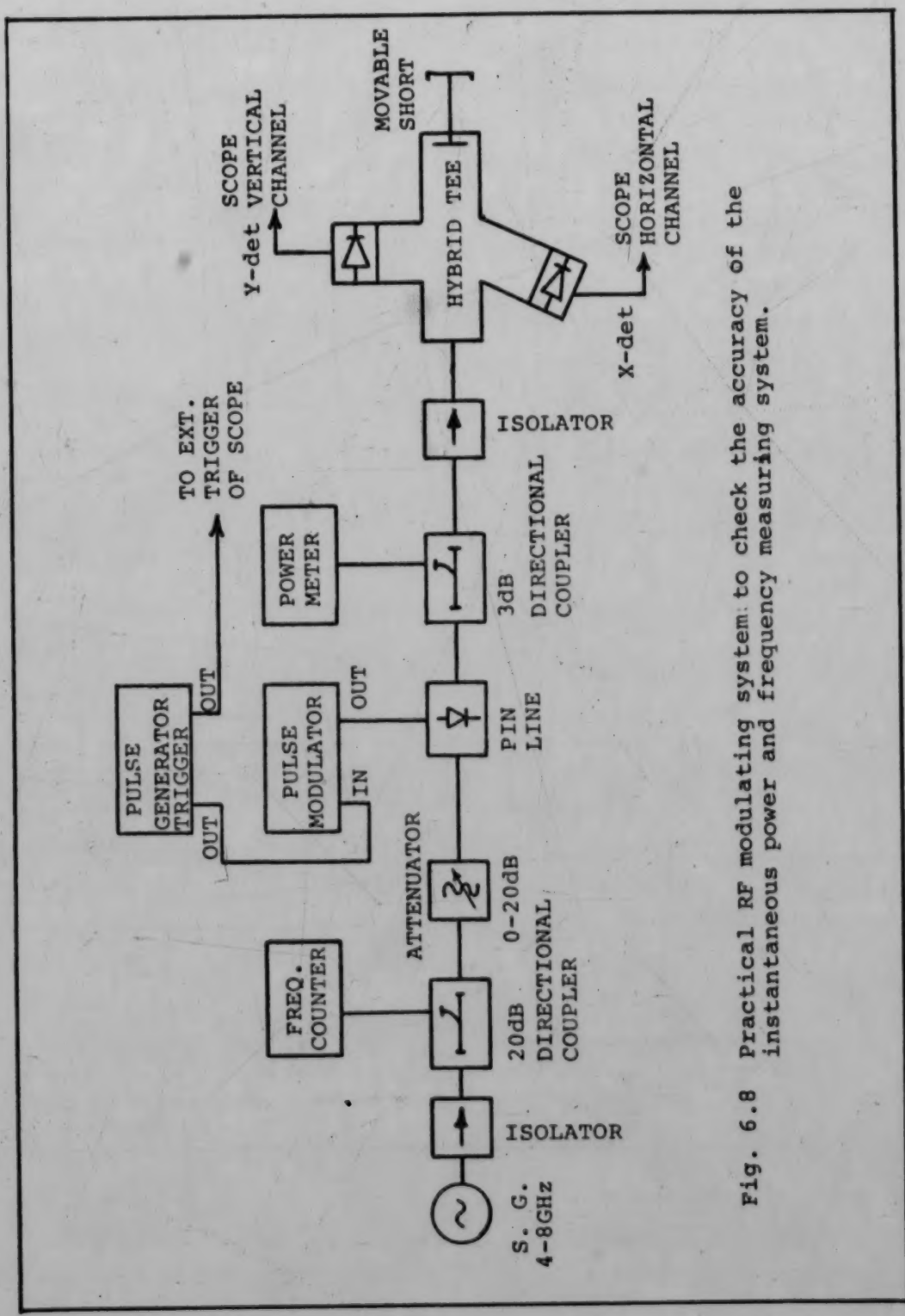

Fig. 6.8 Practical RF modulating system to check the accuracy of the instantaneous power and frequency measuring system.

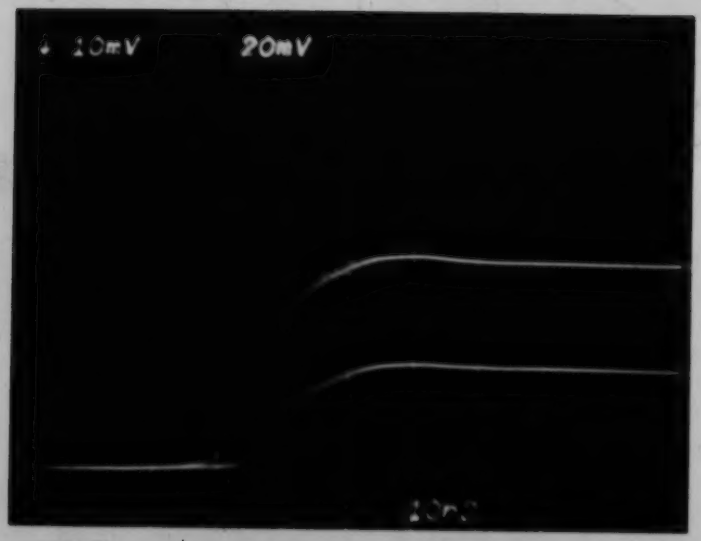

Fig. 6.9. The two RF envelopes recorded by the X- (top trace: 20 mV/cm) and Y-detector (bottom trace: 10 mV/cm). A modulating pulse of 3 V-amplitude, 2 μs-period is used to modulate an RF source (6 GHz) by means of a PIN diode modulator.

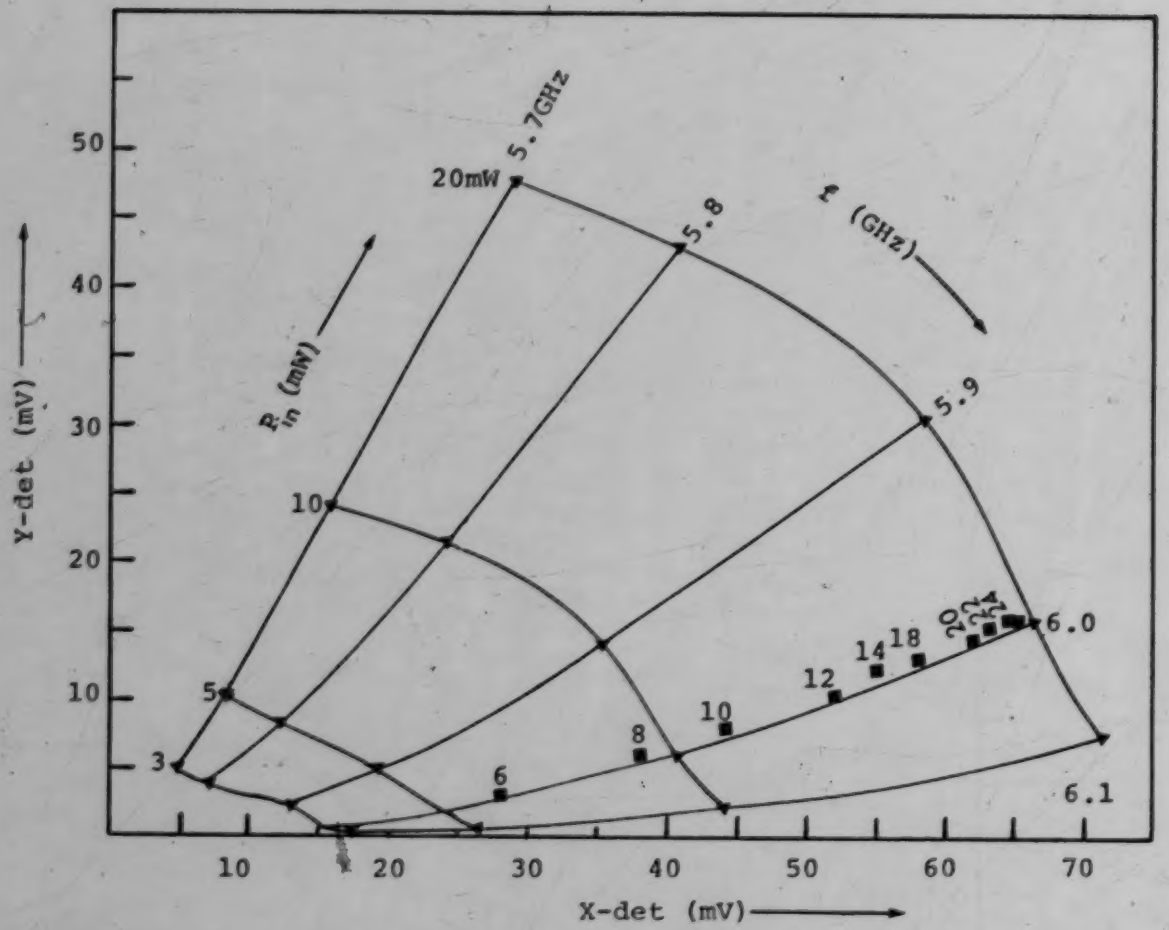

Fig. 6.10 Enlarged section of the constant power and frequency curves of Fig. 6.7 showing the results extracted from the traces in Fig. 6.9.

(restricting the rise time of the resulting RF envelope to about 15 ns). The RF envelope recorded by the two detectors is shown in Fig. 6.9. The top trace corresponds to the D_4 detector and the bottom trace corresponds to the D_3 detector. In order to evaluate the instantaneous frequency, at various time instants, starting from the leading edge of the two RF envelopes, the amplitude is recorded off the RF envelope of each detector. These values are plotted on the calibration curves of the system (X-Y polar display) and by interpolation, the instantaneous frequency and power are determined for each time instant. These points are numbered 1,2,..., etc. corresponding to different time intervals along subsequent points on the RF envelope graphs. Here, the points of interest, are those on the top portion of the RF envelopes which are numbered 20, 22, 24 and 26 (Fig. 6.10). The measured instantaneous frequency does not differ by more than 4 MHz from that measured on the counter (6 GHz). It can also be noted, that the measured instantaneous peak power never differs from the figure calculated from the measured average power by more than 4%.

CHAPTER VII

THEORETICAL STUDY ON TRANSIENT AND STEADY STATES IN OSCILLATORS

7.1 Introduction

The dynamic behaviour of a microwave oscillator, which is characterized by the time dependence of its instantaneous frequency and amplitude, is described by Eq. (2.66). Two initial conditions are required in order to find unique solutions for the amplitude A and the frequency $\omega(t)$ related to the known x by

$$\omega(t)=\bar{\omega} + d\phi/dt = \bar{\omega} + x \ .$$

The physically accepted initial conditions are definable either by the conditions at the start of oscillations (i.e. the start of the transients) or by the conditions immediately following the transient stage, referred to as the "almost steady" state conditions. The solution based on initial conditions that characterize the start of oscillation build up will be called the forward recursive method, because it progresses along with the build up of oscillations. Since oscillations are initiated by thermal noise generated in lossy components of the circuit, an amplitude value very close to zero may be used as one of the conditions for the forward recursive method. In this case, the starting value for

$\omega(t)$ is determined mainly by the characteristics of the passive and active components of the oscillator. The alternative solution will be called the backward recursive method. Here, the initial conditions are taken at a point close to the steady state value. The forward recursive method can be easily implemented in the case of an oscillator with a simple passive circuit, e.g. a simple parallel GLC circuit. When applied to an actual oscillator circuit, the numerical solutions based on the forward recursive method very often diverge. This could be due to the fact that the build up of oscillations is exponential, and the numerical solution fails to converge to the steady state on account of cumulative round-off errors during successive iterations. On the other hand, the backward recursive method has proved to be a very effective method for the evaluation of the transient behaviour of practical oscillators.

Differential equations are often numerically solved by transforming them to difference equations. Solving difference equations by backward schemes is well known in the theory of recursive computations. The first algorithm for such a backward scheme was introduced by Miller in 1954 to compute values of the modified Bessel functions I_n and the procedure is generally known as the Miller algorithm [55,56]. This algorithm has the distinct advantage over the forward

recursive scheme of being stable since cumulative round-off errors in forward computations seem to grow with the number of operations, as mentioned earlier.

This chapter describes the methods for obtaining numerical solutions of the equations characterizing the steady and transient states of an oscillator. In the first section, equations and circuit parameters (evaluation of passive and active d-coefficients and $\bar{\omega}$) common to both the transient and steady states are derived. The next section outlines the numerical steps followed in order to arrive at the steady state solution. Subsequently, the numerical algorithms developed are applied for computing the oscillator transients using measured large signal admittance for the Impatt diode #2, and also by utilizing the data published by Scharfetter and Gummel [28].

7.2 Derivation of equations and parameters describing steady and transient states in oscillators

The steady state amplitude and frequency of the oscillator are needed to provide the proper starting conditions for the backward recursive method. Since the amplitude and frequency of oscillations are constant under steady state conditions, all derivatives in the describing equation (2.66) are identically zero. Thus, the steady state operation is described by the following

set of two nonlinear algebraic equations

$$A^{o} = 0 \quad , \quad R_3R_4 - R_6R_2 = 0 \tag{7.1a}$$

$$x^{o} = 0 \quad , \quad R_2R_4 - R_1R_5 = 0 \quad . \tag{7.1b}$$

Here, the R_n's are nonlinear functions in A, x and the quasistationary frequency $\bar{\omega}$.

Generally, it is extremely difficult to solve the two nonlinear equations (Eqs. (7.1)) in the two unknowns. On the other hand, one nonlinear equation in one unknown can easily be solved using available computer routines. It has been found that the proper solution can be obtained by reducing the problem to the solution of two nonlinear equations in a single unknown by treating the A variable as a known parameter. This requires arranging R_n as follows:

$$\begin{aligned}
R_1 &= \sum_{n=1}^{7} R_{1n}\, x^6 \\
R_2 &= \sum_{n=1}^{7} R_{2n}\, x^6 \\
R_3 &= \sum_{n=1}^{6} R_{3n}\, x^5 \\
R_4 &= \sum_{n=1}^{6} R_{4n}\, x^5 \\
R_5 &= \sum_{n=1}^{7} R_{5n}\, x^6 \\
R_6 &= \sum_{n=1}^{5} R_{6n}\, x^4
\end{aligned} \tag{7.2}$$

where R_{mn} are nonlinear functions in A and $\bar{\omega}$. Therefore Eqs. (7.1) are transformed to

$$\sum_{n=0}^{11} B_n x^n = 0 \qquad (7.3a)$$

$$\sum_{n=0}^{11} C_n x^n = 0 \qquad (7.3b)$$

and the coefficients B_n and C_n are nonlinear functions in A and $\bar{\omega}$ as shown in Appendix II.

Selecting values for A and using the predetermined value of $\bar{\omega}$, to be evaluated in section 7.2.3, Eqs. (7.3a) and (7.3b) represent two equations in one unknown, x. Each equation can be then solved using known numerical routines. Generally, the sets of the eleven complex roots are different. The values of A have to be selected in such a way that the real roots of the two equations coincide.

Most of the numerical routines used for the solution of nonlinear algebraic equations, such as those of Eqs. (7.3), require analytically defined equations and thus the R coefficients have to be determined by means of the d-(spline) coefficients of the passive and active circuits. The quasistationary frequency, $\bar{\omega}$, has also to be determined because the B_n and C_n coefficients in Eqs. (7.3) are functions of $\bar{\omega}$.

7.2.1 Evaluation of the active device d-coefficients

To evaluate the d-coefficients, the measured or theoretically evaluated device large-signal admittance data Y_{MN} have to be expressed, as in Chapter II, in the form

$$Y_{MN} = G(A_M^2, \omega_N^2) + j\omega_N \frac{B(A_M^2, \omega_N^2)}{\omega_N} = G(A_M^2, \omega_N^2) + j\omega_N S(A_M^2, \omega_N^2). \quad (7.4)$$

Next, the natural bicubic spline is fitted through the $M \times N$ functional values, e.g. $G_{11}, \ldots, G_{MN}$ or $S_{11}, \ldots, S_{MN}$, corresponding to two sets of grid points, namely $A_1, \ldots, A_M$, $\omega_1, \ldots, \omega_N$. The computer routine returns the coefficients of the bicubic spline interpolate on the MN subrectangle $[A_M, A_{M+1}] \times [\omega_N, \omega_{N+1}]$ in a 4×4 matrix. The spline interpolate is then given by

$$G_{MN}(A^2, \omega^2) = \sum_{i=1}^{4} \sum_{j=1}^{4} g_{ij} (A^2 - A_M^2)^{i-1} (\omega^2 - \omega_N^2)^{j-1} \quad (7.5)$$

and

$$S_{MN}(A^2, \omega^2) = \sum_{i=1}^{4} \sum_{j=1}^{4} s_{ij} (A^2 - A_M^2)^{i-1} (\omega^2 - \omega_N^2)^{j-1} . \quad (7.6)$$

During the buildup of oscillations, the device conductance and susceptance for a given amplitude A and frequency ω, which lie between known amplitude and frequency values given by the device $Y(A^2, \omega^2)$ characteristics, may be evaluated by the use of Eqs. (7.5) and (7.6). These can be transformed into the convenient forms

$$G_{MN}(A^2,\omega^2) = \sum_{i=0}^{3}\sum_{j=0}^{3} GM_{ij}(A_M^2,\omega_N^2)\ A^{2j}\omega^{2i} \qquad (7.7)$$

$$S_{MN}(A^2,\omega^2) = \sum_{i=0}^{3}\sum_{j=0}^{3} SM_{ij}(A_M^2,\omega_N^2)\ A^{2j}\omega^{2i} \quad . \qquad (7.8)$$

The last two equations together with the complementary device admittance are related to the d-coefficients through the $c\mathcal{D}$'s as

$$G_{MN}(A^2,\omega^2) = \sum_{m=0}^{3} (-1)^m\ {}_{MN}c\mathcal{D}_{2m}(A^2)\ \omega^{2m} \qquad (7.9)$$

$$B_{MN}(A^2,\omega^2) = \sum_{m=0}^{3} (-1)^m\ {}_{MN}c\mathcal{D}_{2m+1,2}(A^2)\omega^{2m} \qquad (7.10)$$

$$\bar{G}_{MN}(A^2,\omega^2) = \sum_{m=0}^{3} (-1)^{m+1}\ {}_{MN}c\mathcal{D}_{2m,2}(A^2)\omega^{2m} \qquad (7.11)$$

$$\bar{B}_{MN}(A^2,\omega^2) = \sum_{m=0}^{3} (-1)^m\ {}_{MN}c\mathcal{D}_{m+1}(A^2)\ \omega^{2m+1} \qquad (7.12)$$

where

$${}_{MN}c\mathcal{D}_{2m} = \sum_{n=0}^{3} (-1)^m\ {}_{MN}d_{2m,2n}A^{2n}\ , \quad m = 0,1,2,3 \qquad (7.13)$$

$${}_{MN}c\mathcal{D}_{2m+1} = \sum_{n=0}^{3} (-1)^m(2n+1)\ {}_{MN}d_{2m+1,2n}A^{2n},\ m = 0,1,2,3 \qquad (7.14)$$

$${}_{MN}c\mathcal{D}_{2m+1,2} = \sum_{n=0}^{3} (-1)^m\ {}_{MN}d_{2m+1,2n}A^{2n},\ m = 0,1,2,3 \qquad (7.15)$$

$${}_{MN}c\mathcal{D}_{2m,2} = \sum_{n=0}^{3} \frac{(-1)^m}{(2n+1)}\ {}_{MN}d_{2m,2n}A^{2n},\ m = 1,2,3 \qquad (7.16)$$

7.2.2 Passive circuit d-coefficients evaluation

The set of N functional values $F_1, F_2, \ldots, F_N$ (for $G_c(\omega)$ and $B_c(\omega)/\omega$) and the corresponding coordinates $\omega_1, \omega_2, \ldots, \omega_N$ are fed into a natural-cubic spline subroutine and an output array c of dimension (3,(N-1)) is obtained. In the N^{th} interval (ω_N, ω_{N+1}) the spline interpolate, $F(\omega^2)$, is given by

$$F_N(\omega^2) = \sum_{m=1}^{4} G_m(\omega_N^2)(\omega^2-\omega_N^2)^{m-1} \quad . \qquad (7.17)$$

In order to evaluate d-coefficients of the passive circuit conductance and susceptance Eq. (7.17) is transformed to

$$N^{G_c}(\omega^2) = N^{d}_{0,0} + N^{d}_{2,0}\omega^2 + N^{d}_{4,0}\omega^4 + N^{d}_{6,0}\omega^6 \qquad (7.18)$$

$$N^{B_c}(\omega^2) = N^{d}_{1,0}\omega + N^{d}_{3,0}\omega^3 + N^{d}_{5,0}\omega^5 + N^{d}_{7,0}\omega^7 \qquad (7.19)$$

where G_c and B_c are the passive circuit conductance and susceptance, respectively, and the d's are functions of higher powers in ω_N^2 specifically up to ω_N^7.

7.2.3 The computation of the quasistationary angular frequency $\bar{\omega}$

In oscillators, the susceptance of the active device is tuned out by the susceptance of the embedding

circuitry at the operating frequency. In practice, oscillations start with an amplitude very close to zero and the steady state frequency deviates only slightly from $\bar{\omega}$ so that it is adequate to evaluate $\bar{\omega}$ at A = 0.

Since the active device susceptance $B_D(A^2,\omega^2)$ is a function of ω^2 and A^2, and the passive circuit susceptance $B_c(\omega^2)$ is a function of ω^2, $\bar{\omega}$ may be evaluated as

$$B_D(A=0, \bar{\omega}^2) + B_c(\bar{\omega}^2) = 0 \ . \qquad (7.20)$$

The substitution of Eqs. (7.10) and (7.19) into Eq. (7.20) yields

$$(d_{10} + c\mathcal{D}12) + (d_{30} - c\mathcal{D}32)\bar{\omega}^2 + (d_{50} + c\mathcal{D}52)\bar{\omega}^4 + (d_{70} - c\mathcal{D}72)\bar{\omega}^6 = 0 \ . \qquad (7.21)$$

The above is a nonlinear algebraic equation in $\bar{\omega}$. To evaluate $\bar{\omega}$, the d-coefficients of the passive circuit for the intervals, N,N+1,...,etc., as well as those of the active device for the various subrectangles (M × N)'s, are evaluated in the previous section. Subsequently Eq. (7.21) may be solved numerically in $\bar{\omega}$ using computer routines based on a Newton-Raphson iterative technique. However, under small-signal conditions (A=0) M= 1 and there may be various values of N corresponding to the various frequency intervals. The routine can then

give different values of $\bar{\omega}$ for the various values of N. If $\omega_N < \bar{\omega} < \omega_{N+1}$, the value $\bar{\omega}$ should be taken as that calculated by the use of the corresponding N coefficients.

7.3 Steady state solutions

Having evaluated the d-coefficients for active and passive circuits, as well as determining $\bar{\omega}$, A is assigned a range of values lying within and conforming to the device characteristic (G and B for various A's) for this value of $\bar{\omega}$. Proceeding further, for each of these chosen values of A, eleven complex roots of x are computed for each equation of (7.3) using the same routine utilized for the evaluation of $\bar{\omega}$. Since the steady state frequency is a real number, all complex roots are disregarded, and only physically acceptable values for x are considered in steady state calculations. It has been observed that for a given oscillator circuit, x has one negative value that leads to a converging solution. Also, it has been found that positive values of x cannot lead to a converging solution. The steady state solutions are the values of A and $\bar{\omega} + x$ which satisfy both the equations of (7.3) simultaneously.

A flow chart demonstrating the different steps to be followed in order to evaluate the steady state values A and $\bar{\omega} + x$ is shown in Fig. 7.1. The calculated amplitude, A, and frequency $\bar{\omega} + x$ may be used as the

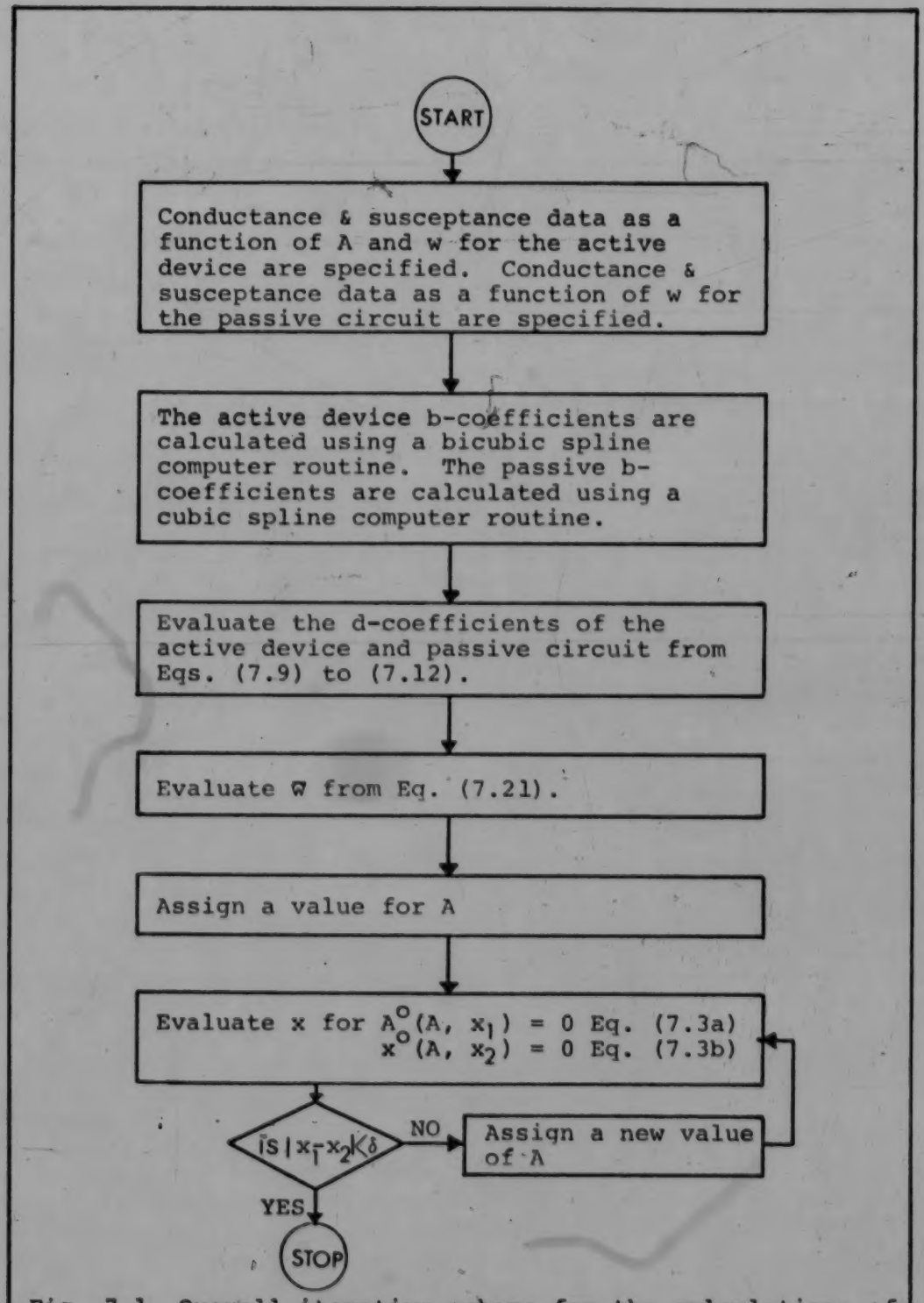
START
Conductance & susceptance data as a function of A and w for the active device are specified. Conductance & susceptance data as a function of w for the passive circuit are specified.
The active device b-coefficients are calculated using a bicubic spline computer routine. The passive b-coefficients are calculated using a cubic spline computer routine.
Evaluate the d-coefficients of the active device and passive circuit from Eqs. (7.9) to (7.12).
Evaluate ϖ from Eq. (7.21).
Assign a value for A
Evaluate x for $A_o^o(A, x_1) = 0$ Eq. (7.3a)
$x^o(A, x_2) = 0$ Eq. (7.3b)
$|x_1 - x_2| < \delta$
NO
Assign a new value of A
YES
STOP

Fig. 7.1 Overall iterative scheme for the calculations of steady state voltage amplitude, A, and frequency $\omega + X$.

initial boundary conditions for the start of the transient solution in the backward recursive approach.

7.4 Transients in Impatt diode oscillators

The transient response of an Impatt oscillator can be analyzed by solving Eqs. (2.66) which are nonlinear differential equations in A and x. The time dependence of A and x ($\bar{\omega}$ taken to be constant) may be determined only by simultaneously solving Eqs. (2.66) using a digital computer. This has been accomplished through the use of a subroutine which utilizes a Runge-Kutta fourth order algorithm [57,58]. It is often difficult and cumbersome to determine the proper size of the integration step in Runge-Kutta type methods for numerical integration of first order nonlinear differential equations. The sub-routine used adopts a modified version of the Runge-Kutta method by Merson. This modification gives an automatic and rapid method for determining the interval (step length) to be used in order to obtain a predetermined accuracy. An accuracy close to that of the machine is used during the initial steps of integration in order to reduce accumulation of round-off errors.

As pointed out before, there are two approaches for the evaluation of the dynamic solution, namely the forward recursive method and the backward recursive

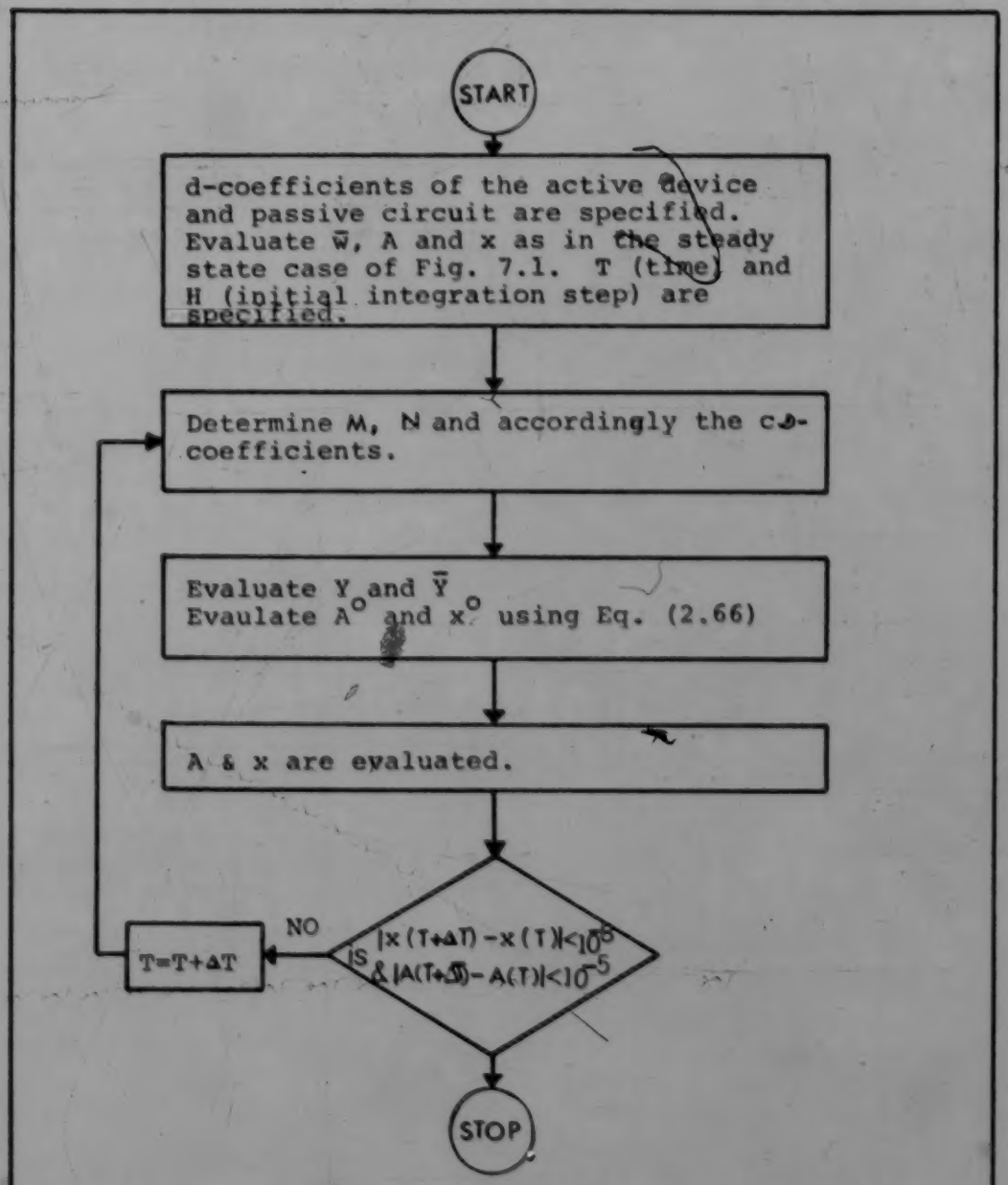
START
d-coefficients of the active device and passive circuit are specified. Evaluate $\bar{w}$, A and x as in the steady state case of Fig. 7.1. T (time) and H (initial integration step) are specified.
Determine M, N and accordingly the c-coefficients.
Evaluate Y_o and $\bar{Y}$
Evaulate A^o and x^o using Eq. (2.66)
A & x are evaluated.
$|x(T+\Delta T)-x(T)|<10^{-5}$ & $|A(T+\Delta T)-A(T)|<10^{-5}$
IS
NO
T=T+ΔT
STOP

Fig. 7.2 Overall iterative scheme for the calculation of the dynamic solution by using forward iterative scheme. (Appendix III).

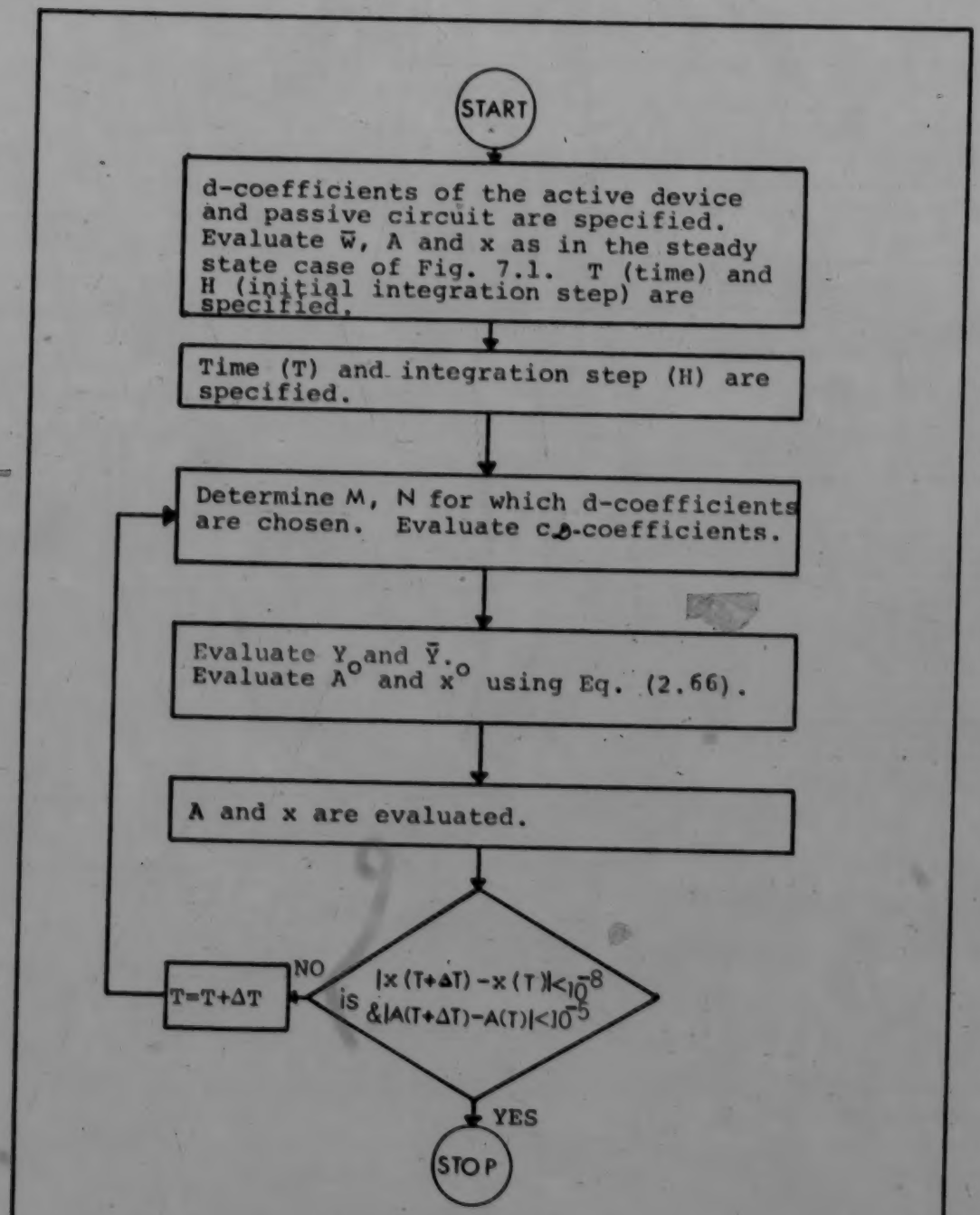
START
d-coefficients of the active device and passive circuit are specified. Evaluate $\bar{w}$, A and x as in the steady state case of Fig. 7.1. T (time) and H (initial integration step) are specified.
Time (T) and integration step (H) are specified.
Determine M, N for which d-coefficients are chosen. Evaluate c-coefficients.
Evaluate Y_o and $\bar{Y}$.
Evaluate A^o and x^o using Eq. (2.66).
A and x are evaluated.
$|x(T+\Delta T)-x(T)|<10^{-8}$ & $|A(T+\Delta T)-A(T)|<10^{-5}$
is
NO
$T=T+\Delta T$
YES
STOP

Fig. 7.3 Overall iterative scheme for the calculation of the dynamic solution using backward iterative method. (Appendix III).

method. The steps followed in the two approaches to obtain the time dependence of A and x, are shown in Figs. 7.2 and 7.3. (Appendix III).

To demonstrate the applicability of the forward and backward recursive solutions, the Impatt oscillator transients are evaluated for a hypothetical oscillator. In these calculations, the Impatt diode, or more precisely the semiconductor chip theoretically investigated by Scharfetter and Gummel, is assumed mounted in the S_4 microwave package [59], (contact area = 10^{-4} cm^2) and operated in a coaxial line-type resonator with a single tuning slug. The external circuit, consisting of the resonator and the lumped package parasitics, is tuned to present at the chip contacts a conductance of 10^{-3} mho in parallel with a susceptance that tunes out the chip small-signal susceptance (corresponding to a bias current of 200 A/cm^2) at 7.4 GHz.

Fig. 7.4 shows the dependence of the active device negative conductance and susceptance upon the operating frequency and RF voltage as published by Scharfetter and Gummel [28]. It also shows the dependence of two passive circuit admittances on the frequency as seen by the device. These admittances are calculated for two sets of parameters for a 7 mm coaxial type resonator shown in Fig. 7.5a and described in detail in Chapter VIII.

Also, indicated in Fig. 7.4 are the M × N values of the various subrectangles corresponding to each set of the d coefficients computed. It is clearly seen that for the five RF voltages and six frequencies available, there will be, respectively, four M and five N values.

In Fig. 7.5b, Y_E is the transformed circuit admittance as seen by the packaged diode, and C_p and L_p are the package capacitance and inductance, respectively. A computer program is developed to calculate the circuit admittance as a function of frequency using the two sets of parameters presented in Table 7.1 and the equivalent circuit of Fig. 7.5b as an input. In these calculations, the discontinuities due to the single slug are included as appropriate discontinuity capacitances [60]. The resonator parameters are adjusted to tune out the total small-signal oscillator susceptance at 7.4 GHz. As mentioned earlier, the forward recursive method fails to converge for practical oscillator circuits. The results obtained on the basis of the backward recursive method for these oscillators, are shown in Figs. 7.6 and 7.7. The amplitude origin is chosen to be 10^{-4} volts which is about the same as the noise threshold level. Comparison of these figures shows that the frequency starts to increase appreciably only after the RF voltage has increased to nearly one volt. Fig. 7.7 shows, that the

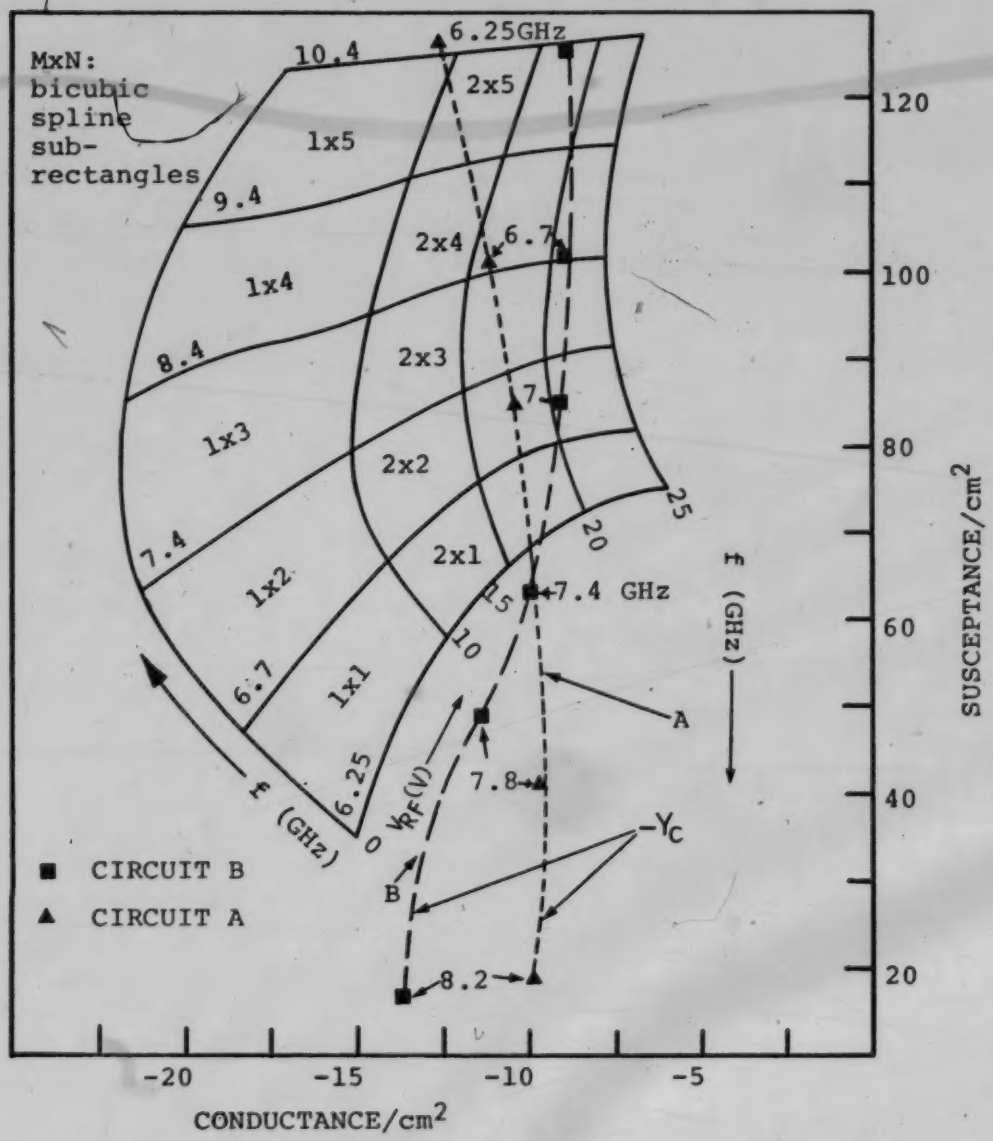

Fig. 7.4 (a) Impatt diode admittance as a function of RF voltage amplitude and frequency at a current density of 200A/cm (After Scharfetter etal. [28]).

(b) Passive circuit admittance, Y_C, as a function of frequency for circuit A (Table 7.1).

(c) Passive circuit admittance as a function of frequency for circuit B (Table 7.1).

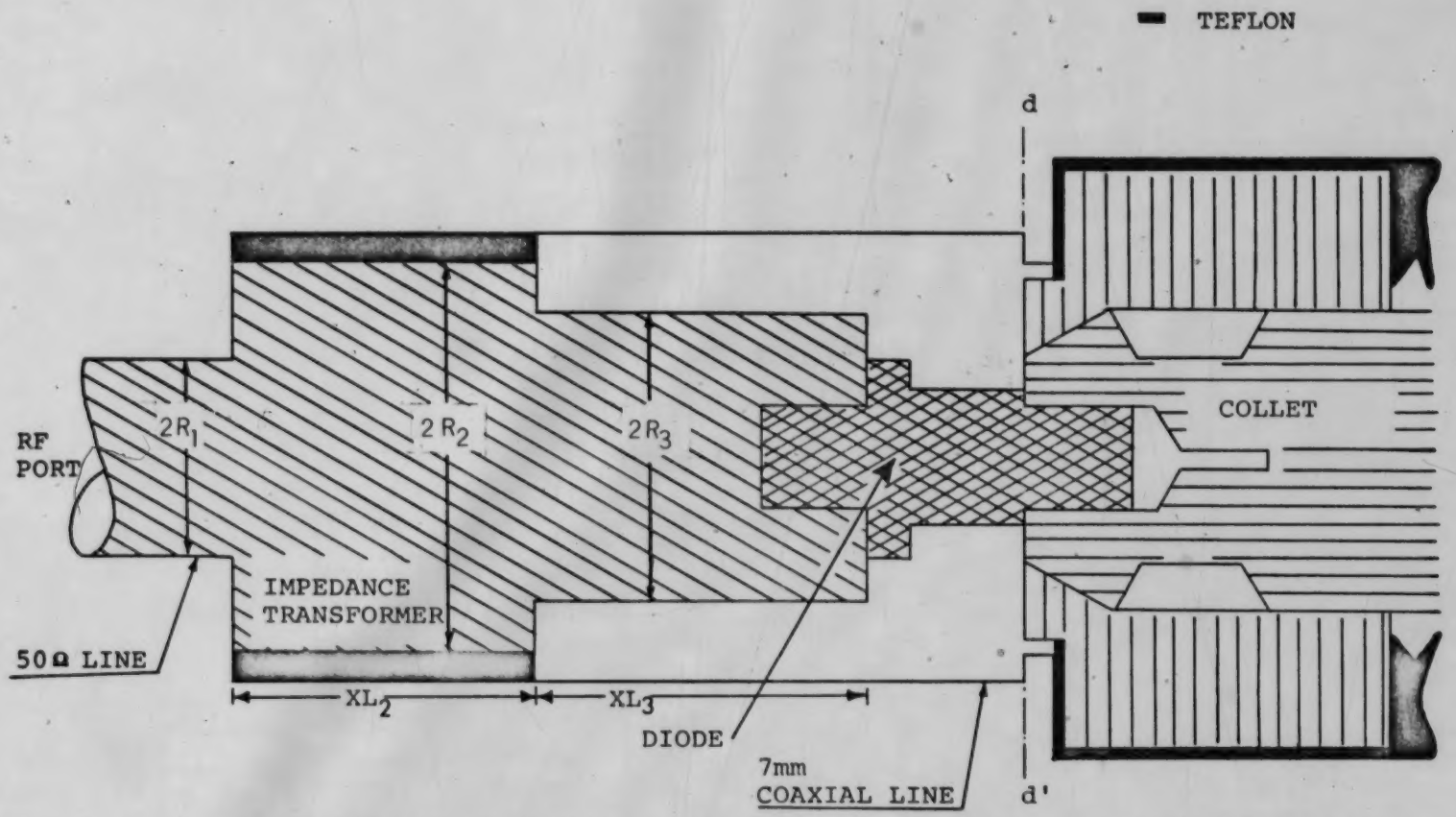

Fig. 7.5a Cross-sectional view of a 7mm coaxial-type resonator embedding the Impatt diode. R_1, R_2, R_3, XL_2 and XL_3 are the resonator parameters (Table 7.1).

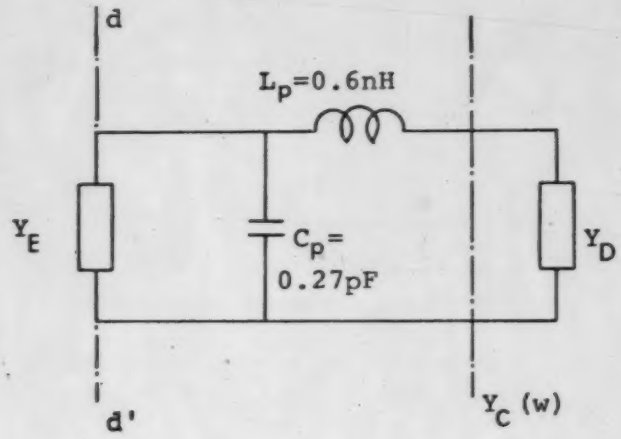

Fig. 7.5b Equivalent circuit of an Impatt diode oscillator.

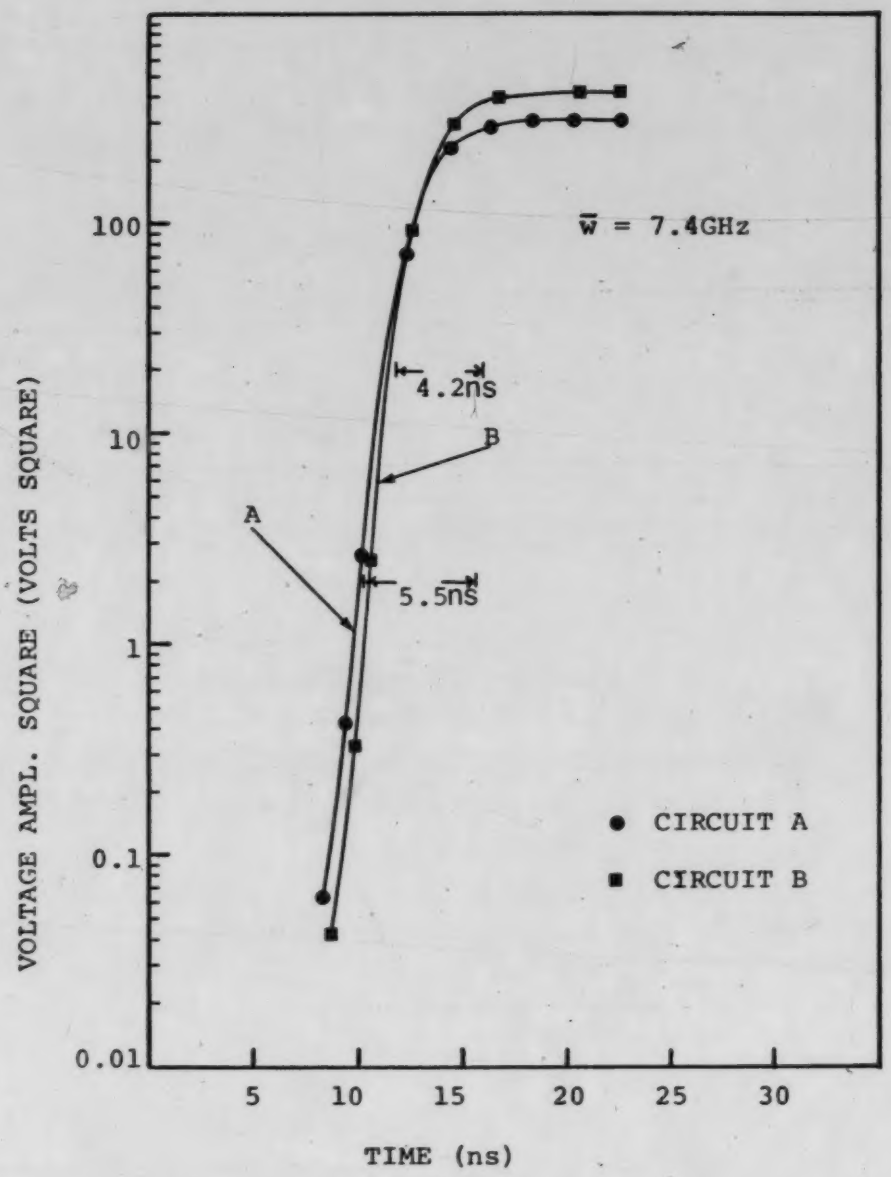

Fig. 7.6 Build up of power in a realistic oscillator for two sets of the 7mm coaxial resonator parameters as given in Table 7.1 (Fig. 7.5).

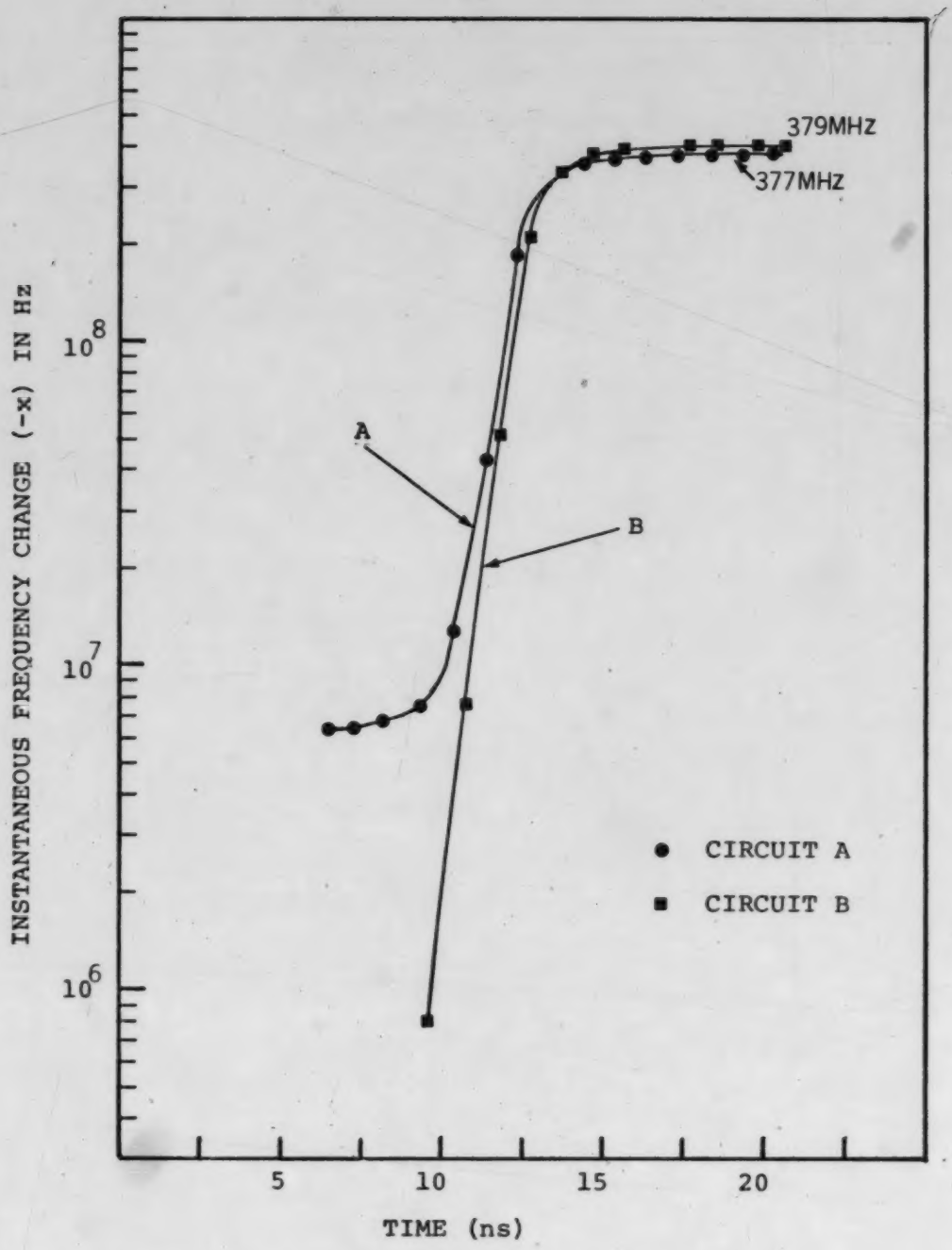

Fig. 7.7 Build up of frequency in a realistic oscillator for two sets of the 7mm coaxial resonator parameters as given in Table 7.1 (Fig. 7.5b).

Table 7.1. The two sets of resonator parameters used to evaluate the passive circuit admittance as a function of frequency for circuits A and B of Fig. 7.4.

Resonator parameters	Set #1 circuit A	Set #2 circuit B
R_1	.152 cm	.152 cm
R_2	.28064 cm	.28318 cm
R_3	.15 cm	.15 cm
XL_2	.796 cm	1.3 cm
XL_3	.56 cm	.469 cm
C_p	.27 pF	.27 pF
L_p	.6 nH	.6 nH

calculated steady state frequency is about the same (within 5%) for the two resonators used, even though the time needed to reach the steady state frequency is different. It is also observed, that the oscillation rise time is different for the two oscillators. This demonstrates that the interaction between the circuit admittance locus and the device characteristic curves plays an important role in the transient behaviour of the oscillator. Therefore, it is possible, by changing the resonator parameters, to optimize these transients.

The characteristics of the Impatt diode oscillator consisting of diode #2 mounted in a 7 mm coaxial line resonator whose design is described in the next chapter, are used to calculate the transients. For this example, the backward recursive solution is obtained by using the admittance parameters measured in Chapter V (Fig. 5.11). In Fig. 7.8 curve (a) shows the RF power build up for this arrangement. From this figure, it can be deduced that the oscillation rise time is approximately 5.4 ns. The frequency build up is shown by curve (b) in this figure. Fig. 7.8 forms the basis for the comparison between the transients calculated by using the backward recursive solution and those measured experimentally for the Impatt diode oscillator developed by the author.

In order to understand the behaviour of microwave oscillators, the evaluated instantaneous amplitude and

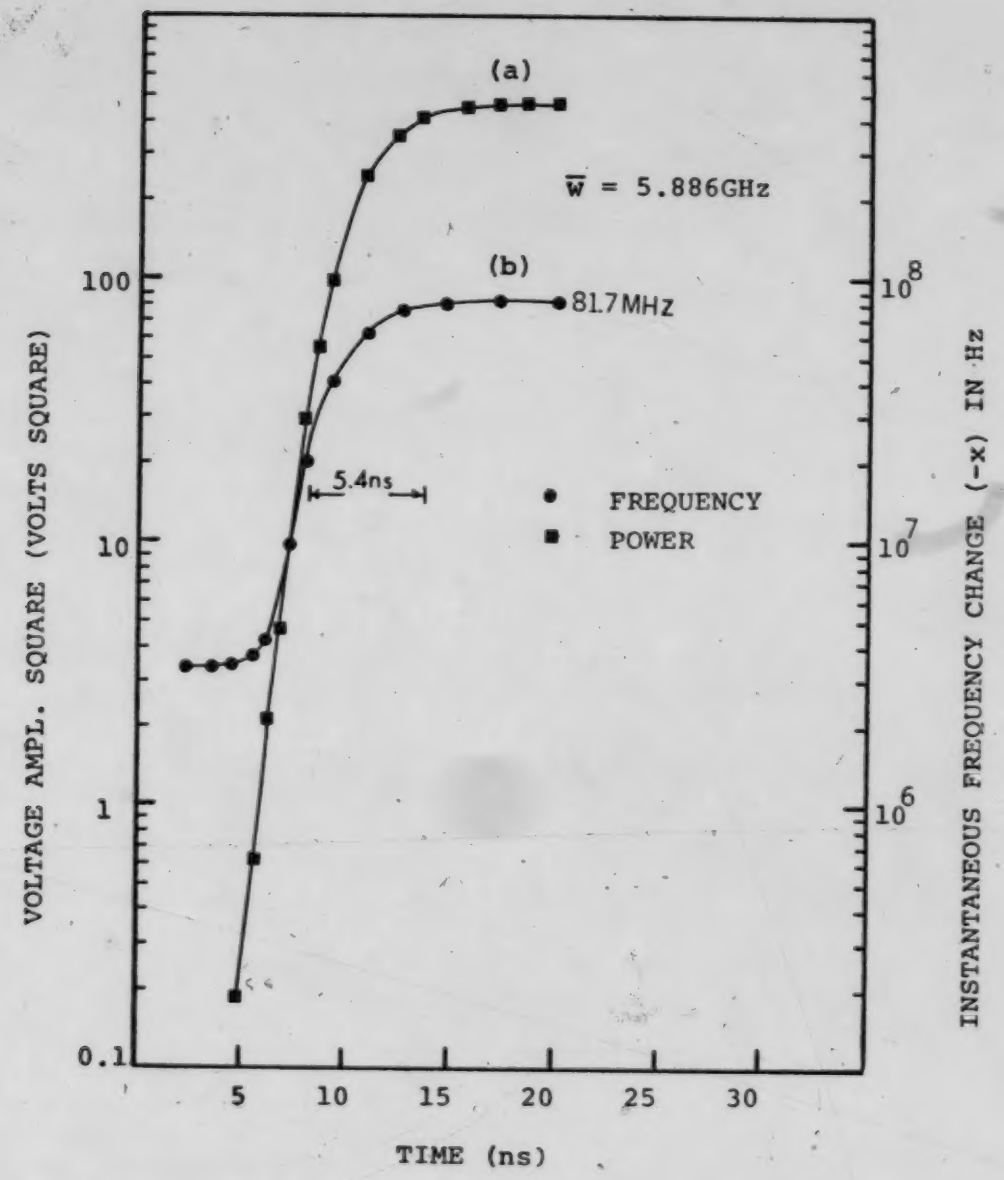

Fig. 7.8 Build up of power (a) and frequency (b) in the Impatt diode oscillator using diode #2 (Ch. VIII). The measured oscillator admittances are shown in Fig. 5.11.

frequency are used to obtain the dependence of the device admittance on the RF voltage. This has been described in Chapter III as the device line [17]. The calculations are performed for the two hypothetical and the developed Impatt diode oscillators. A computer program is developed for this purpose in which the active and passive d-coefficients, A(t), x(t) and $\bar{\omega}$ are fed as inputs. The program outputs both conductance and susceptance values as a function of the RF voltage. These calculations are also useful, since they give the behaviour of the device admittance with time during the transient stage. Fig. 7.9 shows the results obtained for the device line together with the admittance locus of the two hypothetical oscillators. The results obtained on the basis of the measured oscillator admittances are shown in Fig. 7.10. In both figures, the arrowheads attached to the locii indicate the direction of increasing ω in case of the admittance locus, and the direction of increasing RF voltage as well as time for the device. The intersection between the device line and admittance locus determine the steady state frequency. The steady state frequency for the hypothetical oscillators is about 7 GHz, and this can be easily seen as the intersection points which are close to 7 GHz ($\bar{\omega}$ = 7.4 GHz). It can be noted from Fig. 7.9 that the device lines of the two oscillators

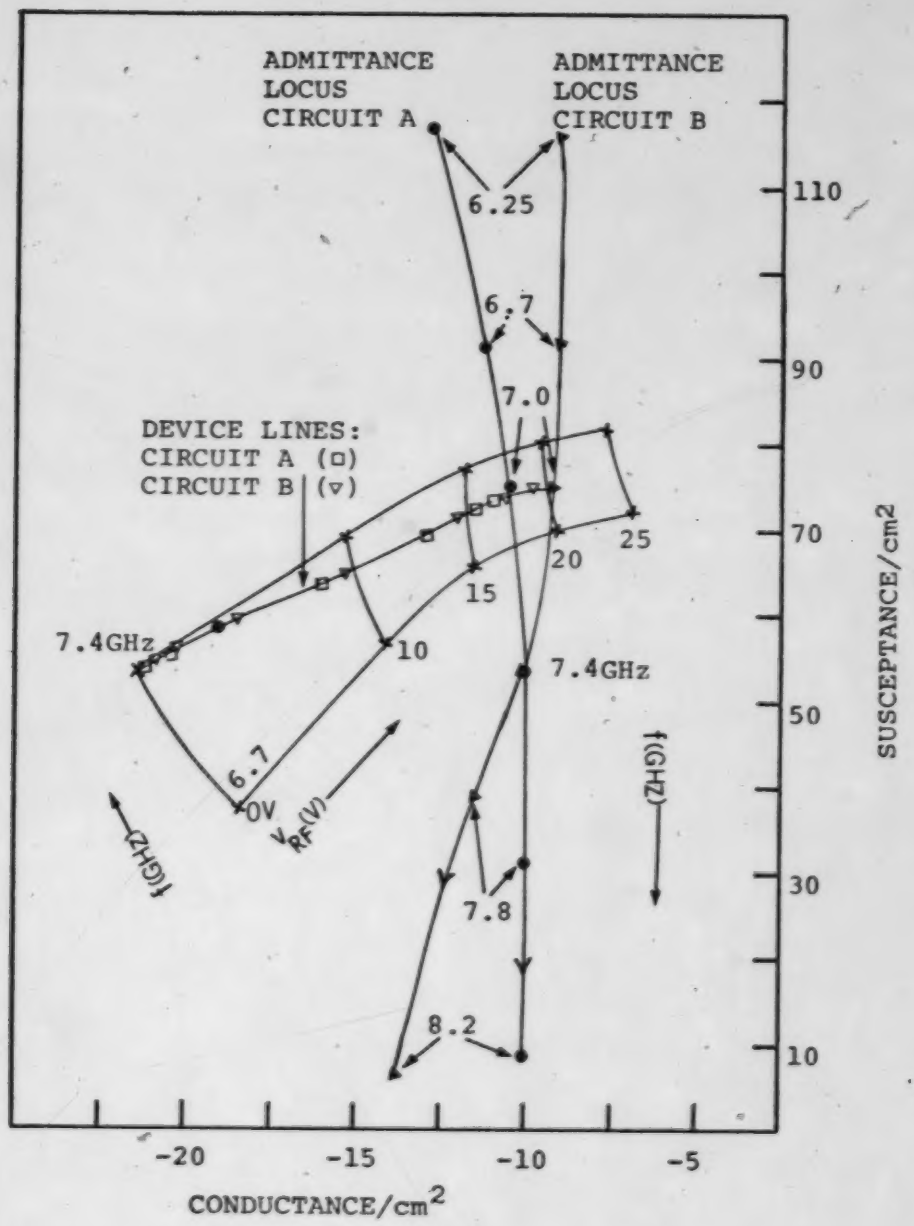

Fig. 7.9 Device line and impedance locus superimposed on a part of Impatt diode admittance characteristics (Fig. 4.9) published by Scharfetter and Gummel [28] ($\bar{w}$ = 7.4GHz).

take the same path. It can also be noted, according to Figs. 7.9 and 7.10, that at the start of oscillation build up, the frequency changes slightly until the RF voltage builds up to more than one volt; thereafter a noticeable change in frequency occurs. These changes are different for various oscillators as shown in Figs. 7.9 and 7.10. In case of the oscillator developed, the steady state frequency is 5.804 GHz and $\bar{\omega}$ = 5.886 GHz, and the change occurring in frequency from that at the start of oscillation build up is only about 81.6 MHz. This is unlike the frequency change in the hypothetical oscillators, which is about 377 MHz. In general, the behaviour of oscillation build up is similar in all oscillators.

A stable oscillatory condition is possible provided that, in addition to the conditions imposed upon the device and circuit admittances, the following requirement be fulfilled [61] at each intersection on the admittance plane plot:

$$- A \frac{\partial G_D}{\partial A} \frac{dG_c}{d\omega} (\tan \phi - \tan \theta) > 0 \qquad (7.22)$$

where

$$\tan \phi = \frac{\frac{dB_c}{d\omega}}{\frac{dG_c}{d\omega}}$$

and

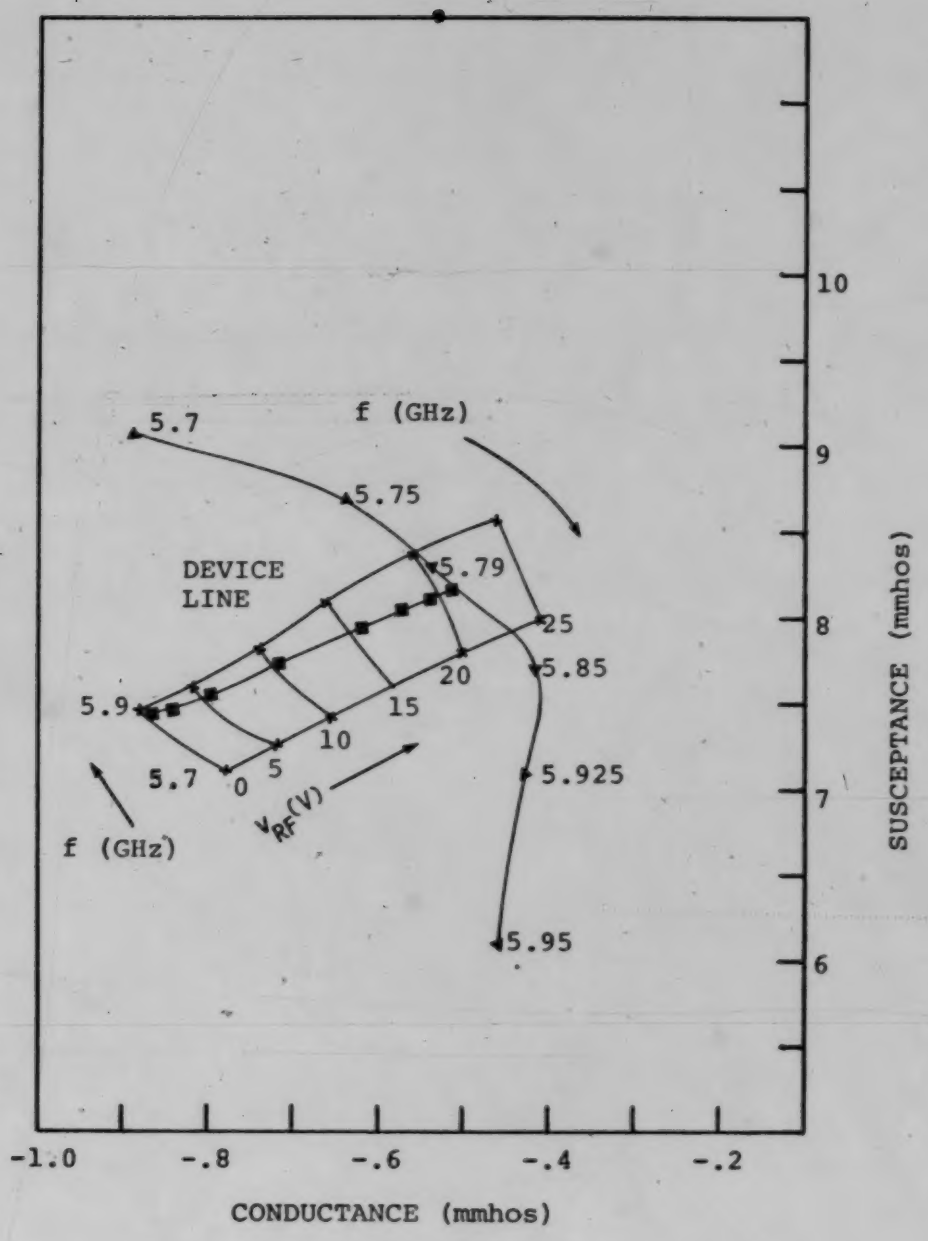

Fig. 7.10 Device line and impedance locus superimposed on the measured Impatt diode admittance characteristics, diode #2, as of Fig. 5.11 ($\bar{W}$ = 5.886GHz).

$$\tan \theta = \frac{\frac{\partial B_D}{\partial A}}{\frac{\partial G_D}{\partial A}} \quad .$$

Using the parameters involved in Eq. (7.22), for the intersections of Figs. 7.9 and 7.10, it can easily be shown that these operating points are stable. Approximate values for these parameters are given in Table 7.2. If $\partial G_D/\partial A$ is positive, then stable oscillations can only be obtained if both $dB_c/d\omega$ and $dG_c/d\omega$ are negative or else $dB_c/d\omega$ must be negative. It should be noted that although the transients for the two hypothetical oscillators are different, the angle between the device line and admittance locus is about the same, and equal to 50°. This angle for the developed oscillator is 80°.

Table 7.2. Hypothetical and developed oscillator parameters of Eq. (7.22).

Oscillator parameters	Hypothetical oscillator		Developed oscillator
	circuit A	circuit B	
$dB_c/d\omega$	-0.8×10^{-11}	$-.52 \times 10^{-11}$	$-.9 \times 10^{-11}$
$dG_c/d\omega$	$-.2 \times 10^{-12}$	$.11 \times 10^{-12}$	$-.24 \times 10^{-11}$
$\partial B_D/\partial v$	$.6 \times 10^{-4}$	$.3 \times 10^{-5}$	$.336 \times 10^{-4}$
$\partial G_D/\partial v$	$.44 \times 10^{-4}$	$.04 \times 10^{-4}$	$.204 \times 10^{-4}$
$\tan \phi$	40.	-47.27	3.75
$\tan \theta$	1.36	.75	1.65

CHAPTER VIII

EXPERIMENTAL STUDIES ON IMPATT DIODE OSCILLATORS

The emphasis so far has been on developing a nonlinear model to describe the behaviour of microwave active circuits embedding a certain class of negative resistance devices. This theory has been applied to Impatt diode oscillators in order to demonstrate how the general theory can be adopted to a particular device, and also to develop an insight into the characteristics of these oscillators under transient and steady state conditions.

For experimental studies, an Impatt oscillator has been designed for pulsed operation. The oscillator design and experimental arrangement for measuring the transients is discussed in the first section of this chapter. In Section 8.2, steady state and transient studies are presented for oscillators using two Impatt diodes whose large signal admittances have been presented in Chapter V. The experimental results are compared with those predicted theoretically in the previous chapter. The operation of the bias modulated oscillators is discussed in the last section.

8.1 Design of Impatt diode oscillator and the measurement system

The system to be used in the transient measurements

consists of a resonator circuit, the bias circuit and the instantaneous frequency and amplitude measuring arrangement. The latter has been discussed in Chapter VI. The measurement system is shown in Fig. 8.1 and an expanded cross sectional view of the oscillator is given in Fig. 8.2. This oscillator is equipped with a unique bias arrangement to make it suitable for pulsed operation mode. Two special terminals, one for monitoring the diode currents and another for monitoring the modulating pulse have been provided.

8.1.1 The resonator circuit

The Impatt diodes, whose specifications are given in Table 8.1, were separately end mounted in a single slug 7 mm coaxial cavity (Fig. 8.3). To ensure that only the TEM mode exists in the cavity, even at the second harmonic of the RF frequency, a 7 mm airline was used for the cavity construction. These diode cavities are of the single transformer, fixed frequency type, so that they could be represented by a simple equivalent circuit. A change of operating frequency requires a change of the center conductor; however, this was a straightforward procedure. The single transformer is designed to match the 50 ohm characteristic impedance of the transmission line to the impedance at the steady state operating frequencies of 5.85 GHz for diode #1 or 5.81 GHz for

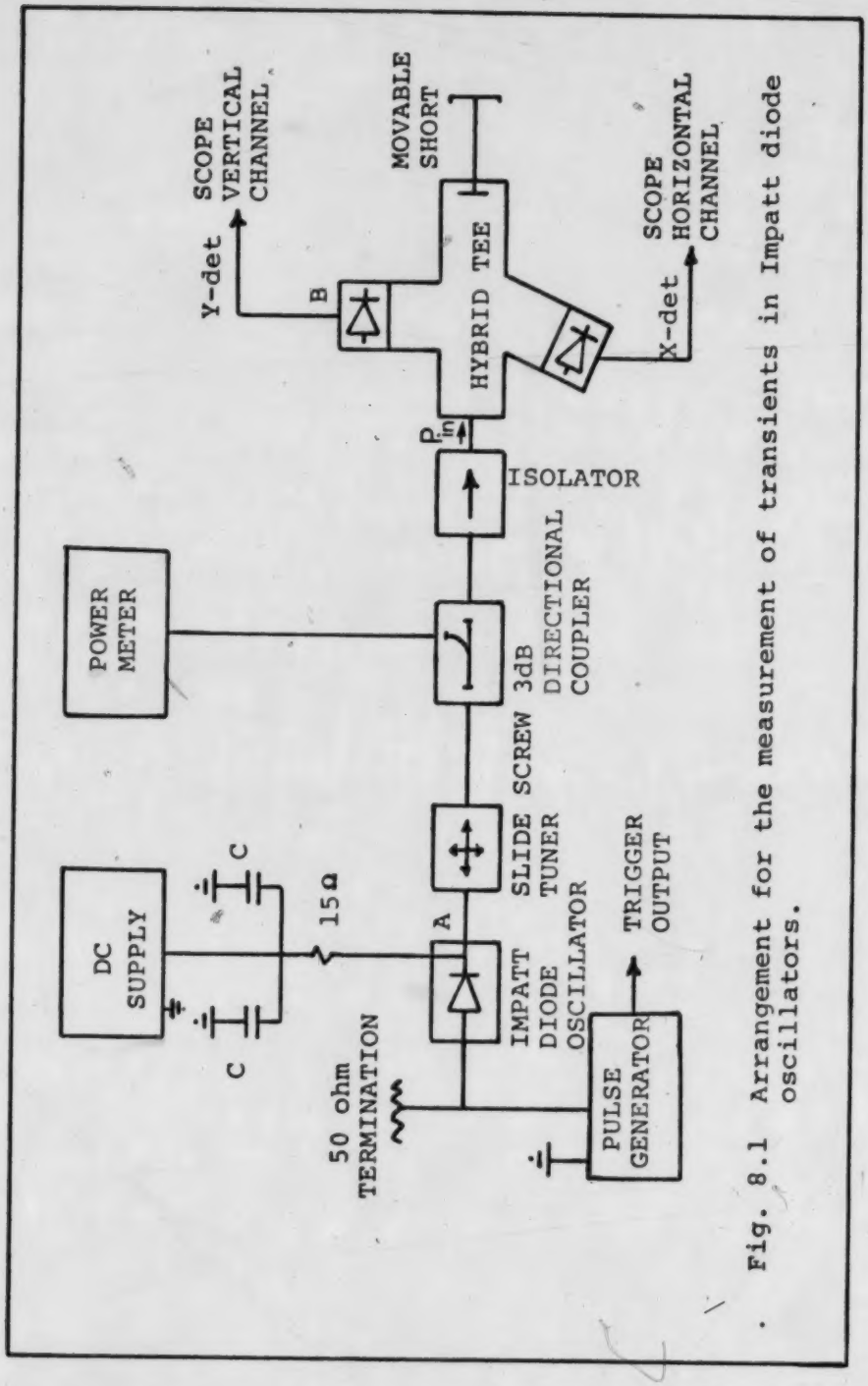

Fig. 8.1 Arrangement for the measurement of transients in Impatt diode oscillators.

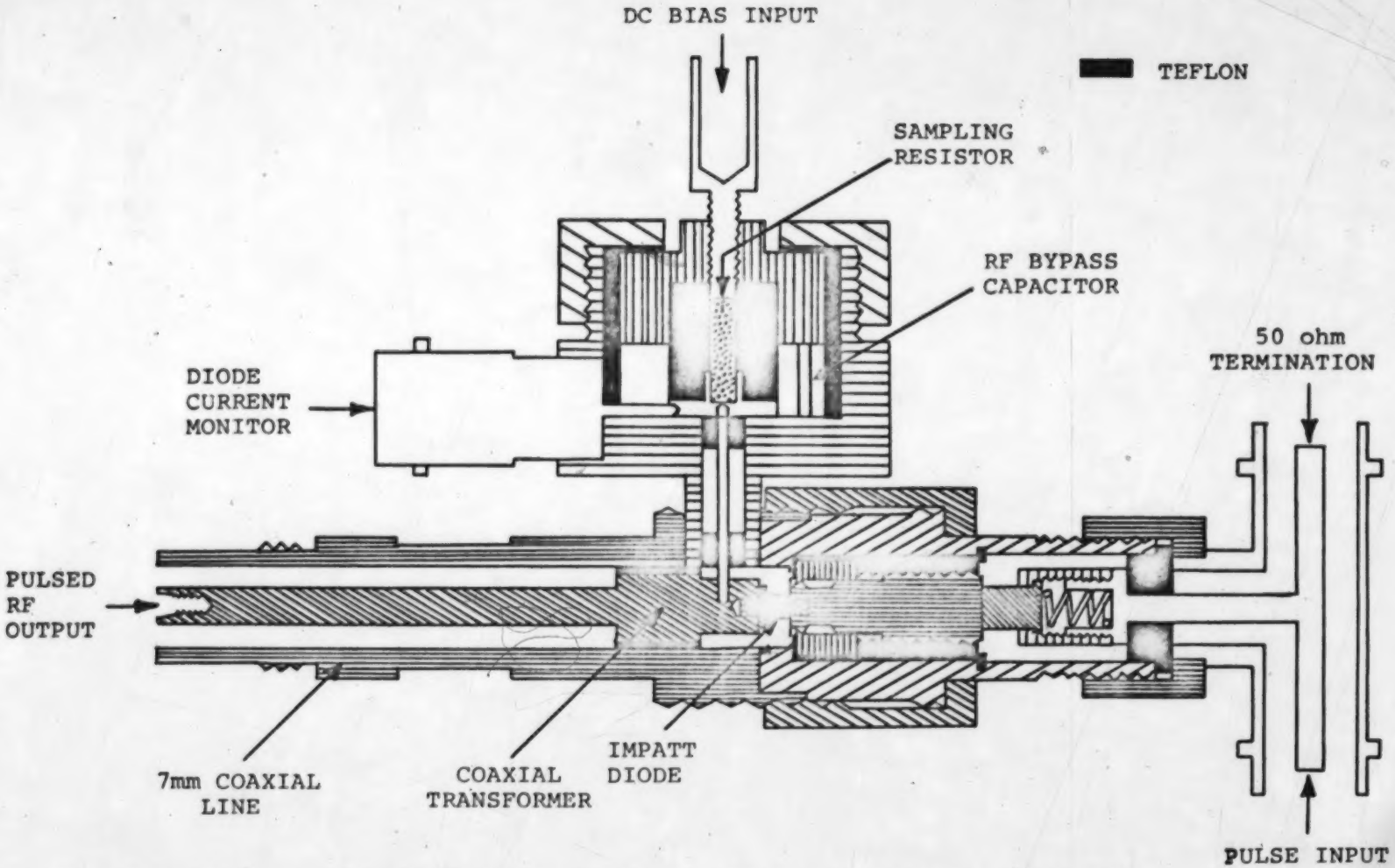

Fig. 8.2 Cross-sectional view of the Impatt diode oscillator used in the measurement of the transients.

diode #2. The impedance transformer is designed using known techniques [61].

In addition, the discontinuities of the transmission line due to the single slug are included as appropriate discontinuity capacitances [62]. The transformed impedance can be put in parallel with the diode impedance, i.e. wafer and package, to obtain a complete model of the circuit. An approximate equivalent circuit representing this transformation is shown in Fig. 7.5b. The diode is biased by using a special arrangement to be discussed in the next section. The diode current is monitored by measuring the voltage across a 15 Ω series resistor in the biasing circuit.

It should be noted that if planes A and B (Fig. 8.3) coincided with each other, then one side of the diode would be effectively grounded. This configuration is suitable for CW operation or for pulsed operation with the pulse generator connected to the ground negative terminals of the dc power supply. This last case is not acceptable because the pulse generator is then loaded by the capacitance of the power supply negative terminal to ground; the value of this capacitance for the HP 6207B dc power supply used is about 1500 pF. Therefore, for pulsed operation, planes A and B are separated by a 2 mil thick teflon sheet and the pulse generator is connected between the heat sink and ground.

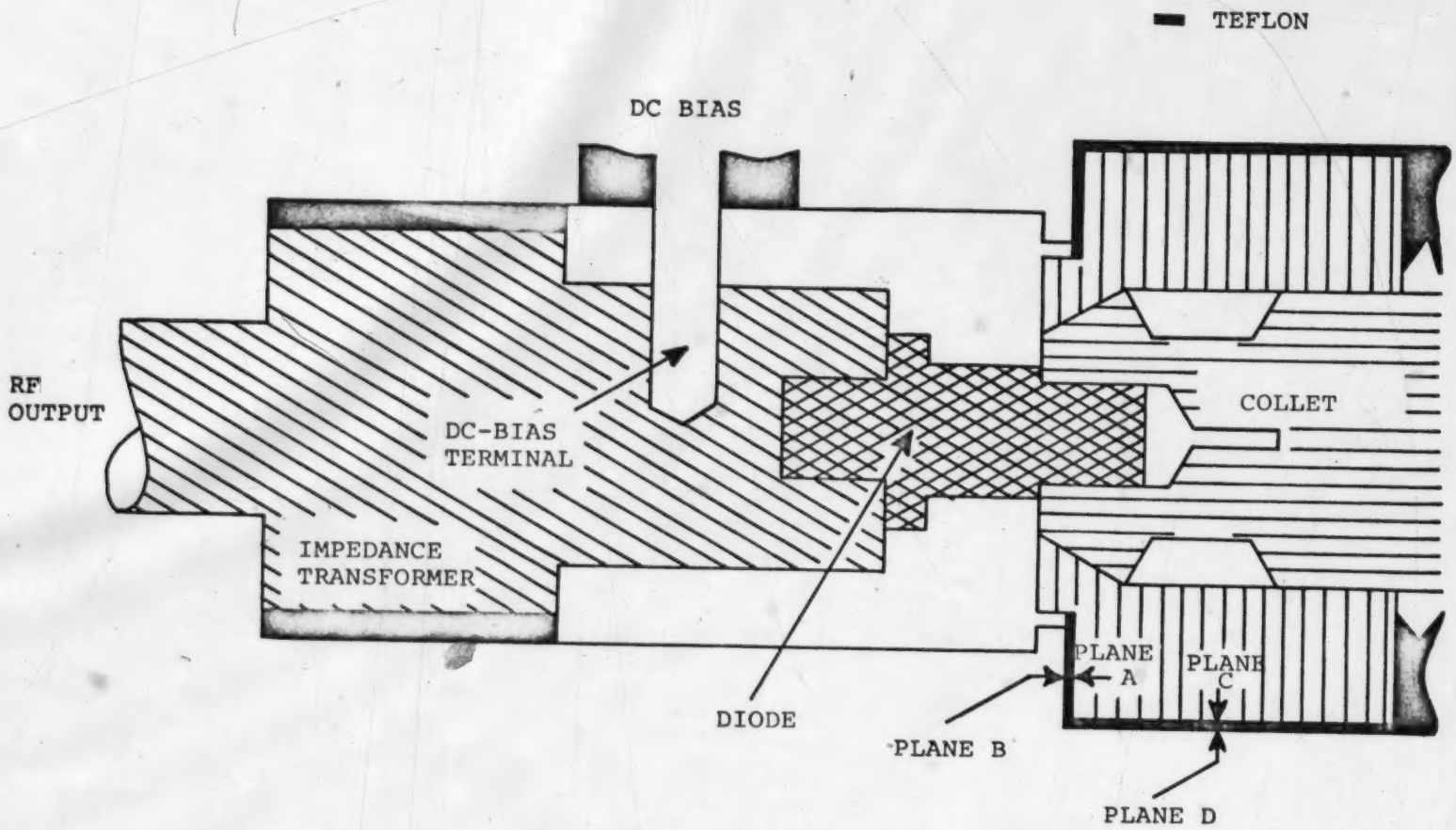

Fig. 8.3 Cross-sectional view of the 7mm coaxial cavity with end mounted Impatt diode.

In addition, there is a capacitance between planes C and D so that the total capacitance between the heat sink and ground is 60 pF as measured on a #71A Boonton meter. At 5.8 GHz this capacitance is equivalent to an impedance of about $1.44/\pi$ ohms. The penalty for decreasing the RF impedance further is a prohibitively high time constant seen by the pulse generator. Noting that the output impedance of the pulse generator is 50 ohms and without including any other capacitances, the time constant for the circuit is 3 ns. There is a distinct trade off between the value of the RF short and the time constant associated with the circuit. The use of a 50 ohm termination in parallel with the output of the pulse generator reduces the time constant of the circuit to 1.5 ns. The value of 60 pF chosen for the RF blocking capacitance (heat sink to ground) is considered near optimum for the circuit used.

8.1.2 The bias circuit

The Impatt diodes in oscillator circuits are usually biased through a biasing element called a bias tee. This arrangement is adequate for CW operation. However, under pulsed operation the capacitance in the RF arm of the bias tee ($\simeq$ 12 pF) and the inductance in its dc arm ($\simeq$ 20 nH at 50 MHz) degrade the rise time of the diode bias current which in turn affects

the rise time of the measured modulated signals (RF envelopes). To alleviate this problem, a different arrangement has been used as shown in Fig. 8.2 in which the dc voltage is supplied directly to the diode through a resistor. Two feed through capacitors (≈ 12000 pF), acting as RF shorts, isolate the RF from the dc power supply. This, together with a 15 ohm resistor inserted in the dc circuit, prevents instabilities which might result in bias oscillations [64]. The bias circuit as seen from the pulse generator terminals can be modelled as shown in Fig. 8.4.

The major contributing factor to the length of the rise and decay times of the diode current is the time constant of the parallel RC circuit loading the pulse generator. This is shown in Fig. 8.4 as a parallel combination of the source resistance R_s, the terminating resistance R_T and the heat sink to ground capacitance C_H. The rise time of this RC circuit can be decreased in one of the two ways:

1. by decreasing the value of C_H
2. by decreasing the value of R_s.

C_H acts as an RF bypass for the cavity. Decreasing this capacitance below 60 pF results in an excessive amount of RF radiation losses through the back of the cavity. Decreasing the value of R_s by further loading the pulse generator results in a very low voltage pulse across the

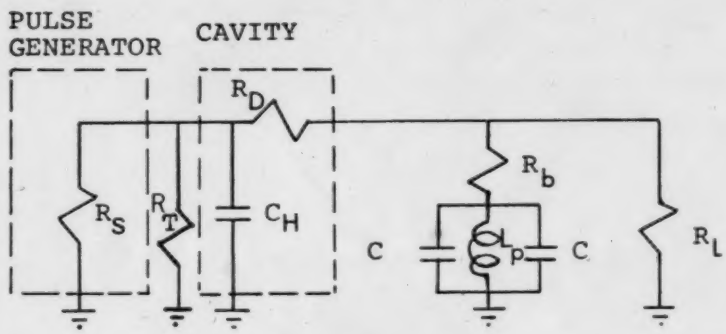

where R_D = diode resistance
R_b = bias current measuring resistor =15Ω
C_H = heat sink capacitance to ground=60pf*
C = feed through capacitor =12000pf
L_p = DC supply input inductance =160nH at 50MHz**
R_S = pulse generator source resistance = 50Ω
R_L = load resistance =50
R_T = load termination = 50Ω

* measured with Boonton 71A inductance-capacitance meter

** measured with Hewlett Packard HP8405A vector voltmeter

Fig. 8.4 Bias circuit as seen from pulse generator terminals.

diode. There is a trade off for high pulse repetition generators between short transients and high amplitudes. With these considerations, the compromise values of R_s and C_H are those given in Fig. 8.4. It may be stressed that these results are restricted to the circuit used in the experiments reported here.

It has been assumed in the above discussion that the RF oscillations start as soon as the pulsed current startsto flow. This assumption is seldom true as will be seen later in this chapter.

The following are the various possibilities for biasing the diode under pulsed operation:

1. biasing at 0 V dc (i.e., no dc bias voltage)
2. biasing at the breakdown voltage
3. biasing below the oscillation threshold but above the breakdown voltage
4. biasing at the oscillation threshold.

A trade off exists in high-prf pulse generators between fast rise times and high pulse amplitudes. For the required rise times of less than 2.5 ns, only 10 V pulse generators are commercially available. Biasing below the breakdown voltage and pulsing the diode into avalanche breakdown results in fluctuations at the leading edge of the diode current pulse. This is due to the statistical nature of the avalanche process. The above considerations preclude biasing the diode

below the breakdown voltage. Biasing below the oscillation threshold introduces some finite time delay before the current reaches the threshold level of oscillations. Therefore, a suitable biasing point for bias-modulation applications is at the oscillation threshold. This is in spite of the fact that there is always a time delay between the RF envelope and the diode current even at this condition; biasing at the oscillation threshold at least minimizes this delay. This biasing point has the added advantage that the diode is already dissipating one or two watts; hence the temperature fluctuations under pulsed conditions are minimized.

8.2 Transient and CW measurements on the oscillators

The two diodes whose large signal admittances have been measured and reported in Chapter V are embedded in the coaxial cavity discussed in Section 8.1. The oscillators are designed for frequencies around 5.8 GHz. The diodes, under both CW and transient conditions, operate well within the frequency range for which their large-signal characteristics have been measured. However, depending upon the microwave circuitry, and functions involved, the diodes can operate over a wider frequency range (see Table 8.1).

Table 8.1 Specifications of HP 5082-0437 and HP 5082-0431 Impatt diodes used in experimental work [63]

Diode parameters	HP 5082-0437	HP 5082-0431
frequency range	5-9 GHz	5-9 GHz
typical operating voltage	110 V	110 V
typical operating current	25 mA	25 mA
breakdown voltage (V_b)	103 V	103 V
junction capacitance	0.29 pF	0.29 pF
output power	100 mW	100 mW
thermal resistance	20°C/W	20°C/W
package capacitance	0.26 pF	0.26 pF
package inductance	1.0 nH	1.0 nH

To measure the CW frequency and power, the measurement set up shown in Fig. 8.1 is employed. The current source shown in Fig. 8.1 is used in order to maintain a constant current in the biasing circuit. Additional dc supply is connected in series with the constant current source because the latter has a maximum output voltage of 100 volts while the diode operating voltage is over 110 volts. For the steady state measurements, the Impatt diode is first reverse biased into avalanche breakdown with I_{dc} = 25 mA and then left for about half an hour to obtain a stabilized condition. The value of this current is chosen to be the same as that for which the diode large-signal admittance has been measured. For each diode the steady state (CW) frequency and power are recorded and compared with those evaluated in the previous chapter, i.e.

$$\omega = \bar{\omega} + x \tag{8.1}$$

$$P = \frac{1}{2} G_D A^2 \tag{8.2}$$

Under CW conditions, both x and A are time independent quantities. The measured and theoretically evaluated CW power and the frequency of two oscillators are given in Table 8.2.

Table 8.2. Theoretical and experimental steady state solutions (frequency and power) of the two Impatt diode oscillators used.

Diode type	CW operating frequency (GHz)		CW operating power (mW)	
	Exp.	Theo.	Exp.	Theo.
#1	5.8475	5.8767	120	134
#2	5.809	5.804	106	116.7

The evaluated and measured steady state quantities compare very well, in the case of the power the difference is about 12% and in the case of frequency the difference is only about 0.5%. Especially for diode #2, the measured and evaluated quantities are very close. Since both the CW power and frequency can be measured with an accuracy better than a few percent, the above differences are mainly due to the inaccuracies associated with the admittance measurement, which are about 12%. Generally, in different cavities the oscillating diodes can see a little different environment at harmonic frequencies compared to that under which the diode admittances were measured. This fact can account for different inaccuracies characterizing the diodes 1 and 2.

In order to compare the theoretical with the measured transients, the oscillator comprising diode #2 is considered under pulsed operation. In this case, contrary to the CW operation, the p-n junction temperature does not remain constant. The effect of junction temperature variation can be minimized by bias modulating the oscillator with pulses of high repetition frequency. With high pulse repetition frequency, on the other hand, the characteristics of the modulated RF will be dependent on the preceeding modulating pulses. This may not simulate well the conditions under which the transients of the oscillator are evaluated theoretically. However, decreasing the duty cycle by using pulses of smaller duration (about 30 ns) and thus increasing the off time, does not result in a noticeable change in the characteristics of the leading edge of the RF envelopes. Therefore a modulating pulse with an amplitude = 1.4 V, period = 30 ns with 10% ON time is used. Fig. 8.5 shows the wave shapes of the modulating pulse, diode current and the RF outputs of the two detectors of the discriminator. The discriminator and microwave components inserted between the diode and the discriminator cause about 10 ns delay between the RF output of the oscillator and the RF output of the discriminator. According to this figure, the applied bias pulse is not completely constant during its flat portion and diode

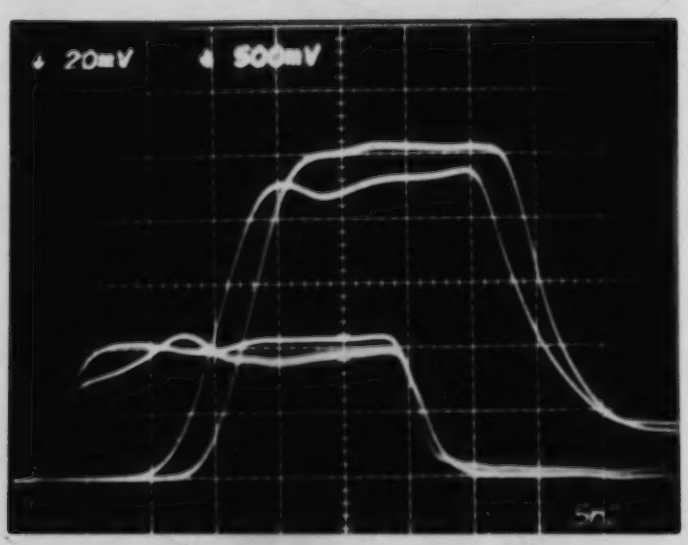

Fig. 8.5. From left to right; the modulating pulse (500 mV/cm), the diode current (100 mV/cm) and the two RF envelopes recorded by the X- and Y-detectors (20 mV/cm), respectively, for diode #2. Modulating pulse amplitude = 1.4 V, period = 300 ns with 10% ON time pulse.

current does not exactly follow the bias pulse (Fig. 8.6). Small parasitic reactive elements in the current measuring circuitry together with junction temperature effects may be responsible for small oscillatory fluctuations on the current waveform at its leading edge. The oscillation growth is taking place under almost isothermal conditions, note that the diode current before the pulse leading edge is constant. The oscillation decay, after the pulse is turned off, is significantly affected by the variable junction temperature. As can be seen, the diode current slowly decreases long after the bias pulse trailing edge and, because the junction temperature has strongly affected the diode RF characteristics, the trailing edge of the measured RF pulse reflects the transients caused by sudden change in the diode negative conductance which is still large enough to compensate for the circuit losses. Note that a relatively rapid transition of a trailing edge of the RF pulse is followed by a slowly varying portion which characterizes the decay of the small residual oscillation directly controlled by the junction temperature of the diode.

The two RF envelopes of Fig. 8.5 together with the calibration curves in Fig. 6.7 are used to evaluate the rise time of the oscillations. This has been achieved by calculating the instantaneous power at various time instants starting from the leading edge

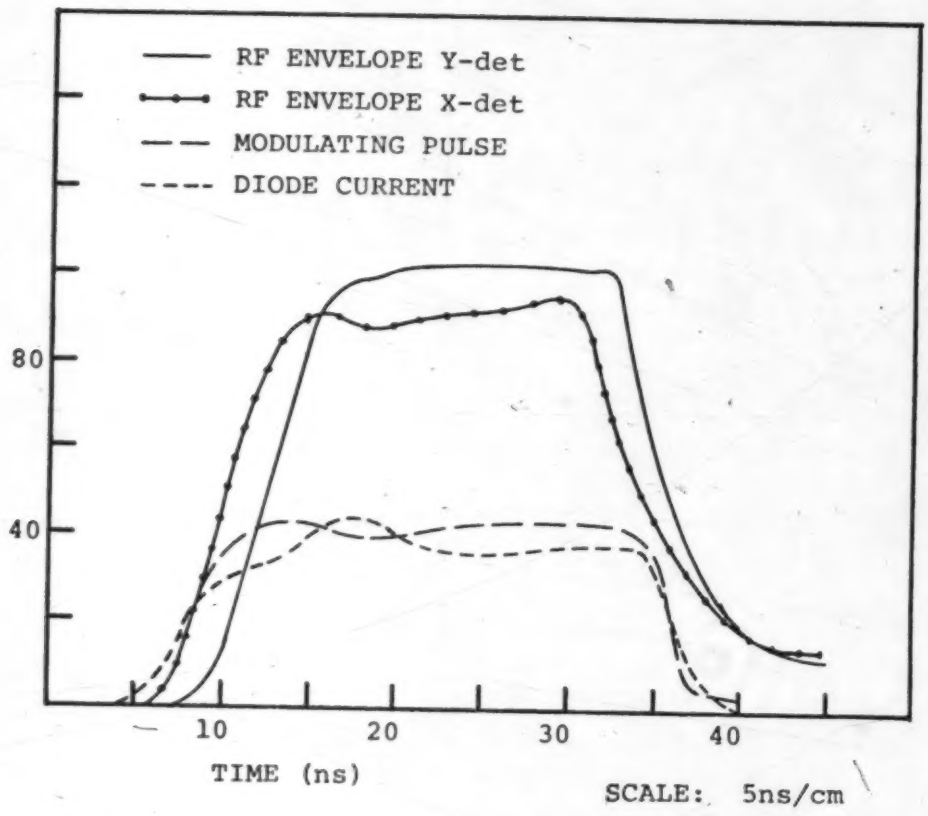

Fig. 8.6 A reproduced copy of Fig. 8.5 with the time scale adjusted for a 10ns delay caused by the measurement system.

of either of the RF envelopes. The values are then plotted on the calibration curves of the system (x-y polar display, Fig. 8.7) and by interpolation, the instantaneous frequency and power are determined for each time instant. The points numbered 1,2,..., are corresponding to different time intervals along successive points on the RF envelope graphs.

Fig. 8.8 shows the growth of the oscillator RF power vs time as obtained from the two experimentally determined RF envelopes in Fig. 8.5 after multiplying by a factor of two to allow for the 3 dB coupler of Fig. 8.1. The figure also shows the growth as calculated on the basis of the backward recursive method (Fig. 7.8). The measured power is shifted in time by 8 ns in comparison to the time scale for the two RF envelopes (Fig. 8.5). The experimental curve indicates that the rise time of the RF oscillations is about 7 ns. In view of the discussion of the transients in the bias circuitry in section 8.1, this value compares fairly well with the value of 5.4 ns calculated on the basis of the backward recursive method (Fig. 7.8). It can also be noted that the measured power corresponding to the flat portion of the bias pulse is about 126 mW as compared to the calculated steady state value of 116.7 mW. This difference can be attributed to the fact that the calculations are based on the diode admittance

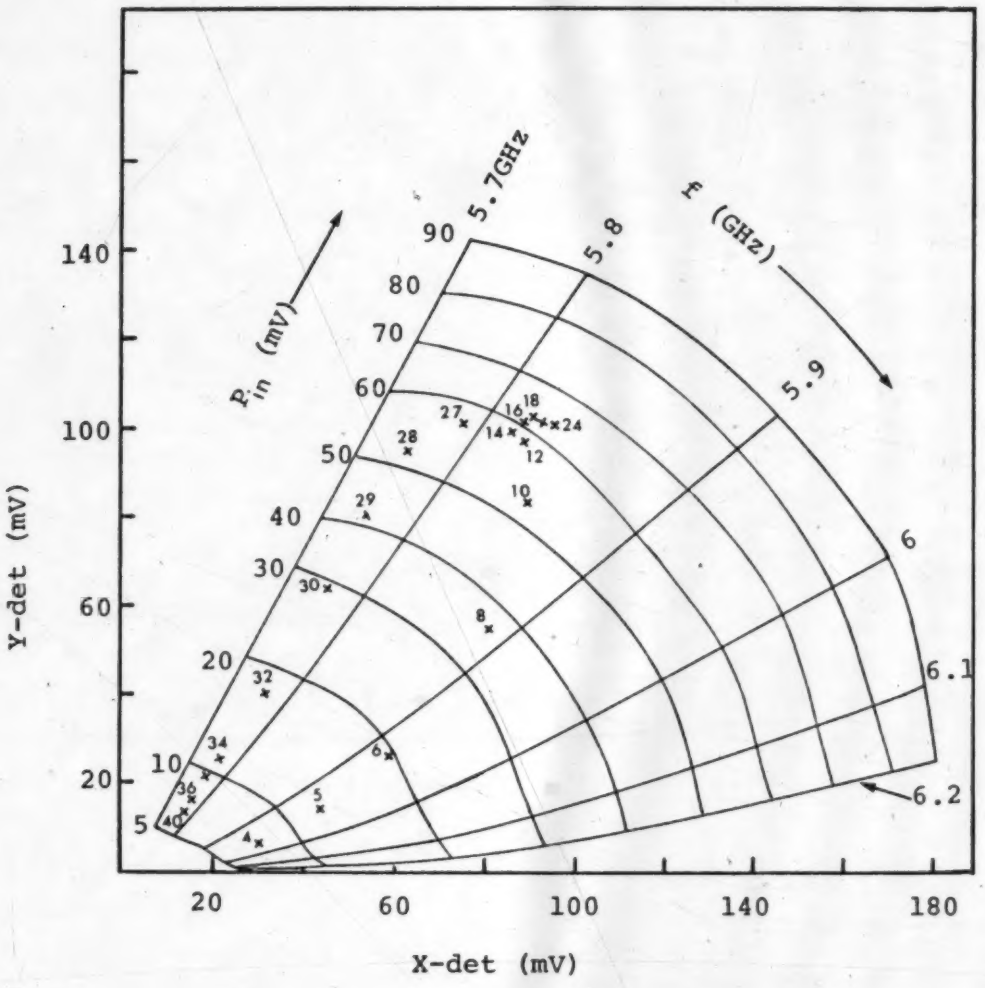

Fig. 8.7 System calibration for instantaneous frequency and at different instance of time on the RF envelopes of Fig. 8.5.

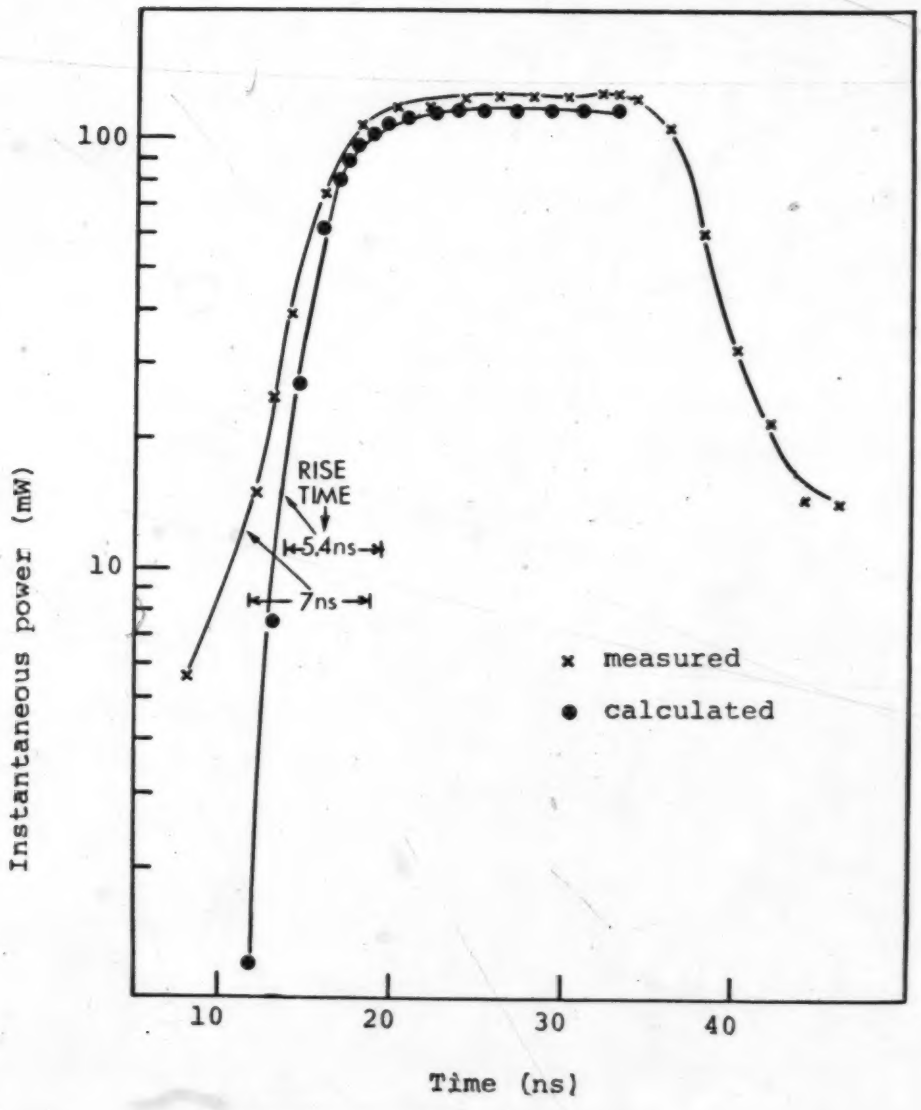

Fig. 8.8 Measured and calculated power waveforms of the Impatt diode oscillator.

which is measured under constant thermal conditions. However, in the pulsed mode of operation (due to the ON and OFF sequence of pulses) the diode junction temperature is slightly different from that at which the large signal admittance is measured.

Fig. 8.9 shows the instantaneous frequency vs time behaviour (the crosses indicate measured values deduced from the two RF envelopes of Fig. 8.5, and the dots show figures calculated from the theoretically determined values of x and $\bar{\omega}$ (Fig. 7.8)). It may also be noted that in this case the time scale for the measured frequency is shifted by 8 ns in comparison to the time scale for the two RF envelopes. The two curves in Fig. 8.9 show a similar trend until about 33 ns. The frequency difference of about 80 MHz is observed at the leading edge of the bias pulse. For the flat portion of the pulse, a frequency difference of only about 10 MHz is observed.

The Impatt diode oscillator used in these measurements is designed to oscillate at about 5.8 GHz if the diode bias current is 25 mA. To avoid the RF pulse jitter and to operate at junction temperature close to that at which the large signal admittance of the diode was measured, the diode is pulsed from about 16 mA (OFF state) to 25 mA (ON state). The bias current reaches a value of 25 mA, and thus the design conditions are

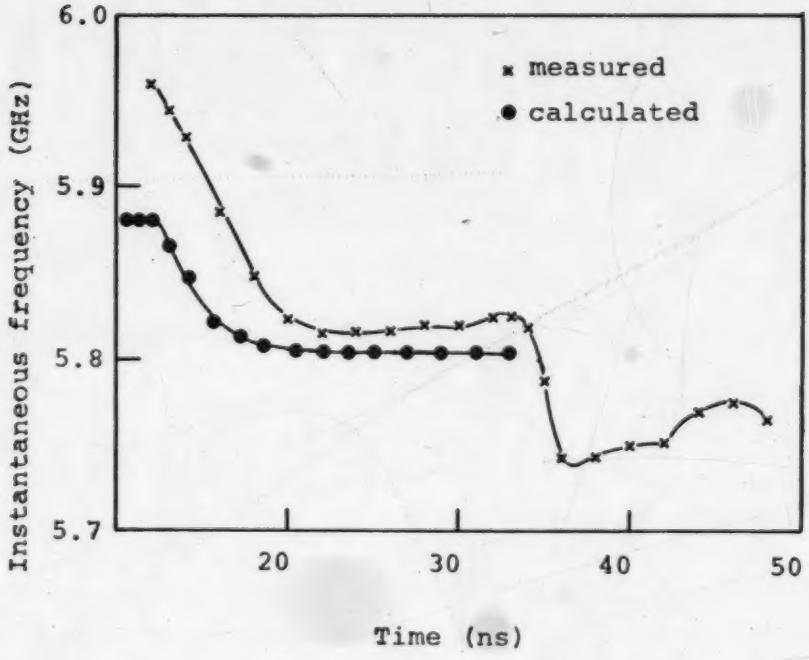

Fig. 8.9 Measured and calculated time dependence of the frequency of the Impatt diode oscillator.

attained during the flat portion of the pulse. In the OFF state, no oscillations should be present in the circuit. When taking measurements, the output of the discriminator diodes was used to determine the OFF pulse current level. Fig. 8.5 shows no oscillations in the OFF state. However, the diode sensitivity is very limited and any low power oscillations can hardly be detected. A spectrum analyzer should be used when selecting the OFF state current level. Fig. 8.9 indicates that low power oscillations were present in the oscillator during the OFF state. The frequency of these oscillations, determined by the circuit impedance and the small signal impedance of the diode bias at 16 mA, seems to be around 6.0 GHz. When the diode is pulsed on, the oscillations grow from the low level oscillations, already present in the resonator, and not from the circuit noise whose frequency is determined by the circuit impedance and the small signal impedance of the diode biased to 25 mA. Thus, at the beginning of the ON pulse, the frequency of the experimental oscillator changes rapidly and the conditions are very different from these used in the calculations. When approaching the flat portion of the pulse, the experimental conditions approach those of the conditions used in the calculation; this is true for both the

frequency and the rate of change of frequency. The undesired oscillations may be avoided if the oscillator is carefully tuned, not only for operation at 25 mA, but also for 16 mA.

The time dependence of the oscillator frequency during and after the trailing edge of the bias pulse, i.e. for instants of time exceeding 33 ns, is determined by the residual oscillations. Note that the measured RF envelopes indicate oscillations far into the OFF state. These oscillations could be prevented if lower bias current for the OFF state is selected or if the circuit is properly tuned.

8.3 Bias modulated Impatt diode oscillators

Bias modulated Impatt diode oscillators can be used in transmitters of digital radio systems. These combine modulation and generation functions in a single stage and depending on output power requirements, RF amplification stages may not be needed. Hence such systems may be economically very attractive. The noise disadvantage of ASK modulation in such simple systems can be partially offset by the fact that higher pulsed power can be obtained from a given

oscillator. If a 50% modulation scheme is adopted, the oscillator pulsed output power can be almost doubled in comparison with its CW outputs.

The spectral distribution of the energy of the transmitted signal is an important consideration in a modulation scheme. In an ideal ASK system, the RF spectrum, centered at the carrier frequency, is identical in shape to the baseband spectrum of the modulating signal. In this case, the percentage of the power in the main lobe of the RF spectrum is the same as the percentage of the power in the main lobe of the baseband spectrum, i.e., the spectrum of the envelope. For an ideal ASK system, the RF spectrum is always symmetrical around the carrier frequency, regardless of the pulse shape.

In a digitally modulated Impatt oscillator, the carrier frequency is not constant and an undesired FM component is present. This is due to the fact that the electronic susceptance is a function of the diode current, the amplitude of RF voltage, and the junction temperature. Hence when the current changes, the frequency will also change. Under pulsed conditions, the shape of the current waveform and that of the applied pulse are similar, resulting in the frequency being decreased during the build up of the oscillations. This observation can be verified from the change of the

instantaneous frequency during the pulse ON period as shown in Fig. 8.9. The frequency also changes during the main part of the pulse due to heating of the diode; this is a consequence of the temperature dependence of breakdown voltage as mentioned earlier.

To give some insight into the limitations of bias modulated Impatt diode oscillators two sets of experiments are performed. The diode is dc biased at the threshold of oscillations and then modulated with pulses of either varying duty cycles or 50% duty cycle with different periods (Tables 8.3 and 8.4).

For the operating conditions described in Tables 8.3 and 8.4 the two RF envelopes detected by the X- and Y-detectors, and the diode current are recorded simultaneously. The results corresponding to the duty cycles of 0.5 and 0.2 are illustrated in Figs. 8.10 and 8.11. These figures show that the shapes of the RF envelopes are different and also the decay time increases with decreasing duty cycle. The latter observation is a consequence of temperature effects. The two instants at which maximum power and .87 maximum power occur are used as reference points for which the corresponding change in frequency is evaluated. These power points correspond approximately to the main portion of the RF envelopes recorded for various duty cycles. Fig. 8.12 shows the measured effect of duty cycle variation on

Fig. 8.10. From left to right; the diode current (100 mV/cm) and the two RF envelopes (20 mV/cm) recorded by the X- and Y-detectors, respectively, under the operating conditions stated in Table 8.3 for a modulating pulse with duty cycle of 0.5.

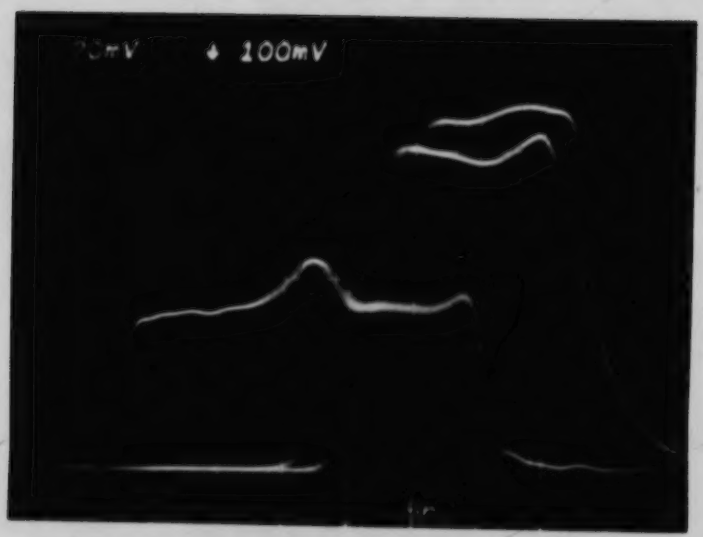

Fig. 8.11. From left to right; diode current (100 mV/cm) and the two RF envelopes (20 mV/cm) recorded by the X- and Y-detectors, respectively, under the operating conditions stated in Table 8.3 for a modulating pulse with duty cycle of 0.2.

Table 8.3. Operating conditions under changing duty cycle from 50% to 10%.

Characteristic	Value
Pulse duration	30 ns
DC bias current	16.2 mA
Applied voltage pulse amplitude	2.1 V

Table 8.4. Operating conditions under fixed (50%) duty cycle and changing pulse period from 60 ns to 300 ns.

Characteristic	Value
Pulse duration	30 ns
DC bias current	16.2 mA
Applied voltage pulse amplitude	2.1 V

frequency during the main portion of the pulse. The dashed line for a given period reflects the frequency change between the two reference points in the main portion of the pulse. It is seen that, for a given pulse length, the frequency variation during the ON time increases as the duty cycle decreases. A similar behaviour is observed for the decay time of the RF envelopes which increases with the decrease in the duty cycle (Fig. 8.13).

Below an OFF time of about 240 ns, the average diode junction temperature increases and there is a smaller temperature variation during the ON time. On the other hand keeping a 50% duty cycle and increasing the pulse period does not show any significant change in frequency because the temperature variation between ON and OFF periods of the pulse is smaller as compared to the smaller duty cycle pulses. A reference point is chosen at the maximum power level. The instantaneous frequency at this point is calculated and plotted against the corresponding pulse period (Fig. 8.14). It is observed that there is insignificant change in the instantaneous frequency with the pulse period employed. It was also noted that there was no significant change in the decay time.

In realistic digital applications, the change of the carrier frequency is undesirable since it will

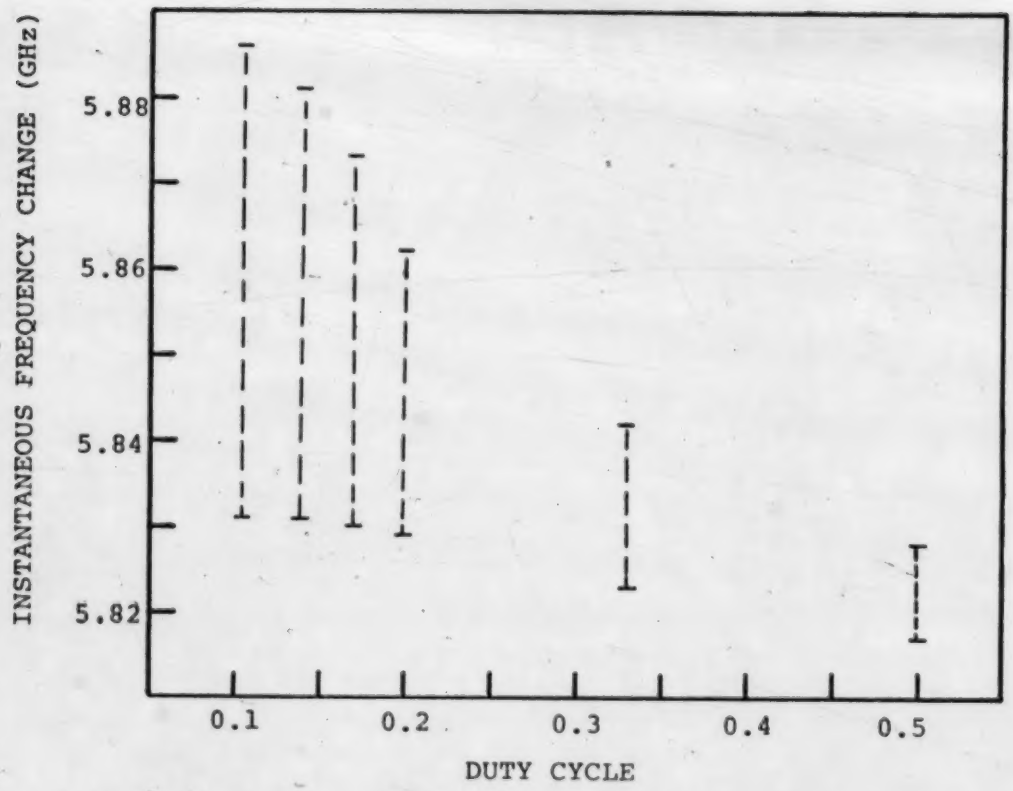

Fig. 8.12 Frequency variation, for pulses of 30ns ON time, as a function of the duty cycle between two instances for which the power changes between its maximum value and 87% of this value.

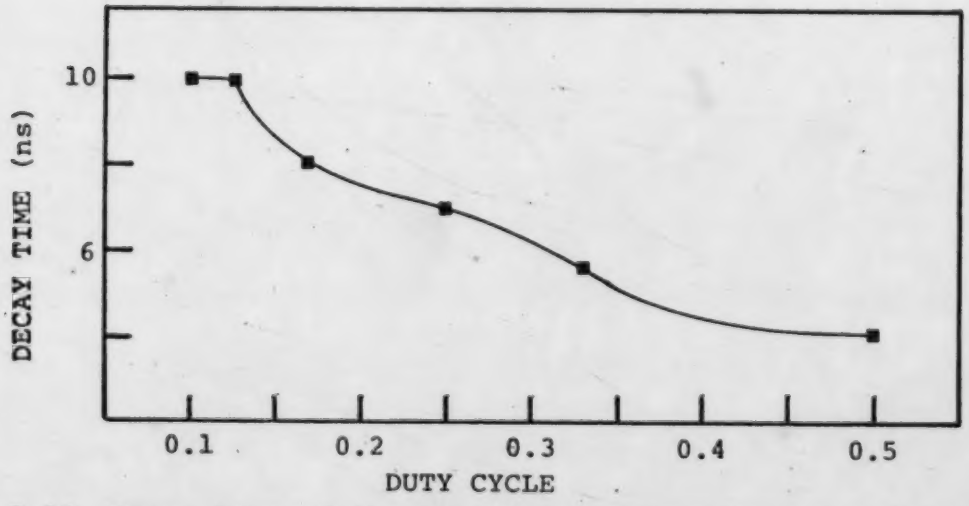

Fig. 8.13 Decay time of the RF envelopes as a function of the duty cycle due to a 30ns ON pulse.

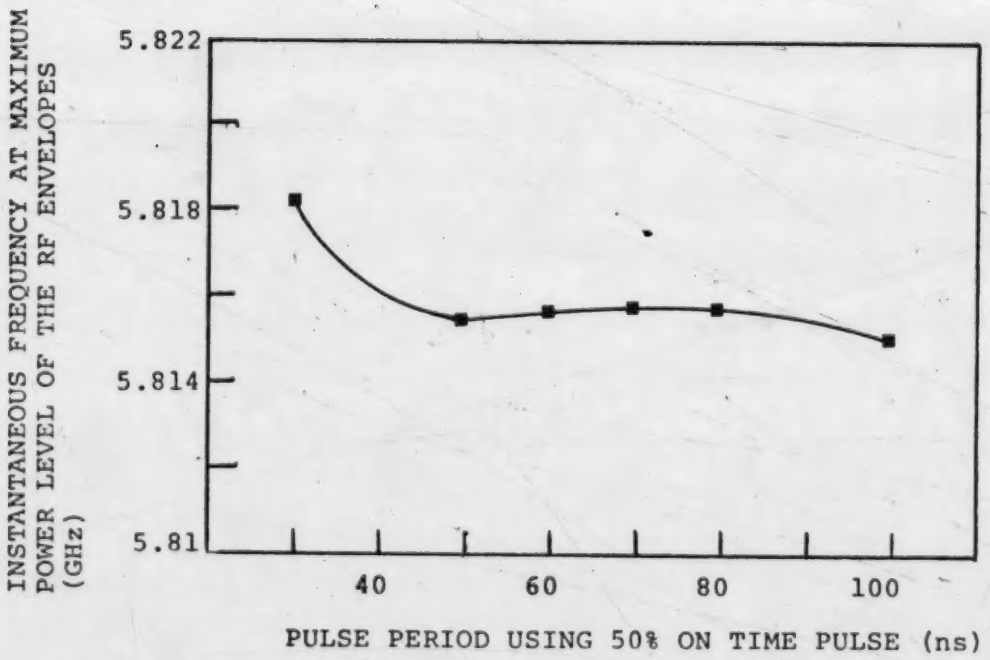

Fig. 8.14 Instantaneous frequency at maximum power level vs. pulse periods (50% ON time pulses).

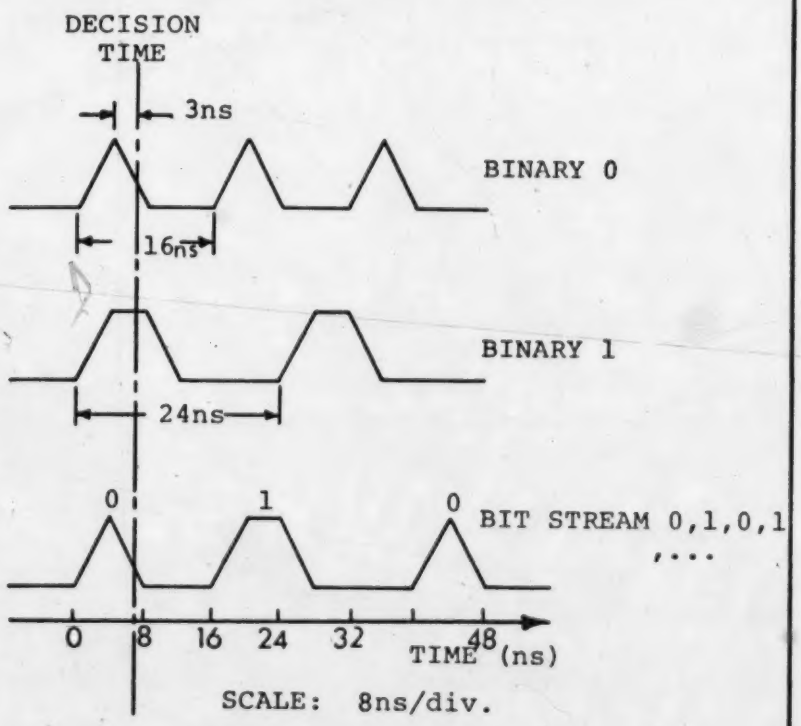

Fig. 8.15 Modulation scheme for utilizing bias modulated Impatt diode oscillator for the transmission of data at nearly 40 Mbits/s.

result in intolerable interference in adjacent channels. The experimental results shown above indicate that the most serious drawbacks of the simple ASK bias modulation associated with the changes in the carrier frequency can be minimized by employing coding schemes based on 50% duty cycle pulses. According to Fig. 8.13, the narrowest pulse which can be handled by the bias modulated Impatt diode oscillator is 8 ns. Adopting a modulation scheme where binary zero is characterized by 8 ns pulses and 50% duty cycle, about 40 M bits pulse stream (see Fig. 8.15) can be handled by the bias modulated Impatt diode oscillators without introducing unwanted interference. To decode such a signal, the decision time instant should be delayed behind the pulse peak by about 3 ns as shown in Fig. 8.15.

Since only a simple peak detector and a constant delay circuit are needed on the receiving side of the system, the above modulation scheme makes the bias modulated Impatt oscillators suitable for digital applications handling bit rates up to 40 Mb/s.

CHAPTER IX

SUMMARY AND CONCLUSIONS

In this study a nonlinear model has been developed for the investigation of microwave circuits with embedded two terminal active devices. The general model is equally well suited for both discretely characterized and analytically described active and passive circuits. It can be used in the design, study and optimization of microwave oscillators and amplifiers.

By separating the passive microwave circuitry from the active device, the active microwave circuit can be well described by two nonlinear differential equations. Unlike the previous models, which take into account the RF voltage dependence of the active device admittance up to a maximum of the third order (e.g. Van der Pol's cubic nonlinearity), the model presented here considers the admittance dependence on both RF voltage and frequency up to the sixth order. Moreover, the previous models, based on single tuned GLC circuits, were restricted in their applicability to simple microwave circuits for narrow band operation. The model presented in this study, on the other hand, is of a more general nature which makes it suitable for any dynamic and steady state study of broad band oscillators and injection locked oscillators. The applicability of the method

has been illustrated with a transient and steady state study of the Impatt diode oscillator.

Numerical methods have been developed for the solution of nonlinear equations describing steady state and transient operation of Impatt diode oscillators. It has been found that the transient study based on a forward recursive method is suitable only for simple GLC circuits while the backward recursive method is found to be, so far, the only alternative for obtaining a solution for the more complex circuits encountered in practice.

The determination of the model parameters requires the large-signal admittance values of the diode and also the admittance of the embedding circuitry. Therefore, an accurate method has been designed and tested for the measurement of both the large-signal admittance of an Impatt diode and the embedding circuitry. The measurement system is characterized by two 2-port networks whose parameters are determined with an error of less than 3%. The method is also readily adopted for measurements at various frequencies. One special feature of the measurement technique is that it effectively eliminates the systematic errors inherent in any microwave measuring system. Two types of Impatt diodes were operated as reflection type amplifiers in a tunable coaxial resonator. The large-signal admittance of these

diodes and their associated circuitry, when embedded in a specially designed oscillator, were measured by the above mentioned technique at different power levels and at a single bias current of 25 mA. The overall error in these measurements is estimated to be in the neighbourhood of 12%. This accuracy is better than that obtained by all other methods except that of Van Iperen and Tjassens. These authors use a more complicated approach which limits the applicability of their system if measurements are sought at various frequencies.

A coaxial type Impatt diode oscillator with a single slug transformer has been designed. Special bias circuitry optimizes the oscillator characteristics under pulsed operation. The rise time of the diode current pulse is about 3 ns or less which compares very well with the 2.0 ns rise time of the applied voltage pulse. The oscillator is capable of handling pulsed modulating signals up to 40 Mb/s.

The two Impatt diodes characterized above were end mounted in two single slug transformers to form two oscillators of the developed type. The steady state power and frequency together with the transient response of the second diode were measured with the help of a frequency discriminator.

In the course of this study, a novel frequency discriminator has been developed to measure the Impatt

diode transient and steady state behaviour. Its simplicity allows the discriminator to measure power and frequency changes in nanosecond time intervals. The discriminator can be calibrated using CW signals. Using a PIN modulator, the discriminator error in measuring the frequency of fast changing signals has been found to be better than 4 MHz.

The measured steady state frequency and power together with the transient response of the two Impatt diode oscillators have been compared with the computed solutions obtained on the basis of the backward recursive method. Fair agreement between the theoretical and experimental data has been found. The steady state power differs by 12% and frequency by 0.5%. On the other hand, the measured rise time of 7 ns is about 1.6 ns longer than that evaluated theoretically.

The backward recursive method has also been used to evaluate the response of the two hypothetical diodes for which the large-signal admittance has been published. These diodes are considered to be embedded in two resonators with different sets of parameters. It has been shown that although the two oscillators are tuned to the same frequency of oscillation, their calculated rise times differ by about 20%. In addition, the following characteristics have been revealed by the studies on Impatt diode oscillators under steady state and transient

conditions:

1. The diode admittance dependence on RF voltage is not as simple as that expected by Van der Pol's cubic nonlinearity.

2. The nonlinear dependence of the diode admittance on frequency cannot be ignored.

3. The calculated steady state and transient parameters of the oscillators determined by using the present model depend on the accuracy by which the admittances of the diodes as well as the passive circuitry is measured.

4. The value of the oscillator transients depends on the interaction between the device characteristics and the circuit loci.

During the course of this work, certain aspects of the study arose which merit further investigation:

a) The influence of the interaction between the device line and circuit locus in optimizing the transients in oscillators.

b) The stability in oscillators and amplifiers.

c) Incorporation of the presented model into available computer aided routines for design analysis and optimization of microwave active circuits.

The model developed here can also be used in dynamic studies on broad band power amplifiers. The presented model has been successfully used in evaluating

distortion and intermodulation products in Impatt diode amplifiers [65].

The discriminator developed for the measurement of instantaneous power and frequency can be adapted, due to its simplicity and very fast response time, to studying the transients in digital communication systems.

REFERENCES

1. W.E. Wilson, "Pulsed LSA and TRAPATT Sources for Microwave Systems", Microwave Journal, vol. 14, pp. 33-41, August, 1971.

2. V.J. Higgins, J.J. Baranowski, "The Utility and Performance of Avalanche Transit Time Diodes and Transferred Electron Oscillators in Microwave Systems", Microwave Journal, vol. 13, pp. 37-42E, July, 1970.

3. D.E. Inglesias, J.C. Irwin, and W.C. Niehaus, "10 W and 12 W GaAs Impatts", IEEE Trans. Electron Devices, vol. ED-22, p. 200, April, 1975.

4. S.M. Sze, Microwave Avalanche Diodes", Proc. IEEE, vol. 59, pp. 1140-1154, August, 1971.

5. H. Kozimo, Y. Ito, H. Ashida, and M. Shinoda, "A .5 W CW Impatt-diode Amplifier for High Capacity 11 GHz FM Radio Relay Equipment", IEEE J. Solid-State Circuits, vol. SC-8, pp. 14-20, February, 1973.

6. S.F. Paik, P.J. Tanzi, and Douglas J. Kelley, "Impatt-Diode Power Amplifiers for Digital Communication Systems", IEEE Trans. Microwave Theory Tech., vol. MTT-21, pp. 716-720, November, 1973.

7. M.E. Hines, "Negative-resistance Diode Power Amplification", IEEE Trans. Electron Devices, vol. ED-17, pp. 1-8, February, 1970.

8. W.J. Evans and G.I. Haddad, "A Large Signal Analysis of Impatt Diodes", IEEE Trans. Electron Devices, vol. ED-15, pp. 708-717, October, 1968.

9. D.R. Decker, C.N. Dunn, and R.L. Frank, "Large-signal Silicon and Germanium Avalanche-diode Characteristics", IEEE Trans. Microwave Theory Tech. (Special Issue on Microwave Circuit Aspects of Avalanche-Diode and Transferred Devices), vol. MTT-18, pp. 872-876, November, 1970.

10. B. Van der Pol, "Forced Oscillations in a Circuit with Nonlinear Resistance (Reception with Reactive Triode)", Phil. Mag., vol. 3, pp. 65-80, January , 1927.

11. N.N. Bogliubov and Y.A. Mitroposky, Asymptotic Methods in the Theory of Nonlinear Oscillations. New York: Gordon and Breach, 1961.

12. H.J. Kuno, "Analysis of Nonlinear Characteristics and Transient Response of Impatt Amplifiers", IEEE Trans. Microwave Theory Tech., vol. MTT-21, pp. 694-702, November, 1973.

13. K. Kurokawa, "Some Basic Characteristics of Broad Band Negative Resistance Oscillator Circuits", Bell System Technical Journal, vol. 48, pp. 1937-1955, July-August, 1969.

14. L. Gustafsson, G.H.B. Hansson, and K.I. Lundstrom, "On the Use of Describing Functions in the Study of Nonlinear Active Circuits", IEEE Trans. Microwave Theory Tech., vol. MTT-20, pp. 402-409, June, 1972.

15. F.L.M.M. Stumpers, "Distortion IF Frequency Modulated Signals in Electrical Networks", Communication News (Philips), vol. 9, pp. 82-92, April, 1948.

16. J.H. Ahlberg, E.N. Nilson, J.L. Walsh, The Theory of Splines and Their Applications. New York: Academic Press, 1967.

17. K. Kurokawa, "Injection Locking of Microwave Solid State Oscillators", Proc. IEEE, vol. 61, pp.1386-1410, October, 1973.

18. R.M. Foster, "A Reactance Theorem", Bell System Tech. J., vol. 3, pp. 259-267, 1924.

19. J.L. Altman, Microwave Circuits, D. Van Nortrand Co., Inc., Princeton, N.J., pp. 31-36.

20. K. Kurokawa, "Noise in Synchronized Oscillators", IEEE Trans. Microwave Theory Tech., vol. 16, pp. 234-240, April, 1968.

21. R.E. Goldwasser and F.E. Rosztoczy, "High Efficiency GaAs lo-hi-lo Impatt Devices by Liquid Phase Epitaxy for X-band, Appl. Phys. Lett., vol. 25, pp. 92-94, July, 1974.

22. W.T. Read, "A Proposed High-frequency Negative Resistance Diode", Bell System Tech. J., vol. 37, pp. 401-446, March, 1958.

23. T. Misawa, "Negative Resistance in p-n Junctions under Avalanche Breakdown Conditions", IEEE Trans. Electron Devices, vol. ED-13, pp. 137-151, January, 1966.

24. S.R. Kovel and G. Gibbons, "The Effect of Unswept Epitaxial Material on the Microwave Efficiency of Impatt Diodes", Proc. IEEE, vol. 55, pp. 2066-2067, November, 1967.

25. S.M. Sze, Physics of Semiconductor Devices. New York: Wiley, 1969.

26. W.E. Schroeder and G.I. Haddad, "Nonlinear Properties of Impatt Devices", Proc. IEEE, vol. 51, pp. 153-182, February, 1973.

27. G.I. Haddad, P.T. Greilling, and W.E. Schroeder, "Basic Principles and Properties of Avalanche Transit-time Devices", IEEE Trans. Microwave Theory Tech., vol. MTT-18, pp. 752-772, November, 1970.

28. D.L. Scharfetter and H.K. Gummel, "Large-Signal Analysis of Silicon Read-Diode Oscillator", IEEE Trans. Electron Devices, ED-16, pp. 64-77, January, 1969.

29. M. Gilden and M.E. Hines, "Electronic Tuning Effects in the Read Microwave Avalanche Diode", IEEE Trans. Electron Devices, ED-13, pp. 169-175, January, 1966.

30. S.M. Sze and R.M. Ryder, "Microwave Avalanche Diodes", Proc. IEEE, vol. 59, pp. 1140-1154, August, 1971.

31. S.M. Sze and W. Shockley , "Unit Cube Expression for Space Charge Resistance", Bell. System Tech. J., vol. 46, p. 837, 1967.

32. W.J. Evans, "Avalanche Diode Oscillators", in Solid State and Quantum Electronics, W.D. Hershberger, Ed. New York: Wiley, 1971.

33. K. Mouthaan, "Nonlinear Analysis of the Avalanche Transit-time Oscillator", IEEE Trans. Electron Devices, vol. ED-16, pp. 935-945, November, 1969.

34. J.L. Blue, "Approximate Large-signal Analysis of Impatt Oscillators", Bell System Tech. J., vol. 48, pp. 383-396, February, 1969.

35. C.N. Dunn, J.E. Dalley, "Computer Aided Small-Signal Characterization of Impatt Diodes", IEEE Trans. Microwave Theory Tech., vol. MTT-17, pp. 691-695, September, 1969.

36. J.W. Gewartowski, and J.E. Morris, "Active Impatt Diode Parameters obtained by Computer Reduction of Experimental Data", IEEE Trans. Microwave Theory Tech., vol. MTT-18, pp. 157-161, March, 1970.

37. Y. Ito, H. Komizo, T. Meguro, M. Sinoda, T. Oya, and Y. Daido, "K-band High-power Single-tuned Impatt Oscillator stabilized by Hybrid-coupled Cavities", IEEE Trans. Microwave Theory Tech., vol. MTT-20, pp. 799-805, December, 1972.

38. P.T. Greiling and G.I.Haddad, "Large-Signal Equivalent Circuits for Avalanche Transit Time Devices", IEEE Trans. Microwave Theory Tech., vol. MTT-18, pp. 842-853, November, 1970.

39. J.G. Josenhaus and T. Misawa, "Experimental Characterization of a Negative-resistance Avalanche Diode", IEEE Trans. Electron Devices, vol. ED-13, pp. 206-208, January, 1966.

40. E.L. Ginzton, Microwave Measurements. New York: McGraw-Hill, 1957, Ch. 6.

41. B.B. Van Iperen, H.J. Tjassens, "Novel and Accurate Methods for Measuring Small-Signal and Large-Signal Impedance of Impatt Diode", Philips Res. Repts., vol. 27, pp. 38-75, 1972.

42. R.A. Hackborn, "An Automatic Network Analyzer System", Microwave Journal, vol. 11, pp. 45-52, May, 1968.

43. G.F. Engen, "Calibration Technique for Automated Network Analyzers with Application to Adaptor Evaluation", IEEE Trans. Microwave Theory Tech., vol. MTT-22, pp. 1255-1260, December, 1974.

44. J.L. Altman, Microwave Circuits. New York: D. Van Nostrand Co., Inc., p. 399, 1964.

45. S.M. Sze, Physics of Semiconductor Devices. New York: Wiley, p. 43, 1969.

46. M.J. Howes and M.L. Jeremy, "Large-Signal Circuit Characterization of Solid State Microwave Oscillator Devices", IEEE Trans. Electron Devices, vol. ED-21, pp. 488-499, August, 1974.

47. R.G. Wiley and E.M. Williams, "Theory and Applications of Broad Band Microwave Discriminators", Microwave/ Systems, Inc., Tech. Memo 6.

48. E.M. Katz and M.M. Schreiber, "Design of Phase Discriminators", Microwaves, vol. 4, pp. 26-33, August, 1965.

49. R.J. Mohr, "Broad-band Microwave Discriminator", IEEE Trans. Microwave Theory Tech. (corresp.), vol. MTT-11, pp. 263-264, July, 1963.

50. M.L. Sisodia and O.P. Gandi, "Octave Bandwidth L- and S-band Stripline Discriminators", IEEE Trans. Microwave Theory Tech. (corresp.), vol. MTT-15, pp. 271 272, April, 1967.

51. S.R. Mishara and R.P. Wadhwa, "Development of an X-band Waveguide Frequency Discriminator", IEEE Trans. Microwave Theory Tech. (corresp.), vol. MTT-18, pp. 660-661, September, 1970.

52. J. Nigrin, N.A. Mansour and W.A.G. Voss, "Single Hybrid Tee Frequency Discriminator", IEEE Trans. Microwave Theory Tech. (Letters), vol. MTT-23, pp. 777-778, September, 1975.

53. J.L. Altman, Microwave Circuits. Princeton, N.J.: Van Nostrand, pp. 60-67, 1964.

54. R.M. Vaillancourt, "Errors in a Magic-tee Phase Changer", IRE Trans. Microwave Theory Tech., vol. MMT-5, pp. 204-207, July, 1957.

55. Y.L. Luke, Mathematical Functions and their Approximations., New York: Academic Press Inc., pp. 483-489, 1975.

56. D. Ludwig and F.W.J. Olver, "Studies in Applied Mathematics", Society for Industrial and Applied Mathematics", vol. 6, pp. 110-123, 1970.

57. L. Fox, Numerical Solution of Ordinary and Partial Differential Equations. London: Pergamon Press, pp. 24-25, 1962.

58. J. Christiansen, "Numerical Solution of Ordinary Simultaneous Differential Equations of the First Order Using a Method for Automatic Step Change", Numer. Math., vol. 14, pp. 317-324, 1970.

59. R.P. Owens and D. Cawsey, "Microwave Equivalent-Circuit Parameters of Gunn-Effect-Devices Packages", IEEE Trans. Microwave Theory Tech., vol. MTT-18, pp. 790-798, November, 1970.

60, R. Whinnery and H. Jamieson, "Coaxial Line Discontinuities", Proc. IRE, vol. 32, pp. 695-709, November, 1944.

61. C. Chao and G.I. Haddad, "Nonlinear Behaviour and Bias Modulation of an Impatt Diode Oscillator", IEEE Trans. Microwave Theory Tech., vol. MTT-21, pp. 619-630, October, 1973

62. R.E. Collins, Foundations for Microwave Engineering, Chapter 4. New York: McGraw-Hill, 1966.

63. Hewlett Packard Application NOte 935 - Microwave Power Generation and Amplification Using IMPATT Diodes.

64. G.A. Brackett, "The Elimination of Tuning-induced Burnout and Bias Circuit Oscillations in Impatt Oscillators", Bell System Tech. J., vol. 52, pp. 271-306, March, 1973.

65. B. Syrett , "Feed Forward Linearization of a Stable Impatt Amplifier", Ph. D. Thesis, Department of Electrical Engineering, University of Alberta, Edmonton, Canada, 1976.

Apperdix I

LARGE-SIGNAL ADMITTANCE OF IMPATT DIODES

```
C THIS PROGRAME EVALUATES THE ABCD PARAMETERS OF THE NETWORK BETWEEN THE
C    MEASUREMENT REFERENCE PLANE AND THE ACTIVE IMPATT DIODE CHIP
C*************
C THE USER MUST SPECIFY VALUES FOR THE FOLLOWING:
C        AEPS:THE ABSOLUTE DIELECTRIC CONSTANT (PF/CM)
C             =1.036 FOR SILICON
C             =1.416 FOR GERMANIUM
C        CONK:A CONSTANT
C             =2.38D+17 FOR SILICON
C             =1.74D+17 FOR GERMANIUM
C        AJ: THE DIODE JUNCTION AREA (CIRCULAR) (SQUARE CM)
C        Z0: THE CHARACTERISTIC IMPEDANCE OF THE MEASURING SYSTEM (OHMS)
C        NN: NUMBER OF MEASUREMENTS (20 MAX )
C        F: FREQUENCY OF MICROWAVE IMPEDANCE DATA (GHZ)
C*******************
      IMPLICIT REAL*8(A-H,O-Z)
      REAL*8 LAMDC,LAMDG,LAMDO
      COMPLEX*16 CHZO,ZCR,YCR
      COMPLEX*16 GM,GE,ONE,GCAL,GAM(20),GAC(20)
      COMPLEX*16     DUMM,YD(20),ZP(20),DET,AC,BC,CC,A,B
      COMPLEX*16 DELZD,DELZM,ZM,AN,BN,CN,AF,BF,CF,DF,REFLC,DUMMY,DF2 ,
     1 CHECK,ZD,ZMC(20)
      DIMENSION DELZD(20),DELZM(20),PIF(20),DIST(20),PIQ(20)
      DIMENSION V(20),CD(20),SHL(20),
     1CDAV(20),CONC(20),RHO(20),DELRD(20),DELXD(20),DELCD(20),X(6),
     3        FX(20),RD(20),XD(20),RM(20),XM(20),THEFF(20)
      DIMENSION RLF(20),THETF(20),PIN(20),VAC(20),R(20),THET(20),RFF(20)
      COMMON/FUNC/ZM(20),ZD(20),NN,NC
      COMMON/ALPHA/A(3,3),B(3,1),GM(20),GE(20),GCAL(20),DET(20),
     *RL(20),THETA(20),GAMMA(20),THETAR(20),WA(60),PI
      DATA SHL/0.0,.1,.15,.2,.25,.3,.35,.4,.45,.5,.55,.6,.65,7*0.0/
      DATA CL,LAMDC   /2.998D10,6.97D0/
      DATA AEPS,CONK,AJ,Z0/1.036,2.38D+17,1.0D-04,50.0/
      DATA CD/3.6,2.35,1.3,.942,.674,.55,.472,.42,.38,.35,.328,.306,.289
     */
      DATA V/0.0,1.,5.,10.,20.,30.,40.,50.,60.,70.,80.,90.,100./
      DATA PIQ/-20.,-10.,0.0,3.,6.,9.,12.,15.,17.,19.,21.,23./
      EXTERNAL UOBJ
C*******************INPUT DATA ROUTINE*********
      NN=13
      NC=13
      PI=3.1415926535D0
      DO 444 III=1,2
      READ(5,441) F
      NPOW=12
```

```
      NNM1=NN-1
  441 FORMAT(F10.5)
      LAMDO=CL/(F*1.D9)
      LAMDG=LAMDO/DSQRT(1-((LAMDO/LAMDC)**2))
      LAMDG=LAMDG/2.54
      READ(5,4) (RL(I),I=1,NC)
      READ(5,4) (THETA(I),I=1,NC)
      CALL ANCALI(X,LAMDG,F,SHL)
      WRITE(6,940)
  940 FORMAT(1H0,3X,'MOVABLE',11X,'REFLECTION',22X,'REFLECTION',20X,
     *'REFLECTION',13X,'DIF IN CALC REFL. COEFF'/4X,'SHORT',13X,'COEFFIC
     *IENT',21X,'COEFFICIENT',19X,'COEFFICIENT'/3X,'POSITION', 7X,'
     *THEORETICAL',21X,'MEASURED',21X,'CALCULATED')
      DO 613 I=1,NC
      WRITE(6,944) SHL(I),GE(I),GM(I),GCAL(I),DET(I)
  613 CONTINUE
  944 FORMAT(2X,F7.3,3X,1P8D15.5)
      NC=NN
      AC=DCMPLX(X(1),X(2))
      BC=DCMPLX(X(3),X(4))
      CC=DCMPLX(X(5),X(6))
      ONE=DCMPLX(1.D0,0.D0)
      READ(5,4) (RL(I),I=1,NN)
      READ(5,4) (THETA(I),I=1,NN)
      WRITE(6,557) (RL(I),I=1,NN)
      WRITE(6,558) (THETA(I),I=1,NN)
  557 FORMAT(1H0,'RL=',13(F8.2,1X))
  558 FORMAT(1H0,'THETA=',13(F8.2,1X))
    4 FORMAT(8F10.4)
      DO 5 I=1,NN
      RL(I)=RL(I)/50.0
      THETA(I)=THETA(I)/10.0
      GAMMA(I)=10.**(RL(I)/20.)
      THETAR(I)=THETA(I)*PI/180.0
      GCOS=GAMMA(I)*DCOS(THETAR(I))
      GSIN=GAMMA(I)*DSIN(THETAR(I))
      GAM(I)=DCMPLX(GCOS,GSIN)
      GAC(I)=(GAM(I)-BC)/(AC-(CC*GAM(I)))
      ZNC(I)=(ONE+GAM(I))/(ONE-GAM(I))
      ZN(I)=(ONE+GAC(I))/(ONE-GAC(I))
    5 CONTINUE
C**************WRITE THE INPUT DATA *******
   21 WRITE(6,22)NN,F,AJ
   22 FORMAT(1H1,10X,'NUMBER OF MEASUREMENTS:',I3/10X,'FREQUENCY OF MEAS
     1UREMENTS:',1X,F10.5,2X,'GHZ'/10X,'AREA OF DIODE JUNCTION:',1X,
     2 1PD15.5,2X,'SQUARE CM'/)
   23 WRITE(6,24)
   24 FORMAT(1H0,4X,'BIAS',2X,'DIODE CAPACITANCE',2X,'NORMALIZED IMPEDAN
     1CE MEASUREMENT',5X,'NORMALIZED IMPEDANCE CALCULATED',13X,'REFLECTI
     $ON'/ 3X,'VOLTAGE',4X,'AT 1 MHZ',16X,'AT FREQUENCY F',22X,'USING
     $ANA-ABC',21X,'COEFFICIENT'/34X,'RESISTANCE',8X,'REACTANCE',8X,
     *'RESISTANCE',8X,'REACTANCE', 8X,'MAGNITUDE', 6X,'PHASE'/3X,'(VOLTS
     *)',6X,'(PF)',100X,'(DEG)')
```

```
      DO 26 I=1,NN
      WRITE(6,25)V(I),CD(I),ZMC(I),ZM(I),GAMMA(I),THETA(I)
   25 FORMAT(2F10.3,5X,1PD20.7,1PD17.7,1PD20.7,1PD17.7,D16.6,D13.3)
   26 CONTINUE
C*******************************
C     CALCULATE IMPURITY CONCENTRATION FROM CAPACITANCE DATA
C*******************************
      DIAM=DSQRT(AJ/PI)*2000./2.54
      DO 32 I=1,NNM1
      CDAV(I)=0.5*(CD(I)+CD(I+1))
      DELCD(I)=CD(I+1)-CD(I)
      DELV=V(I+1)-V(I)
      CONC(I)=-(CONK*DELV*CDAV(I)*3)/(DELCD(I)*DIAM**4)
   32 CONTINUE
C*******************************
C             CALCULATE RESISTIVITY
C      FOR N-TYPE SILICON:
C*******************************
      DO 34 I=1,NNM1
      RHO(I)=DEXP(28.3637-.7861*DLOG(CONC(I)))
   34 CONTINUE
C*******************************
C   WRITE CONCENTRATIONS AND RESISTIVITIES IN THE VOLTAGE INTERVALS
C*******************************
      WRITE(6,41)
   41 FORMAT(1H1,3X,'VOLTAGE',11X,'IMPURITY',10X,'RESISTIVITY'/3X,
     1 'INTERVAL',8X,'CONCENTRATION'/18X,'(PER CUBIC CM)',10X,
     2 '(OHM-CM)'//)
      DO 43 I=1,NNM1
      WRITE(6,42)I,CONC(I),RHO(I)
   42 FORMAT(5X,I3,4X,1P2E20.7)
   43 CONTINUE
C*****************************************
C     CALCULATE CHANGES IN 1 MHZ AND VHF IMPEDANCE DATA
C                    IN THE VOLTAGE INTERVALS
C*****************************************
      DO 51 I=1,NNM1
      DELRD(I)=-AEPS*RHO(I)*(1./CD(I+1)-1./CD(I))
      DELXD(I)=(500.*DELCD(I))/(PI*F*CD(I)*CD(I+1))
      DELXD(I)=-1.*DELXD(I)
      DELZD(I)=DCMPLX(DELRD(I),DELXD(I))
      DELZM(I)=ZM(I+1)-ZM(I)
   51 CONTINUE
C*************************************
C   WRITE THE CHANGES IN THE 1 MHZ AND VHF IMPEDANCE DATA
C       IN THE CORRESPONDING VOLTAGE INTERVALS
C*************************************
      WRITE(6,61)
   61 FORMAT(1H0,3X,'VOLTAGE',9X,'CHANGES IN 1 MHZ IMPEDANCE DATA',
     1 7X,'CHANGES IN MICROWAVE IMPEDANCE DATA'/3X,'INTERVAL'/19X,
     3 'RESISTANCE',11X,'REACTANCE',10X,'RESISTANCE',11X,'REACTANCE'/21X
     3,'(OHMS)',14X,'(OHMS)',14X,'(OHMS)',14X,'(OHMS)'//)
      DO 64 I=1,NNM1
```

```
      WRITE(6,63)I,DELRD(I),DELXD(I),DELZM(I)
   63 FORMAT(5X,I3,4X,1P4E20.7)
   64 CONTINUE
C*************************************
C     CALCULATE ABSOLUTE VALUE OF 1MHZ IMPEDANCE
      RD (NN)=0.0
C*************************************
      DO 71 I=1,NNM1
      J=NN-I
      RD (J)=RD (J+1)-DELRD(J)
   71 CONTINUE
      DO 72 I=1,NN
      XD(I)=-500.0/(PI*F*CD(I))
      ZD(I)=DCMPLX(RD(I),XD(I))
      RM(I)=DREAL(ZM(I))
      XM(I)=DIMAG(ZM(I))
   72 CONTINUE
C*****************************************
C   ALL NECESSARY EXPERIMENTAL DATA HAS NOW BEEN OBTAINED
C       PROCEED WITH THE OPTIMIZATION ROUTINE
C      DEFINE SCALAR VARIABLES REQUIRED BY ZXPOWL
C*****************************************
      EPS=1.D-12
      ITMAX=10000
      M=NN
      N=6
C*****************************************
C      CALCULATE INITIAL VALUES BY SOLVING SYSTEM OF LINEAR EQUATIONS
C        WITH COMPLEX COEFFICIENTS OBTAINED FROM 3 SETS OF IMPEDANCE DATA
C*****************************************
      AAR=1.0
      AAI=0.0
      DO 73 I=1,3
      J=3*I+4
      A(I,1)=ZD(J)
      A(I,2)=DCMPLX(AAR,AAI)
      A(I,3)=DCMPLX(XD(J)*XM(J)-RD(J)*RM(J),-RD(J)*XM(J)-RM(J)*XD(J))
      B(I,1)=ZM(J)
   73 CONTINUE
      CALL LEQT1C(A,3,3,B,1,3,0,WA,IER)
      X(1)=DREAL(B(1,1))
      X(2)=DIMAG(B(1,1))
      X(3)=DREAL(B(2,1))
      X(4)=DIMAG(B(2,1))
      X(5)=DREAL(B(3,1))
      X(6)=DIMAG(B(3,1))
      WRITE(6,74)
   74 FORMAT(///,'THE STARTING ABCD PARAMETERS ARE:'/)
      WRITE(6,82)X(1),X(2)
      WRITE(6,83)X(3),X(4)
      WRITE(6,84)X(5),X(6)
```

```
   82 FORMAT(1HO,4X,'A =',1PD20.7,2X,'+J ',1PD20.7)
   83 FORMAT(1HO,4X,'B =',1PD20.7,2X,'+J ',1PD20.7)
   84 FORMAT(1HO,4X,'C =',1PD20.7,2X,'+J ',1PD20.7)
      WRITE(6,85)
   85 FORMAT(1HO,4X,'D =',10X,'1.0', 9X,'+J ',11X,'0.0'//)
      CALL ZXPOWL (UOBJ,EPS,N,X,FMIN,ITMAX,WA,IER)
      WRITE(6,81)
   81 FORMAT(1H1,4X,'THE NORMALIZED ABCD PARAMETERS ARE:'/)
      WRITE(6,82) X(1),X(2)
      WRITE(6,83) X(3),X(4)
      WRITE(6,84) X(5),X(6)
      WRITE(6,85)
C*************************************
C        CALCULATE THE ABSOLUTE ABCD PARAMETERS
C*************************************
      AN=DCMPLX(X(1),X(2))
      BN=DCMPLX(X(3),X(4))
      CN=DCMPLX(X(5),X(6))
      DF2=1./(Z0*(AN-BN*CN))
      DX=DSQRT((DREAL(DF2)+CDABS(DF2))/2.0)
      DY=0.5*DIMAG(DF2)/DX
      DF=DCMPLX(DX,DY)
      AP=Z0*AN*DF
      BP=Z0*BN*DF
      CP=CN*DF
      WRITE(6,87)
   87 FORMAT(4X,'THE ABSOLUTE ABCD PARAMETERS ARE:'/)
      WRITE(6,82) AP
      WRITE(6,83) BP
      WRITE(6,84) CP
      WRITE(6,88) DF
   88 FORMAT(1HO,4X,'D =',1PD20.7,2X,'+J ',1PD20.7//)
      CHECK=AP*DF-BP*CP
      WRITE(6,89) CHECK
   89 FORMAT(10X,'THE VALUE OF AD-BC =',1PD20.7,2X,'+J ',1PD20.7)
C*************************************
C      CHECK THE OPTIMUM NORMALIZED A,B,C,D
C*************************************
      WRITE(6,92)
   92 FORMAT(1HO,'THE CALCULATED IMPEDANCES ARE:'//)
      WRITE(6,93)
   93 FORMAT(6X,'BIAS',15X,'1 MHZ IMPEDANCE DATA',19X,'MICROWAVE IMPEDAN
     1CE DATA',17X,'DIF IN CALC IMPEDANCES'
     1        /5X,'VOLTAGE'/19X,'RESISTANCE',11X,'REACTANCE',10X,
     2 'RESISTANCE',11X,'REACTANCE',16X,'DIFR',16X,'DIFX'/
     221X,'(OHMS)',14X,'(OHMS)')
      DO 95 I=1,NN
      ZMC(I)=(AN*ZD(I)+BN)/(CN*ZD(I)+1.0)
      DET(I)=(ZM(I)-ZMC(I))
      WRITE(6,94) V(I),ZD(I),ZMC(I),DET(I)
   94 FORMAT(2X,F10.3,1P6D20.7)
   95 CONTINUE
      ERR=0.0
```

```
      DO 300 I=1,NN
      DUMM=(AN*ZD(I)+BN)/(CN*ZD(I)+1.0 )-ZM(I)
      ERR=ERR+CDABS(DUMM)**2
  300 CONTINUE
      WRITE(6,301)ERR
  301 FORMAT(1HO,'ERROR=',D20.7)
  601 FORMAT(1HO,2(10X,F10.3))
  500 FORMAT(8F10.4)
      DO 251 I=1,NPOW
      PIN(I)=PIQ(I)
  251 CONTINUE
      DO 1222 IQ=1,2
  222 READ(5,500) (RLF(K),K=1,NPOW)
      READ(5,500) (THETF(K),K=1,NPOW)
      DO 600 I=1,NPOW
      WRITE(6,601)RLF(I),THETF(I)
  600 CONTINUE
      DO 501 K=1,NPOW
      PIF(K)=0.001*(10.**(PIN(K)/10.))
      RFF(K)=RLF(K)/50.
      THEFF(K)=THETF(K)/10.
      GAMMA(K)=10.**(RFF(K)/20.)
      THETAR(K)=THEFF(K)*PI/180.
      GCOS=GAMMA(K)*DCOS(THETAR(K))
      GSIN=GAMMA(K)*DSIN(THETAR(K))
      ZF(K)=DCMPLX(1.+GCOS,GSIN)/DCMPLX(1.-GCOS,-GSIN)
      YD(K)=(CN*ZF(K)-AN)/(BN-ZF(K))
      CONSV=CDABS((AN+CN)+((BN+1.)*YD(K)))
      VAC(K)=DSQRT(8.PIF(K)*CDABS(AN-(BN*CN)))/CONSV
  501 CONTINUE
      IF(IQ .EQ. 1) WRITE(6,229)
      IF(IQ .EQ. 2) WRITE(6,228)
      WRITE(6,502)
      DO 505 K=1,NPOW
      WRITE(6,503)PIF(K),VAC(K),YD(K)
  505 CONTINUE
C          SMALL SIGNAL ADMITTANCE
      NPOW=7
      DO 220 I=1,NPOW
      PIN(I)=-20.
  220 CONTINUE
 1222 CONTINUE
  444 CONTINUE
  228 FORMAT(1H1,'SMALL SIGNAL ADMITTANCE')
  229 FORMAT(1H1,'LARGE SIGNAL ADMITTANCE')
  503 FORMAT(1HO,6X,4(D15.7,10X))
  502 FORMAT(1HO,//10X,'INPUT POWER',13X,'AC-VOLTAGE',20X,'GD',24X,'BD')
      STOP
      END
```

```
      FUNCTION UOBJ(X)
      IMPLICIT REAL*8(A-H,O-Z)
      COMMON/FUNC/ZM(20),ZD(20),NN,NC
      COMPLEX*16 AN,BN,CN,DELZD,DELZM,ZM,DUMMY,ZD
      DIMENSION X(6)
      AN=DCMPLX(X(1),X(2))
      BN=DCMPLX(X(3),X(4))
      CN=DCMPLX(X(5),X(6))
      UOBJ=0.0
      DO 100 I=1,NC
      DUMMY=(AN*ZD(I)+BN)/(CN*ZD(I)+1.0)-ZM(I)
      UOBJ=UOBJ+CDABS(DUMMY)**2
  100 CONTINUE
      RETURN
      END
      SUBROUTINE ANCALI(X,LAMDG,F,SHL)
      IMPLICIT REAL*8(A-H,O-Z)
      REAL*8 LAMDG
      COMPLEX*16 GM,GE,AC,BC,CC,GCAL,ONE,UU,A,B          ,ZM,ZD,DET
      DIMENSION X(6),SHL(20)
      COMMON/FUNC/ZM(20),ZD(20),NN,NC
      COMMON/ALPHA/A(3,3),B(3,1),GM(20),GE(20),GCAL(20),DET(20),
     *RL(20),THETA(20),GAMMA(20),THETAR(20),WA(60),PI
      EXTERNAL UOBJ
      N=6
      EPS=1.D-10
      WRITE(6,55)(RL(I),I=1,NC)
      WRITE(6,56)(THETA(I),I=1,NC)
   55 FORMAT(1H0,'RL=',13(F8.2,1X))
   56 FORMAT(1H0,'THETA=',13(F8.2 ,1X))
      DO 5 I=1,NC
      RL(I)=RL(I)/50.0
      THETA(I)=THETA(I)/10.0
      GAMMA(I)=10.**(RL(I)/20.)
      THETAR(I)=THETA(I)*PI/180.0
      GCOS=GAMMA(I)*DCOS(THETAR(I))
      GSIN=GAMMA(I)*DSIN(THETAR(I))
      GM (I)=DCMPLX(GCOS,GSIN)
    5 CONTINUE
      DO 666 I=1,NC
      COSV=DCOS(4.0*PI*SHL(I)/LAMDG)
      SINV=DSIN(4.0*PI*SHL(I)/LAMDG)
      GE(I)=DCMPLX(-COSV,SINV)
  666 CONTINUE
      DO 20 I=1,3
      J=I
      A(I,1)=GE(J)
      A(I,2)=DCMPLX(1.D0,0.D0)
      A(I,3)=-GM(J)*GE(J)
      B(I,1)=GM(J)
   20 CONTINUE
```

```
      CALL LEQT1C(A,3,3,B,1,3,0,WA,IER)†
      WRITE(6,51)IER
   51 FORMAT(1H0,'AN-LEQT1C IER=',I5)
      X(1)=DREAL(B(1,1))
      X(2)=DIMAG(B(1,1))
      X(3)=DREAL(B(2,1))
      X(4)=DIMAG(B(2,1))
      X(5)=DREAL(B(3,1))
      X(6)=DIMAG(B(3,1))
      WRITE(6,74)
   74 FORMAT(///,'THE STARTING ABCD PARAMETERS FOR ANALIZER-CALI ARE:'/)
      WRITE(6,82)X(1),X(2)
      WRITE(6,83)X(3),X(4)
      WRITE(6,84)X(5),X(6)
      DO 220 I=1,NC
      ZD(I)=GE(I)
      ZM(I)=GM(I)
  220 CONTINUE
      CALL ZXPOWL (UOBJ,EPS,N,X,FMIN,20000,WA,IER)†
      WRITE(6,52)IER
   52 FORMAT(1H0,'AN-ZXPOWL IER=',I5)
      WRITE(6,81)
   81 FORMAT(1H1,4X,'THE OPTIMIZED ABC   PARAMETERS FOR ANALYZER-CALI
     * ARE:'/)
      WRITE(6,82)X(1),X(2)
      WRITE(6,83)X(3),X(4)
      WRITE(6,84)X(5),X(6)
C**************************************
C      CHECK THE OPTIMUM NORMALIZED A,B,C FOR ANALYZER CALIBRATION
C**************************************
      ERR=0.0
      AC=DCMPLX(X(1),X(2))
      BC=DCMPLX(X(3),X(4))
      CC=DCMPLX(X(5),X(6))
      ONE=DCMPLX(1.D0,0.D0)
      DO 600 I=1,NC
      GCAL(I)=(GE(I)*AC+BC)/(GE(I)*CC+ONE)
      UU=GM(I)-GCAL(I)
      DZT(I)=UU
      ERR=ERR+CDABS(UU)**2
  600 CONTINUE
      WRITE(6,945)ERR
  945 FORMAT(1H0,'ERROP-AN=',D20.7)
   82 FORMAT(1H0,4X,'AN=',1PD20.7,2X,'+J ',1PD20.7)
   83 FORMAT(1H0,4X,'BN=',1PD20.7,2X,'+J ',1PD20.7)
   84 FORMAT(1H0,4X,'CN=',1PD20.7,2X,'+J ',1PD20.7)
      RETURN
      END
```

---

† Subroutines LEQT1C and ZXPOWL were used from the International Mathematical and Statistical library (IMSL).

Appendix II

STEADY STATE SOLUTIONS IN OSCILLATORS
A & $\bar{w} + x$

It is achieved by the following five programs.

First: Evaluates the bicubic-spline coefficients g(i,j) or s(i,j) knowing conductance and susceptance data of Impatt diode. (Here FR = w and V = A)

```
      IMPLICIT REAL*8(A-H,O-Z)
      DIMENSION FK(5),V(6),FR(6),GR(6,6),C(4,4),WK(340),V1(6)
      DATA V/0.0D0,.025D0,.1D0,.225D0,.4D0,.625D0/
      DATA V1/     .025D0,.1D0,.225D0,.4D0,.625D0/
      DATA FR/.3249D0,.3481D0,.3844D0,.4225D0/
      DATA FK/        .3481D0,.3844D0,.4225D0/
      DATA GR/12.441881D-3,12.731653D-3,13.033675D-3,13.347953D-3,
     *13.674482D-3,14.013265D-3,12.625276D-3,12.874356D-3,13.270122D-3,
     *13.731654D-3,14.178031D-3,14.528331D-3,13.186755D-3,13.458182D-3,
     *13.498415D-3,13.73418D-3,13.998617D-3,14.291723D-3,14.613502D-3,
     *14.963952D-3/
C     SPLINE COEFFICIENTS FOR DIODE SUSCEPTANCE B(A2,W2)/F
      SUM=0.0D0
      DO 2 K=1,5
      DO 1 L=1,3
      CALL ICS2CU(GR,V,FR,6,4,K,L,6,C,WK,IER)†
      WRITE(6,10)K,L,IER
   10 FORMAT(1H1,//5X,'K=',I4,5X,'L=',I4,5X,'IER=',I4)
      WRITE(6,11) ((C(I,J),J=1,4),I=1,4)
      WRITE(7,21) ((C(I,J),J=1,4),I=1,4)
   11 FORMAT(' ',////4D18.9,5X)
      D=V1(K)-V(K)
      B=FK(L)-FR(L)
      SUM=C(1,1)+(C(1,2)*B)+(C(1,3)*(B**2))+(C(1,4)*(B**3))+(C(2,1)*D)+
     1(C(3,1)*(D**2))+(C(4,1)*(D**3))
      DO 9 M=2,4
      DO 7 N=2,4
      SUM =SUM +C(M,N)*(D**(M-1))*(B**(N-1))
    7 CONTINUE
    9 CONTINUE
      WRITE(6,20)V1(K),SUM
   20 FORMAT(2(5X,D18.11))
    1 CONTINUE
    2 CONTINUE
   21 FORMAT(4(2X,D18.11))
      STOP
      END
```

† Subroutine ICS2CU was used from the International Mathematical and Statistical library (IMSL).

SECOND:

Evalutes the d-coefficients of the diode knowing the bicubic spline coefficients.

```
C     THIS PROGRAM CALCULATES THE D-COEFFICIENTS OF GD(A2,W2),@
C     BD(A2,W2)
      IMPLICIT REAL*8(A-H,O-Z)
      DIMENSION C(4,4),B(4,4),CN(4,4),A1(5,5,4,4),V(6),FR(6)
      DATA V/0.0D0,.025D0,.1D0,.225D0,.4D0,.625D0/
      DATA FR/.3249D-2,.3481D-2,.3844D-2,.4225D-2/
      SUM=0.0D0
      DO 8 K=1,5
      DO 8 L=1,3
    8 READ(5,21)((A1(K,L,I,J),J=1,4),I=1,4)
   21 FORMAT(4(2X,D18.11))
      DO 1 K=1,5
      DO 2 L=1,3
      DO 15 I=1,4
      DO 15 J=1,4
      C(I,J)=A1(K,L,I,J)
   15 CONTINUE
      B(1,1)=C(1,1)-C(1,2)*FR(L)+C(1,3)*(FR(L)**2)-C(1,4)*(FR(L)**3)
     *+(-C(2,1)+C(2,2)*FR(L)-C(2,3)*(FR(L)**2)+C(2,4)*(FR(L)**3))*V(K)
     *+(C(3,1)-C(3,2)*FR(L)+C(3,3)*(FR(L)**2)-C(3,4)*(FR(L)**3))*V(K)**2
     *+(-C(4,1)+C(4,2)*FR(L)-C(4,3)*(FR(L)**2)+C(4,4)*(FR(L)**3))*V(K)**
     *3
      B(1,2)=C(1,2)-2.*C(1,3)*FR(L)+3.*C(1,4)*(FR(L)**2)
     *+(-C(2,2)+2.*C(2,3)*FR(L)-3.*C(2,4)*(FR(L)**2))*V(K)
     *+(C(3,2)-2.*C(3,3)*FR(L)+3.*C(3,4)*(FR(L)**2))*V(K)**2
     *+(-C(4,2)+2.*C(4,3)*FR(L)-3.*C(4,4)*(FR(L)**2))*V(K)**3
      B(1,3)=C(1,3)-3.*C(1,4)*FR(L)+(-C(2,3)+3.*C(2,4)*FR(L))*V(K)
     *+(C(3,3)-3.*C(3,4)*FR(L))*V(K)**2-(C(4,3)-3.*C(4,4)*FR(L))*V(K)**3
      B(1,4)=C(1,4)-C(2,4)*V(K)+C(3,4)*(V(K)**2)-C(4,4)*(V(K)**3)
      B(2,1)=C(2,1)-C(2,2)*FR(L)+C(2,3)*(FR(L)**2)-C(2,4)*(FR(L)**3)
     *-2.*(C(3,1)-C(3,2)*FR(L)+C(3,3)*(FR(L)**2)-C(3,4)*(FR(L)**3))*V(K)
     *+3.*(C(4,1)-C(4,2)*FR(L)+C(4,3)*(FR(L)**2)-C(4,4)*(FR(L)**3))*V(K)
     1**2
      B(2,2)=C(2,2)-2.*C(2,3)*FR(L)+3.*C(2,4)*(FR(L)**2)
     *+2.*(-C(3,2)+2.*C(3,3)*FR(L)-3.*C(3,4)*(FR(L)**2))*V(K)
     *+3.*(C(4,2)-2.*C(4,3)*FR(L)+3.*C(4,4)*(FR(L)**2))*V(K)**2
      B(2,3)=C(2,3)-3.*FR(L)*C(2,4)+2.*(-C(3,3)+3.*C(3,4)*FR(L))*V(K)+3.
     1*(C(4,3)-3.*C(4,4)*FR(L))*V(K)**2
      B(2,4)=C(2,4)-2.*C(3,4)*V(K)+3.*C(4,4)*(V(K)**2)
      B(3,1)=C(3,1)-C(3,2)*FR(L)+C(3,3)*(FR(L)**2)-C(3,4)*(FR(L)**3)
     *+3.*(-C(4,1)+C(4,2)*FR(L)-C(4,3)*(FR(L)**2)+C(4,4)*(FR(L)**3))*V(K
     *)
      B(3,2)=C(3,2)-2.*C(3,3)*FR(L)+3.*C(3,4)*(FR(L)**2)
     *+3.*(-C(4,2)+2.*C(4,3)*FR(L)-3.*C(4,4)*(FR(L)**2))*V(K)
```

```
      B(3,3)=C(3,3)-3.*C(3,4)*FR(L)+3.*(-C(4,3)+3.*C(4,4)*FR(L))*V(K)
      B(3,4)=C(3,4)-3.*C(4,4)*V(K)
      B(4,1)=C(4,1)-C(4,2)*FR(L)+C(4,3)*(FR(L)**2)-C(4,4)*(FR(L)**3)
      B(4,2)=C(4,2)-2.*C(4,3)*FR(L)+3.*C(4,4)*(FR(L)**2)
      B(4,3)=C(4,3)-3.*C(4,4)*FR(L)
      B(4,4)=C(4,4)
      DO 30 I=1,4
      DO 30 J=1,4
      FM=(FR(L+1)**(J-1))
      AM=(V(K+1)**(I-1))
      SUM=SUM+(B(I,J)*FM*AM)
   30 CONTINUE
   60 FORMAT(1H ,5X,2D18.11)
   11 FORMAT(' ',////4 D18.11,5X)
      WRITE(6,50)
   50 FORMAT(1H1,'CN-COFF',10X,'SUSCEPTANCE AS A FN OF W2 FOR TRANSIENT
     * CALCU.')
      WRITE(6,11)((B (I,J),J=1,4),I=1,4)
      WRITE(7,21)((B (I,J),J=1,4),I=1,4)
      WRITE(6,60)SUM
      SUM=0.0D0
    2 CONTINUE
    1 CONTINUE
      STOP
      END
```

THIRD:

Evaluates the passive circuit cubic-spline coefficients as well as the corresponding d-coefficients (Here x=w)

```
      IMPLICIT REAL*8(A-H,O-Z)
      DIMENSION  GR(6),X(6),C(3,5),WK(70),BK(5,4)
      DATA X/.390625D0,.4489D0,        .5476D0,.6084D0,.6724D0/
      DO 2  J1=1,2
      READ(5,40)(GR(M),M=1,5)
   40 FORMAT(6(D16.9,4X))
      WRITE(6,41)(GR(M),M=1,5)
   41 FORMAT(1H1,6(4X,D16.9))
      CALL ICS1CU(GR,X,5 ,C,WK,IER)†
      WRITE(6,10)IER
   10 FORMAT(1HO,'IER=',I10)
      WRITE(6,20)((C(I,J) ,J=1,5 ),I=1,3)
   20 FORMAT(1H    5(2X,D16.9))
      DO  1  I=1,4
      P1=X(I)
      P2=P1**2
      P3=P1**3
      P4=X(I+1)
      P5=P4**2
      P6=P4**3
```

---

† Subroutine ICS1CU was used from the International Mathematical and Statistical library (IMSL).

```
      BK(I,1)=GR(I)-C(1,I)*F1+C(2,I)*F2-C(3,I)*F3
      BK (I,2)=C(1,I)-2.*C(2,I)*F1+3.*C(3,I)*F2
      BK(I,3) =C(2,I)-3.*C(3,I)*F1
      BK(I,4)=C(3,I)
      SUM=BK(I,1)+BK(I,2)*F4+BK(I,3)*F5+BK(I,4)*F6
      WRITE(6,30)SUM
   30 FORMAT(1H ,D16.9)
    1 CONTINUE
      WRITE(6,15)((BK(K,L),L=1,4),K=1,4)
   15 FORMAT(1H0,4(2X,D18.11))
      WRITE(7,21)((BK(K,L),L=1,4),K=1,4)
    2 CONTINUE
   21 FORMAT      (4(2X,D18.11))
      STOP
      END
```

FOURTH:

Evaluates the quasistationary frequency w
Having the active and the passive d-coefficients
the value of w is determined by solving sixth
order non linear algebriac equation (Eq. 7.20).

```
      IMPLICIT REAL*8(A-H,O-Z)
      DIMENSION BK(4,4),GN(5,3,4,4),CN(5,3,4,4),GK(4,4),XCOF(7 ),COF(7 )
     *,RR1(6 ),RIM1(6 )
      DIMENSION GD(6),GT(6)
      DO 6 K=1,5
      DO 6 L=1,3
    6 READ(5,33)((GN(K,L,I,J),J=1,4),I=1,4)
      DO 8 K=1,5
      DO 8 L=1,3
    8 READ(5,33)((CN(K,L,I,J),J=1,4),I=1,4)
      READ(5,33)((GK(I,J),J=1,4),I=1,3)
      READ(5,33)((BK(I,J),J=1,4),I=1,3)
   33 FORMAT(4(2X,D18.11))
      D13=1./3.
      D15=1./5.
      D17=1./7.
      A=0.0D0
      A2=A**2
      A4=A**4
      A6=A**6
      K=1
      DO 994 M=1,3
      DO 995 L=1,2
      CD0=GN(K,L,1,1)+GN(K,L,2,1)*A2+GN(K,L,3,1)*A4+GN(K,L,4,1)*A6
      CD1=CN(K,L,1,1)+3.*CN(K,L,2,1)*A2+5.*CN(K,L,3,1)*A4+7.*CN(K,L,4,1)
     1*A6
      CD2=-GN(K,L,1,2)-GN(K,L,2,2)*A2-GN(K,L,3,2)*A4-GN(K,L,4,2)*A6
      CD3=-CN(K,L,1,2)-3.*CN(K,L,2,2)*A2-5.*CN(K,L,3,2)*A4-7.*CN(K,L,4,2
     1)*A6
```

```
      CD4=GN(K,L,1,3)+GN(K,L,2,3)*A2+GN(K,L,3,3)*A4+GN(K,L,4,3)*A6
      CD5=CN(K,L,1,3)+3.*CN(K,L,2,3)*A2+5.*CN(K,L,3,3)*A4+7.*CN(K,L,4,3)
     1*A6
      CD6=-GN(K,L,1,4)-GN(K,L,2,4)*A2-GN(K,L,3,4)*A4-GN(K,L,4,4)*A6
      CD7=-CN(K,L,1,4)-3.*CN(K,L,2,4)*A2-5.*CN(K,L,3,4)*A4-7.*CN(K,L,4,4
     1)*A6
      CD12=CN(K,L,1,1)+CN(K,L,2,1)*A2+CN(K,L,3,1)*A4+CN(K,L,4,1)*A6
      CD22=-GN(K,L,1,2)-D13*GN(K,L,2,2)*A2-D15*GN(K,L,3,2)*A4-
     1D17*GN(K,L,4,2)*A6
      CD32=-CN(K,L,1,2)-CN(K,L,2,2)*A2-CN(K,L,3,2)*A4-CN(K,L,4,2)*A6
      CD42=GN(K,L,1,3)+D13*GN(K,L,2,3)*A2+D15*GN(K,L,3,3)*A4+
     1D17*GN(K,L,4,3)*A6
      CD52=CN(K,L,1,3)+CN(K,L,2,3)*A2+CN(K,L,3,3)*A4+CN(K,L,4,3)*A6
      CD62=-GN(K,L,1,4)-D13*GN(K,L,2,4)*A2-D15*GN(K,L,3,4)*A4-
     1D17*GN(K,L,4,4)*A6
      CD72=-CN(K,L,1,4)-CN(K,L,2,4)*A2-CN(K,L,3,4)*A4-CN(K,L,4,4)*A6
      WRITE(6,30)A,K,L,M
   30 FORMAT(1H ,'A=',D18.11,3I5)
      B0=BK(M,1)+CD12
      B1=0.0D0
      B2=BK(M,2)-CD32
      B3=0.0D0
      B4=BK(M,3)+CD52
      B5=0.0D0
      B6=BK(M,4)-CD72
      XCOF(1)=B0
      XCOF(2)=B1
      XCOF(3)=B2
      XCOF(4)=B3
      XCOF(5 )=B4
      XCOF(6 )=B5
      XCOF(7 )=B6
      CALL POLRT(XCOF,COF,6 ,RR1,RIM1,IER)†
      WRITE(6,40)IER
      WRITE(6,50)
      WRITE(6,51)RR1
      WRITE(6,52)
      WRITE(6,51)RIM1
      DO 200 KK1=1,6
      W1=RR1(KK1)
      W2=W1**2
      W3=W1**3
      W4=W1**4
      W5=W1**5
      W6=W1**6
      GD(KK1)=CD0-CD2*W2+CD4*W4-CD6*W6
      GT(KK1)=CD0+GK(M,1)+(GK(M,2)-CD2)*W2+(GK(M,3)+CD4)*W4
     *+(GK(M,4)-CD6)*W6
  200 CONTINUE
```

† Subroutine POLRT was used from the Scientific Subroutine Package library (SSPLIB).

```
      WRITE(6,800)
      WRITE(6,51)       (GD(I),I=1,6)
      WRITE(6,801)
      WRITE(6,51)       (GT(I),I=1,6)
  995 CONTINUE
  994 CONTINUE
   40 FORMAT(1H0,'IER=',I10)
   50 FORMAT(1H ,'REAL ROOTS')
   51 FORMAT(1H ,5(2X,D23.16))
   52 FORMAT(1H ,'IM ROOTS')
  800 FORMAT(1H0,'DIODE CONDUCTANCE')
  801 FORMAT(1H0,'TOTAL CONDUCTANCE')
      STOP
      END
```

FIFTH:

Having $\bar{w}$ and d-coefficients, this program evaluates the series state frequency $w + x$, assuming Λ, by solving eleventh order non linear algebraic equations (Eqs. 7.3)

```
C     THIS PROGRAM EVALUATES THE ROOTS OF DA/DT=0 & DX/DT=0 AS FN OF
C     X(FREQ.) IN 11 TH ORDER. IN THE TWO EQNS. X HAS TO BE THE SAME.
C     EACH FN SET IN THE FORM: B0+B1*X+B2*X**2+B3*X**3+...+B11*X**11=0
      IMPLICIT REAL*8(A-H,O-Z)
      DIMENSION BK(4,4),CN(5,3,4,4),CN(5,3,4,4),GK(4,4),XCOF(12),COF(12)
     *,RR1(11),RIM1(11),RR2(11),RIM2(11)
      W1=.5886494335896001D-1
      W2=W1**2
      W3=W1**3
      W4=W1**4
      W5=W1**5
      W6=W1**6
      W7=W1**7
      D13=1./3.
      D15=1./5.
      D17=1./7.
      DO 6 K=1,5
      DO 1 L=1,3
      READ(5,33)((GN(K,L,I,J),J=1,4),I=1,4)
    1 CONTINUE
    6 CONTINUE
      DO 8 K=1,5
      DO 2 L=1,3
      READ(5,33)((CN(K,L,I,J),J=1,4),I=1,4)
    2 CONTINUE
    8 CONTINUE
      READ(5,33)((GK(I,J),J=1,4),I=1,3)
      READ(5,33)((BK(I,J),J=1,4),I=1,3)
   33 FORMAT(4(2X,D18.11))
      L=1
      M=2
```

```
      READ(5,111)AA,DA,N
      WRITE(6,112)AA,DA,N
  111 FORMAT(2D23.16 ,I5)
  112 FORMAT(1H0,'AA=',D23.16,5X,'DA=',D23.16,'N=',I5)
      DO 61 I1=1,N
      AA=AA+DA
      A=AA/(10.D0*DSQRT(10.D0))
      IF(A     .GE. 0.0D0         .AND.  A    .LT.  .158114D0)  GO TO 100
      IF(A     .GE. 0.158114D0    .AND.  A    .LT. .316228D0 )  GO TO 200
      IF(A     .GE. 0.316228D0    .AND.  A    .LT.  .474342D0)  GO TO 300
      IF(A     .GE. 0.474342D0    .AND.  A    .LT.  .632456D0)  GO TO 301
      IF(A     .GE. 0.632456D0    .AND.  A    .LE.  .790569D0)  GO TO 302
  100 K=1
      GO TO 24
  200 K=2
      GO TO 24
  300 K=3
      GO TO 24
  301 K=4
      GO TO 24
  302 K=5
   24 A2=A**2
      A4=A**4
      A6=A**6
      CD0=GN(K,L,1,1)+GN(K,L,2,1)*A2+GN(K,L,3,1)*A4+GN(K,L,4,1)*A6
      CD1=CN(K,L,1,1)+3.*CN(K,L,2,1)*A2+5.*CN(K,L,3,1)*A4+7.*CN(K,L,4,1)
     1*A6
      CD2=-GN(K,L,1,2)-GN(K,L,2,2)*A2-GN(K,L,3,2)*A4-GN(K,L,4,2)*A6
      CD3=-CN(K,L,1,2)-3.*CN(K,L,2,2)*A2-5.*CN(K,L,3,2)*A4-7.*CN(K,L,4,2
     1)*A6
      CD4=GN(K,L,1,3)+GN(K,L,2,3)*A2+GN(K,L,3,3)*A4+GN(K,L,4,3)*A6
      CD5=CN(K,L,1,3)+3.*CN(K,L,2,3)*A2+5.*CN(K,L,3,3)*A4+7.*CN(K,L,4,3)
     1*A6
      CD6=-GN(K,L,1,4)-GN(K,L,2,4)*A2-GN(K,L,3,4)*A4-GN(K,L,4,4)*A6
      CD7=-CN(K,L,1,4)-3.*CN(K,L,2,4)*A2-5.*CN(K,L,3,4)*A4-7.*CN(K,L,4,4
     1)*A6
      CD12=CN(K,L,1,1)+CN(K,L,2,1)*A2+CN(K,L,3,1)*A4+CN(K,L,4,1)*A6
      CD22=-GN(K,L,1,2)-D13*GN(K,L,2,2)*A2-D15*GN(K,L,3,2)*A4-
     1D17*GN(K,L,4,2)*A6
      CD32=-CN(K,L,1,2)-CN(K,L,2,2)*A2-CN(K,L,3,2)*A4-CN(K,L,4,2)*A6
      CD42=GN(K,L,1,3)+D13*GN(K,L,2,3)*A2+D15*GN(K,L,3,3)*A4+
     1D17*GN(K,L,4,3)*A6
      CD52=CN(K,L,1,3)+CN(K,L,2,3)*A2+CN(K,L,3,3)*A4+CN(K,L,4,3)*A6
      CD62=-GN(K,L,1,4)-D13*GN(K,L,2,4)*A2-D15*GN(K,L,3,4)*A4-
     1D17*GN(K,L,4,4)*A6
```

```
      CD72=-CN(K,L,1,4)-CN(K,L,2,4)*A2-CN(K,L,3,4)*A4-CN(K,L,4,4)*A6
      R11=CD1-CD3*3.*W2+CD5*5.*W4-CD7*7.*W6+BK(M,1)+BK(M,2)*3.*W2+
     1 BK(M,3)*5.*W4+BK(M,4)*7.*W6
      R12=-CD3*6.*W1+CD5*20.*W3-CD7*42.*W5+BK(M,2)*6.*W1+BK(M,3)*20.*W3
     1+BK(M,4)*42.*W5
      R13=(BK(M,2)-CD3)*3.D0+(BK(M,3)+CD5)*30.D0*W2+(BK(M,4)-CD7)*105.D0
     1*W4
      R14=(BK(M,3)+CD5)*20.D0*W1+(BK(M,4)-CD7)*140.D0*W3
      R15=(BK(M,3)+CD5)*5.D0+(BK(M,4)-CD7)*105.D0*W2
      R16=(BK(M,4)-CD7)*42.D0*W1
      R17=(BK(M,4)-CD7)*7.D0
      R21=GK(M,1)+CD0+(GK(M,2)-CD2)*W2+(GK(M,3)+CD4)*W4+(GK(M,4)-CD6)*W6
      R22=(GK(M,2)-CD2)*2.D0*W1+(GK(M,3)+CD4)*4.D0*W3+(GK(M,4)-CD6)*6.D0
     1*W5
      R23=GK(M,2)-CD2+(GK(M,3)+CD4)*6.D0*W2+(GK(M,4)-CD6)*15.D0*W4
      R24=(GK(M,3)+CD4)*4.D0*W1+(GK(M,4)-CD6)*20.D0*W3
      R25=GK(M,3)+CD4+(GK(M,4)-CD6)*15.D0*W2
      R26=(GK(M,4)-CD6)*6.D0*W1
      R27=GK(M,4)-CD6
      R31=(BK(M,2)-CD3)*3.D0*W1+(BK(M,3)+CD5)*10.D0*W3+(BK(M,4)-CD7)*21.
     *D0*W5
      R32=(BK(M,2)-CD3)*3.D0+(BK(M,3)+CD5)*30.D0*W2+(BK(M,4)-CD7)*105.D0
     1*W4
      R33=(BK(M,3)+CD5)*30.D0*W1+(BK(M,4)-CD7)*210.D0*W3
      R34=(BK(M,3)+CD5)*10.D0+(BK(M,4)-CD7)*210.D0*W2
      R35=(BK(M,4)-CD7)*105.D0*W1
      R36=(BK(M,4)-CD7)*21.D0
      R41=(CD22-GK(M,2))*2.D0*W1-(CD42+GK(M,3))*4.D0*W3+(CD62-GK(M,4))*
     16.D0*W5
      R42=(CD22-GK(M,2))*2.D0-(CD42+GK(M,3))*12.D0*W2+(CD62-GK(M,4))*30.
     1D0*W4
      R43=-(CD42+GK(M,3))*12.D0*W1+(CD62-GK(M,4))*60.D0*W3
      R44=-(CD42+GK(M,3))*4.D0    +(CD62-GK(M,4))*60.D0*W2
      R45=-(CD42+GK(M,3))+(CD62-GK(M,4))*30.D0*W1
      R46=(CD62-GK(M,4))*6.D0*W1
      R51=CD12*W1-CD32*W3+CD52*W5-CD72*W7+BK(M,1)*W1+BK(M,2)*W3+
     1BK(M,3)*W5+BK(M,4)*W7
      R52=CD12-CD32*3.*W2+CD52*5.*W4-CD72*7.*W6+BK(M,1)+BK(M,2)*3.*W2+
     1BK(M,3)*5.*W4+BK(M,4)*7.*W6
      R53=-CD32*3.*W1+CD52*10.*W3-CD72*21.*W5+BK(M,2)*3.*W1+
     1BK(M,3)*10.*W3+BK(M,4)*21.*W5
      R54=BK(M,2)-CD32+(BK(M,3)+CD52)*10.D0*W2+(BK(M,4)-CD72)*35.D0*W4
      R55=(BK(M,3)+CD52)*5.D0*W1+(BK(M,4)-CD72)*35.D0*W3
      R56=BK(M,3)+CD52+(BK(M,4)-CD72)*21.D0*W2
      R57=(BK(M,4)-CD72)*7.D0*W1
      R61=CD22-GK(M,2)-(CD42+GK(M,3))*6.D0*W2+(CD62-GK(M,4))*15.D0*W4
      R62=-(CD42+GK(M,3))*12.D0*W1+(CD62-GK(M,4))*60.D0*W3
      R63=-(CD42+GK(M,3))*6.D0+(CD62-GK(M,4))*90.D0*W2
      R64=(CD62-GK(M,4))*60.D0*W1
      R65=(CD62-GK(M,4))*15.D0
      WRITE(6,30)AA,K,L,M
   30 FORMAT(1H ,'AA=',D23.16,3I5)
```

```
      B0=R31*R51-R61*R21
      B1=R31*R52+R32*R51-R61*R22-R62*R21
      B2=R31*R53+R32*R52+R33*R51-R61*R23-R62*R22-R63*R21
      B3=R31*R54+R32*R53+R33*R52+R34*R51-R61*R24-R62*R23-R63*R22-R64*R21
      B4=R31*R55+R32*R54+R33*R53+R34*R52+R35*R51-R61*R25-R62*R24-R63*R23
     *-R64*R22-R65*R21
      B5=R31*R56+R32*R55+R33*R54+R34*R53+R35*R52+R36*R51-R61*R26-R62*R25
     *-R63*R24-R64*R23-R65*R22
      B6=R31*R57+R32*R56+R33*R55+R34*R54+R35*R53+R36*R52-R61*R27-R62*R26
     *-R63*R25-R64*R24-R65*R23
      B7=R32*R57+R33*R56+R34*R55+R35 *R54+R36*R53-R62*R27-R63*R26
     1-R64*R25-R65*R24
      B8=R33*R57+R34*R56+R35*R55+R36*R54-R63*R27-R64*R26-R65*R25
      B9=R34*R57+R35*R56+R36*R55-R64*R27-R65*R26
      B10=R35*R57+R36*R56-R65*R27
      B11=R36*R57
      XCOF(1)=B0
      XCOF(2)=B1
      XCOF(3)=B2
      XCOF(4)=B3
      XCOF(5 )=B4
      XCOF(6 )=B5
      XCOF(7 )=B6
      XCOF(8 )=B7
      XCOF(9 )=B8
      XCOF(10)=B9
      XCOF(11)=B10
      XCOF(12)=B11
      CALL POLRT(XCOF,COF,11,RR1,RIM1,IER)
      WRITE(6,40)IER
      WRITE(6,50)
      WRITE(6,51)RR1
      WRITE(6,52)
      WRITE(6,51)RIM1
      C0=R41*R21-R11*R51
      C1=R41*R22+R42*R21-R11*R52-R12*R51
      C2=R41*R23+R42*R22+R43*R21-R11*R53-R12*R52-R13*R51
      C3=R41*R24+R42*R23+R43*R22+R44*R21-R11*R54-R12*R53-R13*R52-R14*R51
      C4=R41*R25+R42*R24+R43*R23+R44*R22+R45*R21-R11*R55-R12*R54-R13*R53
     *-R14*R52-R15*R51
      C5=R41*R26+R42*R25+R43*R24+R44*R23+R45*R22+R46*R21-R11*R56-R12*R55
     *-R13*R54-R14*R53-R15*R52-R16*R51
      C6=R41*R27+R42*R26+R43*R25+R44*R24+R45*R23+R46*R22-R11*R57-R12*R56
     *-R13*R55-R14*R54-R15*R53-R16*R52-R17*R51
      C7=R42*R27+R43*R26+R44*R25+R45*R24+R46*R23-R12*R57-R13*R56-R14*R55
     *-R15*R54-R16*R53-R17*R52
      C8=R43*R27+R44*R26+R45*R25+R46*R24-R13*R57-R14*R56-R15*R55-R16*R54
     *-R17*R53
```

```
      C9=R44*R27+R45*R26+R46*R25-R14*R57-R15*R56-R16*R55-R17*R54
      C10=R45*R27+R46*R26-R15*R57-R16*R56-R17*R55
      C11=R46*R27-R16*R57-R17*R56
      XCOF(1)=C0
      XCOF(2)=C1
      XCOF(3)=C2
      XCOF(4 )=C3
      XCOF(5 )=C4
      XCOF(6 )=C5
      XCOF(7 )=C6
      XCOF(8 )=C7
      XCOF(9 )=C8
      XCOF(10)=C9
      XCOF(11)=C10
      XCOF(12)=C11
      CALL POLRT(XCOF,COF,11,RR2,RIM2,IER)
      WRITE(6,40)IER
   40 FORMAT(1H0,'IER=',I10)
      WRITE(6,50)
   50 FORMAT(1H ,'REAL ROOTS')
      WRITE(6,51)RR2
   51 FORMAT(1H ,5(2X,D23.16))
      WRITE(6,52)
   52 FORMAT(1H ,'IM ROOTS')
      WRITE(6,51)RIM2
   61 CONTINUE
      STOP
      END
```

Appendix III

OSCILLATOR TRANSIENT SOLUTIONS A(t) & x(t)

It is obtained by solving two non linear differential equations in A, x and time(t).
The user must supply the following parameters.
- d-coefficients of the diode
- d-coefficients of the passive circuit
- w qusistationary frequency
- The initial values of A and x

```
      IMPLICIT REAL*8(A-H,O-Z)
      DIMENSION X0(2),WK(15)
      COMMON /ONE/GN(5,3,4,4),CN(5,3,4,4),BK(4,4),GK(4,4)
      COMMON /TWO/G,W1
      EXTERNAL F
      PI=3.141592D0
      H=-10.D0
      AA=-49500.D0
      X0(1)=.9624812145501785D-2/(10.D0*DSQRT(10.D0))
      X0(2)=-.3341535974404524D-04
      W1=.5886494335896001D-1
      N=2
      DO 6 K=1,5
      DO 6 L=1,3
    6 READ(5,33)((GN(K,L,I,J),J=1,4),I=1,4)
      DO 8 K=1,5
      DO 8 L=1,3
    8 READ(5,33)((CN(K,L,I,J),J=1,4),I=1,4)
      READ(5,33)((GK(I,J),J=1,4),I=1,3)
      READ(5,33)((BK(I,J),J=1,4),I=1,3)
   33 FORMAT(4(2X,D18.11))
      BB=-100.D0
      DO 100 I=500,1200,5
      B=BB*I
      CALL DASCRU(F,AA,B,H,N,X0,WK)†
      AA=B
      AMPL=10.D0*DSQRT(10.D0)*X0(1)
      FREQ=X0(2)*1.D11
      TIME=B/(2.D0*PI*1.D11)
      WRITE(6,200)AMPL,FREQ,TIME,H,B
  100 CONTINUE
  200 FORMAT(1H ,'AMPL=',D23.16,1X,'FREQ=',D23.16,3X,'T=',D15.7,1X,'H=',
     *D13.7,1X,'B=',D15.7)
      STOP
      END
```

† Subroutine DASCRU was used from the International Mathematical and Statistical library (IMSL).

```
      SUBROUTINE F(X0,T,N,YP)
      IMPLICIT REAL*8(A-H,O-Z)
      DIMENSION X0(2),YP(2)
      COMMON /ONE/GN(5,3,4,4),CN(5,3,4,4),BK(4,4),GK(4,4)
      COMMON /TWO/G,W1
      X=X0(2)
      X2=X**2
      X3=X**3
      X4=X**4
      X5=X**5
      X6=X**6
      A=X0(1)
      A2=A**2
      A4=A**4
      A6=A**6
      W2=W1**2
      W3=W1**3
      W4=W1**4
      W5=W1**5
      W6=W1**6
      W7=W1**7
      D13=1./3.
      D15=1./5.
      D17=1./7.
      IF(A     .GE. 0.0D0        .AND.  A    .LT.  .158114D0) GO TO 100
      IF(A     .GE. 0.158114D0   .AND.  A    .LT. .316228D0 ) GO TO 200
      IF(A     .GE. 0.316228D0   .AND.  A    .LT.  .474342D0) GO TO 300
      IF(A     .GE. 0.474342D0   .AND.  A    .LT.  .632456D0) GO TO 301
      IF(A     .GE. 0.632456D0   .AND.  A    .LT.  .790569D0) GO TO 302
  100 K=1
      GO TO 21
  200 K=2
      GO TO 21
  300 K=3
      GO TO 21
  301 K=4
      GO TO 21
  302 K=5
   21 IF(W1+X  .GE. .057 D0  .AND.  W1+X  .LT. .059D0 )GO TO 400
      IF(W1+X  .GE. .0590D0  .AND.  W1+X  .LT. .062D0 )GO TO 500
      IF(W1+X  .GE. .0620D0  .AND.  W1+X  .LE. .065D0 )GO TO 600
  400 L=1
      GO TO 22
  500 L=2
      GO TO 22
  600 L=3
   22 IF(W1+X  .GE. .057 D0  .AND.  W1+X  .LT. .0575D0)GO TO 150
      IF(W1+X  .GE. .0575DQ  .AND.  W1+X .LT. .05825D0)GO TO 250
      IF(W1+X .GE. .05825D0  .AND.  W1+X .LE. .05925D0)GO TO 350
  150 M=1
      GO TO 23
  250 M=2
      GO TO 23
  350 M=3
```

```
23 CD0=GN(K,L,1,1)+GN(K,L,2,1)*A2+GN(K,L,3,1)*A4+GN(K,L,4,1)*A6
   CD1=CN(K,L,1,1)+3.*CN(K,L,2,1)*A2+5.*CN(K,L,3,1)*A4+7.*CN(K,L,4,1)
  1*A6
   CD2=-GN(K,L,1,2)-GN(K,L,2,2)*A2-GN(K,L,3,2)*A4-GN(K,L,4,2)*A6
   CD3=-CN(K,L,1,2)-3.*CN(K,L,2,2)*A2-5.*CN(K,L,3,2)*A4-7.*CN(K,L,4,2
  1)*A6
   CD4=GN(K,L,1,3)+GN(K,L,2,3)*A2+GN(K,L,3,3)*A4+GN(K,L,4,3)*A6
   CD5=CN(K,L,1,3)+3.*CN(K,L,2,3)*A2+5.*CN(K,L,3,3)*A4+7.*CN(K,L,4,3)
  1*A6
   CD6=-GN(K,L,1,4)+GN(K,L,2,4)*A2-GN(K,L,3,4)*A4-GN(K,L,4,4)*A6
   CD7=-CN(K,L,1,4)+3.*CN(K,L,2,4)*A2-5.*CN(K,L,3,4)*A4-7.*CN(K,L,4,4
  1)*A6
   CD12=CN(K,L,1,1)+CN(K,L,2,1)*A2+CN(K,L,3,1)*A4+CN(K,L,4,1)*A6
   CD22=-GN(K,L,1,2)-D13*GN(K,L,2,2)*A2-D15*GN(K,L,3,2)*A4-
  1D17*GN(K,L,4,2)*A6
   CD32=-CN(K,L,1,2)-CN(K,L,2,2)*A2-CN(K,L,3,2)*A4-CN(K,L,4,2)*A6
   CD42=GN(K,L,1,3)+D13*GN(K,L,2,3)*A2+D15*GN(K,L,3,3)*A4+
  1D17*GN(K,L,4,3)*A6
   CD52=CN(K,L,1,3)+CN(K,L,2,3)*A2+CN(K,L,3,3)*A4+CN(K,L,4,3)*A6
   CD62=-GN(K,L,1,4)-D13*GN(K,L,2,4)*A2-D15*GN(K,L,3,4)*A4-
  1D17*GN(K,L,4,4)*A6
   CD72=-CN(K,L,1,4)-CN(K,L,2,4)*A2-CN(K,L,3,4)*A4-CN(K,L,4,4)*A6
   R11=CD1-CD3*3.*W2+CD5*5.*W4-CD7*7.*W6+BK(M,1)+BK(M,2)*3.*W2+
  1 BK(M,3)*5.*W4+BK(M,4)*7.*W6
   R12=-CD3*6.*W1+CD5*20.*W3-CD7*42.*W5+BK(M,2)*6.*W1+BK(M,3)*20.*W3
  1+BK(M,4)*42.*W5
   R13=(BK(M,2)-CD3)*3.D0+(BK(M,3)+CD5)*30.D0*W2+(BK(M,4)-CD7)*105.D0
  1*W4
   R14=(BK(M,3)+CD5)*20.D0*W1+(BK(M,4)-CD7)*140.D0*W3
   R15=(BK(M,3)+CD5)*5.D0+(BK(M,4)-CD7)*105.D0*W2
   R16=(BK(M,4)-CD7)*42.D0*W1
   R17=(BK(M,4)-CD7)*7.D0
   R21=GK(M,1)+CD0+(GK(M,2)-CD2)*W2+(GK(M,3)+CD4)*W4+(GK(M,4)-CD6)*W6
   R22=(GK(M,2)-CD2)*2.D0*W1+(GK(M,3)+CD4)*4.D0*W3+(GK(M,4)-CD6)*6.D0
  1*W5
   R23=GK(M,2)-CD2+(GK(M,3)+CD4)*6.D0*W2+(GK(M,4)-CD6)*15.D0*W4
   R24=(GK(M,3)+CD4)*4.D0*W1+(GK(M,4)-CD6)*20.D0*W3
   R25=GK(M,3)+CD4+(GK(M,4)-CD6)*15.D0*W2
   R26=(GK(M,4)-CD6)*6.D0*W1
   R27=GK(M,4)-CD6
   R31=(BK(M,2)-CD3)*3.D0*W1+(BK(M,3)+CD5)*10.D0*W3+(BK(M,4)-CD7)*21.
  *D0*W5
   R32=(BK(M,2)-CD3)*3.D0+(BK(M,3)+CD5)*30.D0*W2+(BK(M,4)-CD7)*105.D0
  1*W4
   R33=(BK(M,3)+CD5)*30.D0*W1+(BK(M,4)-CD7)*210.D0*W3
   R34=(BK(M,3)+CD5)*10.D0+(BK(M,4)-CD7)*210.D0*W2
   R35=(BK(M,4)-CD7)*105.D0*W1
```

```
      R36=(BK(M,4)-CD7)*21.D0
      R41=(CD22-GK(M,2))*2.D0*W1-(CD42+GK(M,3))*4.D0*W3+(CD62-GK(M,4))*
     16.D0*W5
      R42=(CD22-GK(M,2))*2.D0-(CD42+GK(M,3))*12.D0*W2+(CD62-GK(M,4))*30.
     1D0*W4
      R43=-(CD42+GK(M,3))*12.D0*W1+(CD62-GK(M,4))*60.D0*W3
      R44=-(CD42+GK(M,3))*4.D0    +(CD62-GK(M,4))*60.D0*W2
      R45=-(CD42+GK(M,3))+(CD62-GK(M,4))*30.D0*W1
      R46=(CD62-GK(M,4))*6.D0*W1
      R51=CD12*W1-CD32*W3+CD52*W5-CD72*W7+BK(M,1)*W1+BK(M,2)*W3+
     1BK(M,3)*W5+BK(M,4)*W7
      R52=CD12-CD32*3.*W2+CD52*5.*W4-CD72*7.*W6+BK(M,1)+BK(M,2)*3.*W2+
     1BK(M,3)*5.*W4+BK(M,4)*7.*W6
      R53=-CD32*3.*W1+CD52*10.*W3-CD72*21.*W5+BK(M,2)*3.*W1+
     1BK(M,3)*10.*W3+BK(M,4)*21.*W5
      R54=BK(M,2)-CD32+(BK(M,3)+CD52)*10.D0*W2+(BK(M,4)-CD72)*35.D0*W4
      R55=(BK(M,3)+CD52)*5.D0*W1+(BK(M,4)-CD72)*35.D0*W3
      R56=BK(M,3)+CD52+(BK(M,4)-CD72)*21.D0*W2
      R57=(BK(M,4)-CD72)*7.D0*W1
      R61=CD22-GK(M,2)-(CD42+GK(M,3))*6.D0*W2+(CD62-GK(M,4))*15.D0*W4
      R62=-(CD42+GK(M,3))*12.D0*W1+(CD62-GK(M,4))*60.D0*W3
      R63=-(CD42+GK(M,3))*6.D0+(CD62-GK(M,4))*90.D0*W2
      R64=(CD62-GK(M,4))*60.D0*W1
      R65=(CD62-GK(M,4))*15.D0
      R1= R11+R12*X+R13*X2+R14*X3+R15*X4+R16*X5+R17*X6
      R2=A*(R21+R22*X+R23*X2+R24*X3+R25*X4+R26*X5+R27*X6)
      R3=A*(R31+R32*X+R33*X2+R34*X3+R35*X4+R36*X5)
      R4= R41+R42*X+R43*X2+R44*X3+R45*X4+R46*X5
      R5=A*(R51+R52*X+R53*X2+R54*X3+R55*X4+R56*X5+R57*X6)
      R6=A*(R61+R62*X+R63*X2+R64*X3+R65*X4)
      YP(1)=(R3*R5-R6*R2)/(R6*R1-R3*R4)
      YP(2)=(R4*R2-R1*R5)/(R6*R1-R3*R4)
      RETURN
      END
```